Spectral Characterisation and Optical Simulation of Innovative Liquid Encapsulants for Design-for-Recycling Silicon Solar Modules

Technical University Delft

Photovoltaic Devices and Materials
Thomas Rijsman

TU Delft

BIOSPHERE SOLAR

Spectral Characterisation and Optical Simulation of Innovative Liquid Encapsulants for Design-for-Recycling Silicon Solar Modules

Technical University Delft

by

Thomas Rijsman

to obtain the degree of Master of Science

at the Delft University of Technology,

to be defended publicly on Monday August 25, 2025 at 14:00.

Student number:	4918053	
Project duration:	9 December 2024 – 25 August 2025	
Thesis committee:	Prof. Dr. A. W. Weeber,	TU Delft, chair or the committee
	Dr. M. R. Vogt,	TU Delft, supervisor
	Dr. Ir. D. van der Born,	TU Delft, external member
	Dr. U. Bothra,	TU Delft, daily supervisor
	MSc Z. Fung-A-Jou,	Biosphere Solar

Cover:	Liquid-filled solar module from Biosphere Solar by Liam McClain (Modified)
Style:	TU Delft Report Style, with modifications by Daan Zwaneveld

An electronic version of this thesis is available at http://repository.tudelft.nl/.

TU Delft

BIOSPHERE SOLAR

Abstract

The transition to renewable energy, led by photovoltaic (PV) energy, is critical for a sustainable future. However, the current linear ”take-make-waste” economy, also used for PV modules, presents a significant challenge to long-term sustainability, creating a massive future waste stream and reliance on virgin materials. The primary obstacle to achieving a circular economy for solar modules is the use of permanently cross-linked solid encapsulants like Ethylene Vinyl Acetate (EVA), which bond all components together and severely hinder repair, reuse, and high-value recycling.

This thesis examines liquid encapsulation as a promising alternative design-for-recycling concept, enabling simple disassembly and material recovery. The primary objective was to determine if liquid encapsulation is a viable alternative from an optical perceptive, compared to conventional solid (EVA) and gas-filled (air) module designs. To achieve this, three sub-goals were formulated and completed.

First, a comprehensive selection strategy was developed based on critical optical, electrical, chemical, and thermal criteria, identifying seven candidate liquids for analysis: deionised water, glycerol, SolaPro Ennogreen glycol, Polydimethylsiloxane (PDMS), and three industrial dielectric oils (Shell Diala S4 XZ-I, Midel 7131, Mivolt). Material compatibility tests with polyisobutylene (PIB) immersed in Midel 7131 and Shell Diala, confirmed that Shell, and therefore mineral oils in general, are incompatible with the use of PIB as a sealant.

Second, the complex refractive index (n and k) of these liquids was experimentally measured over the 300–1200 nm solar spectrum using a novel hybrid method. This involved a specialised ellipsometer and dual cuvette measurements with spectrophotometry, generating the nk data needed for detailed optical modelling. Measurements made by Semilab’s liquid-specialised ellipsometer using a 2-term Cauchy model yielded excellent fits ($R^2 > 0.97$) for all liquids, in good agreement with literature values. The dual cuvette method revealed extremely high transparency for all liquids, even slightly yellowish fluids Midel and Shell Diala. A SNR analysis established a confidence threshold at $k \approx 5 * 10^{-8}$.

Finally, these optical properties were used as inputs for detailed optical modelling and simulation, in GenPro4, to quantify and compare the photocurrent generated by liquid encapsulation compared to standard EVA and air, in various solar module configurations. The optical model and its simulated output are validated through experiments and datasheets, showing excellent agreement around the Δ J_{ph} = 0.2 mA/cm^2. The results revealed a fundamental trade-off: while the liquids have lower refractive indices, leading to higher initial reflection losses compared to conventional EVA with UV blockers, their superior transparency resulted in lower parasitic absorption. This balance allowed top-performing liquids, notably Mivolt (highest photocurrent and lowest reflector, J_{ph} = 40.90 - 41.81 mA/cm^2) and PDMS (lowest absorber, J_{ph} = 40.85 - 41.75 mA/cm^2), to generate a photocurrent comparable to, and in some cases higher than, UV-transparent EVA (J_{ph} = 40.92 - 41.81 mA/cm^2). However, the optical performance of the other liquids was very close (especially Midel and Shell, but also glycerol and glycol, followed within 0.17 mA/cm^2), meaning that based on optics alone, they should not be excluded, as other design benefits might justify their selection. A critical insight emerged from annual energy yield simulations, which demonstrated that PDMS delivered the highest yearly energy output (0.07% higher than EVA-UVT, 0.086% to Mivolt), due to its extremely low absorption. The simulations showed that mitigating reflection losses through tailored Anti-Reflection Coatings (ARCs) or glass texturing can further unlock the full potential of liquid-encapsulated modules.

In conclusion, this thesis provides the first comprehensive optical validation for liquid encapsulation in standard silicon PV modules. It successfully demonstrates that, from an optical standpoint, liquids are a highly viable technology, worthy of further research. Their primary drawback of higher reflection is compensated by superior transparency and can also be further mitigated with existing ARC and glass texturing technologies. This work establishes a robust foundation for future research, confirming that liquid encapsulation is not only a promising pathway toward a circular economy for PV but is also an optically competitive alternative to established solid encapsulants.

Acknowledgements

First of all, I would like to thank my supervisors, Malte Vogt and Urvashi Bothra, for their guidance, valuable feedback, and support throughout this thesis. There advice was motivating and helped me focus on properly performing one task at a time, instead of 100 task in a mediocre way. I am especially grateful for their open and approachable attitude, it gave me the feeling I was allowed to discuss, think and critize freely, a feeling I greatly enjoy and value a lot.

I am thankful to everyone at Biosphere Solar for the fun interactions and thought-provoking discussions, and in particular to Alberto Poli for his sharp mind and scientifically critical thinking. But most of all for his easy going and reassuring mindset, and of course for educating me in some Italian culture and words.

Special thanks go to Stefaan Heirman and Tim Velzeboer for ensuring smooth lab work, their helpful insights, fruitful discussions, and the light-hearted conversations that made the lab a pleasant place.

I am indebted to Semilab for enabling refractive index measurements with their specialized ellipsometer setup, as well as for their valuable discussions on the complex refractive index of liquids. Especially Bálint Fodor and László Makai, for their explanations and pleasant contact.

My appreciation extends to the staff at the PVMD department and TU Delft, especially Youri Blom, Paul Procel Moya, Katarina Kovačević, Federica Saitta, and Rudi Santbergen for taking the time to answer my many questions. Also for Juan Camilo Ortiz Lizcano for his helpful answers and curiosity regarding ARC and glass texturing. I am grateful to Wim Termorshuizen and Luis Castro Heredia from the High Voltage department for sharing their expertise on dielectric liquids in high voltage applications.

I would like to acknowledge all the researchers whose work this thesis is built upon, and in particular Matthew Clarke and Han Xinyue for kindly sharing data from their studies.

To my family, friends, and roommates, thank you for your endless support and the distractions that kept me balanced during this project. I especially want to thank Marijn de Rijk for helping me rediscover the joy of data analysis.

Contents

List of Figures

List of Tables

Nomenclature

Abbreviations

Abbreviation	Definition
AM1.5G	Air Mass 1.5 Global spectrum
ASTM	American Society for Testing and Materials
EOL	End-of-life
EQE	External quantum efficiency
EVA	Ethylene vinyl acetate
FF	Fill factor
GW	Gigawatt
IBC	Interdigitated back contact
IEC	International Electrotechnical Commission
IQE	Internal quantum efficiency
IRENA	International Renewable Energy Agency
Jsc	Short-circuit current density
kWh	Kilowatt-hour
NICE	New industrial cell encapsulation
PDMS	Polydimethylsiloxane
PAO	Polyalphaolefin
PET	Polyethylene terephthalate
PIB	Polyisobutene
PID	Potential induced degradation
POE	Polyolefin elastomer
PV	Photovoltaic
PVMD	Photovoltaic Materials and Devices
SHJ	Silicon heterojunction
STC	Standard Test Conditions
TOPCon	Tunneling oxide passivated contact
TPO	Thermoplastic polyolefin
TW	Terawatt
UV	Ultraviolet
Voc	Open-circuit voltage
PFAS	Per- and polyfluoroalkyl substances
PFC	Perfluorocarbons
PFPE	Perfluoropolyethers
HFE	Hydrofluoroethers
FK	Fluorketones
PCBs	Polychlorinated biphenyls
GWP	Global Warming Potential

Symbols (Latin)

Symbol	Definition	Unit
I_{ph}	Photogenerated current	[A]
I_{sc}	Short-circuit current	[A]
J_{ph}	Photocurrent density	[mA/cm^2]

Symbol	Definition	Unit
J_{sc}	Short-circuit current density	[mA/cm^2]
n	Real part of refractive index	[–]
k	Extinction coefficient (imaginary part of refractive index)	[–]
$\tilde{n} = n + ik$	Complex refractive index	[–]
α	Absorption coefficient	[cm^{-1}]
A	Absorptance	[– or %]
R	Reflectance	[– or %]
T	Transmittance	[– or %]
V	Voltage	[V]
V_{oc}	Open-circuit voltage	[V]
λ	Wavelength	[nm or µm]
c_p	Specific heat capacity	[J/kg·K]
κ	Thermal conductivity	[W/m·K]
α_T	Thermal expansion coefficient	[K^{-1}]
T_f	Freezing point	[°C]
T_b	Boiling point	[°C]
T_{fp}	Flash point	[°C]
T_{pp}	Pour point	[°C]
σ	Electrical conductivity	[S/m]
ρ_e	Electrical resistivity	[Ω·m]
ε_r	Relative dielectric constant (relative permittivity)	[–]
E_b	Breakdown voltage / dielectric strength	[kV/mm]
η	Dynamic viscosity	[Pa·s]
ρ	Density	[kg/m^3]
β	Compressibility	[Pa^{-1}]
Hazen number	Colour index (0 = clear, 500 = yellow)	[–]
ASTM D1500	Colour scale for petroleum products	[–]

Symbols (Greek)

Symbol	Definition	Unit
Ψ	Ellipsometric amplitude ratio	[°]
Δ	Ellipsometric phase difference	[°]
ρ	Density	[kg/m^3]
ε	Dielectric permittivity	[F/m]
μ	Dipole moment	[C·m]

1

Introduction

We have entered a remarkable era, one in which technologies are being developed that could potentially ensure an ”endless” supply of energy for generations to come. Renewable energy systems, particularly solar photovoltaics (PV), offer the vision of a future where humanity sustains itself by harvesting the power of the sun, one of the most abundant and reliable energy sources in the universe.

In 2021, the International Energy Agency (IEA) stated that solar energy became the cheapest form of electricity in history, with 0.044 USD per kilowatt-hour (kWh) in 2023 [1]–[3]. This price is projected to decline further thanks to research, large-scale production and supporting policies [4]–[6]. Providing clean and affordable energy to people around the world, with modular systems able to be deployed in large production sites or decentralised off-grid solutions.

However, from a ”the glass is half empty” viewpoint, this vision is far from realised. The pace of global emissions, degradation of ecosystems, and loss of biodiversity provides mounting evidence for a more sobering scenario. As global demand for energy, infrastructure, and technology continues to grow, so too does the pressure on Earth’s finite resources. Our current economic model, linear and built on a foundation of extraction, production, use, and disposal, is showing its limits. This ”take–make–waste” system not only leads to significant material losses but also generates vast quantities of waste, much of which remains unmanaged. In response to this challenge, the concept of a circular economy has emerged as a compelling alternative. Rather than relying on continuous extraction, a circular system seeks to retain value within the economy by prioritising reuse, repair, and recycling. It offers a pathway to reduce environmental impact while addressing material scarcity and long-term supply risks.

In this context, solar PV modules offer both a challenge and a unique opportunity. They are one of the most promising technologies for delivering clean energy, yet they are typically not designed for disassembly, reuse, or recycling. As the global solar market continues to grow, so too does the looming issue of end-of-life panel waste and reliance on virgin materials. With an impressive 1865 GW PV power currently installed, installation rates have been explosive and surpassed many forecasts [7]. However, this is generating a large and fast-growing PV waste stream that is going to hit in the upcoming years, estimated to reach 200 Mt globally by 2050 [8], [9].

This thesis combines two of the most important pillars in the pursuit of a truly self-sustaining society: the provision of renewable energy and the implementation of a circular economy. Where there are great challenges, there are also great opportunities—and this is especially true for circular solar module design. Solar panels offer the potential for a near-limitless energy supply, lasting for as long as the sun continues to shine. By extending this sustainability to the materials themselves—through smart, circular design—solar energy can fulfil its promise not only as a renewable power source, but as a fully regenerative system fit for the future.

1.1. Circular economy

Moving to a fully circular economy, in which products can be repaired, reused and recycled, will be crucial to ensure a sustainable future. Most production lines are still linearly shaped; raw materials are mined to produce a product, which is then used and, after use, thrown away. In a circular economy, mining is reduced by extending the lifetime of products (repairs) and reusing and recycling them at the end of their life to form new products, as seen in Figure 1.1. A step even further would be the blue economy, an emerging principle which shares many values with the circular economy. Also closing the loop and using waste to produce, but focusing on possible interconnections of resource loops between industries, limits of nature and local production [10]. Since the two concepts are similar and can build on each other, only the circular economy is addressed further in this thesis.

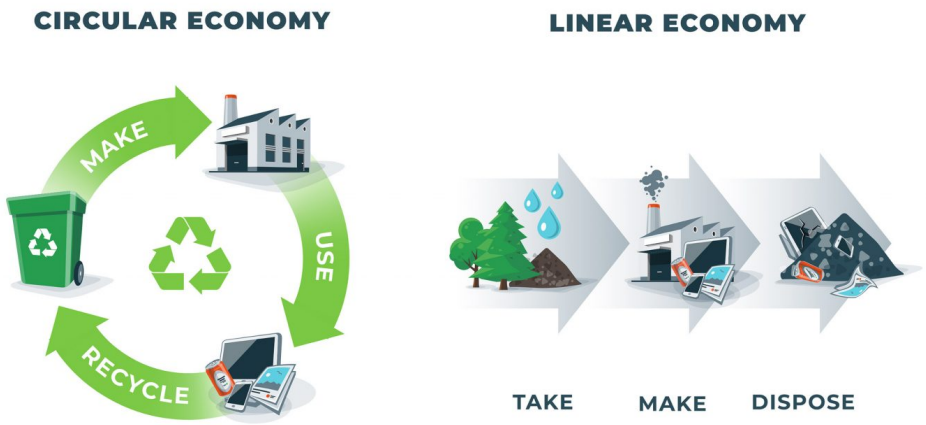

Figure 1.1: Circular and linear economy [11]

This change in production and logistic chains is needed in all sectors; in some, it is already the standard, such as the reuse of beer crates and bottles, others have emerging initiatives such as the FairPhone or Patagonia, but unfortunately, in most sectors, it is only in the early stages of research and implementation [12], [13]. The linear economy creates 3 main problems:

- Raw materials: There is only a limited amount of materials available on our planet, which can run out with current production levels. This can also create a dependence on other countries, using it in geopolitics, which is why the EU is focusing on these (critical) raw materials [14].
- Mining: Extracting raw materials is a very polluting and energy-intensive activity. It produces large quantities of carbon emissions, but also negatively affects the local environment, biodiversity and people [15]–[18].
- Waste stream: The linear economy is producing a large waste stream through all products that are disposed of after use. This can have very dramatic consequences for the environment, wildlife and health [19]–[22].

This nicely highlights which opportunities a circular economy can offer, such as an alternative supply of raw materials. Currently, the recycling and collection rate of PV modules is relatively low. However, improving this rate can significantly contribute to securing critical materials needed for future PV production. If the collection rate is improved to 100%, recycled PV modules could supply 20-64% of the materials required for PV production by 2050, depending on production levels [23].

This is the reason why it is sometimes referred to as urban mining, gaining valuable materials out of (urban) waste streams. This new supply creates three main advantages: firstly, creating another supply of materials helps bring potential shortages of that material down. Secondly, recycling materials is less energy intensive and polluting than mining them [17], [18]. Lastly, there is less dependence on other countries that produce or have a monopoly on a certain material.

Furthermore, there are local benefits to the environment and health of the population by having fewer mines and landfills [15], [16], [20]. Most PV modules end up in landfills due to the high cost of recycling

and limited infrastructure. This poses environmental risks, such as the leaching of heavy metals like lead and cadmium [21], [22], [24]. Reducing the waste that ends up in nature will be beneficial to its ecosystems and wildlife, potentially limiting the amount of microplastics in living organisms, for example.

It is possible to increase efficiency significantly by using products longer, repairing, reusing and only recycling them if no other option is possible. Extending the lifetime of a product makes it more economically attractive and also reduces its carbon emission (fewer new products are needed) [25].

1.1.1. Solar modules as circular product

Solar modules are a good candidate for a circular production line since most of their materials could be separated. Solar modules contain some critical raw materials (EU definition) and some materials that might become scarce according to future forecasts, which will be discussed later [14], [23], [26], [27]. Given the main goal of the industry, providing green energy for a sustainable future, it is well-suited to set an example of truly becoming 100% sustainable. Not only harnessing the (relatively) endless supply of solar energy, but also being able to do this forever by repairing, reusing and recycling its products.

To better understand what a circular economy means for solar modules and which obstacles are in the way, we will start with the current status and then see what options there are to improve this. To do this, we will start with the build-up of a solar module, which materials are used and which parts. Then, the current recycling options will be discussed, with their disadvantages and advantages. This helps to show how we could improve the repair, reuse and recycling of solar modules in the future. As a rule of thumb, for a product to be circular, it needs to be modular. This means that it should be possible to take the components apart to repair or replace them with other components. This also allows for the separation of materials at the end of life, making it possible to reuse or recycle them in case repairing is not possible. This separation of materials is crucial since you need to have a pure material to produce something new from it, in general.

1.1.2. Solar module parts and raw materials

Solar modules consist of critical raw materials and more abundant materials, of which the definition can change with time. As can be seen in Figure 1.2, the main component (by weight) in a standard Si solar module is glass (76%), followed by a plastic polymer, often EVA (10%), then aluminium (8%), the solar cell, which is a bulk of silicon (5%) with some interesting material layers and interconnections making up the last 1% [28]–[31]. First, these layers and interconnections will be discussed and after that, the larger parts and their materials.

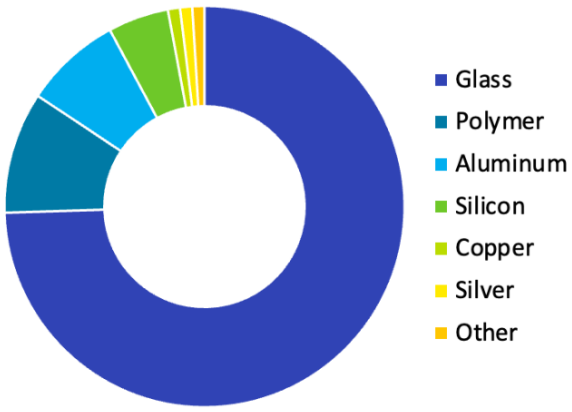

Figure 1.2: Material composition of standard silicon solar module [29]

It is the silicon solar cell with its thin layers and the interconnections that contain most of the critical raw materials. Depending on which architecture is used, the following materials can be found in solar cells that are listed as critical (or strategic) raw materials by the EU as of 2023: bismuth, boron, germanium,

copper, phosphorus, silicon metal, and nickel (indium present in 2020 list) [14]. Some materials are not listed by the EU but could potentially become scarce due to their intense usage, as is predicted in some forecasts. This is the case for silver, tin, bismuth, and indium [23], [26], [27]. These lists of critical raw materials and forecasts show which materials might form a problem for PV production. This will depend on future trends in solar cell technology and material intensity. A table with the solar cell technologies and their material is displayed in Table 1.1.

Table 1.1: Valuable materials in different solar cell technologies

Solar Cell Technology	(Critical) Materials
PERC	Silver (Ag), Silicon (Si), Aluminium (Al)
TOPCon	Silver (Ag), Silicon (Si), Aluminium (Al), Phosphorus (P), Boron (B)
HJT	Silver (Ag), Indium (In), Silicon (Si), Tin (Sn)
CdTe	Tellurium (Te), Cadmium (Cd), Silver (Ag)
CIGS	Indium (In), Gallium (Ga), Selenium (Se), Silver (Ag)
Perovskite	Lead (Pb), Iodine (I), Tin (Sn), Gold (Au) or Silver (Ag)
Tandem/Multi-Junction	Indium (In), Gallium (Ga), Arsenic (As), Germanium (Ge), Silver (Ag)
GaAs	Gallium (Ga), Arsenic (As), Germanium (Ge), Indium (In)
InP	Indium (In), Phosphorus (P)

This small fraction of the total solar module, the solar cell, may contain the most valuable materials; the remaining bulk can also be used in the circular economy. Currently, it is difficult to take solar modules apart due to their layout, which will be further discussed to better understand the problem. As can be seen in Figure 1.3, the standard solar module consists of an aluminium frame that protects the edges and provides mounting points [25], [32], [33]. The top layer is a sheet of low-iron (solar) glass, bonded to an encapsulation layer that surrounds the solar cells on both the front and back surfaces. This encapsulation layer is typically made of a transparent polymer, such as ethylene vinyl acetate (EVA), and is attached to either a polymer-based backsheet or another glass panel.

The solar cells are crystalline silicon (c-Si) wafers connected in series to form a cell string. Electrical interconnection is achieved through silver-based front and back contact grids, linked via copper busbars using lead-tin solder. The encapsulation process optically and mechanically binds these components together, with the module edge sealed using a specialised adhesive. Beneath the backsheet, the junction box houses the electrical connections, linking the individual strings to the external system.

This general layout applies to most silicon-based PV modules, which currently dominate the market, accounting for approximately 98% of global production [34], [35]. However, a major challenge with this design is the difficulty in separating the encapsulation from the solar cells and glass during recycling [36]–[38]. These layers are essentially ”glued” together, making both repair and material recovery complex. The parts can be summarised as follows:

- Front and backsheet
- Silicon solar cells
- Aluminium frame
- Interconnection and junction box
- encapsulation

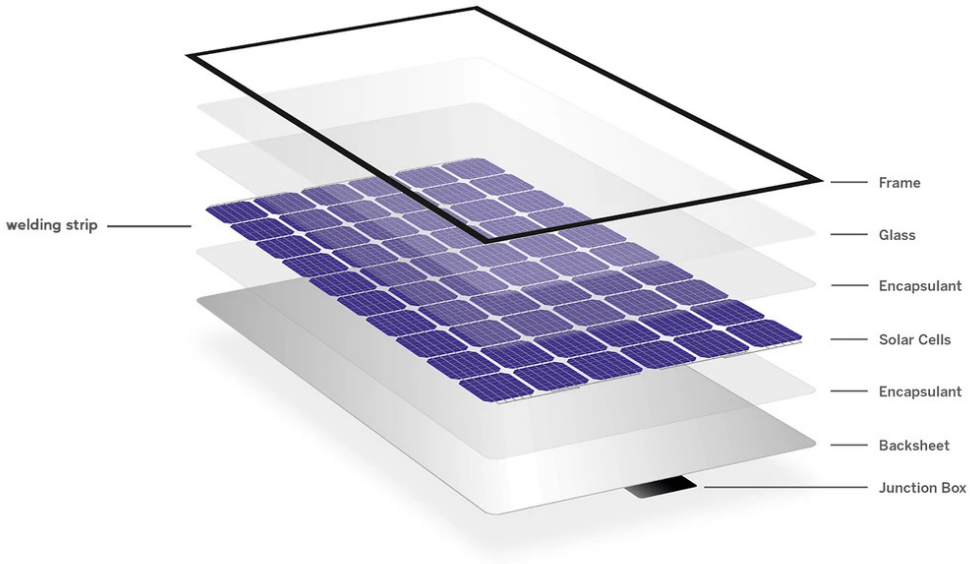

Figure 1.3: Layer build up of standard solar module [39]

Front and backsheet

Front and backsheets are essential components of solar modules, acting as the rear cover that protects solar cells from moisture and UV radiation. They provide electrical insulation and block moisture ingress, crucial for preventing corrosion. Low iron glass is used as a front sheet for the solar module due to its extremely high optical transparency, mechanical strength and good weather resistance [34], [40]. Usually, tempered glass with an anti-reflection coating (ARC) is used [40]. Tempered glass is stronger than normal glass by chemically or thermally treated. In general, standard glass is well recyclable and is currently being recycled [40]. However, this process can become difficult if glass panels deviate in quality and composition (iron content, ARCs, ect), which is the case for solar glass due to missing regulations and the sharing of glass properties by manufacturers.

Typically, backsheets have a multilayer structure, Kynar-based materials have the largest market share (44%) followed by other materials (PPE, CPC), while Tedlar-based and Polyolefin-core-based are losing market share in the upcoming years [34], [41]. Due to the rise of bifacial solar modules dominating the market at the moment, the back sheet of the module is primarily made of glass, to allow light entering from the back [34]. These glass-glass modules now hold a 50 % market share, which is forecasted to grow to 85+ % in the upcoming years.

Silicon solar cell

The silicon solar cell is where the magic happens; here, the light is absorbed and converted to electricity, and all other components function to optimise this process. As mentioned earlier, the solar module market is dominated by silicon-based technologies [34]. Silicon is the second most abundant material in the Earth's crust, after oxygen, so from a geological perspective it should be abundant [42]. However, the high-purity silicon needed for solar cells and semiconductors is listed as a critical material for a couple of reasons. There are only a couple of countries in the world that produce the high-purity quartz needed. Production of high-grade silicon is energy-intensive. It is a crucial material for PV and electronics.

The most used silicon solar cell technologies with their market share in 2024, are Passivated Emitter and Rear Contact/Locally-diffused (PERC/PERL) ($\approx$ 35%), Tunnel Oxide Passivated contact (TOPCon) ($\approx$ 56%) and Silicon Hetero Junction (SHJ) ($\approx$ 5%), Interdigitated Back Contact (IBC) cells are expected to grow the upcoming years to a market share up to 33%, as can be seen in Figure 1.4. Each has its

benefits and drawbacks over the other, which for this thesis will be limited to their current and predicted efficiency and materials used. These architectures will be further discussed in chapter 5.

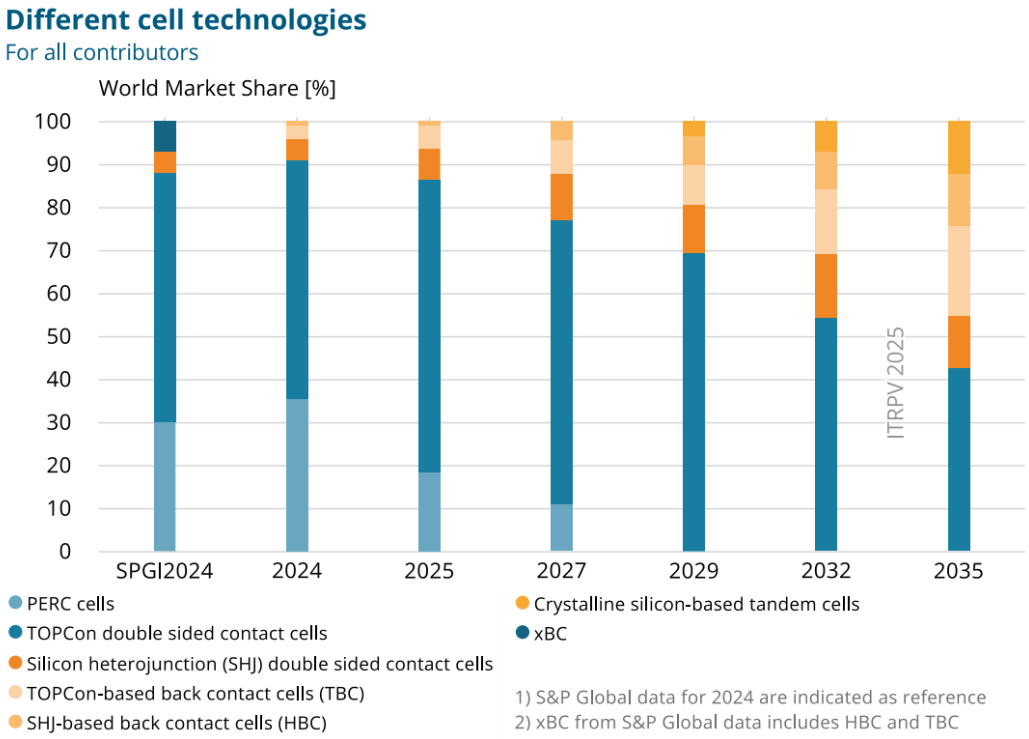

Figure 1.4: Different cell technologies and their market share in 2024 [34]

Aluminium frame

Aluminium is most often used for the frame, 94% market share, which protects the edges of the layers and provides mounting points [34]. It is a light-weight metal and is used in many industries and applications due to its low cost and high performance. It is the most abundant metal in Earth's crust (third place in total) [42], but also listed as a critical raw material, bauxite [14]. In most forecasts, it is not identified as a bottleneck material for PV production, and in general, it is also relatively easy to recycle [23], [26], [27].

Interconnection and junction box

Interconnections electrically connect solar cells within a module and between modules, ensuring efficient current flow and minimising resistive losses. Traditionally, lead-containing solders have been used, but lead-free alternatives are available, particularly for silicon heterojunction (SHJ) and interdigitated back contact (IBC) cells [34].

Junction boxes protect electrical connections and serve as the interface between the module and the external system. They house bypass diodes, which reduce power losses from shading.

Encapsulation

The primary functions of encapsulation in solar modules are to bond the glass, solar cells, and backsheet while providing mechanical strength, electrical insulation, and optical coupling. Additionally, encapsulation protects solar cells from UV radiation, vibration, shock, moisture, and dust.

Historically, EVA has been the dominant encapsulation material, and still is with just over half the market share in 2024, as seen in Figure 1.5 [34]. However, its share is projected to decrease as alternative materials such as Polyolefins (POE) and EVA/POE mix gain popularity due to higher reliability [34]. EVA is processed as a thermoplastic sheet containing various additives, such as UV stabilisers, thermo-oxidative stabilisers, glass adhesive promoters, rheology modifiers, and most importantly, a

radical initiator to facilitate cross-linking [25], [43]. During the lamination process, EVA undergoes a transformation from a thermoplastic to a thermosetting material by cross-linking.

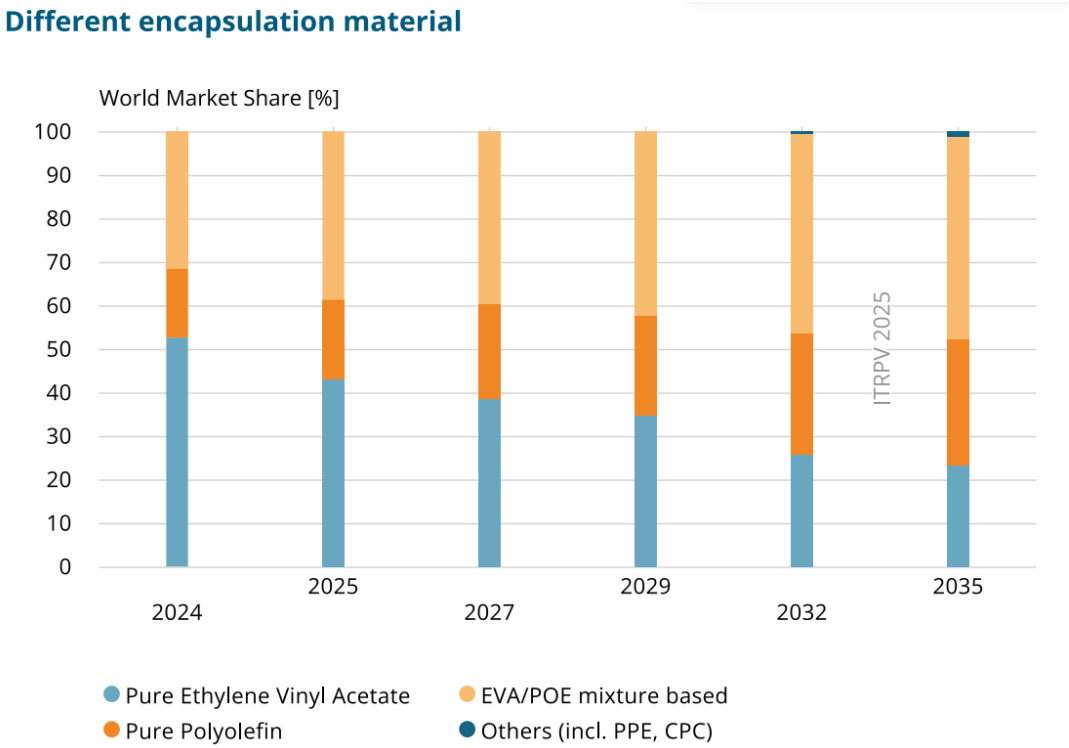

Figure 1.5: Different encapsulation materials and their market share [34]

EVA is widely used in PV module encapsulation due to its low cost, good processability, high transparency, flexibility, and lightweight properties [25], [43]. However, the drawbacks are that EVA is prone to degradation from UV radiation, which can cause discolouration unless stabilising additives are incorporated. Additionally, the cross-linking process necessitates extra chemicals, potentially introducing contaminants into the material. Over time, EVA encapsulation can lead to ageing-related issues such as acetic acid formation, moisture penetration, thermal degradation, and the development of hot spots, all of which can reduce module performance. Furthermore, EVA complicates recycling due to its thermoset nature and the presence of potentially hazardous additives, raising environmental concerns. This is why the search for alternative materials continues, which we also see in forecasts.

Polyolefin-based encapsulants, particularly Polyolefin Elastomer (POE) and Thermoplastic Polyolefin (TPO), are gaining traction as alternatives to conventional EVA, visualised by their growing market share in Figure 1.5 [25], [34], [41]. POE, currently holding a market share of around 15%, is increasingly favoured due to its superior moisture resistance, UV stability, and lower susceptibility to Potential Induced Degradation (PID). POE does not produce acetic acid during degradation, reducing long-term performance losses. However, POE undergoes a cross-linking reaction similar to EVA, requiring additional energy and additives. Despite limited long-term studies, POE is particularly well-suited for bifacial modules and advanced solar cell architectures such as TOPCon and SHJ cells.

TPO, on the other hand, is a non-cross-linking thermoplastic encapsulant with advantages such as shorter lamination times, lower energy consumption, and the elimination of toxic stabilisers or cross-linkers [25]. Studies indicate that TPO exhibits better degradation behaviour than EVA, with lower fluorescence and yellowing under UV exposure and a lower reduction in performance under humid heat conditions. Additionally, it does not produce acid-related degradation by-products. While TPO has better recyclability compared to EVA, its lower glass transition temperature can lead to embrittlement and delamination in cold conditions.

A hybrid approach is seen in the rise of ethylene propylene elastomer (EPE), a co-extruded structure

combining EVA and POE. With a 30+% market share, EPE offers a balance between the process ability and adhesion of EVA and the moisture resistance and stability of POE [34], [41]. This makes it an attractive option for manufacturers seeking to enhance module durability while maintaining cost-effectiveness. An overview or their pros and cons can be seen in Figure 1.6.

Other alternative encapsulation materials operate more in niche or are still being researched, such as polyvinyl butyral (PVB), polyurethane and ionoplasts/ionomers [25]. These ionomers offer enhanced mechanical stability and tear resistance, although current research is limited, and aspects such as adhesion could be a problem [44]. Another interesting alternative is silicone, Polydimethylsiloxane (PDMS), which was used as encapsulation in the past. It has excellent properties and shows a long lifetime for modules in multiple studies, but is no longer used due to its higher cost [25], [45], [46].

Encapsulation Material	EVA	TPO	POE	PVB
Price	+++ [11,36]	++++ [36,37]	++ [36]	++++ [36,37]
Structural support	+++ [11,33]	+++ [11,39]	+++ [42]	+++ [43]
Optical transmission	+++ [11,33]	+++ [11]	+++ [41]	+++ [11,43]
Degradation	++ [11,33,34,37]	+++ [11,37–39]	+++ [38]	+++ [11]
Recyclability	+ [2,10,11,18,19,34]	++ [2,37,40]	+ [2,37,41]	++ [2,37,44–46]

Evaluation spectrum: very good (++++), good (+++), neutral (++) and poor (+) evaluation.

Figure 1.6: Comparison of the main encapsulation materials used at the moment [25]

These alternative materials to EVA are mainly highlighted since EVA is hindering the deconstruction of PV modules at the moment, which will be further discussed in the next section. There are two ways of replacing the EVA: (i) an alternative material such as those listed above, (ii) an alternative encapsulation method, which will be discussed in the following sections.

1.2. Solar module recycling

Recycling can solve crucial problems and offer interesting opportunities, such as a new raw material supply, reducing PV waste in the environment and in landfills, and reducing its negative effect as mentioned in section 1.1. PV recycling at the moment is limited for multiple reasons, among a missing specialised recycling infrastructure and economic incentives [47].

Recycling processes for PV modules can be broadly categorised by two dimensions: the value of recovered materials (low-value bulk downcycling versus high-value re-/upcycling) and the methods employed (mechanical, thermal, chemical, and hybrid/innovative approaches) [25], [38], [47]. First, the high and low economic division will be addressed, followed by the methods used and researched, to conclude with the challenges and potential solutions.

1.2.1. High and low level recycling

A clear distinction can be made between bulk recycling and high-value recycling. Bulk recycling focuses on recovering materials that constitute large mass percentages in the module, such as the aluminium frame and glass [25]. In contrast, high-value recycling aims to recover more precious components, like the silicon solar cell and interconnections, by employing more complex and resource-intensive processes. Most existing processes cover low-value bulk recycling, resulting in downcycling, where recovered materials are of lower quality than the original, thereby reducing their economic value [36], [48].

The typical recycling process involves the removal of external components (cables, junction box, and frame), followed by delamination and the separation of individual materials. However, the current lack of specialised solar module recyclers forces most modules to be processed using standard glass or electronic waste recycling methods [38], [49]. The first outputs of these processes are usually the aluminium frame, cables, and fragmented glass/cullets. While the aluminium and copper can be readily reused, the glass fragments often do not meet the quality requirements for reuse in PV. Meaning they will often be used as low-value filler materials.

High-value recycling, on the other hand, employs additional (expensive) steps such as complex delamination, chemical etching, or leaching processes to recover high-purity silicon wafers and precious metals like silver [25], [38]. The advanced re-/upcycling methods under development do hold significant promise by enabling nearly complete (94+%) recovery of materials in lab scale and R&D lines [23].

It might be difficult to justify these higher costs since the recycling is often not economically viable at the moment. Early cost estimates suggest that while recycling a PV module in the Netherlands may cost around 15€ per panel, advanced processes aimed at high-grade recovery can range from 14€ to 23€ per panel [36], [48]. For the revenues, the majority at the moment is derived from the aluminium frame, with other components being more challenging to economically recover. It is estimated that the revenues can range from 7€ to 21€, depending on the market price of the material (21€ being the historically highest market price). In addition, the recovered silicon (or other materials) extracted after 25 years might be of lower quality/price than the market standard at that moment (so in 2050, although this will always play a role in every product). These fluctuations and uncertainty make recycling less attractive at the moment.

1.2.2. Recycling methods

The main methods used for recycling photovoltaic (PV) modules today are briefly discussed. To get an idea of the share in applications per method, a study from IEA PVPS conducted a survey among recyclers and checked patents per method [38]. The methods and materials obtained are visualised for overview in Figure 1.7 [36].

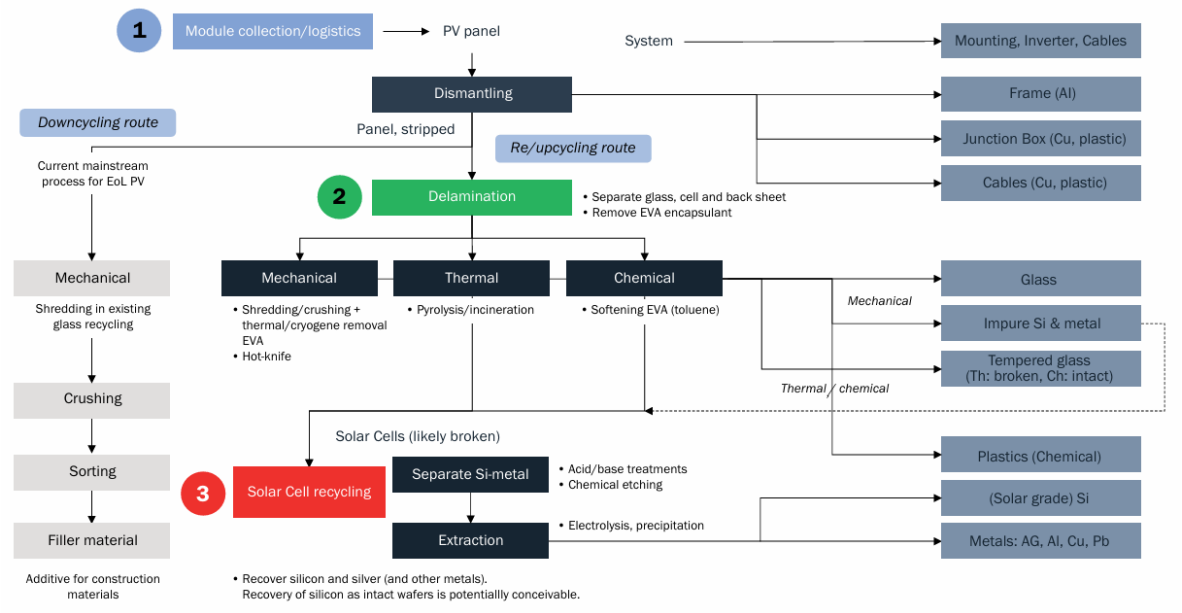

Figure 1.7: Overview of recycling methods and their material extraction[36]

Mechanical Recycling

This method is dominant and involves physical processes such as cutting, shredding, grinding, and blasting to separate and recover materials. This means the glass (encapsulation and silicon solar cells) is reduced to cullet and needs to be separated from other materials. It is of lower quality and cannot be directly reused in the PV industry, but is used as filler or insulating material [25], [36]. It is the most common method and is often performed in e-waste or glass recycling plants, accounting for approximately 40% of patents related to PV recycling [38]. It performs well on cost, capacity and output, but generally it downcycles the modules and is not able to recover important materials such as silicon and silver [38], [50].

Thermal Recycling

This method uses heat treatments to break down the encapsulation and separate the components in processes like pyrolysis, incineration, and hydrothermal processes [25]. These processes often require high temperatures and thus more energy, as well as potentially harmful gases that can be emitted. It represents about 15% of patents [38].

Chemical Recycling

This method involves using solvents and reactive chemicals (acids or alkaline solutions) to extract valuable materials in processes like metal substitution, electrolysis or precipitation [25]. It is rather costly, slower than thermal and mechanical and has a lower throughput, resulting in less focus on these methods [36], [48]. It accounts for about 19% of patents [38].

Combination of Methods and emerging methods

Many recycling processes use a combination of mechanical, thermal, and chemical treatments to optimise material recovery. Examples include light pulse treatment, green chemistry approaches, cryogenic separation, and automated component removal systems. This approach is used in about 25% of patents for c-Si modules and 64% for thin-film modules [36], [38]. The hot knife method and waterjet can enable intact delamination and separation of the solar glass. This allows for the reuse of the glass, but does not give access to the higher value materials in the encapsulation [36].

For thin-film modules, additional methods like electrochemical techniques such as electrodynamic fragmentation, laser, or flash lamp annealing, make up 4% and optical separation 9%. These methods are applied to different types of PV modules, including crystalline silicon (c-Si), cadmium telluride (CdTe), and copper indium gallium selenide (CIGS) modules. The choice of method often depends on the specific materials and construction of the PV modules being recycled. many technologies are still in lower Technologies Readiness Levels (TRL) [36].

To summarise, mechanical has the highest throughput and lowest cost, but leads to downcycling and does not give access to higher value materials such as silver and silicon. For this, more specialised thermal and chemical methods need to be used. Less attention is going into chemical due to its slow processes, higher energy consumption and low throughput. Thermal methods can offer solar-grade glass and potentially higher-grade silicon, but proper separation from the encapsulation remains difficult. New technologies and methods are being researched more, but remain in lower TRL, making it difficult to access them properly and give a proper cost analysis, which is crucial. At the moment, the cost generally outweighs the profits, making it economically unviable. This means that supporting structures and financing are needed to properly recycle the PV modules at End-of-Life (EoL). Bringing down the cost means improving the recycling by either enhancing the current recycling processes or design-for-recycling, which will be discussed in the following section.

1.3. Design for recycling

In order to improve the recycling of solar modules, two main approaches exist, which are strongly connected. (i) Improving the current recycling techniques; making it easier to open up solar modules to separate components and materials, or (ii) design-for-recycling, considering their end of life at design and production, so they will be easier to open up, which is also promoted by several studies [25], [26]. This second option also allows repairs on the module and easier reuse, making them suitable for the circular economy. As we saw in the previous section, the main problem with repairing and recycling at the moment is the difficulty of opening the module with the components intact and separating them. In this section, these problems will be briefly addressed, discussing potential concepts and what research needs to be conducted.

The encapsulation ”glues” all components together, which is good during operations but troubling for repairs and recycling [25]. In subsection 1.1.2, we explored alternatives to EVA, but most have the same problem, although TPO or PVB could be easier to recycle [25]. Instead of these solid encapsulation materials bonding the components together, a gas or liquid could be an interesting alternative. These studies exploring design-for-recycling for solar modules are relatively new, and research into this field has been limited [51]–[59].

TPedge

The TPedge concept was a glass–glass module designed for building-integrated photovoltaic (BIPV) that uses air as encapsulation with an edge sealant, resulting in a frameless and polymer-free module for silicon solar cells [51]. The sealing consists of a thermoplastic spacer (TPS) filled with drying silicates inside the spacer, and a silicone that provides the mechanical stability of the module. Front glass with double-sided ARC is employed to minimise reflection losses as seen in Figure 1.8. The second glass-air interface introduces extra reflection losses, due to the lower refractive index of air, which will be discussed in more detail in chapter 5. This gas-filled design not only reduces production time but also cuts module material costs by approximately 15.3% compared to standard modules, primarily through savings on encapsulation foils and framing. Testing of TPedge modules has demonstrated their robustness, as evidenced by successful performance in thermal cycling, damp-heat, hail, potential-induced degradation, hot spot endurance, UV stability and mechanical load tests.

Moreover, they have been installed at the Fraunhofer ISE since August 2013, with additional modules added in September 2015, showing durability over two years, with electroluminescence inspections revealing no cell degradation and power loss. The technology has been successfully demonstrated with various commercially available solar cells, including back-contact cells and structured interconnections.

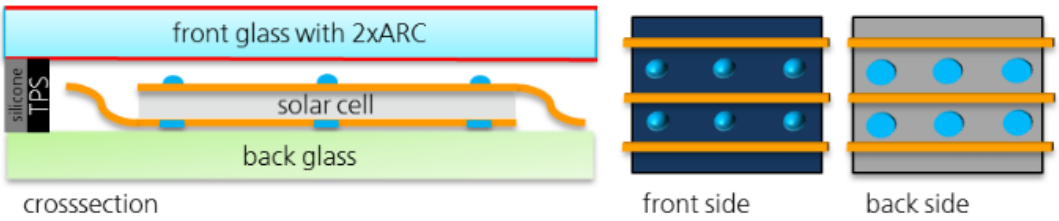

Figure 1.8: TPedge cross section [51]

NICE

The New Industrial Solar Cell Encapsulation (NICE) technology from Apollon Solar utilises nitrogen gas as encapsulation, combined with edge sealant [52], [53], specifically aiming for a recyclable design. The NICE modules employ polyisobutylene (PIB) for edge sealing, which is used for double-insulated windows as well, providing an effective barrier against external effects. In this design, an under-pressure within the module presses the front and back glasses together, forcing the copper ribbons directly onto the cell busbars to create the electrical series connection, as can be seen in Figure 1.9. This enhances the recyclability of the module at the EoL, able to extract components and materials [54]

Although initial simulations by SunSolve indicate that NICE modules may exhibit 1–2% lower performance due to optical losses, these losses are expected to be offset by lower degradation rates and extended operational lifetimes [53]. This stems from the same reflection losses as with air encapsulation, as all gases have a refractive index close to 1. Therefore, they use an ARC on the solar cell (although details on this ARC are missing), which is better suited to the refractive index of the gas.

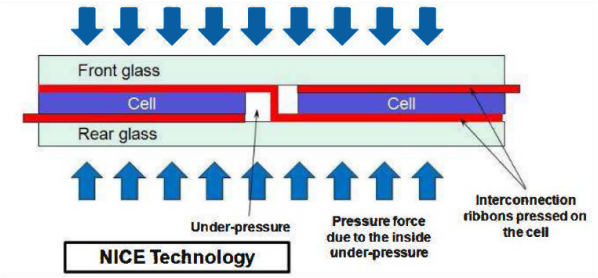

Figure 1.9: Nice module cross section [52]

Biosphere Solar and TU Delft

Biosphere and TU Delft have developed a module with air encapsulation and dessicated PIB sealing, also designed for more circular use, allowing repairs and recycling [60]. Pre-compliance tests for the IEC61215 are currently being performed, as well as outdoor testing.

Next to the air-filled module, liquid encapsulation studies at TU Delft and Biosphere started in 2024, for potentially better protection, improved thermal management and higher optical transmittance [56]–[59]. As mentioned before, the glass-air interface on the inside of the module introduces more reflection losses, which can be reduced by using a liquid. The air also functions as thermal insulation, potentially hindering the cooling of the solar cells, causing them to heat up, which could cause their efficiency to decrease. Research into these liquid encapsulations is still in the early phase. Initial optical, thermal cycling, and damp-heat tests are showing promising results.

CEA-INES

The CEA-INES concept is a glycerol-filled module, which also uses a liquid encapsulation layer to address concerns over metallization material consumption and module recyclability by eliminating dispersive interconnection materials and total solid encapsulation while maintaining high performance [55]. Derived from NICE and TPEdge concepts, this innovative glass–glass design still uses a solid polymer (Ionomer) layer melted onto the internal side of the glass plates to secure connector positioning and a transparent glycerol layer applied around the cells for optical coupling and preventing the polymer from adhering to cell surfaces as can be seen in Figure 1.10.

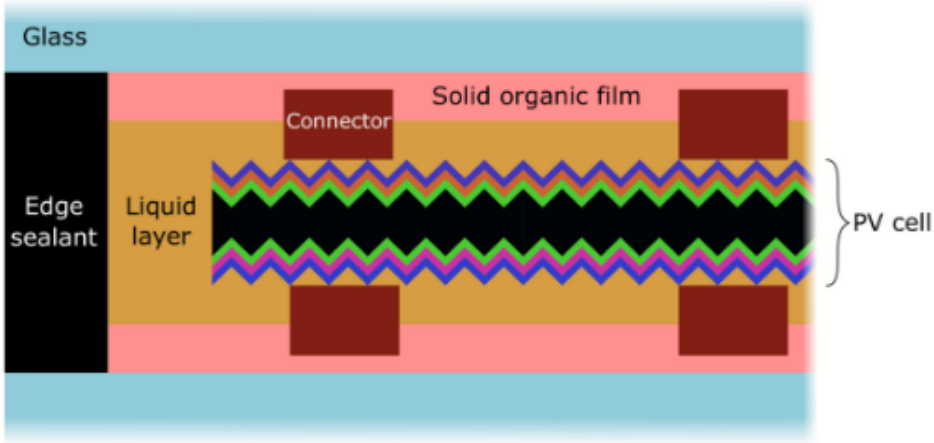

Figure 1.10: CEA-INES module cross section [55]

Optical simulations confirm the design's proper light transmission, while thermal modelling demonstrates its effective heat dissipation. Proof-of-concept one-cell modules have been fabricated and subjected to accelerated ageing, heat-cycling and damp-heat tests. Simulation and tests have shown good results with a slight increase in photocurrent for the optical modelling and a small increase in heat dissipation, resulting in lower cell temperature. The design further minimises critical material consumption by reducing interconnection components to standard copper ribbons, which can be easily recovered and recycled in a closed-loop process. Recycling has been demonstrated in which all components were easy to separate. Glycerol is soluble in water, meaning it can be easily washed off. Further optimisation of the optical index of the liquid layer is proposed, as well as longer degradation testing and finer modelling on optical and thermal aspects.

These concepts show the state-of-the-art and where research is heading; it is still very limited, but showing promising first results. The gas/air-filled modules are easy to fabricate and recycle, but could fall short in terms of efficiency and protection due to lower light transmission and heat dissipation. Liquid encapsulation could potentially solve these problems with better optical coupling and lower temperatures. Also, it adds more protection against external influences while still allowing easy recycling. To

evaluate if liquids are suitable as encapsulation, they need to perform some key functions, which will be discussed in the following section and chapter 3.

1.4. Liquid Encapsulation

Liquid encapsulation is proposed as a promising alternative to traditional solid encapsulants such as EVA, with the aim of improving the recyclability of PV modules. For effective encapsulation, the liquid must fulfil several key criteria to protect the solar cells and ensure proper module performance. These include high optical transparency, chemical stability, and strong electrical insulation, among other requirements described in chapter 3.

In order to achieve this, suitable liquids must be identified and thoroughly evaluated. While thermal, electrical, and chemical properties are relatively well documented for many liquid candidates, a significant gap remains in the literature when it comes to their optical properties. This is especially problematic, as extremely high optical transmittance is one of the most crucial characteristics for any encapsulation material used in solar modules. It directly affects the amount of light reaching the solar cells, and therefore the overall energy yield. With optical properties such as the complex refractive index, n and k values, over the required wavelength range (300 - 1200 nm), it is possible to optically compare the liquid encapsulation to traditional and gas-filled modules. This can be done through an optical analysis and modelling, which will shortly be discussed.

1.5. Optical Modelling

To evaluate and compare different encapsulation strategies, such as liquids, solids, or gas-filled modules, optical modelling is essential. By simulating how light interacts with the multilayer structure of a solar module, it is possible to estimate how much light is transmitted to the solar cell and how much is lost through reflection or absorption. This thesis uses the GenPro4 simulation tool, which is well-suited for modelling layered optical systems under standard test conditions while maintaining computational efficiency.

Accurate modelling requires wavelength-dependent optical input parameters for each material layer, specifically the refractive index (n) and extinction coefficient (k). These define the light's behaviour at each interface and within each layer. For many liquids, this optical data is often missing or incomplete, highlighting the need for further characterisation. A more detailed explanation of the modelling process, assumptions, and validation is provided in chapter 5.

1.6. Research Gap

Although some studies have investigated solar cells immersed in dielectric liquids, the field remains under-explored, particularly concerning liquids as permanent encapsulants in standard PV modules. Multiple papers have highlighted this lack of research and call for further exploration into the topic [61]–[66]. Early work mainly examined solar cells submerged in liquids as an experimental comparison to air, or as part of active cooling systems in concentrated photovoltaic (CPV) applications. In these cases, liquids were not intended as encapsulation layers but as cooling media. Some optical measurements have been performed, typically limited to transmittance, to screen for potential candidates. However, detailed optical analyses, with complex refractive index (n and k values) over the range 300 to 1200 nm, are often missing.

Almost no liquids (except water, silicone oil, glycol, glycerol and 3 edible oils) have had their full wavelength-dependent refractive index (n) and extinction coefficient (k) values reported across the solar-relevant range of 300 to 1200 nm. Furthermore, no liquid encapsulation concepts have been proposed besides the CEA-INES concept published in January. This study does not consider a broader range of candidate liquids, nor does it provide in-depth optical comparisons to conventional solid or gas-filled encapsulates.

This thesis addresses this gap by reviewing potential liquid encapsulants and investigating their suitability for PV modules, with a specific focus on their optical performance. Since manufacturers rarely report comprehensive optical properties, such as transmittance, reflectance, absorption, and full-spectrum n and k values, experimental measurements or simulation-based modelling become essential. Without

this data, it is difficult to properly assess or compare the viability of liquid encapsulation against traditional options. With it, however, optical modelling can be used to evaluate performance and identify promising candidates for circular and efficient solar module designs.

In summary, the major research gap lies in the limited understanding of the optical properties of potential liquid encapsulation. Without complete spectral data, including refractive index and extinction coefficient, the feasibility and efficiency of implementing liquid encapsulation in standard silicon solar modules remain unvalidated.

1.7. Thesis Objective

The overarching objective of this thesis is to explore the feasibility of using liquids as an alternative encapsulation material in standard silicon solar modules, with a particular focus on their optical performance. Liquids present improved recyclability, yet their optical performance needs to be analysed and compared to conventional solid encapsulation and gas-filled modules.

Main goal

To perform an optical analysis and modelling of multiple suitable liquids for use as encapsulation in standard silicon solar modules, as compared to EVA and air encapsulation.

Sub-goals

- **Develop a strategy for liquid selection.**
  A selection methodology needs to be created to identify promising candidate liquids based on a combination of known optical, physical, thermal, chemical, and electrical properties. Based on literature, datasheets, industry, experts and experiments. Eventually identifying suitable candidate liquids..
- **Obtain complex refractive index through experiments.**
  The refractive index (n) and extinction coefficient (k) of selected liquids will be experimentally measured over the solar-relevant wavelength range of 300 to 1200 nm. These measurements are crucial, as they provide the input parameters required for accurate optical modelling and comparison to conventional encapsulation.
- **Perform optical modelling and simulation.**
  Using the obtained optical properties, simulations will be performed with the GenPro4 tool to assess the optical behaviour of solar modules using each liquid as encapsulation. Based on the modelling results, the optical losses in each configuration will be analysed to determine which liquids offer the best performance. Real-world simulations using the PVMD Toolbox and optimisation of the best-performing liquids will help assess the full potential of liquid encapsulation.

1.8. Thesis Outline

This thesis is structured as follows. chapter 1 introduces the motivation and context of the research, emphasising the need for sustainable energy solutions and the role of circular design in photovoltaic modules. It outlines the research gap and defines the scope and objectives of the work. chapter 2 presents the literature review on liquid encapsulation in solar applications, with a focus on optical, electrical, and thermal properties, and highlights the limited existing research in this field. chapter 3 describes the liquid selection process by outlining the methodology; literature to select the most crucial criteria, identifying suitable liquid groups/families, eliminating liquids and groups based on criteria and selecting the most suitable fluids. chapter 4 explains the experimental methods used to measure the complex refractive index, n and k values, of the selected liquids. chapter 5 introduces the optical simulation tool GenPro4, outlines the modelling approach, and describes how the models were validated. It presents the simulation results and performance comparisons between candidate liquids and traditional encapsulants. Finally, chapter 6 concludes the thesis with a summary of findings, evaluates the feasibility of liquid encapsulation based on optical criteria, and provides recommendations for future work.

2

Literature review

2.1. Literature review

This review was performed to see what is known today and which aspects require further research, and how this thesis can fit in there. It continues with the design for recycling introduced in the previous section, then research related to solar cells immersed in liquid is discussed. Followed by papers regarding concentrated photovoltaic (CPV) and concentrators, after which comes the section on optics and beam splitting. Finally, the patents are briefly discussed, and a conclusion is drawn.

2.2. Design for recycling

Several design-for-recycling concepts, such as NICE, TPEdge, biosphere-TU Delft and CEA-INES concepts, have been discussed in chapter 1. Here, the literature regarding this field will be briefly addressed.

While there are multiple studies into the recycling of solar modules, there is only a limited amount about the design for recycling. This is probably due to the lower priority of recycling when designing a PV module at the moment. Several papers regarding recycling mention this method as interesting, facilitating easier repairs, reuse and recycling [25], [26], [33].

The interest of larger institutions such as TNO or IEA's PV Power Systems Program (PVPS) highlights the importance of design for recycling and also shows that its development is in the early stages. TNO conducted multiple studies into the recycling of solar modules, giving valuable insights and focusing on circular design in their PILATUS project [36], [67]. PVPS Task 12 has put forth guidelines for the design of recycling solar modules, which incorporate interesting ideas and lessons [68]. Among others, it includes guidelines like: ”minimising non-reversible adhesives or similar bonds, especially over whole surfaces and for dissimilar materials, can facilitate disassembly and material liberation”, ”design for disassembly (DfD) can improve recyclability” and ”minimising encapsulant use or using reversible encapsulants can facilitate disassembly of PV modules”. These could include materials other than EVA or different phases such as gases and liquids, which will be briefly discussed in the following paragraphs.

Interestingly, noted by Heat et al. (2020), changes in design to minimise cost or materials can influence recycling in good and bad ways, often without direct intentions. Recent trends include the drastic reduction of silver usage in solar cells, the shift toward thinner silicon wafers, and the increasing prevalence of double-glass bifacial modules. These changes not only alter the material composition and recovery value of end-of-life modules but also introduce new technical challenges, such as increased fragility (cells break more easily, for example) and compatibility with existing separation processes. For example, double-glass modules reduce fluoropolymer content, potentially lowering emissions in thermal treatments, but require adaptations in glass-handling systems and a greater emphasis on maintaining low-iron glass purity for reuse. These design trends often prioritise cost, efficiency, and durability, but rarely consider end-of-life recovery, making it harder for recycling infrastructure to keep pace.

The paper ”The Design Value for Recycling End-of-Life Photovoltaic Panels” underscores the critical

importance of integrating Design for Recycling (DfR) and Design for Durability [47]. The study identifies several actionable design strategies to improve PV module recyclability without compromising durability. It repeats previously mentioned guidelines for minimising or replacing non-reversible adhesives, especially EVA encapsulants, facilitating easier disassembly. Selecting recyclable backsheets and optimising sealants used in aluminium frames can prevent components from being damaged during separation. Using finite element analysis, the authors show how adjusting geometric tolerances between layers could enhance durability, mechanical resilience and end-of-life recovery. Their focus is more on the design of the recycling process instead of the solar module, unfortunately, as well as their design improvements, focusing on durability and minimising failure modes.

Other options for a more circular design include two encapsulation layers, in which the bottom layer does not attach to the cells and can be easily released, as seen in Figure 2.1 [25], [69]. Although this does facilitate easier recycling, the optical performance (and efficiency) is decreased by the additional transparent film. It has some similarities with the CEA-INES concept, which also uses an ionomer layer on the inside of the glass, with the glycerol being in contact with the solar cells. This does not seem to affect the optical performance negatively (even slightly positive), making it an interesting option to further examine in this thesis as well.

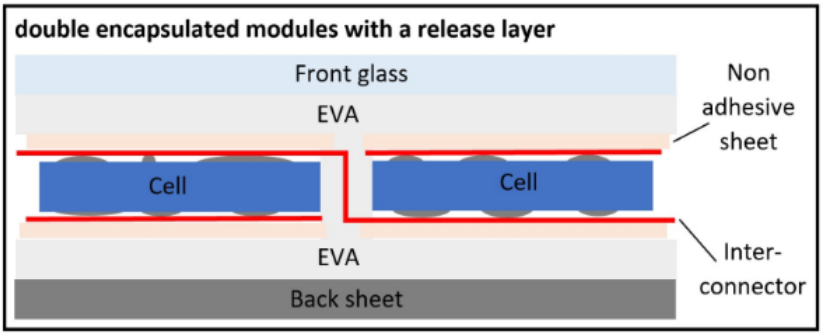

Figure 2.1: Cross section of the double encapsulation with release layer [69]

The Dutch company Solarge is developing lightweight, polymer-based PV panels that aim to reduce environmental impacts by replacing traditional materials like glass and aluminium with polymers [70]. Utilising polyolefin as encapsulation, which should make the solar modules better recyclable, although detailed information about this process is missing. It does provide an interesting alternative possessing several advantages, such as lightweight, recyclability and high production standards.

By far the most mentioned concept with improved circular design in other studies is the NICE module, which has multiple published papers showing good results [52]–[54]. Although having multiple years of proper performance in real climate conditions and plans for setting up larger-scale production lines, the idea was abandoned without further explanation.

However, the recent paper on the CEA-INES concept has similarities to the NICE module, such as the interconnections, but adding a liquid as encapsulation for the first time in a standard Si module [55]. The concept is performing well; they modelled the optical behaviour using CROWN. A simple thermal model was constructed, which shows slightly lower temperatures for the glycerol concept compared to EVA (and air). For future work, they propose finer simulations for optical and thermal aspects, looking into fine-tuning of the optical index of the liquid layer and using higher purity glycerol. This fits well with the objectives of this thesis, with a more elaborate optical analysis on multiple potential liquids. To better understand which fluids could be used and the effect of using fluids with (direct immersion) solar cells, the following sections discuss the relevant literature about these topics.

2.3. Solar cells immersed in liquid

One of the first papers on solar cells immersed in a dielectric liquid was published in 1980, with the paper ”Efficiency increase of solar cells operated in dielectric liquid” [71]. This research was conducted after Tanaka found that solar cell efficiency increases when operating in a dielectric liquid, which he later

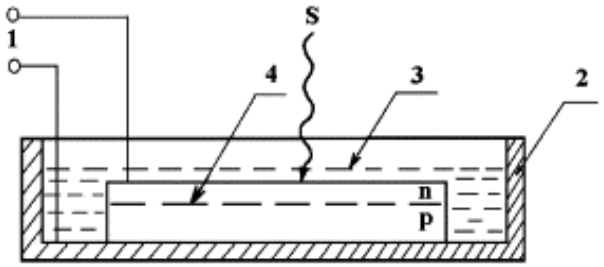

Figure 2.2: Test setup cross-section with solar cell in a vessel with glycerol: 1—contact terminals, 2—vessel, 3—glycerol, 4—solar cell (p-n-junction) [76]

also patented [72], [73]. The liquids investigated with different dielectric constants were benzene, water, methyl alcohol, acetone, ethyl ether and ethyl alcohol. The focus was on determining if the reason for the increased efficiency was due to the absorption of polarizable molecules or increased light collection thanks to refraction and internal reflection of the liquids. From the results, they see a stronger correlation of increased short circuit current with the permanent electric moment of the molecules in the liquid than refractive index or dielectric constant. Proposing two possible mechanisms for the increase in current: the suppression of surface recombination by adsorption of polarizable molecules, or an increase in photoconductance due to band bending at the surface.

The following computational study investigates the impact of submersion depth on the spectral distribution of solar radiation and its effects on the performance of silicon solar cells [74]. As sunlight penetrates water, both its total energy and spectral bandwidth decrease, particularly in the longer wavelengths, due to absorption by water. Using a computational model, the authors reconstructed the solar spectrum and silicon cell spectral response at various depths, calculating the relative efficiency of the cell compared to its performance at the surface. Results show that while solar energy and short-circuit current decline with depth, the relative efficiency initially increases due to spectral filtering that favours the silicon cell's optimal absorption range, peaking around 0.05 m before gradually decreasing and reaching the same level as out of the water around 3.5 m. These findings highlight the potential for spectrum filtering, which will be discussed further in a later section.

In the paper "Effect of liquid dielectrics on the efficiency of silicon solar cells" an increase of efficiency was also observed [75]. Liquids were chosen with low electrical conductivities, namely: glycerol, acetone, isopropyl alcohol, deionised water, butanol and dioxane. They mention that all liquids show similar results and therefore only glycerol is reported, since this gave the best results. The solar cells are put in a vessel (petri dish, see setup at Figure 2.2) and immersed in the liquid; later, glass is also placed on them, resulting in a similar effect as increased thickness of the liquid. They saw an average efficiency increase of 40-60%, with the largest increase going from 8 % to 14%. They also ascribe this effect to reduced surface recombination and increased bend-bending at the surface. Also suggesting that there is an increased brightening effect due to the liquid, since the efficiency depended on the layer thickness of the liquid or of the glass covering it. It could also be that these older cells did not have proper surface passivation yet and that the liquid is fulfilling that role, an interesting aspect to further examine.

A couple of years later, the same authors published an extension on the previous paper called "The efficiency of solar cells immersed in liquid dielectrics" using an identical test set-up as in Figure 2.2 (adding an extra liquid: toluol) [76]. It highlights an optimum liquid thickness of 5-6 mm; however, it also states the dependents on the conduction of the solar cell surface, among other factors. They propose various reasons for the increased efficiency, again the reduced surface recombination velocity. Also, an increase in the barrier height of the n-p-junction. The two most important factors, according to the authors, are an increase in the separation of charge carriers generated by incoming light and a decrease in the reflected radiation.

"The performance of silicon solar cells operated in liquids" further investigates the effect of the liquids on solar cells [61]. It has a slight focus on concentrated solar cells and tries to see if the increased efficiency is due to optical or electrical properties of the solar cells. Based on previous papers, it focuses on the polarity of liquids, with polar liquids glycerin and ethanol, non-polar silicone oil and benzene, and tap water and inorganic distilled water. There were two tests set up, which are depicted in Figure 2.3, both

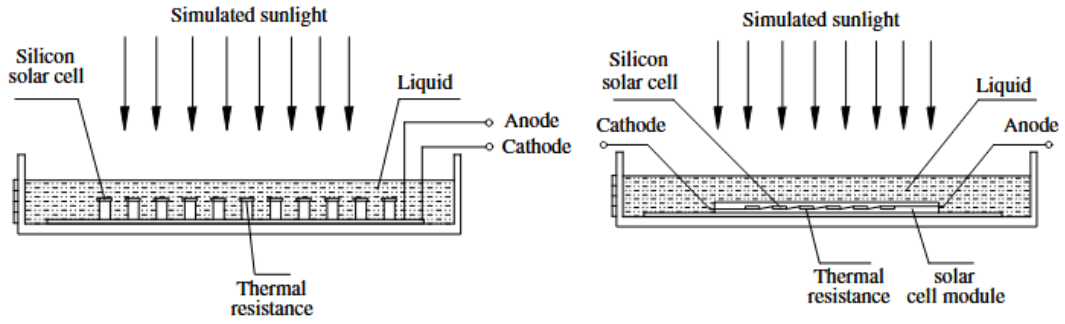

Figure 2.3: Test setup with on the left the bare solar cells and on the right solar cells encapsulated in EVA

with the solar cells in petri dishes immersed in the liquid. In one of the test setups ups the solar cells were also wrapped in a layer of EVA to exclude the electrical effect of the liquid on the solar cell. With the solar modules (EVA coated), the current and voltage of the cells change minimally, not more than 3.37%. While with the bare solar cells in the liquid, all currents increase by up to 30.34%, and all voltages drop by a max of 24.47%. They give a more detailed explanation of the electrical effects of polarizable molecules in liquids. They can create electrical fields at the cells' back and front surfaces in the same direction as the built-in electrical field of the cell, which can suppress the surface recombination. On the other hand, the electrical fields can also decrease the shunt resistance by causing electrical leakage. So the intensity of the electrical fields influences this balance. The non-polar silicone oil showed the best results; therefore, they concluded that non-polar liquids are preferable.

In the paper "Accelerated ultraviolet test and high temperature test on dielectric liquid for immersing solar cells" the durability of some dielectric liquids (silicone oil, glycerol, ethanol) was examined [62]. They concluded that the first UV and high-temperature test showed promising results. Although the silicone oil was experiencing some yellowing, probably due to impurities, which highlights the importance of using pure liquids.

The durability of some more fluids (glycerol, ethylene glycol, three kinds of paraffin oils, a synthetic hydrocarbon, and silicone oil) was further tested in "Durability of dielectric fluids for concentrating photovoltaic systems" [77]. They received an equivalent sun dose of 3 years. The pure paraffin performed best in these conditions. They also noted the good performance of silicone oil; however, this liquid was not included in all the tests.

2.4. CPV and Concentrator solar cells

As shown in the previous section, only a limited amount of research has been conducted on the direct immersion of solar cells in liquids. At the time of writing, only one other known study uses liquid encapsulation in the same way, retaining the solar module structure while replacing the solid (EVA) encapsulant with a liquid. However, relevant insights can also be drawn from the field of CPV, where liquids are sometimes used for direct immersion cooling. These studies not only explore thermal performance but also reveal electrical and optical effects of the liquids on the solar cells. The following papers are therefore reviewed to understand the current state of knowledge and identify areas requiring further research. Although some papers produced by the group at TianJin University (China) report no research before 2008, the review of Marta Vivar and Vernie Everett provides a look back at the development and progress of the CPV and solar concentration field [63], [64], [78]–[81].

2.4.1. Early concepts CPV (1970 - 1990)

The extensive review of Marta Vivar and Vernie Everett "A review of optical and thermal transfer fluids used for optical adaptation or beam-splitting in concentrating solar systems" gives good insights in the development of liquids in CPV and concentrating solar systems [64]. It nicely shows potential obstacles also experienced at Biosphere and TU Delft, and suggests some solutions, providing valuable lessons and advice. The first concepts, before 1990, will be discussed briefly, after which the more recent developments will be analysed.

Work on concentrator systems featuring front-surface liquid cooling and immersed solar cells began in the late 1970s and early 1980s. Featuring special mirrors and newly designed bifacial solar cells, immersed in deionised water initial designs involved encapsulated cells surrounded by fluid, avoiding direct contact [64], [82], [83]. However, the study proposed that in cases where encapsulation was unfeasible, direct immersion of the solar cells in dielectric fluids could be a viable solution, the start of the immersed solar cell concept. A dielectric fluid was used by Mills and Giutronich in 1978 with a liquid prism concentrator, using Dow Corning silicone oil (DC 200), which exhibited strong thermal and chemical stability, but was expensive at the time, prompting exploration of more economical alternatives [84]. In 1987, Edmonds et al. developed a related static concentrator that pushed the exploration of liquid immersion for both cooling and optical coupling [85], [86]. Using water and mineral oil as immersion media to obtain a more ideal refractive index. Their design specifically aimed at reducing system costs, and raised early concerns regarding the weight of filled systems, the long-term stability of both the fluids and sealing materials. These issues, especially degradation and sealing integrity, remain challenging today.

2.4.2. Continuation concepts CPV (2008 - 2014)

Between 1990 and 2008, research into immersed CPV systems was sparse. Two significant post-2008 developments revived the concept. First, IES-UPM developed the ‘Fluidreflex’ concentrator, a single-stage system using an aspherical mirror and high-efficiency solar cells immersed in a static dielectric fluid [87]. Second, a hybrid CPV-T dish system was proposed by Tianjin University, Australian National University and the University of Nevada, featuring circulating fluid around immersed cells to co-generate heat and electricity [63], [78]–[81].

In the Fluidreflex system, the cells were immersed in an unspecified fluid, although the researchers listed desirable fluid characteristics: optical transparency matching the spectral response of the cells, high electrical resistivity, thermal conductivity, non-corrosiveness, and long-term physical and chemical stability [87]. The team also tested several candidate fluids under UV exposure, noting visible degradation in some cases, though no detailed results were published; they emphasised the critical importance of fluid longevity and resistance to photochemical degradation.

The second group of universities published and shared more findings, which started of with ”Heat dissipation performance of silicon solar cells by direct dielectric liquid immersion under intensified illuminations” by Liu et al., where normal silicon solar cells are used in a concentrator set-up [79]. In this study, cells are immersed directly in dimethyl silicone oil, allowing heat to be removed from both the front and rear surfaces, which can be seen in Figure 2.4. Under turbulent flow and high irradiance levels (up to 70 kW/m²). Optical tests on the silicone oil are performed, and its absorption curve over the range of 200 - 900 nm and 800 - 2500 nm is reported. Electrical testing showed that while open-circuit voltage (V_{oc}) remained stable under immersion, short-circuit current (I_{sc}) degraded. This is attributed to increased series resistance and degradation of fingers and contacts under high current loads, as well as the use of standard silicon cells not optimised for concentration.

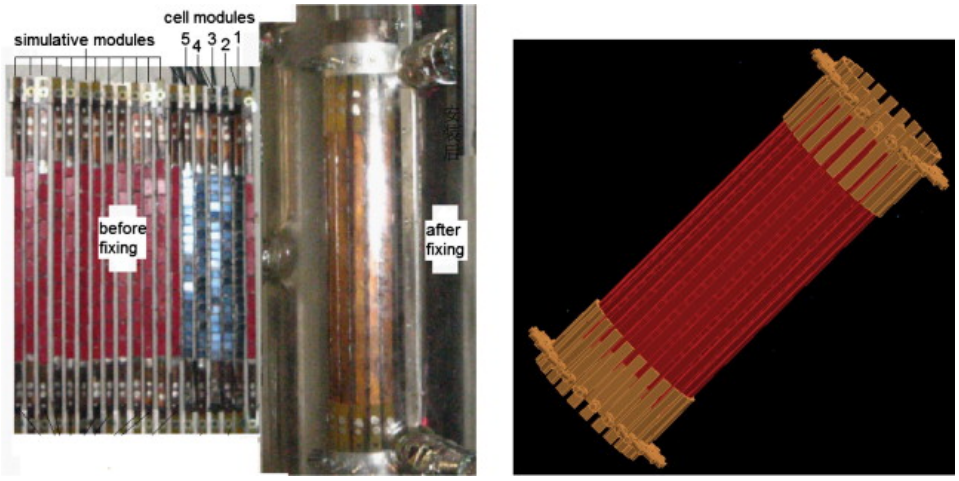

Figure 2.4: CPV concept in which a liquid could be past through [79]

The same group investigated the use of (DI) water immersion cooling for PV cells in a 250-sun concentration system [78]. While the method provided a uniform temperature distribution and initially stable electrical performance, the study observed clear degradation in short-circuit current (I_{sc}), fill factor (FF), and maximum power (Pmax) after three days of immersion. This occurred despite maintaining high water resistivity (perhaps not high enough), suggesting that factors such as electrolytic reactions at cell contacts may play a role in performance decline. The findings highlight potential reliability concerns when using water as a cooling medium for long-term operation.

To better understand the effects water has on the cells, Han et al. (2011) evaluated the long-term performance of silicon CPV cells immersed in deionised water at 65 °C [81]. Comparing bare cells with two types of tabbed cells, those using Pb-Sn solder and those with pure copper tabs. The bare cells showed no visible corrosion or degradation in performance, even after months of immersion, demonstrating DI water's compatibility with silicon solar cells. In contrast, tabbed cells suffered significant (I_{sc}) loss when exposed to sunlight, with degradation more severe in cells using copper tabs. This was attributed to galvanic corrosion between dissimilar metals, leading to metal oxide deposits that blocked light. Although rinsing and re-soldering often reversed the damage, water conductivity increased over time due to ion leaching, and transmittance dropped slightly, particularly in the UV. The study concluded that while bare silicon cells are stable in DI water, careful material selection is essential for tabbed cells in immersed CPV systems.

They then dove deeper and researched multiple interesting liquids (DI water, IPA, ethyl acetate, and dimethyl silicone oil), in the same configuration proposed earlier. The paper "Electrical and thermal performance of silicon concentrator solar cells immersed in dielectric liquids" investigates the optical, electrical, and thermal effects of these liquids on CPV cells [63]. It also focuses on the use of concentrator solar cells using the liquid to cool the cells. The cells are tested with the following interfaces: glass, air, ARC, solar cell, where the air is swapped with 1.5 mm liquid and compared to the air sample. Again, reporting the transmittance curves, depicted in Figure 2.5, over the range 20 - 2000 nm for the liquids mentioned. The cells were tested under various light intensities (10, 20, and 30 suns), in all cases, the efficiency increases, which they attribute to both an optical effect and an electrical effect. The optical effect is estimated using the Fresnel equations and the refractive index, calculating the reduced reflection compared to air. This increased transmittance is then used to estimate the resulting photocurrent enhancement [insert equations?]. The liquids tested have similar refractive index values (1.33–1.40), leading to a comparable optical contribution of about 7% to the relative efficiency increase. However, a larger total efficiency increase (up to 15.2%) was measured, which is attributed to an electrical effect. As in previous studies, this is explained by reduced surface recombination due to the surface adsorption of polar molecules.

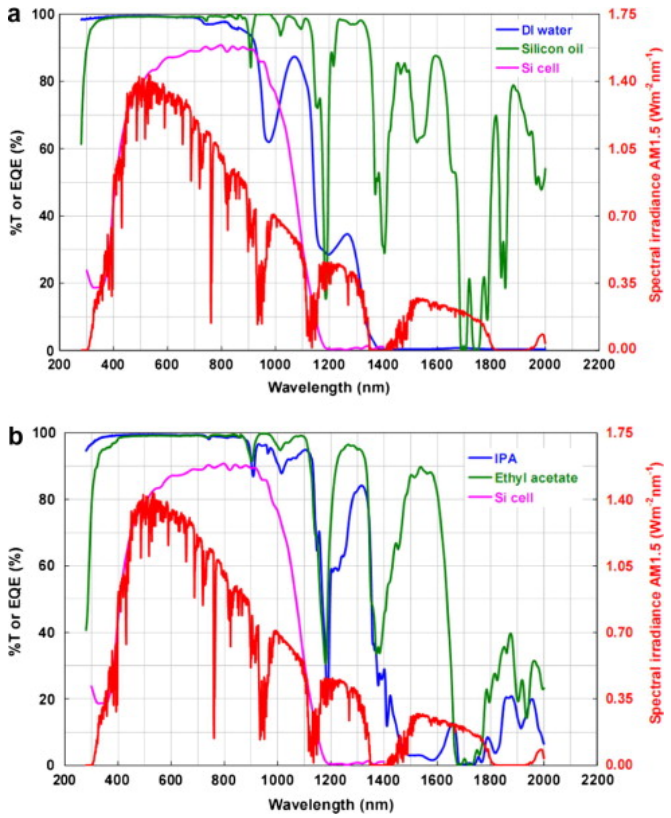

Figure 2.5: Transmission measurements of several liquids, both figures contain the EQE of a Si solar cell, the irradiance spectrum and transmission measurements of 2 different liquids (top: water and silicone oil, bottom: IPA and ethyl acetate). All liquids show good transmittance over the relevant wavelength spectrum. [63]

They expanded this study with more experiments, an increased liquid thickness (1.5 and 9 mm) and long-term degradation tests (same liquids and sun concentrations) [88]. The findings indicate that immersion in a 1.5 mm liquid layer improves cell efficiency, with IPA showing the highest performance boost (15.2%), followed by dimethyl silicone oil (10.2%) and DI water (8.5%). This improvement is attributed, again, to both optical effects (reduced light reflection) and electrical effects (lower surface recombination). In contrast, for thicker 9 mm liquid layers, the positive effects are diminished due to greater light absorption by the liquid. Long-term tests show stable performance for cells immersed in silicone oil, while the water is showing degradation, consistent with earlier findings. In the first experiments IPA and ethyl acetate cause degradation over time, likely due to interactions with the silicone sealant. When the silicone sealant is excluded in later tests, this degradation is not observed, which means there is a negative interaction between these liquids and the sealant. This highlights the importance of not only a suitable liquid, but also a proper sealant concerning material compatibility.

Focusing more on the promising dimethyl silicone oil, longer, real-climate tests were conducted with mono-crystalline silicon solar cells immersed within a narrow rectangular channel designed for a linear CPV system [80]. Over 270 days of real-climate testing under a concentration of 9.1 suns, the immersed cells maintained stable electrical performance, with no significant efficiency degradation observed. Efficiencies remained around 13.5% at 15°C and 12.6% at 30°C. These findings again support the potential of direct liquid-immersion of silicon solar cells using silicone oil, showing stability over longer periods and in real-life conditions. The main differences with the proposed biosphere-TU Delft concept are the higher sun concentration (and use of concentrator solar cells) and the flow of the liquid instead of a static encapsulation.

Silicone oil was further examined, and additives were used to increase its performance, monitoring the electrical and optical effect while subjecting the modified oils to accelerated ageing under high UV and temperature conditions per IEC 62108 standards [89]. Their results showed that all additives reduced degradation, with the combined formulation best preserving the fluid's viscosity and optical transmit-

tance over time. Importantly, none of the additives negatively affected solar cell performance; the combination of UV-9 (a UV absorber) and GW-783 (a hindered amine light stabiliser) showed the best results. This study highlights that properly selected additives can significantly enhance the durability of immersion fluids; there is also more attention for the optical properties and their behaviour, a switch that persists in the following papers.

Clarke (2012) conducted a comprehensive techno-economic analysis of liquid cooling in low-concentration CPV receivers, proposing important fluid criteria and potential candidates [65]. Listing properties such as dielectric behaviour, high transparency, operating temperature, chemical and UV stability, environmental safety (non-toxic, recyclable), and cost-effectiveness, emphasising the inevitability of leaks and long-term exposure risks. Also putting forth interesting challenges, such as potential extra optical losses due to drupelets forming, among others. Clarke identified DI water, silicone oils, and hydrofluorocarbons as promising candidates, each offering dielectric properties and optical transparency. However, he highlighted practical trade-offs: affordable fluids (organic) often required expensive encapsulants or posed flammability risks, while chemically inert options like HFCs were prohibitively expensive. Ultimately, he concluded that dielectric immersion (DI) cooling may be interesting but needs further studies on fluid–cell interactions to address long-term compatibility and performance.

This, in combination with the review of Vivar and Everett, draws important lessons from earlier developments in liquid-based concentrator systems, particularly the distinctions between static and circulating fluid configurations, type of cells, and (non)tracking, among others, are useful [64]. Static configurations demand exceptional sealing, as fluid leakage can lead to rapid performance degradation and environmental concerns. Moreover, chemical compatibility between fluids and sealants is critical to avoid long-term degradation. Thermal expansion of enclosed fluids must also be carefully managed, requiring dedicated expansion volumes or flexible seals, which few historical designs explicitly addressed [86]. A further lesson is that fluid choice matters significantly, for thermal properties, electrical insolation, long-term optical stability and material compatibility. Despite the diversity of early efforts using water, mineral oils, alcohols and silicone oils (among others theoretically considered), an ideal liquid choice remains inconclusive. The review also highlights that while front-side cooling without full immersion (using encapsulation of cells, for example) is possible, it has seen limited adoption due to added complexity and cost. Overall, these findings stress the importance of fluid stability, system sealing, electric resistivity, thermal management, and optical coupling in any liquid-based concentrator design. It gives some helpful tables listing the necessary liquid criteria and proposes some potential candidates and their properties, which helps in the search for interesting liquids. They also call for more extensive optical analysis since this is missing and unknown for most liquids. Their review highlights a shift in interest in CPV into beam-splitting options by using the liquid as a spectrum filter. An interesting addition which gives more focus on the optical properties of the fluids and therefore contains some valuable information, which will be discussed in the following section.

2.4.3. Focus on optics and beam splitting CPV (2014+)

In addition to the cooling function of the liquids, there is the ability to absorb wavelengths not utilised by the solar cells (thermilization) and redirecting this energy into heat for thermal applications while also cooling the cells to enhance electrical efficiency. The review by Imenes and Mills in 2003 includes multiple technologies of this spectral beam splitting method, one of them being the liquid absorption filters with research dating back to the 1980s [90]–[94]. Although these earlier concepts do not include direct immersion of solar cells, but transparent liquid-filled channels or tubes positioned above PV cells, their optical analysis and measurements are interesting and relevant for this thesis. They include early transmittance measurements over a broad wavelength range (300 - 1500 nm) of several liquids in search of sharp absorption edges, which can be used for the spectrum splitting. Again, practical limitations, including liquid degradation, environmental concerns, scattering losses, non-ideal spectral matching, and complexity of fluid circuits, remain key challenges. They propose more research into characterising interesting fluids, as well as their cost analysis, since at that time, there was yet a suitable non-degradable liquid for the liquid absorption application. These studies give some interesting insights but lack refractive index data, direct cell immersion and seem to contain semi-useful transmittance data since the focus is on filtering instead of high transparency over the whole range. More recent studies (2014+), which will be discussed in the following paragraphs, do address some of these issues but still have a different objective (light filtering) than this thesis (complete transparency).

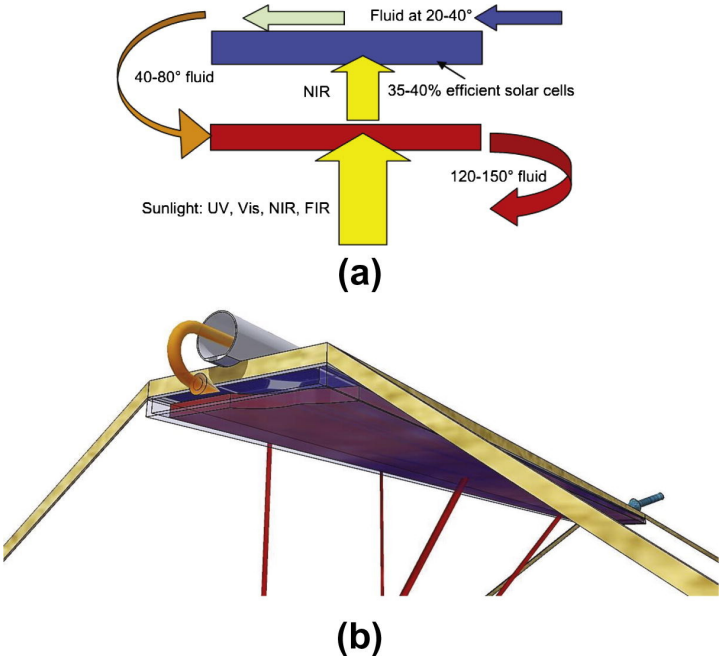

Figure 2.6: Spectrum beam splitting concept [95]

18 interesting liquids, categorised as glycols, synthetic oils, silicone oils and mineral oils, were studied for use in hybrid photovoltaic-thermal (PV-T) micro-concentrator systems employing spectral beam-splitting for heat recovery, which can be seen in Figure 2.6 [95]. Fluids were first screened for optical transmittance using UV/VIS/NIR spectrophotometry and then subjected to accelerated degradation tests at 75° C, 150° C, and under UV exposure to simulate long-term use. Among the candidates, industrial-grade Propylene Glycol (PG) demonstrated the most favourable balance of spectral selectivity (transparent in 640–1080 nm), chemical and thermal stability, and cost, especially when modified with a stable inorganic red dye such as Oil Red 235 to enhance filtering in the visible range. The silicone oils showed the highest transmittance over the entire spectrum, making them interesting for the biosphere-TU Delft application. However, this made them unsuitable for beam splitting, and they were therefore excluded from the degradation testing, unfortunately. Also interesting to note is that they displayed their transmittance data without correcting for the cuvette in which the liquids were measured. So it includes reflection (and absorption) losses from the cuvette's walls, which was pointed out by the following study, which did apply a correction.

The study is a continuation of the earlier work at Tianjin University, again measuring de-ionised water, IPA, dimethyl silicone oil, ethyl acetate, and now adding glycerol as well [66]. They perform the needed cuvette correction mentioned above by measuring an identical piece of quartz glass as the cuvette wall, which can then be corrected for. Their measurements of water show better agreement with values reported in the literature than the previous study. Interestingly, results showed that all liquids outperformed conventional EVA and silicone encapsulants in the 300–1100 nm range. Non-polar liquids, particularly dimethyl silicone oil and ethyl acetate, exhibited superior transmittance in the near-infrared region and caused less photocurrent reduction in MJ cells (focus of their study), making them more suitable for such applications. Long-term immersion tests up to 180 days demonstrated minimal degradation for dimethyl silicone oil, while other liquids showed minor losses in the UV region.

2 years later they expanded this study with more liquids (Therminol VP-1, three white/paraffin oils (A/B/C), and two alkanes (C14 n-alkane and C16 iso-alkane)), durability tests (UV exposure, damp heat, low- and high-temperature tests) and introduced a new method for measuring the transmittance [96]. They perform the needed cuvette correction mentioned above by using a double optical path-length method, measuring the transmittance in two cuvettes with different optical pathway lengths (5 and 10 mm), which can then be corrected using the Equation 2.1, which will be discussed in more detail in chapter 4. All liquids demonstrated excellent optical transmittance (above 95%) in the 400–1100 nm

range. Accelerated ageing tests, including UV exposure (56.8 kWh/m² at 60° C), damp heat (85° C at 85% RH for 1400 h), and thermal cycling (700 h at 65° C followed by 300 h at 100 °C), were used to evaluate long-term stability. Dimethyl silicone oil, again, exhibited the best performance, with optical transmittance losses below 0.5% under all stress conditions, attributed to the strength of its Si–O bonds. White oil C and C14 n-alkane also showed acceptable durability, with losses under the 5% threshold defined by IEC 62108. In contrast, C16 iso-alkane and Therminol VP-1 degraded significantly under UV exposure and were deemed unsuitable. Giving strong indications for suitable candidates and a valuable method for accurately measuring the transmittance of liquids.

$$\alpha(\lambda) = [-1/(x_2 - x_1)] \ln [T_2(\lambda)/T_1(\lambda)] \tag{2.1}$$

The same group produced a beam-splitting study as well, in which they incorporated earlier findings and added new liquids such as aqueous salts and some mixtures [97]. Their shift to absorption filters steers away from the complete transparency this thesis is interested in, making their conclusions on suitable liquids less relevant. However, the new transmittance graphs are interesting, especially the mixture of water, glycol and glycerol shows good transmission. This is reassuring since it is beneficial to add water to glycol and glycerol to lower their freezing point [98].

The same is true for the other spectrum beam splitting papers, where more focus is put on thermal behaviour or the absorption abilities of the liquids. In the case of Chemisana et al. (2018), which offers some good analysis, again, some mixtures are reported that show improved results for their thermal and optical properties [99]. They also give more emphasis on the importance of the refractive index of the liquids to minimise reflection; other papers lack this, unfortunately. In another study, refractive index matching with glass is also listed as a reason for improved light collection, notably the coconut oil is performing well, sparking interest in similar bio liquids [100]. Ma et al. (2025) are adding new elements by evaluating perovskites, proposing nanofluids and using optical modelling, which was hardly done before [101].

Most recent research is going into these nanofluids, which is unfortunate for the biosphere-TU Delft concept (and this thesis) because the addition of these nanoparticles lowers the transmittance, which is not desirable, making the research less relevant [102]–[105].

2.5. Patents

Several patents have proposed ideas related to the biosphere-TU Delft concept, though they often lack relevant details or interesting data and are therefore not discussed in depth. One of the earliest related inventions is a concentrated solar system with directly immersed solar cells, already proposed in 1977 [106]. Later, Tanaka filed two patents using various liquids to immerse solar cells directly, aiming to enhance their performance, first in 2003 [72] and then with a refined concept in 2007 [73]. Similarly, the use of PDMS silicone oil for immersion cooling is described in a patent by Carcangiu [107].

Other patents focus on optical and thermal enhancements, such as beam splitting to spectrally filter sunlight before it reaches the photovoltaic material [94], or the use of mirrors and concentrator solar cells in combination with a transparent cooling liquid [108], [109]. Some patents also use a liquid encapsulation for the manufacturing process, which is then solidified later [110], [111].

Although less directly related, additional concepts like fluid-based solar collectors [112] and sealed PV module designs for concentrated light exposure [113] are also of interest in the broader context of liquids used in the PV industry [114].

2.5.1. Apollon Solar Patents

The following patents are all from Apollon Solar, the company behind the NICE module, and share a common interest in lamination-free PV module construction. Several filings explore innovative mechanical assembly techniques using plates, spacers, or controlled vacuum environments to encapsulate cells without traditional lamination [115]–[119]. Others address improved integration of materials or cell connections, such as metal-supported designs or alternative electrical architectures [120], [121].

2.6. Conclusion

The reviewed literature highlights the potential of using liquids in PV systems beyond their traditional role as thermal media. Early concentrator PV and CPV concepts explored direct immersion for optical and thermal improvements, yet faced persistent challenges such as fluid degradation, sealing complexity, and material compatibility. More recent studies, especially from Tianjin University, reaffirm the benefits of immersion, such as improved efficiency through reduced reflection and surface recombination, while emphasising the critical role of fluid stability and material selection for long-term reliability. The findings clearly show that both optical and electrical performance are strongly influenced by the choice of immersion liquid. Research into the electrical effect that liquids have on solar cells is needed to confirm early positive findings.

Subsequent research has shifted toward optical properties, particularly in spectrum beam-splitting applications, with newer studies introducing refined methods for measuring liquid transmittance and more liquids being considered. Silicone oils consistently emerge as the most promising candidate due to their chemical stability and optical clarity, although other fluids such as glycols, hydrocarbons and glycerol also show potential. Across all works, the importance of optical performance, electrical insulation, chemical compatibility, and minimal degradation under UV and heat is underscored. These insights provide a robust foundation for further exploring liquid-filled PV concepts like the Biosphere-TU Delft concept, while identifying knowledge gaps in optical properties of liquids and material compatibility, among others.

Complex refractive index data, n and k values, over the relevant spectral range (300 - 1200 nm) remain poorly reported. Optical properties are often considered irrelevant in traditional applications, hence their absence in datasheets. For implementation and solid optical analysis for PV application, this data is crucial. That is why the thesis starts with focusing on obtaining this data in the following chapter, after which an optical model will be developed and used to perform the optical analysis of the liquids.

3

Liquid selection

In order to successfully replace EVA (or other solid) encapsulation with a fluid, a suitable liquid has to be found. We will first have a look at what has currently been used in similar applications in the literature. Then, from this research, the most important properties are identified and used to eliminate liquids and select usable candidates.

The liquid used in the solar panel has to meet certain criteria, some of which are easily formulated and searched, others, among optical properties, form a challenge. Therefore, it is interesting to research and model these optical properties, such as refractive index and extinction coefficient. Before this investigation, other criteria can be checked to evaluate if a liquid has potential. The relevant criteria for these liquids are as follows:

Optical

- Real part refractive index ($n \approx 1.5$)
- Imaginary part refractive index, extinction coefficient k as low as possible

Thermal

- Freezing and boiling point beyond -40 °to 85 °Celsius
- High thermal conductivity
- High heat capacity
- Low thermal expansion

Electrical Properties

- Low electrical conductivity
- High breakdown voltage (high dielectric constant)
- Non-polar (no permanent electric moment)

Chemical

- Material compatibility with glass, edge seal and solar cell (corrosion, to chemical reactivity)
- UV resistant
- Non-toxic
- Non-flammable
- Biodegradable

Physical

- Protection (moisture/water, shock/breakage)

- Low viscosity
- Low density
- Compressibility

Socio-Economical

- Widely abundant material
- Low cost
- Recyclability
- Safety

3.1. Methodology

In order to find suitable liquids, it is crucial to have a well-structured search, which will be explained in this section. Relevant information was found in (technical/safety) datasheets, contact with companies/experts, (review) studies on solar cells immersed in liquids and other related topics like dielectric transformer oils, among others. To search most efficiently, the following steps were taken:

1. **Material property filtering:** Narrow down from all relevant criteria to the most essential properties (transparency, dielectric, chemically stable, temperature range) which will be discussed in more detail in the following paragraphs. It is crucial to be able to discard unusable liquids as soon as possible, not wasting time researching all properties
2. **Literature survey:** Collecting and searching for data and properties on candidate liquids was mainly streamlined in two ways. First, using the studies with solar cells directly immersed in liquids to identify suitable liquids and learn more about their performance. Second, check which fields of research focus on the essential properties, such as the transformer fluid research for dielectric liquids.
3. **Grouping and example liquids:** Liquids are grouped into families (hydrocarbon oils, silicones, esters, fluorocarbons, water-based, alcohols, nanofluids, etc.) and investigated. Within each group, representative examples are identified that were already tested with PV or in electrical applications, making it possible to eliminate whole groups (although exceptions will still be possible).

In the following subsections, the essential properties are discussed, and why these are chosen. Followed by the liquid candidates, their appearance in literature, datasheets, contact with industry and experts, and experiments.

3.1.1. Optical

Optical transparency and minimal light reflection are crucial for proper PV performance, governed by the complex refractive index, which is discussed in more detail in chapter 4. To very briefly summarise, it requires ultra-high transmittance across the PV-relevant spectrum (300–1200 nm), which translates to low absorption or extinction coefficients. Reflection is minimised by refractive index grading or matching, which for the liquid selection means the n values should be similar to glass ($n \approx 1.5$).

These complex refractive index values are often not known for liquids over the relevant range (more in chapter 4), which makes it difficult to assess and search liquids on this criterion. Sometimes, refractive index n values are reported for 1 wavelength. For some liquids that are researched in PV (among others), more about their transparency is known, but this is limited to a selected amount of liquids, which will be discussed in the following section [66], [96], [97], [122]. More widely available optical data are colour indications like Hazen, which ranges from 0 (clear/colourless) to 500 (distinct yellow), or the ASTM D1500 test method, which defines a visual colour scale for petroleum products, ranging from 0.5 (lightest) to 8.0 (darkest). There are others, but these are mainly used/found; they should have the lowest value possible, meaning less light absorption. Since most liquids that have been measured so far have a refractive index value between $n \approx 1.3$ - 1.8, this criterion might be less crucial than transparency [123], [124]. This is reasoned by the following: a slightly higher reflection could be acceptable for further

testing, but low transmittance could have a larger negative effect. Although currently, the exact balance between these is unknown, their influence and dominance are further researched in chapter 5.

3.1.2. Electrical

The liquid must be a strong electrical insulator. If the liquid is not dielectric, it conducts electricity, making it unusable since it will short-circuit and malfunction, making the solar module unusable. This means extremely low ionic or electronic conductivity, and a high breakdown voltage is needed. Extended research into dielectric liquids has been done in the field of transformer fluids, meant to electrically insulate high voltage equipment or electronic [125]. They need to withstand kV-scale gaps without flashover and have high dielectric resistivity (typically $> 10^{12} cm$), higher also means better shunt resistance, meaning less electrical leakage. Since this field of electrically insulating electronic components with liquids is well researched, it is very useful for identifying potential candidates. Focusing on the optical and chemical performance to find usable fluids.

Non-polar liquids could potentially have a higher open circuit voltage, meaning a higher efficiency. This was observed in some studies as mentioned in the chapter 2 [61], [63]. Several mechanisms were proposed, but none seemed to fully explain what caused the increased efficiency. One hypothesis we propose is that the cells tested were not well passivated, and the liquids filled this passivation role, giving higher efficiencies. This would definitely be interesting to further research, for example, measuring the difference between a non-passivated and a well-passivated solar cell operated in several liquids. For searching potential liquids, this permanent electrical moment was not taken into account, but could potentially explain extra efficiency gains if present.

3.1.3. Chemical

Chemical stability is a broad term, which for now is focused on material compatibility (no chemical reactivity, in contact with other components or over time), non-flammability, UV resistance and toxicity. Biodegradability is important and might exclude liquids at a later stage, but testing of liquid encapsulation of non-biodegradable liquids is still possible and would work in a solar module, and is therefore chosen not to be a restricting criterion at this moment. The biodegradability of the liquid can be a benefit, less environmental harm during a leakage, but also a drawback if it degrades over time in the module (or with moisture ingress, for example). For most liquids, the flammability and toxicity are known to a certain extent (for example, PFAS, for which we are still learning the negative consequences), which are important factors to exclude a liquid since it is highly unlikely that a flammable or toxic liquid will be used in a solar module. Therefore, toxic and flammable liquids are excluded. Most information is taken from datasheets and contact with manufacturers and experts.

Material compatibility between materials is often unknown; in some cases, it can be deduced based on the chemical structure. Where it is not known and other criteria all show promising results, material compatibility tests might be needed and should be included in further research. Compatibility with the glass should not form a problem; the metal interconnections could corrode (with water, for example), the solar cell surface could also be reactive with certain liquids, but the bottleneck so far seems to be the PIB sealant used. Some liquids have been used in PV research as discussed in chapter 2, which are therefore assumed to be compatible with the solar cells and interconnections if not otherwise addressed.

PIB will be used as the edge seal in order to keep the liquid inside and protect against the outside conditions. For the mineral oils, this might form a problem since they are nonpolar hydrocarbons. PIB is also made of long chains of hydrocarbons and non-polar, meaning it might dissolve or swell in the non-polar hydrocarbons (paraffinic/naphthenic mineral oils or synthetic PAOs) based on the ”like dissolves like” principle [126]. There have been some manufacturers that mention that PIB, and butyl rubber, generally dissolve in hydrocarbon fluids [127]–[129]. The silicon cells seem fine in most studies; interconnections could be subjected to oxidation. PIB seems to cause the most problems so far.

3.1.4. Thermal

In order to be in the liquid state during operation, the boiling point should be above 85°C and the freezing point below –40°C. Other useful properties for determining this and providing additional information are the flash point, which is the temperature at which a liquid gives off enough vapour to be ignited (related

to flammability), and which is undesirable and should therefore also be higher than 85 °C (which results automatically in a higher boiling point as well). The pour point is the temperature where the liquid still has its flow characteristic, meaning it ”behaves” like a liquid, which is also beneficial.

Other important, but not crucial, thermal properties include the thermal conductivity (for efficient heat removal), heat capacity (enables lower temperature) and coefficient of thermal expansion (less expansion is better, lower pressure).

3.1.5. Physical

None of the general properties is limiting, but they can be strived for in further research or application. Proper protection from shock and vibration is a plus, as well as limiting moisture ingress. Low viscosity is preferred for easier manufacturing. Solubility in water could be nice for cleaning the solar cells, but it is a disadvantage in operation if water gets inside, same with water diffusion. Low density gives a lighter panel, reducing stress on components, and low viscosity enables easier production (but could also mean more leakage in case of breakage).

3.1.6. Socio-Economic

While previously mentioned criteria remain the primary focus for liquid selection at this research stage, socio-economic factors provide important secondary guidance. Even if they are not currently limiting the selection, they help shape the long-term viability, safety, scalability, and sustainability of the chosen liquid, crucial for eventual application.

Cost and availability

The cost and availability of a liquid are fundamental to its practical application. EVA has been so widely adopted because of its low price. Beyond the initial purchase price for the raw material, there are additional costs related to the manufacturing steps involved, storage, and disposal procedures, among others. To financially compare the liquids against standard encapsulation, such as EVA, a brief calculation on price will be done after selecting the liquids for further research; only the raw material cost will be considered.

The selected liquids should be widely available, which is, in general, strongly linked to their price. It is undesirable to add another valuable or critical material to the module. Speciality fluids, besides being more expensive, with limited suppliers, unstable supply chains or long delivery times, which could delay experimental timelines or complicate production or replication. Availability on short notice and in manageable quantities is a practical advantage during the testing phase. Furthermore, a widely available fluid allows local production, repairs and recycling.

Environmental and Circular Economy

A crucial aspect of sustainability is the liquid’s environmental impact throughout its entire lifecycle, from production to its EoL, since the ultimate purpose of this research is a more environmentally friendly solar module. This can be assessed through a Life Cycle Assessment (LCA), which evaluates the energy and resources consumed during its fabrication (production footprint) and its EoL handling.

In line with circular economy principles, liquids that can be easily recovered, purified, and reused are highly desirable. This minimises waste and reduces the environmental burden associated with chemical disposal. If the liquid can degrade over time or under illumination, this also plays into its long-term circularity.

Safety: Toxicity, Flammability and Health

As mentioned before, safety risks like flammability or toxicity can form important grounds to exclude a liquid. Often grouped as Environment, Health, and Safety (EHS), they can be a strong indicator of a liquid’s suitability for broader applications. During this research stage, it might be interesting to further examine liquids for scientific reasons, which might be excluded later on due to EHS compliance. Although laboratory guidelines are crucial to respect, and naturally favour safe liquids.

Furthermore, Non-toxic and non-flammable fluids reduce the need for specialised equipment (e.g., fume hoods, Personal Protective Equipment (PPE), specialised storage and handling) and limit health risks in the event of spills or leaks. This factor also has implications for the environmental release of

the fluid. Choosing less hazardous options is aligned with responsible research practices and lowers the burden on waste management systems. Using flammable liquids increases both risk and regulatory hurdles and may necessitate additional fire suppression measures or laboratory certifications, especially since solar panels can heat up significantly and are exposed to direct irradiation. Banned or restricted liquids (PFAS for example) are less desirable since they would need to pass more certifications (probably for good reason). These factors are typically detailed in a Safety Data Sheet (SDS) or known by manufacturers, which serves as a primary source of information.

Socio-Economic Outlook

Ultimately, the socio-economic dimension of a liquid directly influences the technology's scalability and social acceptance. A liquid that is inexpensive, readily available from a stable supply chain, non-toxic, non-flammable, and environmentally safe is more likely to be successfully commercialised and deployed globally, also in developing regions or low-infrastructure contexts. By considering these factors early in the research phase, it reminds to not only strive for efficient but also safe, sustainable, and economically viable technology.

3.2. Liquid candidates

3.2.1. Alcohols

Most alcohols are less suitable since they have low boiling and flash points. This is related to their flammability, making it more difficult to work with and deploy in the field. An exception to this is glycol and glycerol, also known as glycerine, which are researched in multiple studies, which is why they are considered a different group. The following two common alcohols were also researched in solar cell-related studies.

Isopropyl alcohol (IPA)

Widely used as a cleaning agent, isopropyl alcohol (IPA) is used in multiple studies into solar cells immersed in liquid [63], [66], [88], most showing good results. One of these studies mentioned yellowing after 1 month of testing a single solar cell immersed in IPA between two glass plates sealed by a silicone sealant [88]. This seems to be a reaction with the silicone sealant, which is confirmed by another 180-day test, concluding that the solar cells can stably operate in the IPA. However, their compatibility with PIB should be checked, since it is incompatible with silicone.

Ethanol

Silicon solar cells operated in ethanol produced somewhat the same power output. Tests with different liquid thickness layers gave mixed results; two thickness layers saw a slight increase, while the thickest thickness layer saw a slight decrease in power output [61], which might be due to more parasitic absorption due to the thicker layer. Ethanol was also tested for accelerated UV radiation and high temperature, which showed no change in chemical or physical properties. However, ethanol has a low flash point and is highly flammable, making it unusable in this application.

Glycols

Glycol has been used in numerous studies as written in chapter 2, many highlighting its excellent stable performance in degradation tests and proper optical transparency [77], [95], [97], [130]. Again, since no chemical reaction was noted in any of the studies, it is assumed that there is no problem with material compatibility when used in solar modules.

In most studies, pure glycol is used, which has a standard liquid composition and does not differ much per manufacturer. The main glycols are ethylene glycol, which is toxic and commonly used in industrial applications like antifreeze, while (mono-)propylene glycol (MPG) is considered safe for human contact and used in food, cosmetics, and pharmaceuticals. When referring to glycol in this thesis, either MPG or the following fluid based on MPG is meant.

There is a solar-specific glycol, Innogreen SolarPro, currently researched by Biosphere and TU Delft, specially designed for use in solar energy, boosting operating range and better thermal stability [131]. Although not disclosed, it consists of a blend of compounds (for which glycol is the main liquid) and additives were used, which can indeed increase performance, but could also result in complications in other areas.

Glycerol

Glycerol also has a standard liquid composition and does not differ much per manufacturer; it is often mixed with water to get a lower viscosity and freezing point [98]. Glycerol has been included in multiple studies, as seen in chapter 2, showing good results in transparency and degradation testing, with no chemical or physical change [55], [62], [66], [75], [77], [97].

3.2.2. Mineral oil

Mineral oil, also known as white oil, is the oldest and most widely used dielectric liquid in electrical applications [125]. Its dominance is largely due to its relatively low cost and wide availability, as it is derived from petroleum products. However, the long-term availability and pricing of mineral oil may become a concern as petroleum resources decline.

Chemically, mineral oils are hydrocarbons divided into three main categories: paraffinic, naphthenic, and aromatic. Paraffinic oils are less suitable for lower temperatures and more susceptible to oxidation. They also react with PIB, as observed in some experiments with OptiCool (synthetic hydrocarbon, discussed in the following paragraph) and were also reported in literature as a solvent for PIB [132]. Naphthenic oils offer better performance at lower temperatures and improved resistance to oxidation. Aromatic oils are no longer produced due to environmental considerations. Typically, mineral oil undergoes hydro-treatment to remove impurities common in refined products. This process enhances its dielectric properties and stability. Despite this treatment, mineral oil-based dielectrics can become yellowish as they age, which may affect their optical properties [133]. Mineral oils are primarily used in outdoor applications, such as transformers, due to their fire risk. The IT industry has largely moved away from these oils because of their low flash point, inconsistent quality, and potential issues with material compatibility. Regarding transparency, specific data for mineral oils is limited, mostly only reported in the Hazen or ASTM colour scale. However, comprehensive transparency data on mineral oil types is not readily available.

The most advanced form of mineral oils are the synthetic hydrocarbons, which are discussed in the following paragraph.

Synthetic hydrocarbons

This group is part of the mineral oil family, containing long chains of hydrocarbons as well, and is synthetically produced, meaning higher purity and enhanced properties. Mineral oils have multiple underperforming properties, such as material compatibility PIB, fire safety and degradation; however, they are one of the most researched and used liquids. So to properly exclude them, the most advanced examples are taken, reasoning that if they are not usable, none of the mineral oils can be used. Prime examples include Opticool, Electrocool and Shell Diala S4 XZ-I.

Both Opticool and Electrocool are frequently used liquids in the field of electronics cooling and are advised to us by manufacturers like Engineering Fluids and Soltex Inc for our specific application [134], [135]. They both perform excellently on all essential criteria (although no proper transmission data is available), and were therefore researched more thoroughly, especially to find out their material compatibility with PIB. As mentioned before, the Opticool seemed incompatible with PIB during testing at Biosphere and TU Delft, as visualised in Figure 3.1, and was therefore excluded. Electrocool is marketed as ”ElectroCool Dielectric Coolants feature the broadest material compatibility profile in the industry”, which gave hope for proper performance. Further research found a material compatibility table([136]), which showed ”not recommended” for PIB and Electrocool. To be certain, it was tested in a liquid-filled module and failed during a damp-heat test by Uravshi Bothra due to PIB swelling, which can be seen in Figure 3.1. This led to the conclusion that if these high-grade, highly engineered hydrocarbons are failing, other mineral oil-based liquids might fail as well. Another type of these highly refined and processed hydrocarbons is discussed in the following paragraph.

Figure 3.1: Damp heat tests of several fluids (left to right: PDMS, Electrocool, Mivolt, Opticool) between two glass sheets sealed with PIB sealant. Electrocool and Opticool show bad material compatibility with PIB, as PIB dissolves in the fluids, tested by Urvashi Bothra at TU Delft.

Other groups are synthetic poly alpha olefins (PAOs) and synthetic motor oil, which could potentially still be used, but have limited research available. They are engineered to improve on mineral oil with fewer impurities, better oxidation resistance, absorption of water and material comparability, improved biodegradability, but also a higher price because of these enhancements.

From the high voltage department at the TU Delft (Wim Termorshuizen and Luis Castro Heredia), two liquids were advised for this application: Midel 7131 (discussed later) and Shell Diala S4 ZX-I. Research related to solar cells on Shell Diala has been limited, but shows good properties, although it is missing interesting degradation and optical measurements [95]. This Shell Diala is made through a Gas-To-Liquid (GTL) process, enabling very precise fabrication of hydrocarbon chains and minimal impurities. it is therefore widely used in high voltage applications and could potentially be PIB compatible, which is tested before further optical experiments.

The test includes submerging pieces of PIB in the Liquid to see if any reaction or swelling can be observed. If this liquid is underperforming, it gives a strong case for dismissing mineral oils entirely. Adding to this, Shell Diala has an ASTM colour scale (ASTM D1500) rating of L0.5. Which will be interesting to test to see how this slight colouring translates to transmittance.

The material compatibility tests showed good results in the early stages (first week), with no sign of the PIB dissolving. However, after several weeks, the PIB was pinched multiple times with tweezers, and the Shell Diala completely dissolved the PIB as seen in Figure 3.2a. This makes the Shell Diala unusable with the PIB sealant. At this point, the optical measurements on Shell were already performed (This paragraph was updated on 25-07-2025), which is why it is still included in the analysis and in case another edge seal material is used in the future.

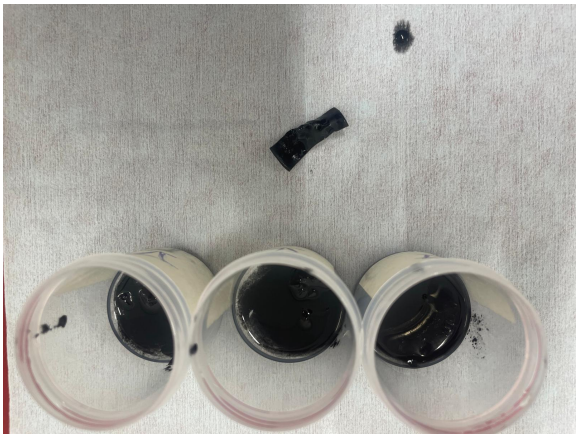

(a) Material compatibility tests for PIB sealant and Shell Diala, showing that the PIB dissolves in the Shell Diala, making it unusable with the PIB

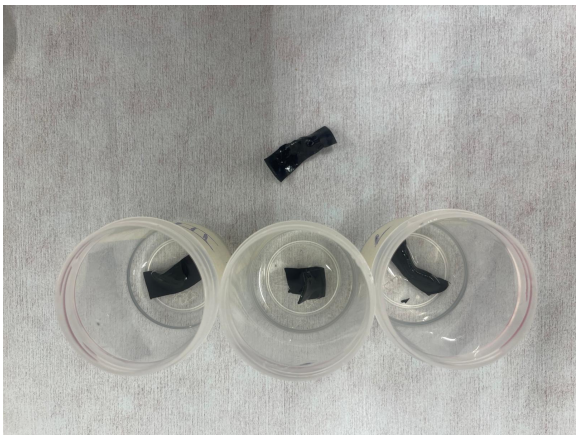

(b) Material compatibility tests for PIB sealant and Midel 7131, the PIB does not dissolve and seems compatible with the Midel

Figure 3.2: Material compatibility tests for PIB sealant with Shell Diala and Midel 7131. Shell Diala is not compatible, and Midel shows good results so far

3.2.3. Silicone fluids

Silicone fluid (industrial or technical application name), also referred to as silicone oil (consumer name), or polydimethylsiloxane (PDMS, which will be used throughout this thesis), is based on the same compounds. They are composed of chains of carbon, hydrogen, oxygen and silicon, showing interesting properties, while having similar dielectric strength as mineral oils, non-toxic, high oxidation resistance, and good heat dissipation. They are less biodegradable, which can be a benefit since they will not degrade easily or a drawback when they spill into nature. But above all, they are well reported in literature with high transparency in the spectral range of interest and degradation testing showed that PDMS was highly stable, with no material compatibility problems reported, making it an excellent candidate [61]–[64], [77], [95], [97], [137]–[139].

3.2.4. Synthetic esters

Derived from alcohol groups and carboxylic acids, this group contains multiple different formulas and brands exhibiting some interesting improvements over earlier fluids. Retaining favourable properties mentioned before but improving on better temperature range, higher biodegradability, good moisture absorption, excellent chemical stability and fire resistance [125]. This does come at a higher cost compared to petroleum-based oils. In addition, their transparency needs to be investigated since very little is known so far, many manufacturers only displaying the hazen colour scale. Values found range between the 0 and 125, so from colourless to light yellow colouring, which might result in substantially higher absorption, needing further investigation. They have been gaining popularity as a replacement for petroleum-based dielectric liquids.

Potential candidates could be Mivolt (tested before at Biodpehre and TU Delft) and Midel 7131 (advised by the high-voltage department of TU Delft). Also, for Midel, there are currently initial material compatibility tests ongoing, the same as for Shell Diala. From these tests, the Midel 7131 seems to be performing well, no sign of the PIB dissolving after being submerged in the liquid for several weeks and pinched by tweezers as can be seen in Figure 3.2b. This gives confidence in the use of Midel, although more tests at high temperatures and damp-heat cycles are needed to ensure material compatibility.

Mivolt DF7 already had some initial degradation tests at TU Delft showing mixed results. Some 1-cell modules tested in damp heat showed proper performance and material compatibility in the test of Uravshi Bothra. However, modules fabricated by Sebastian Weemaes failed during production, where leaking of the PIB seemed to be the problem [58], [59]. The hypothesis at the moment is that Mivolt can create a problem if it comes in between the PIB and glass, thus resulting in a manufacturing problem as observed by Sebastian Weemaes. However, if a module is sealed properly, then it does not react with the PIB as we see in Figure 3.1. Further research is needed in this matter to be able to validate Mivolt as a usable liquid.

3.2.5. Plant based oils

In the search for a more biodegradable dielectric alternative to petroleum-based liquids, plant-based oils are considered the most promising [125]. They are non-toxic, biodegradable and have a high flash point. However, they are vulnerable to rapid oxidation, especially in the presence of certain metallic catalysts, such as copper or zinc [125], [140]. This could render them unusable, so more research is needed into their oxidation stability and material compatibility with the interconnections. Already, efforts have been made in this aspect with the formation of natural esters.

As for their optical properties, there is one detailed study which determines the complex refractive index of peanut, soybean and sunflower oil, which all show very good results [122]. With refractive index n values around 1.45 and extinction coefficient going down to $10^{-7} - 10^{-8}$ in the relevant spectral range. While in the first instance these liquids were considered less transparent due to their yellowish colour and therefore unusable, this study shows that this might not be the case, making them interesting to further consider.

3.2.6. Natural esters

Made from plant-based products, natural esters pose a solution to the problems plant-based oils experience, such as oxidation stability. They have favourable properties such as low toxicity, highly biodegradable, high ignition point and significant moisture absorption capacity. Their oxidation stability is improved, but they are still outcompeted by mineral oils on this aspect (as well as cost, freeze point, viscosity), limiting their wide-scale adoption [125], [141]. They do form an interesting candidate, but first, these oxidation risks should be addressed, which could cause them to be incompatible with the interconnections. Material compatibility tests should be performed to check if this is the case and see if their oxidation is indeed a problem.

Ethyl acetate

Ethyl acetate could be considered as a natural ester, which showed similar problems to IPA as it seemed to react with the silicone sealant, producing bubbles [88]. This is confirmed with a 180-day test by excluding the silicone sealant, which enables the stable operation of solar cells. These promising results are also mentioned in [63]. But due to the low flash and boiling point of ethyl acetate, it is not further considered.

3.2.7. Nanofluids

These fluids are composed of a base liquid such as a mineral oil or synthetic/natural ester, containing nanoparticles with a size ranging from 1 to 100 nm. The particles are added to improve the properties of the liquid, such as the dielectric properties, thermal conductivity and chemical and thermal stability. They are being researched and studied more and more, but still, some crucial information is missing, and some show contradictory results. Perhaps because there is no clear definition or standard for producing the nanofluids. Data on their dielectric, optical, thermal and chemical properties is missing. In addition, adding nanoparticles will probably reduce the transparency of the liquid, making it less interesting for use in solar panels. How much less is yet to be determined, perhaps these liquids could be interesting in the future, but are not realistic because of the earlier mentioned reasons, as well as their availability, long-term stability and high cost [97], [125], [142].

3.2.8. Water

DI water (often referred to as water, deionised water is meant), especially mixed with other liquids, is widely used in the cooling of electronics because of its good heat dissipation. However, there are some questions about its use with solar panels because of the high oxidation and possible corrosion of the cells and interconnections. It should therefore be checked how, for example, water/glycol or water/glycerol mixtures affect the solar cells and PIB. It does show very good optical properties, fully biodegradable, low cost and wide availability [143]. Also, deionised water has been used in earlier studies, which will be discussed in the following paragraph.

Used in multiple studies because of its good heat dissipation, optical transparency, wide availability and research already conducted, DI water performance in combination with solar cells varies. Some studies conclude good compatibility after 170 days of testing, as in [88]. However, they also note that the stable electrical performance of the solar cell was difficult to achieve. This is in agreement with other

papers, which saw a declining photocurrent in DI water immersion [81]. However, after cleaning the cell, they saw some recovery of the electrical performance, meaning that the cells were not damaged by the DI water [81]. Tap water showed a significant decrease in power output as noted in [61]. It was also mentioned in another study that it might be the interconnections forming larger problems, which concluded that ion concentration alone is not the only factor to consider when selecting DI water [78]. Electrolytic reactions at the electrodes or interconnections of the solar cells may pose additional challenges and could lead to performance degradation. The resistivity of the DI water might not be high enough, as mentioned before; higher resistivity can reduce the electric leakage.

Add to this the fact that water can be corrosive for materials in the interconnection or cells themselves, we see more research of CPV looking for alternatives. Also, its low freezing point (0 ° C) makes it a less suitable option for standard solar panels, which need to handle temperatures well below freezing [64].

3.2.9. Heat transfer liquids

In principle, all liquids could be categorised with the ability to transfer heat, but what is meant here is when the liquids are specifically used or made for transferring heat from or to an application (such as liquids in refrigerators or air conditioning). These include other groups like water, glycols, mineral oils, silicone oils, (natural/synthetic) esters; therefore, this group is used for all other liquids not described in their section. In literature, they are also mentioned as heat transfer liquids sometimes without specifying their chemical composition [92], [95]. Clarke's work has already reviewed several liquids, including many heat transfer liquids and multiple chemical compounds [65]. Most of these liquids were excluded from further consideration because of their high toxicity, flammability (and some even explosive), low flash and boiling point, or insufficient information available. Fluids proposed as suitable candidates include water, silicone oil and several heat transfer liquids such as Dupont Vertrel XF, and Solvay SV55, which are both PFAS liquids and should be avoided, as will be explained in the following paragraph.

Fluorcarbon fluids

Already briefly mentioned in chapter 2 for their good properties but deemed too expensive and questionable environmental compatibility, they seem not suitable [65]. Fluorinated hydrocarbons and perfluorinated compounds, exhibiting similar properties or chemistries, with the main groups of Perfluorocarbons (PFCs), Perfluoropolyethers (PFPEs), Hydrofluoroethers (HFEs) and Fluorketones (FKs), which are considered PFAS materials. Making them questionable in terms of toxicity and ability to break down, again raising environmental concerns. They are a relatively new group of fluids with limited research compared to other fluids like mineral oils. They possess excellent dielectric properties, are thermal and chemically stable, with no flash point, which makes them perfect in terms of fire resistance. Their boiling points range from 50 °to 270 °C. They have a relatively high vapour pressure, meaning high evaporation rates, which can make it tricky to work with. PFCs and PFPEs have a longer history of computer cooling, but show concerns in terms of Global Warming Potential (GWP) [65]. They produce F-gases, which are damaging to the environment and require special qualifications to work with. Therefore, HFEs and FKs have recently been developed to address this, although they also emit F-gases to some degree. Many of these PFAS materials have sparked controversy, for good reason, in last couple of years, especially in the Netherlands, due to their environmental and health risks. They are therefore deemed unsafe and excluded from consideration until proper, independent, long-term research has been conducted.

Several manufacturers (like 3M and BestSolve) were contacted, and some liquids were further examined to see if they also possessed the negative properties mentioned earlier, which seemed the case. The liquids considered were: 3M Fluorinert FC-40, 3M Novec 7300 and BestSolv™ 7300 [144]–[146].

A similar family is Chlorinated diphenyls, for example, polychlorinated biphenyls (PCBs), which are chlorinated rather than fluorinated and have been taken out of production because of environmental and toxicity concerns.

Therminol

Used in other studies into CPV systems, this synthetic heat transfer liquid shows good thermal and optical properties [95], [96]. However, after 41.5 hours of UV exposure, it showed a significant colour shift from clear to orange-brown, which excluded it from further considerations [96]. This was also

observed in another study, which made them unusable [147]. Adding to this, it is also a hazardous compound needing special procedures to be removed in case of a spill [64].

3.3. Liquids selected

After identifying the crucial criteria and searching the literature for suitable candidates, several liquid groups were selected for consideration. Their overall properties and characteristics have been discussed, and are simplified in Table 3.1 for easy comparison. Blank means no data/knowledge available, red is bad or unusable compared to other liquids, orange is not good/bad, but could form a problem, and green is good performance. As expected, optical data is missing for most liquids, since for many fluids, wavelength-dependent data is missing and only the refractive index at one wavelength is reported.

Alcohols (except glycol and glycerol) score badly on multiple criteria, and are therefore excluded due to their high flammability and flash point, toxicity, and potential lower refractive index.

Heat transfer fluids are excluded due to their safety concerns, environmental damage, and toxicity, as many are PFAS-based or exhibit similar problems.

Nanofluids are missing data since they are relatively new; therefore, they are excluded at this point, among the earlier-mentioned reasons.

Natural esters and plant-based oils are not involved in further testing due to questions regarding material compatibility (oxidation) and transparency, as most are yellow (or darker) tinted. They could, however, be an interesting candidate if these problems are addressed. Therefore, there will be liquids with a slight yellowish tint included in the optical measurements to see the effects and determine if other liquids can be excluded based on these visual observations. The 7 liquids eventually chosen for further testing are listed below.

Table 3.1: Liquid families/groups are compared to each other for the most relevant criteria. Blank means no data/knowledge available, red is bad compared to other liquids, orange is not good/bad, could be a problem, but not sure yet and green is good performance. Optical is missing a lot of data, same as for nanofluids, alcohols score badly on multiple criteria, and most fluid groups with a red mark get excluded.

Liquid group	**Optical** Refractive index (n)	Extinction coefficient (k)	**Electrical** Resistance (ohm*m)	Breakdown V (kV/cm)	**Chemical** Material compatability	Flammability	Toxicity	**Thermal** Pour point (C)	Flash point (C)
Alcohol									
Heat transfer liquid									
Mineral oil									
Silicone fluid									
Synthetic ester									
Plant-based oil									
Natural esters									
Nanofluids									
Water									
Glycol (alcohol)									
Glycerol (alcohol)									

The following liquids have been selected for further optical experiments due to their promising properties, as seen in Table 3.1, their relevant material properties can be found in the appendix in Figure A.1 [58]. The following four liquids (DI water, PDMS, glycerol and glycol) have been researched in solar energy applications before. DI water has multiple negative properties, as discussed before; however, it is well reported in the literature, giving a proper benchmark and might be mixed with other liquids, which is why it will be tested in the optical experiments. PDMS has been a proper candidate in multiple liquids and therefore chosen, XIAMETER™ PMX-561 Transformer Liquid [148] is used [61]–[64], [77], [95], [97], [137]–[139]. Glycerol is used in the most similar concept published so far, which will be interesting to compare [55]. The solar-specific Innogreen SolarPro is selected as a glycol candidate, which could show different results than pure glycol in a good or bad way.

The liquids that did not have any solar-related research performed (and lack most optical data) are Shell Diala S4 XZ-I, Midel 7131 and Mivolt DF7. Shell Diala is included to represent the mineral oil group and seemed compatible with PIB at the moment of selecting the liquids; it has an ASTM D1500 colour scale rating of L0.5. For the synthetic esters, Midel and Mivolt are selected. Midel has a hazen

colour scale rating of 125, which will be interesting to see how this slightly yellow colour performs in the optical measurements.

To see how the financial cost of these selected liquids compares to standard EVA and future POE encapsulation, a brief calculation is made in the following section.

3.4. Cost analysis liquids

As mentioned before, encapsulation cost is crucial for its eventual application; the low price of EVA is a strong aspect for it being the industry standard choice at the moment. Therefore, a brief calculation is done on a standard solar module from Biosphere Solar (480 Wp), to compare the encapsulation cost (only raw material) of using standard EVA, UV transparent EVA, POE, EVA/POE mixture and the liquids (air encapsulation would be 0 for raw material cost) [60]. It is important to note when comparing these prices that only raw material costs are considered; there might be more or less cost involved in manufacturing with liquids. The process is expected to be less energy intensive as EVA lamination is performed around 140 ° C and for liquids this is 95 ° C with lower pressure (modules manufactured at TU Delft and Biosphere [58], [59]). Also, prices are taken from market analysis (EVA, POE, glycol, glycerol), meaning that these are raw material prices and not the ready-to-use encapsulation sheets (for EVA and POE), which will be slightly higher. For the other liquids (PDMS, Shell Diala, Midel), shipping/port data was used to get the price as close to the bulk price as possible. Since the liquids do not need further processing and can be used directly, while the EVA and POE need to be made in specialised solar sheets, their prices are expected to increase, giving a conservative approximation. Furthermore, prices could differ for solar module manufacturer and the liquids could potentially be reused, reducing their cost. The prices are taken at 06/08/2025 for the European market, as Biosphere Solar and TU Delft fabricate the modules in the Netherlands, Europe.

These prices, listed in Table 3.2, should only be considered as an indication and should be further researched in the future. Density is taken from datasheets, the mass required is calculated from these densities and the volume of a standard Biosphere module with 0.45 mm encapsulation on the front and back of the solar cells (0.9 mm in total). The volume for solid (EVA and POE) and liquid encapsulation is assumed to be the same, assuming that solids also use an edge seal like PIB. For liquid encapsulation, an air bubble might be implemented for thermal expansion, but it is not yet determined how large ($\approx$ 5 - 15 % of encapsulation volume) and will not be considered in the calculation, which, again, gives a more conservative approximation.

- Total encapsulation thickness: 0.0009 m (0.45 mm front and back)
- Panel area: 2.21 m^2
- Volume: 2.21 $m^2 * 0.0009$ m $= 0.001989 m^3$

Table 3.2: Raw material cost comparison for standard EVA, POE, EVA/POE mix and the 7 liquids selected. For two liquids, no price could be found. Although these can differ a lot through making various assumptions, it is interesting to see that some liquids offer better pricing than the solid encapsulation, which can be an important advantage.

Material	Density (kg/m^3)	Price (€/kg)	Mass per module (kg)	Cost per module (€)
EVA [149], [150]	950	1.98	1.89	3.74
POE [145], [151]	880	2.44	1.75	4.27
EVA/POE mix (50/50)	915	2.21	1.82	4.02
Glycerol [152], [153]	1250	0.82	2.49	2.04
Glycol [154], [155]	1036	1.39	2.06	2.86
SolarPro Glycol [131]	1360	-	2.71	-
Deionized Water [156]	1000	0.50	1.99	1.00
PDMS (PMX-561) [157], [158]	960	2.37	1.91	4.53
Shell Diala S4 XZ-I [159], [160]	805	1.38	1.60	2.21
Midel 7131 [161], [162]	970	2.77	1.93	5.35
MIVOLT DF7 [163]	916	(12.54)	1.82	-

The Table 3.2 shows the data for the materials selected under the assumptions made, with relatively low cost for some liquids. Especially pure liquids like water, glycol, and glycerol give a significantly lower price than the standard EVA encapsulation, and even larger improvement compared to future

materials like POE. As mentioned before, this price difference is expected to be even larger as the raw EVA and POE also have to be processed into solar sheets. Other liquids like the PDMS and Midel are more expensive than expected, Shell Diala is relatively cheap, which is expected for a mineral oil. Prices for SolarPro Glycol and Mivolt DF7 were not publicly available and are expected to be the same price or slightly higher than the Midel 7131.

Regarding the weight of the encapsulation, they are all around the same 1.8 - 2.0 kg, with the lowest being Shell Diala of 1.60 kg and the highest SolarPor Glycol with 2.71kg. This would be an increase of 0.82 kg, which on a total module weight of 37.0 kg (2.2% increase) would not be a major problem.

To give an idea for the influences the assumption can have, EVA cost 3 years ago peaked at 3.87€, resulting in a price of 7.31€ per module. If you take the EVA price in China (where most production takes place), the price would be 1.24€ for EVA, meaning 2.34€ per module. Still outcompeted by some liquids like water, glycerol and glycol, but with less dramatic effect (although all prices, also liquids drop for China). Current solar module produced by Biosphere Solar has PIB as edge seal costing 4.85€ per module, an increasing number of standard EVA solar modules have an edge seal as well, although it is not clear if it is the same price.

Therefore, it is important to keep in mind that these prices function as an indication and more research is needed. That being said, all prices are in the same order of magnitude, and some liquids even outcompete EVA, which is known for its low cost, giving confidence in their eventual adaptation. The industry is already moving away from EVA to more expensive POE (mixtures), which might allow a slightly more expensive liquid, such as PDMS or Midel 7131, to be implemented as well.

3.5. Conclusion

To identify a suitable liquid encapsulant in place of EVA, information was found in photovoltaic immersion studies, transformer oil research, datasheets, manufacturers and experts. From this review, we distilled a set of critical performance criteria: optical transparency across 300–1200 nm with refractive index near 1.5 or higher, dielectric strength to avoid electrical leakage, chemical inertness toward PV materials and PIB edge-seal, and thermal stability as a liquid from –40 °C to +85 °C. Additional considerations include low viscosity and density for handling, minimal moisture uptake, UV and oxidation resistance, non-toxicity, and economic factors such as availability and cost, among others. As seen in a brief calculation, under various assumptions, liquids could potentially be cheaper than EVA (and POE) and, in any case, comparable in price, supporting their wider adoption.

The selection methodology began by rapidly eliminating any fluids that failed one or more essential criteria. Then, more information was gathered on promising candidates via immersion experiments reported in the PV literature, detailed transformer-fluid datasheets, as well as contact with various companies and experts. Finally, viable fluids were divided into families: hydrocarbon oils, heat transfer liquids, silicones, esters, water, glycols, glycerol and alcohols, and focused on representative examples that had already demonstrated relevant performance.

From this process, seven fluids were chosen for optical measurements. Silicone oil (PDMS) emerged as a leading candidate due to its colourless transparency, high dielectric strength, UV stability, and extensive validation in PV tests. Deionised water serves as a benchmark, despite known challenges with corrosion and freezing. Glycerol offers a high refractive index and chemical inertness, but is hindered by high viscosity and a freezing point near 17 °C (potentially needs mixing with water or glycol). Glycol, represented by SolarPro Ennogreen glycol, performs well in multiple studies. Among transformer fluids, the synthetic ester MIDEL 7131 seems promising, as well as Shell Diala and MIVOLT, with potential compatibility issues to be confirmed. After the optical measurements and analysis, the Shell Diala was confirmed incompatible with the PIB, and therefore, the mineral oils were excluded when using PIB sealant (Midel showed good results in similar tests).

The next chapter will measure each liquid's complex refractive index over the relevant wavelength range to determine its optical performance and use this data in chapter 5.

4

Complex refractive index

For many liquids, general properties are known as shown in the previous section. Still, optical properties such as the spectrally resolved complex refractive index, with real n (refractive index) and imaginary k (extinction coefficient), are often unknown, which are essential for optical modelling and solar module performance. The complex refractive index is wavelength depended, but $n(\lambda)$ and $k(\lambda)$ values will not be presented with the (λ) each time for simplicity, each time refractive index values of a material are reported (for example, n = 1.0 for air) this is at the wavelength 632 nm unless otherwise stated. Most materials used in solar modules, glass, encapsulation, solar cells and their layers, have their complex refractive index reported in literature since they are well studied and researched in order to optimise the performance. Optical data for the liquids is missing since they have rarely been used in the solar sector (only in CPV application and glycerol concept as seen in chapter 2) and no other industries are interested in detailed optical data over the range of 300 - 1200 nm. Therefore, these complex refractive indices of interesting liquids will be measured and compared to values that are present in the literature, after which they can be used in the optical modelling. First, the measuring methods and available data in the literature will be discussed to see what is missing. After that, the methodology will be addressed to see what options there are to find the complex refractive index of liquids and which will be used. After which, the results will be discussed and compared to available literature, followed by the discussion and conclusion.

4.1. Measuring methods and theory

The complex refractive index values depend on each other and should therefore be measured together. Refractive index (n) values are the most reported, but only for one wavelength and for specific liquids. Extinction coefficient k values are even rarer; if reported at all, it is a limited range and often not measured below k = 10^{-5}, which is not enough for highly transparent mediums such as encapsulation material. The extinction coefficient is strongly linked to transmission and could be translated from transmission measurement, which are present in some papers mentioned in chapter 2.

The complex refractive index is temperature and pressure-dependent (among others) [164]–[166]. In general, higher temperature gives lower values, and higher pressure gives higher values (since the complex refractive index is also proportional to density). This effect can be significant for larger temperatures, but for the operation range (-20 to 85 degrees Celsius), it is rather small (less than 0.02 for n and k not significant) [164]–[166]. This could be different for the liquids studied, but it is not investigated further in this thesis due to its small effect. The same goes for the Kerr effect, where the refractive index of a material changes when an electric field is applied. For PDMS, this effect does not give a significant change, and this is assumed to be similar for other liquids, also because of the weak electric field [167].

To measure the complex refractive index (or a part of it), multiple instruments can be used, namely the following. The two most used methods, spectrophotometer and ellipsometry, are discussed further with papers utilising these methods.

- Spectrophotometer

- Spectroscopic ellipsometer
- Abbe refractometer (only n)
- Reflectometer (only n) (used by glycerol concept [55])
- Interferometry (FTIR, Swanepoel method and Fabry–Pérot)
- Brewster Angle method (Measures the angle of reflection where no linearly polarised light is reflected from the sample surface)
- Modelling and simulation using density functional theory (DFT) and the Forouhi-Bloomer model (currently researched at TU Delft)

4.1.1. Spectrophotometer

When measuring the transmittance or reflection of a material, one of the most used devices is a spectrophotometer, often a UV/Vis/NIR LAMBDA PerkinElmer as used in [63], [66], [95]–[97], [168]. Since the liquids need to be measured in a cuvette, additional Fresnel reflection and absorption losses are introduced. The optical path goes from air to glass to sample to glass to air, which gives 2 more material changes due to the glass. This needs to be corrected for, as well as the absorption of the glass cuvette walls. This absorption is rather small, depending on the quality of the cuvette. Higher quality quartz cuvette absorbs less light, but especially in the UV range, there is still some absorption. The reflection losses between the glass-liquid interfaces can be calculated by the Fresnel equation Equation 4.1. These two losses introduced by using a cuvette to measure the sample can then be used to correct the measured values, which can make a significant impact, as can be seen in Figure 4.1 [63].

$$R = \frac{|\tilde{n}_1 - \tilde{n}_2|^2}{|\tilde{n}_1 + \tilde{n}_2|^2} \tag{4.1}$$

R is the reflection at the interface of two media, $\tilde{n}_1$ is the complex refractive index of the first medium and $\tilde{n}_2$ of the second medium.

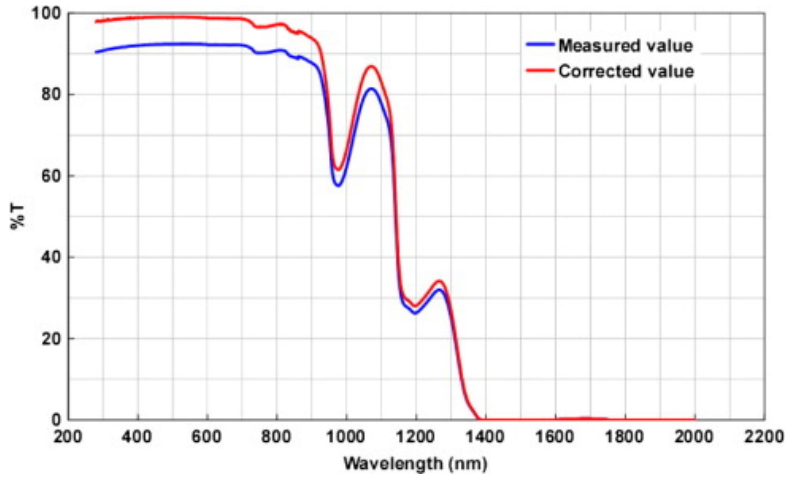

Figure 4.1: Corrected transmittance measurements of DI water in a quartz glass cuvette [63]

This method is used in multiple studies since measurements with the LAMBDA spectrophotometer are relatively accurate and easy to perform. After this study, the same authors followed a similar method, but instead of measuring the cuvette, they measured an identical piece of glass with twice the thickness of the cuvette wall to exclude the inner air-glass interfaces [66]. After cross-checking with other transmittance studies of water, they found this method to be more accurate, which can be seen in Figure 4.2. It is important to note that in both studies, they assumed the refractive index to be constant and wavelength independent for the Fresnel reflection losses calculations. The refractive index is, in fact, wavelength-dependent, but they made this assumption since the difference is small and the values of the glass and liquids are close to each other.

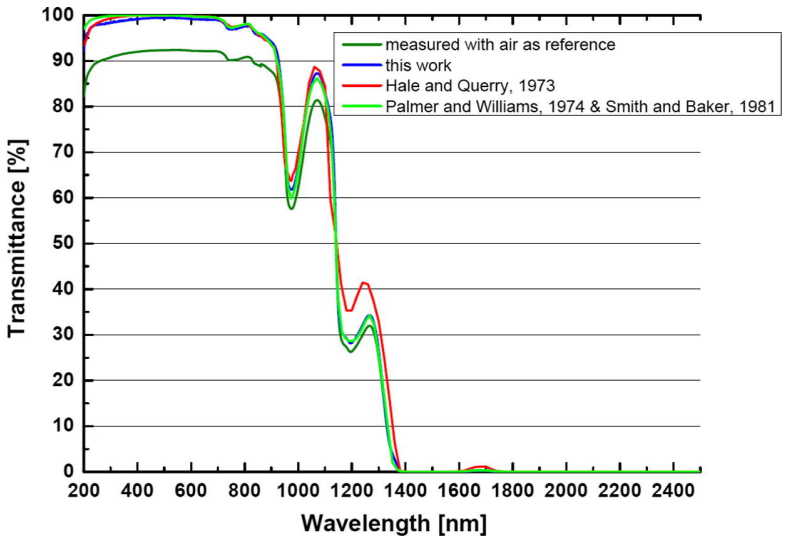

Figure 4.2: New method of measuring transmittance of water, along with other reported water transmittance measurements [66]

In their most recent research, and other studies, they use another method called the ”double optical path-length transmittance method” or ”dual cuvette method”, which will be used in this thesis and explained in the methodology section in more detail [96], [97], [130], [137], [169]. They introduced this method because of the difficulty of finding a piece of identical glass twice the thickness of the cuvette glass [96]. The new method shows a 1.2% deviation from already reported data, concluding that the method is suitable to use.

In some studies of optical characterisation, this correction for the cuvette was not applied, which showed lower transmittance values because of it [95]. Many of the liquids show transmission values of around 90%, while in other studies, with correction, they are closer to 100% in the interested spectral range. While less accurate, this study still shows interesting results of some heat transfer liquids, again highlighting the good optical properties of PDMS and glycol.

4.1.2. Spectroscopic ellipsometry

In general, the spectroscopic ellipsometer gives the most accurate results and is widely used in industry and academia for determining the complex refractive index of materials (solids). However, the standard setup of an ellipsometer is to measure solids/thin films; exchanging this for liquids introduces some problems. The two main problems mentioned in the literature are the levelling of the sample and the vibrations of the device affecting the surface of the liquids.

The ellipsometer measures the change in the phase Δ and amplitude Ψ of polarised light reflected from a sample at different angles. This data can then be fitted by certain models to find properties such as the complex refractive index. In order to receive the reflected beam of light at the centre of the analyser, the angle of the stage on which the sample is placed is adjusted slightly with 2 knobs. However, this method poses a problem for liquids since they will level due to gravity (spirit levelled) instead of following the same angle as the stage. To solve this problem, the instrument can be levelled with active pneumatic isolators, as seen in Figure 4.3 in which three isolators level the baseplate [138]. They also dampen the vibrations of the ellipsometer, which would otherwise give the liquid surface an additional roughness, distorting the measurement.

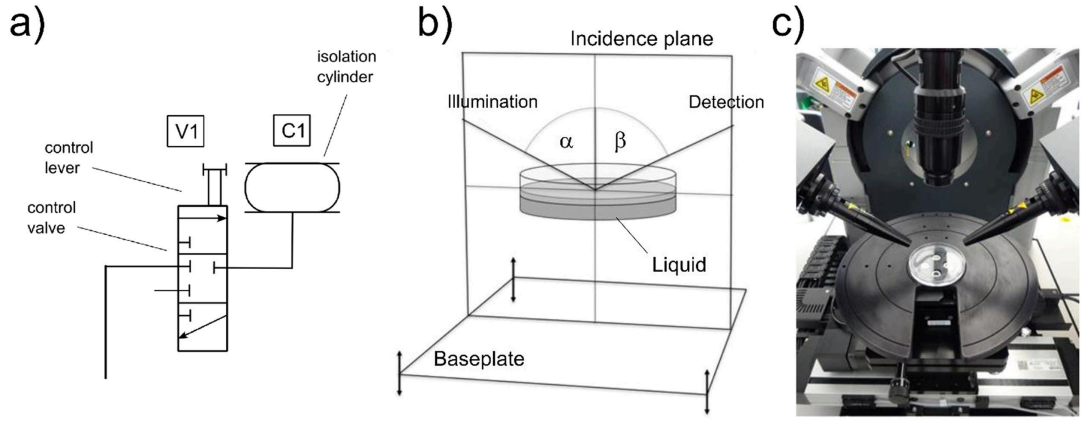

Figure 4.3: Ellipsometer setup at Semilab (a) Shows the schematic of controlling the pneumatic isolators. (b) Gives the layout with the points on the baseplate where the pneumatic isolators are secured. Controlling the level of the machine and thereby the liquid sample. (c) Shows how the sample is measured in the petridish [138]

A solution for eliminating the waves on the liquid surface is placing a prism on top of the liquid [170]. Mentioning that the liquids should not have a refractive index similar to the prism and a sensitivity for k of 10^{-4}, which is not accurate enough for the application in the optical model, unfortunately.

A paper measuring the complex refractive index of organic solvents combines spectroscopic ellipsometry with transmission measurements, addressing the limitations of ellipsometry alone in weakly absorbing media [171]. While ellipsometry provides high sensitivity to refractive index (n), it struggles to accurately capture the absorption index (k) in semi-transparent liquids, which is instead derived from transmittance data [172]. They also noted this in their earlier work on highly transparent solids, in which they introduced another method of using an ellipsometer for the double optical pathway transmission measurements, although not performed on the organic solvents [164], [173]. To mitigate interference from reflections at the liquid–dish interface, they use a focusing probe to create a micro-sized illumination spot and a semi-open cover to shield against stray light and reduce solvent evaporation. This setup ensures that only the reflection from the air–liquid surface reaches the detector, enabling more accurate measurements. They show promising results, with k values going down to 10^{-8}, although there is generally also more uncertainty after passing 10^{-7}.

In older work, Li et al. did use the ellipsometer for the double optical pathway method for liquids (previously only used on solids), in their study on edible oils and sodium chloride solutions [122], [174]. They use a model to minimise the difference between the calculated transmission and the measured values. They used these transmission measurements to obtain n and k in combination with a Seilmeir fit for n and a Gaussian function for k in the ultra-transparent region of 300 - 700 nm (below 10^{-7}). They do note that n is especially sensitive to transmittance errors.

Lastly, another group performed ellipsometry measurements on solids and two liquids, PDMS and glycol, combining the ellipsometry measurements with transmission measurements [130], [137]. They obtain the n values by normal ellipsometry measurements and a Seilmeir fitting. For obtaining the extinction coefficient, they use the double optical pathways method with 2 cuvettes explained earlier in spectrophotometry. Instead of computing transmission values, they use them to calculate the k values of the liquids (similar formulas are used). They obtain values for k in the range of 10^{-5}, which is probably due to the accuracy of the ellipsometer in transmission mode.

To conclude, spectrophotometry (often with a Perkin Elmer Lambda) is used to obtain transmission and reflection values, but liquids introduce new problems since they need to be contained in a vessel (like a cuvette), which gives extra reflection and absorption. This can be corrected by measuring the glass, but the double optical pathway method seems more accurate, easier and has been used in multiple studies. Ellipsometry is used for obtaining n values, but is less accurate in k values for weakly absorbing materials, such as the liquids being researched. Therefore, the ellipsometer could be used in transmission mode, in combination with the double optical pathway method. The disadvantage here is that a spectrophotometer, like the Lambda, gives more accurate transmission results. That is why

the combination might give the best results, using the ellipsometer for the n values and the Lambda for the k values. This option is further explored in the following section, paying attention to the dependent nature and influence that the values have on each other.

4.2. Methodology complex refractive index

The complex refractive index of the liquids is measured with ellipsometry and spectrophotometry combined, which is why their methodology is divided into two sections, which will be justified in the following paragraph. All ellipsometry measurements (n values) are performed by the ellipsometry R&D application group at Semilab Hungary, using a Semilab SE 2000 spectroscopic ellipsometer equipped with active vibration isolation described in [138]. This is an ellipsometer with specialised equipment for measuring liquids, currently not available at TU Delft. All the spectrophotometry measurements (k values) using the Perkin Elmer Lambda 1050+ UV/Vis/NIR Spectrophotometer were performed at the Electrical Sustainable Power (ESP) lab at the Technical University of Delft.

Several options exist for measuring the complex refractive index, which needs to be measured simultaneously due to its dependent nature; this has proven to be difficult for liquids. Which is why three main approaches were tried: (i) a simultaneous fit by the ellipsometry with transmission measurements from the ellipsometry, (ii) a simultaneous fit with transmission measurements from the lambda (Spectrophotometry) and (iii) n values from the ellipsometry and k values from the dual cuvette method using the Lambda (used in this thesis).

Ellipsometry tends to be less accurate in transmission measurements compared to spectrophotometry, which can cause the k values computed by the simultaneous fit to deviate from literature values. Especially compared to the k values computed from Lambda transmission measurements, explained in the following section, which showed good agreement with literature values, making them a reliable basis for subsequent simultaneous fitting. Because of the better transmission measurements from the Lambda, the successive method tried the simultaneous fit using the transmission data from the Lambda. While the CompleteEASE software used at TU Delft did not support the import of external transmission data, Semilab's SEA software offered greater flexibility by allowing such data to be integrated into the analysis. Although the current version of the SEA software does not support modelling of multiple incoherent ("thick") layers, such as the cuvette structure (glass/sample/glass), due to the loss of interference information beyond the coherence length, this limitation is rooted in fundamental physical constraints. There are workarounds available, but they were considered too uncertain for this study and were therefore not pursued.

Nevertheless, the initial simultaneous fit using the ellipsometry transmission data (which still had good agreement with the lambda data) did give interesting insights. Namely, the n values were hardly influenced by the simultaneous fit as compared to the k = 0 assumption, as the k values are close to 0, which could legitimise their separate measurement. Since k values were more sensitive to the fitting method, they were measured using the dual-cuvette approach, which accounts for the interdependent nature of n and k, as detailed in the methodology section on extinction coefficient measurements.

4.2.1. Refractive index (n) of liquids

All ellipsometry measurements (n values) were performed with a Semilab SE-2000 spectroscopic ellipsometer fitted with active pneumatic isolators under its base plate, as seen in Figure 4.3 [138]. Three individually controlled cylinders level the ellipsometer in such a way that the reflected light from the sample can be collected, while simultaneously damping environmental vibrations. A micro-spot optic (400 μm) enabled focusing on the liquid/air interface, serving also to reduce backside (liquid/Petri dish) reflections. Liquids were poured into a clean Petri dish and allowed to rest for several minutes until surface waves subsided. Spectra were collected over the wavelength range 245–975 nm at multiple angles of incidence (AOI) near each liquid's Brewster angle (where polarised light is transmitted into the material, no reflection, around 53-55° for water, glycol, glycerol and PDMS), extrapolated to the 1200 nm range with the Cauchy parameters.

Ellipsometry measures the change in the phase Δ and amplitude Ψ of reflected polarised light, which can then be fitted by a model to find refractive index (n) (and extinction coefficient (k)). These measurements were performed in two modes, standard measuring of Δ and Ψ, and so-called mirror mode

(two-zone measurement). SE-2000 is a rotating compensator ellipsometer. The compensator is contentiously rotating during measurement while the polarisers are at a fixed position. In mirror mode, two measurements are taken with one polariser at two azimuth angles (A = +45° and A = -45°), and the results are combined [175], [176]. This technique is highly effective at improving accuracy by eliminating most systematic errors, particularly those arising from azimuthal misalignment. By cancelling these systematic biases, a more accurate determination of Δ and Ψ is achieved. For this reason, the mirror mode was selected. The measured Δ and Ψ can be fitted directly, or transformed to Alpha α and Beta β using the following formulas:

$$\alpha = -\cos(2\Psi) \quad \beta = \sin(2\Psi)\,\cos(\Delta)$$

This is often done for isotopic bulk-like materials near the Brewster Angle, as they tend to "re-weight" the values of Δ, reducing its noise (which is more significant near the Brewster angle). These parameters can then be fitted by a model to obtain the wanted n (and k) data as described in the following section.

Ellipsometry model and fitting

To determine the wanted nk values, the measured Δ and Ψ, or here α and β, can be fitted by a dispersion model through regression analysis. Simply put, the model simulates the measured values (Δ and Ψ) by assuming/estimating certain parameters like layer thickness/roughness, refractive index (n) and extinction coefficient (k) (among others), of the material layers defined in the software. If the simulated values from the model and the measured values align well (minimal deviation), there is a good fit, and the assumed parameters mentioned before are correct (close to reality). Several options for the dispersion model, such as Cauchy, Urbach, Sellmeier, and B-spline, are possible, from which the 2-parameter Cauchy (displayed below) was selected. This model is chosen for its relative simplicity and application to transparent materials where k = 0 is assumed (a fair assumption, as later shown).

$$n(\lambda) = A + \frac{B}{\lambda^2} \tag{4.2}$$

Where n (λ) is the wavelength-dependent refractive index, A and B are the fitted coefficients. To better match the measured values (mainly used when k is not 0), certain oscillators can be added to the model to create a better fit. They model light-matter interaction and are related to the absorption of a material and material properties, so not all oscillators can be used, as some do not make physical sense for the liquids used. In the first fit, k is assumed to be zero; in the second fit with the transmission measurements, k is no longer zero, and Gaussian oscillators are used to match the k values. As mentioned before, this gave a less accurate curve than literature values compared to the dual cuvette method, with the lambda, explained later on. Therefore, no oscillators were used in the fit, only the 2-term Cauchy dispersion law and the following material layer build-up fed into the software.

The sample layers were modelled with a three-phase system: Air – surface interface – liquid, visualised in Figure 4.4. The air had a refractive index of n = 1. The surface of the liquid is never perfectly smooth due to surface roughness and a transition region (evaporation effect); therefore, it is common to introduce a surface interface layer. This is modelled as a thin Bruggeman Effective Medium Approximation (BEMA) layer, which produced the refractive index (n) in the transition region from the air and liquid n values in a 50/50% void ratio [177]. The liquid layers are described by the Cauchy 2-term equation, for which the parameters are found, along with the roughness/surface interface thickness, by regression analysis, described in the following paragraph.

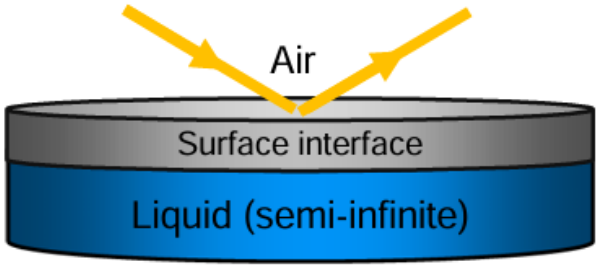

Figure 4.4: Material layer build-up used in the ellipsometry software

The regression analysis (model fitting) minimises a monotone function of the Root Mean Squared Error (RMSE) between the measured and simulated spectra. For fit quality indication and comparisons, which will be shown in the results section, the coefficient of determination (R^2) is more suitable as it is independent of the number of free parameters (A, B and roughness thickness) and spectral points; a value closer to 1 means a better fit. The values were measured in the range of 249 – 975 nm, where there is less absorption in general, which gives a better fit with the Cauchy model (assumption k = 0). The refractive index is extrapolated to 1200 nm with the Cauchy parameters. The values measured from the experiments showed good reproducibility. For glycerol, it was expected to deviate the most, as the highest evaporation was expected. For glycerol, the standard deviation between measurements was n 0.0003, which showed good repeatability.

All modelling and fitting were performed using Semilab's SEA software. The full raw datasets (Ψ, Δ and α, β), fit summaries, and repeatability tables can be made available on request.

To conclude, the refractive index (n) of the 7 liquids was obtained from ellipsometry measurements, using the experimental set-up of Semilab over the range 249 - 975 nm (extrapolated to 1200 nm). The measured values were fitted using a 2-term Cauchy model with a three-phase system: Air – surface interface (BEMA) – liquid. Through regression analysis, the RMSE is minimised between simulated and measured values, and the quality of the fit is expressed in R^2. The measured values (Ψ, Δ and transformed α, β) will be presented together with the produced refractive index values over the wavelength range in the results section.

4.2.2. Extinction coefficient (k) and transmittance of liquids

The second half of the complex refractive index, the imaginary part, is the extinction coefficient k, which governs the light absorption in a material. They are normally, for solids, measured and simultaneously fitted by ellipsometry, taking into account that n and k depend on each other. For liquids, this is challenging because of their nature and the need for a holding vessel such as a cuvette. Therefore, they require specialised transmission measurements to eliminate the cuvettes and measure ultra-low absorption. First, the theory and measuring methods will be explained, followed by the procedure of the transmission measurements and finally the results in the following section.

The liquids need a holder such as a cuvette, but this introduces new materials and interfaces that are also being measured. There are a couple of techniques to exclude these; in this thesis, the focus will be on the following two. Transmission data was converted to extinction coefficients (k) by two methods: the "dual-cuvette approach" (k1) and the "reference beam approach" (k2). We compare both methods against each other and the literature values.

Dual cuvette method (k1)

By using the dual cuvette method, used in several other papers, the reflection of all interfaces (air/-glass/sample) is taken into account by correcting with the other cuvette. The only difference between the 5 and 10 mm cuvettes is 5 mm of additional liquid sample inside the 10 mm cuvette. So the difference between the transmittance measured of the 5 and 10 mm cuvette is only caused by the absorption of the 5 mm of extra liquid, excluding the other reflection and absorption effects which the cuvette glass

walls have on the measurement.

The extinction coefficient can be calculated by rewriting the Beer-Lambert law, absorption coefficient and definition of transmission:

$$T(x) = \frac{I(x)}{I_0} = e^{-\alpha(\lambda)x} = e^{(-\frac{4\pi k(\lambda)}{\lambda}x)} \tag{4.3}$$

where $T(x)$ is the transmittance at distance x, which is the light intensity at x ($I(x)$), divided by the initial light intensity ($x = 0$). $\alpha(\lambda)$ the absorption coefficient at distance x in the material and can be expressed in $k(\lambda)$, the extinction coefficient, and λ, the wavelength in nanometres.

Transmittance is thus depended on the thickness of the material, while absorption and extinction coefficient are material properties which can be computed from the two cuvette measurements. The cuvettes of path□lengths $z_1 = 5$ mm and $z_2 = 10$ mm are both measured, yielding transmittances T_1 and T_2. The extinction coefficient follows from the following equation [130], [137]:

$$k_1(\lambda) = \frac{\lambda}{4\pi} \frac{\ln(T_1(\lambda)/T_2(\lambda))}{z_2 - z_1} \tag{4.4}$$

In principle $T_2 < T_1$ since 10 mm absorbs more light due to its longer optical pathway, but measurement noise (instrument precision, measuring deviations, slight differences in cuvette cleanliness) can produce $T_2 > T_1$ and hence non□physical k1 values (negative, so not displayed on graphs).

Reference beam method (k2)

The ”reference beam method”, proposed by Stefaan Heirman, follows the same principle, but performs the correction by the Lambda directly, instead of calculating it afterwards. This is done by placing the 5 mm cuvette in the reference beam, so that losses due to reflections and glass□wall absorption are, again, taken into account, and the only difference between the 10 mm cuvette is 5 mm of the liquid inside. However, the difference in transmittance is now subtracted from each other instead of using the formula, which can cause slightly different results due to the following reason.

The difference is not the first 5 mm of the liquid but the last 5 mm (from 5 to 10 mm), which has lower light intensity and thus absorption, following not a linear trend but an exponential decline according to Lambert's law. Hence $k_2 < k_1$ in general, especially expected at high k for which the absorption is higher and therefore the difference more evident. Nevertheless, when we look at the light intensity curve for materials with low k (10^{-5}) over a distance of 10 mm, the behaviour looks more linear than exponential, which can explain why the curves overlap in higher k regions, leading to $k_2 \approx k_1$.

Transmission measurements

Transmission measurements were performed with a Perkin Elmer Lambda 1050+ UV/Vis/NIR Spectrophotometer with integrating sphere, over the range of 300 - 1200 nm, step size 5 nm [168]. Tungsten and D2 lamp (below 319 nm), 2 mm slit width, detector PMT response of 0.60 s and auto gain, PbS detector with 0.40 s and 12 gain, detector changed to PbS at 860 nm. The liquids are measured in Hellmex cuvettes (5 and 10 mm optical pathway) [178]. Each measurement was performed 3 times. Standard deviation (STD) and maximum deviation for the 3 measurements of each cuvette of each liquid are computed. Between the measurement of each liquid, the cuvettes are thoroughly cleaned as explained in the following paragraph. The process of transforming the transmittance to extinction coefficient (k) is depicted below; each step is shown in more detail for water in the results section.

1. Three datasets per liquid (7 liquids) and per cuvette optical path-length (5, 10 mm and reference beam method (10 mm)) (63 in total) are obtained. They are normalised with the reference measurement (100 % measurement before experiments). If needed, the transmission measurements are corrected for potential dirt on the cuvettes.
2. Mean and standard deviation of measurements
3. k1 is computed from the 5 and 10 mm cuvette measurement, and k2 from the reference beam measurement

4. Calculate signal to noise ratio (SNR), determine appropriate Threshold
5. Check effect of threshold on optical simulations
6. k1 and k2 values are plotted and compared to literature values and each other
7. nk files are produced

Cuvette cleaning

Before measurement, cuvettes were cleaned sequentially with isopropanol (IPA), acetone, and deionised water. Alternative agents (e.g. Nebol, Hellmanex) or ultrasonic baths could also be used, although the ultrasonic bath could damage the cuvettes, depending on their fabrication. After each cleaning protocol, the cuvettes were measured without liquid samples (air) and compared against the unused cuvette measurements (reference) to determine if the cleaning was successful. During the testing, the cuvettes seemed to be cleaned relatively well (less than 1% difference). The ”cleanliness” of a cuvette refers to any residue, dust, fingerprints, scratches or other, on its surfaces that can interfere with incoming light. Because this factor can vary between the two cuvettes and even between cleaning cycles, it can become a more important effect in the very low absorption regions (k = 10^{-7}).

4.3. Results and discussion

4.3.1. Refractive index (n) of liquids

Here, the results of the refractive index measurements by ellipsometry, described earlier, are presented and visualised. First, the measured (Ψ, Δ and transformed α, β) values will be presented for water, together with their refractive index fit of simulated and measured values, to illustrate the data processing. This data is then compared to literature values for all liquids with available literature (water, glycol, glycerol and PDMS).

Water refractive index

Psi (Ψ) and Delta (Δ) Water

In Figure 4.5, the Psi Ψ and Delta Δ at the angles 51°, 53° and 55° are displayed over the range 245 - 975 nm. As expected, the measurement of Δ 53° shows more dispersion since that is close to the Brewster angle of water (53°). Other liquids showed similar graphs and patterns, with glycerol, glycol and PDMS showing more dispersion in the 53° and 55° measurements, because their Brewster angles are slightly higher. These values are transformed to α and β as explained in the methodology.

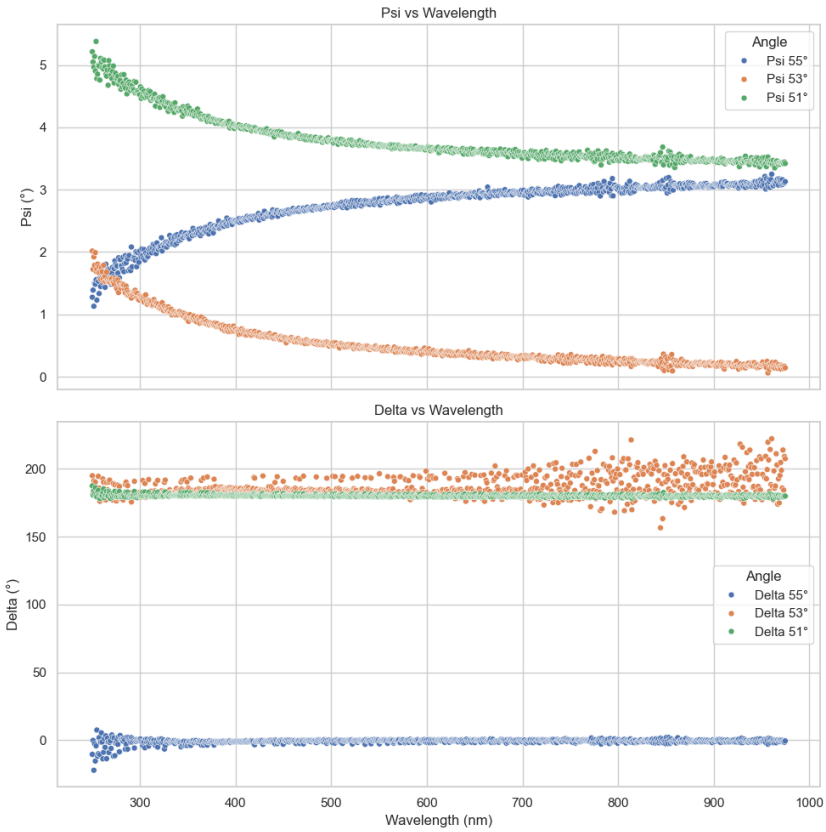

Figure 4.5: Ψ and Δ of water, measured at angles 51°, 53°, and 55°

Alpha α and Beta β Water

The α and β of water for the angles 51°, 53° and 55° are presented over the range 245 - 975 nm in Figure 4.6. They follow a nice curve with less distortion due to the ”re-weighing’ of the parameters explained in the methodology. Therefore, these values are used for the fitting, which is shown in the following paragraph.

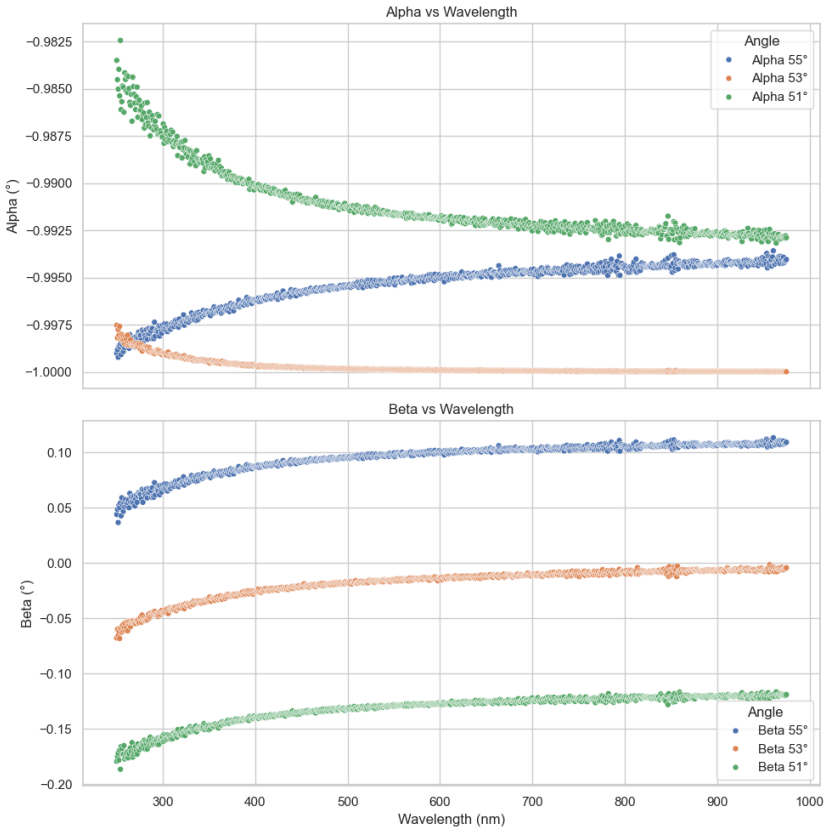

Figure 4.6: Alpha α and Beta β measured and transformed at angles 51°, 53°, and 55°

Fitting model and parameters

The 2-term Cauchy law is fitted on the Alpha α and Beta β values, to obtain the parameters A, B and interface surface thickness through regression analysis explained in the methodology. This fitting graph of simulated and measured alpha and beta values, as seen in the SEA software, is displayed in Figure 4.7. The RMSE is minimised and this delivered a quality of fit of R^2 = 0.9867. The parameters of water were found to be A = 1.32888, B = 0.003487 and roughness layer thickness = 2.3 nm. Finally, the refractive index value can be computed from the Cauchy model and compared to literature values.

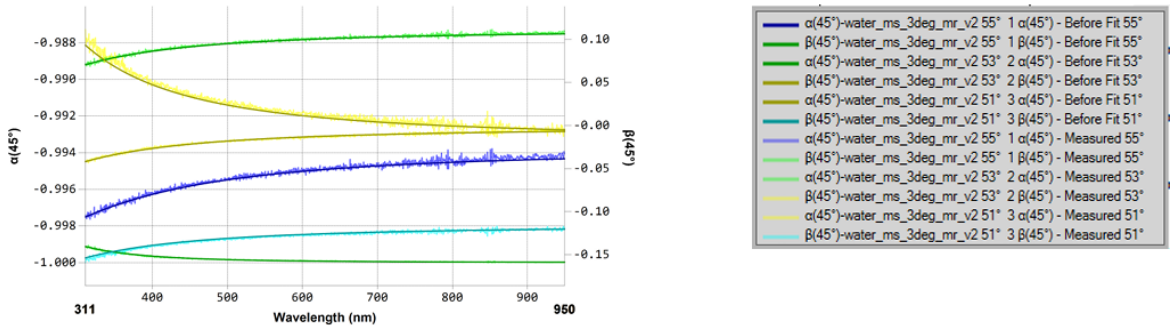

Figure 4.7: SEA software fitting graph of simulated and measured alpha and beta values

Comparison with literature value

From the obtained Cauchy model, the refractive index values, over the range 245 - 975 nm (extrapolated to 1200 nm later on), can be obtained. These are plotted together with literature values of water in Figure 4.8 and provided with a marker at 632 nm. The values seem to align relatively well, with slightly

lower n values measured by Semilab (this thesis) in general [179]. Near the end (1200 nm), there is the most deviation of Δ n = 0.011. For water, there was a refractive index difference between these values and the method of simultaneous fitting using the transmission data of Δ n = 0.0002. This showed that the simultaneous fit had minimal effect on the refractive index values.

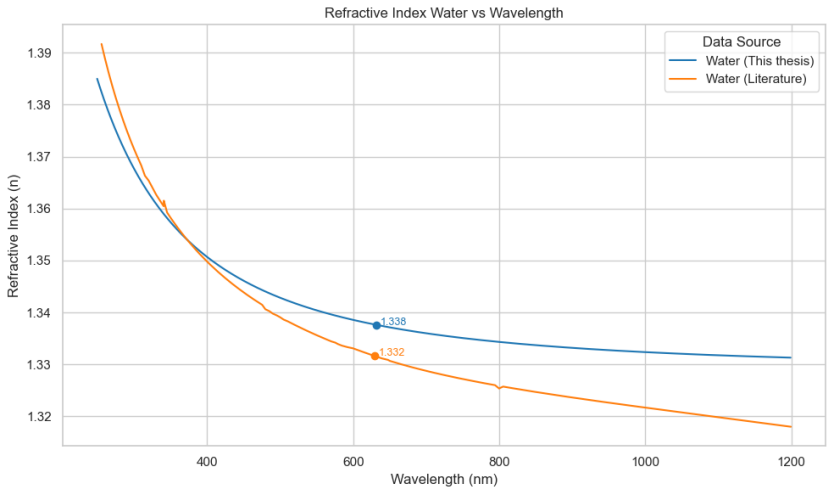

Figure 4.8: Refractive index of water compared to literature values, showing good agreement [179]

Glycerol refractive index

For glycerol (and all following liquids), the measured Ψ, Δ values are not displayed; only the α and β simulated and measured are displayed in the SEA graph, as well as the fitted parameters and the refractive index values compared to literature.

Fitting model and parameters

This fitting graph of simulated and measured alpha and beta values, as seen in the SEA software, is displayed in Figure 4.9. The RMSE is minimised and this delivered an excellent quality of fit of R^2 = 0.9954, which is the highest of all liquids. The parameters of glycerol were found to be A = 1.46175, B = 0.0040152 and roughness layer thickness = 4.1 nm. Finally, the refractive index value can be computed from the Cauchy model and compared to literature values.

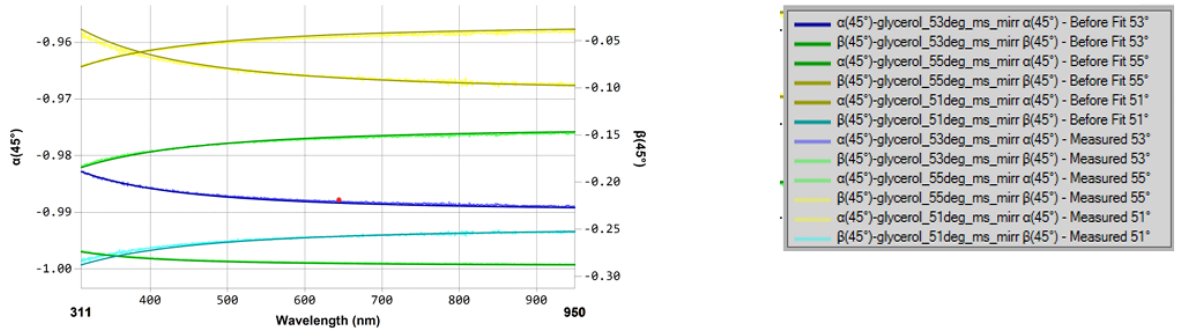

Figure 4.9: SEA software fitting graph of simulated and measured alpha and beta values for glycerol

Comparison with literature value

From the obtained Cauchy model, the refractive index values over the range 245 - 975 nm (extrapolated to 1200 nm later on) are plotted together with literature values of glycerol in Figure 4.10 and provided with a marker at 632 nm [55].

The values seem to align relatively well with the literature values from the Glycerol concept, with slightly higher n values measured by Semilab (this thesis), a difference of Δ n = 0.005 [55]. This could poten-

tially be due to mixing of water with the glycerol in the literature, as this is often done, which lowers the refractive index. For glycerol, there was a refractive index difference between these values and the method of simultaneous fitting using the transmission data of Δ n = 0.0006. This showed that the simultaneous fit had minimal effect on the refractive index values.

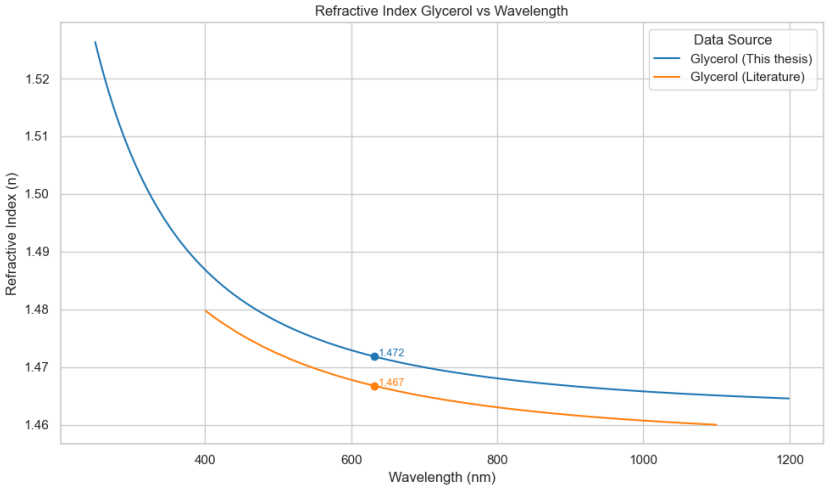

Figure 4.10: Refractive index of glycerol compared to literature values, showing good agreement [55]

PDMS refractive index

Fitting model and parameters

This fitting graph of simulated and measured alpha and beta values, as seen in the SEA software, is displayed in Figure 4.11. The RMSE is minimised and this delivered a quality of fit of R^2 = 0.9762, which was the lowest of all fits. The parameters of PDMS were found to be A = 1.39713, B = 0.004374 and roughness layer thickness = 0.4 nm.

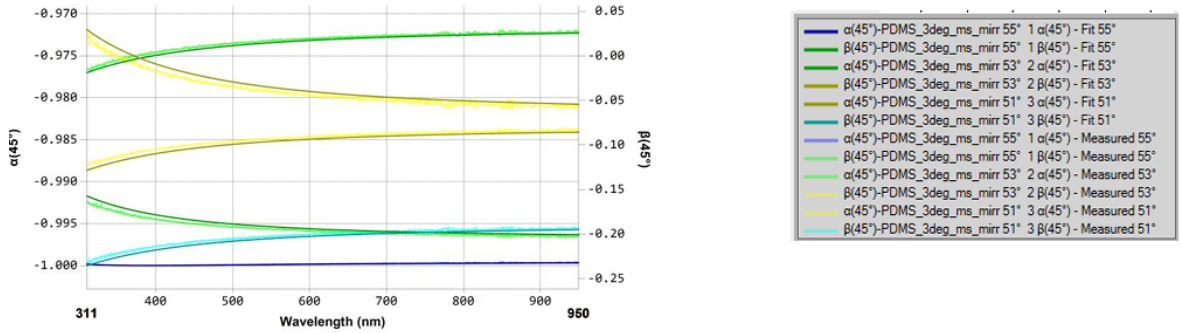

Figure 4.11: SEA software fitting graph of simulated and measured alpha and beta values of PDMS

Comparison with literature value

From the obtained Cauchy model, the refractive index (n) values over the range 245 - 975 nm (extrapolated to 1200 nm later on) are plotted together with literature values of PDMS in Figure 4.12 and provided with a marker at 632 nm [137].

Although PDMS has the lowest fit quality R^2 and the largest difference with the simultaneous fit method, the values correspond well with the literature, with a deviation around the Δ n = 0.009. For PDMS, there was a refractive index difference between these values and the method of simultaneous fitting using the transmission data of Δ n = 0.0025, which was the highest of all liquids. This is the highest difference in refractive index values between the simultaneous fit and is still rather small, so expected to have an insignificant effect on the optical simulations.

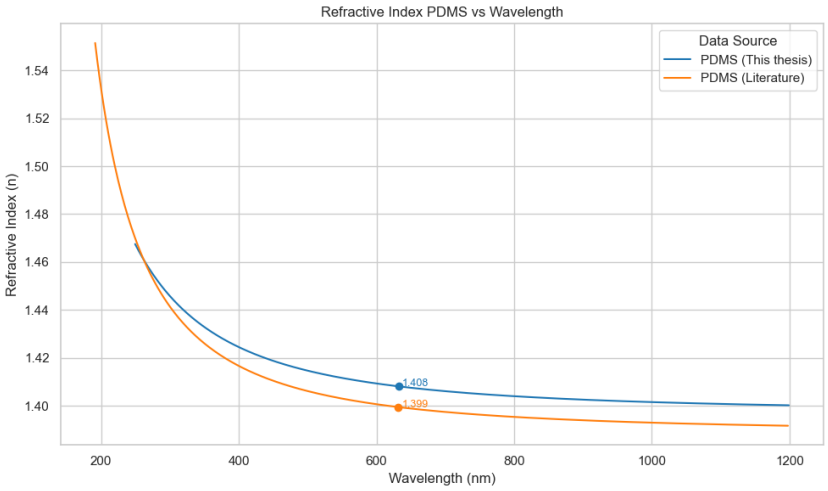

Figure 4.12: Refractive index of PDMS compared to literature values, showing good agreement [137]

Glycol refractive index

Fitting model and parameters

This fitting graph of simulated and measured alpha and beta values, as seen in the SEA software, is displayed in Figure 4.13. The RMSE is minimised and this delivered a quality of fit of R^2 = 0.9784. The parameters of glycol were found to be A = 1.40077, B = 0.0043271 and roughness layer thickness = 2.6 nm.

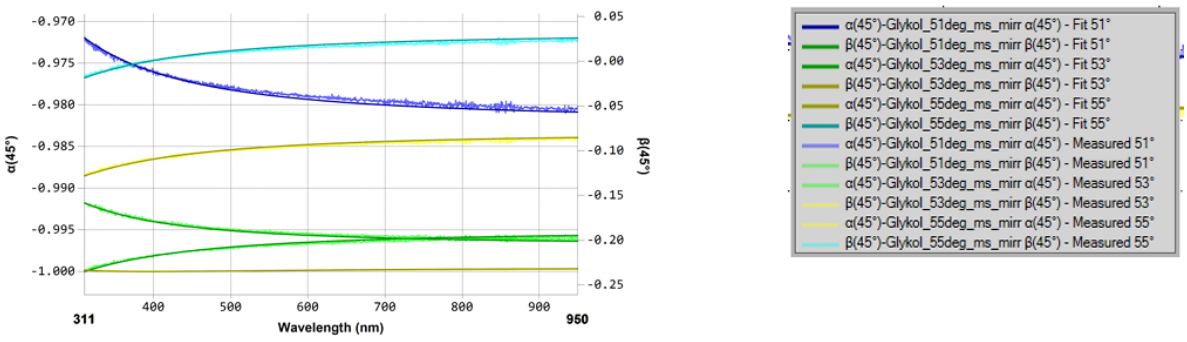

Figure 4.13: SEA software fitting graph of simulated and measured alpha and beta values for glycol

Comparison with literature value

From the obtained Cauchy model, the refractive index values over the range 245 - 975 nm (extrapolated to 1200 nm later on) are plotted together with literature values of glycol in Figure 4.14 and provided with a marker at 632 nm [130].

For glycol, the refractive index values deviated the most from the values found in literature. This is because not pure glycol is used, but Innogreen SolarPro, a modified liquid based on glycol for solar application, likely containing additives [130], [131]. The difference is around Δ n = 0.042, the largest of all liquids. The hypothesis is that this is due to the inhibitors added, such as ”vaporisable corrosion inhibitors”. They also mention that the liquid is a blend of chemical compounds, of which glycol is assumed to be the main component. When looking at the refractive index listed in the datasheet, n = 1.39 - 1.43, this seems to align well with the measured values, supporting the idea that the SolarPro Innogreen glycol might be more different to standard 100% pure glycol than initially expected [131]. For glycol, there was a refractive index difference between these values and the method of simultaneous fitting using the transmission data of Δ n = 0.0015. Again showing that the simultaneous fit had minimal effect on the refractive index values.

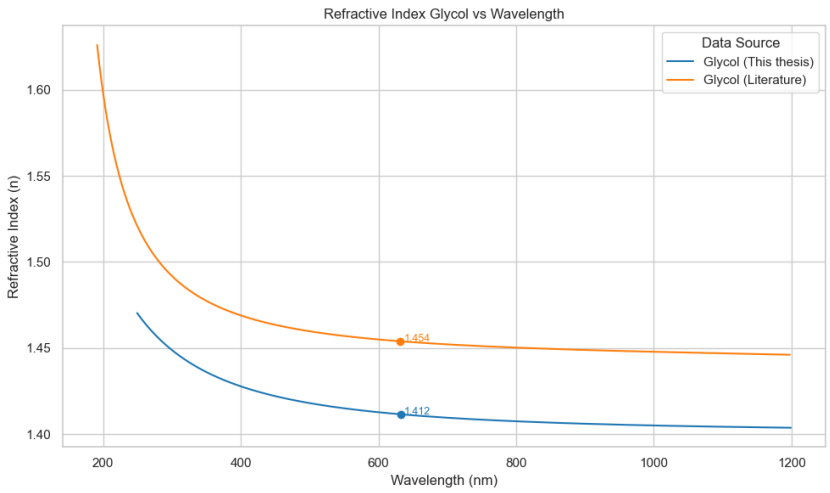

Figure 4.14: Refractive index of glycol compared to literature values, showing the most deviation of all liquids [130]

Shell Diala refractive index

Fitting model and parameters

This fitting graph of simulated and measured alpha and beta values, as seen in the SEA software, is displayed in Figure 4.15. The RMSE is minimised and this delivered an excellent quality of fit of R^2 = 0.9948. The parameters of Shell Diala were found to be A = 1.44639, B = 0.0043761 and roughness layer thickness = 1.8 nm.

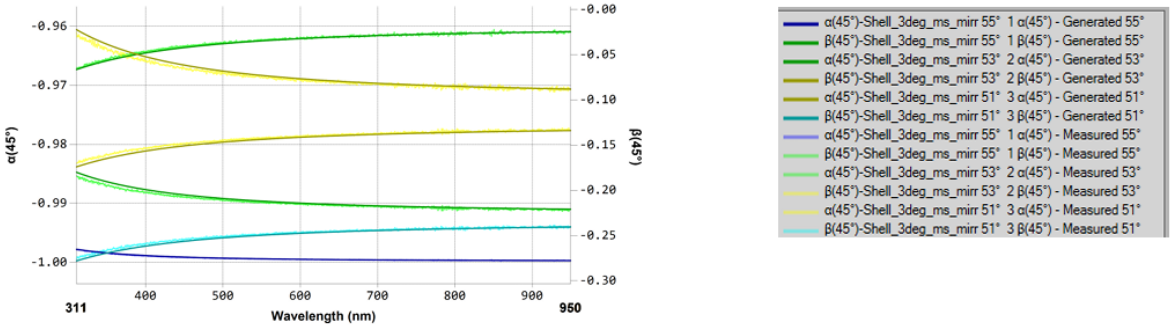

Figure 4.15: SEA software fitting graph of simulated and measured alpha and beta values for Shell Diala

Refractive index curve Shell Diala

From the obtained Cauchy model, the refractive index values over the range 245 - 975 nm (extrapolated to 1200 nm later on) are plotted in Figure 4.16 and provided with a marker at 632 nm.

For Shell Diala S4 XZ-I, no literature values exist to compare against, but other Shell Diala oils have a refractive index in the range of 1.468 to 1.490, which aligns well. The values follow a smooth curve; they are considerably higher than most other liquids, meaning they will reflect less, as will be seen in the following chapter. For Shell Diala, there was a refractive index difference between these values and the method of simultaneous fitting using the transmission data of Δ n = 0.0012. Again showing that the simultaneous fit had minimal effect on the refractive index values.

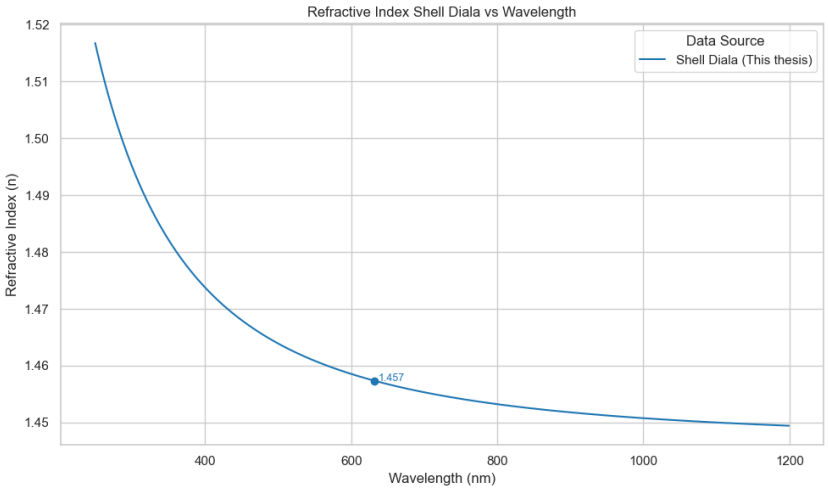

Figure 4.16: Refractive index of Shell Diala, there are no literature values available

Mivolt refractive index

Fitting model and parameters

This fitting graph of simulated and measured alpha and beta values, as seen in the SEA software, is displayed in Figure 4.17. The RMSE is minimised and this delivered an excellent quality of fit of R^2 = 0.9950. The parameters of Mivolt were found to be A = 1.44592, B = 0.0043922 and roughness layer thickness = 1.4 nm.

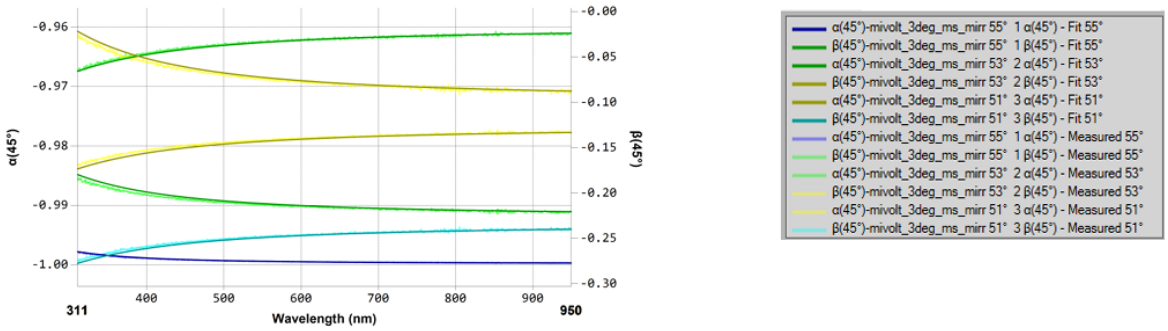

Figure 4.17: SEA software fitting graph of simulated and measured alpha and beta values for Mivolt

Refractive index curve Mivolt

From the obtained Cauchy model, the refractive index values over the range 245 - 975 nm (extrapolated to 1200 nm later on) are plotted in Figure 4.18 and provided with a marker at 632 nm.

The values follow a smooth curve; they are considerably higher, just like Shell Diala. For Mivolt, there was a refractive index difference between these values and the method of simultaneous fitting using the transmission data of Δ n = 0.0009. Again showing that the simultaneous fit had minimal effect on the refractive index values.

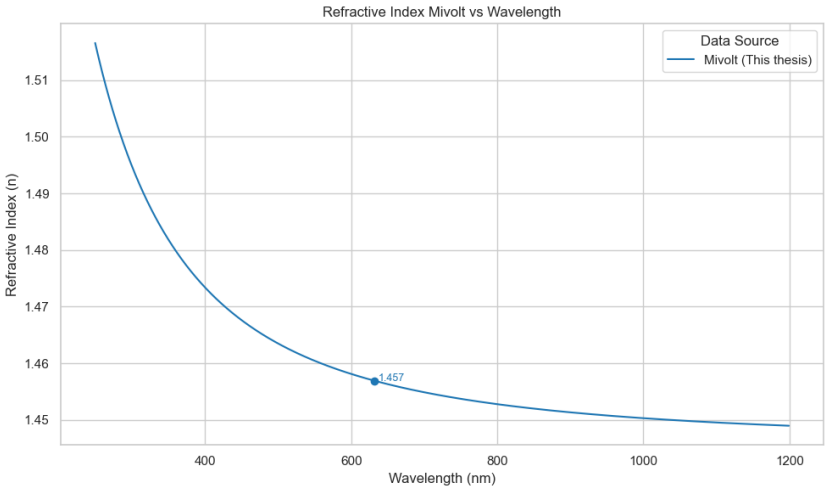

Figure 4.18: Refractive index of Mivolt, there are no literature values available

Midel 7131 refractive index

Fitting model and parameters

This fitting graph of simulated and measured alpha and beta values, as seen in the SEA software, is displayed in Figure 4.19. The RMSE is minimised and this delivered an excellent quality of fit of R^2 = 0.9940. The parameters of Midel were found to be A = 1.44298, B = 0.0043556 and roughness layer thickness = 1.6 nm.

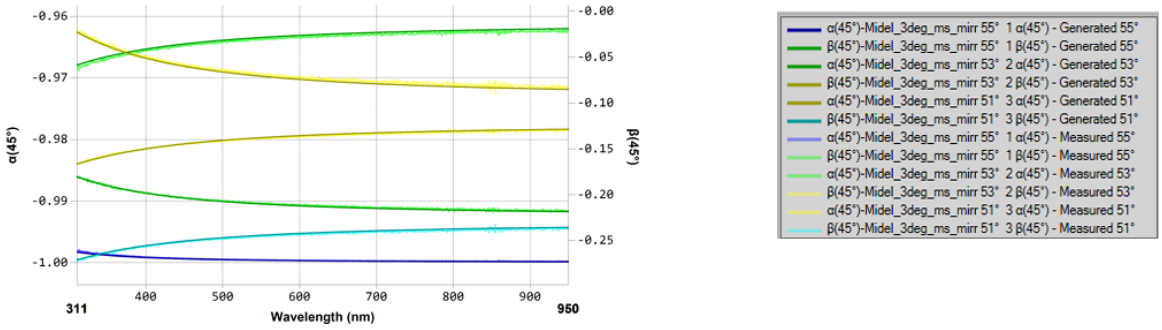

Figure 4.19: SEA software fitting graph of simulated and measured alpha and beta values for Midel 7131

Refractive index curve Midel 7131

From the obtained Cauchy model, the refractive index values over the range 245 - 975 nm (extrapolated to 1200 nm later on) are plotted in Figure 4.20 and provided with a marker at 632 nm.

The values follow a smooth curve, and they are very comparable to Mivolt, which makes sense since both are synthetic esters. For Midel, there was a refractive index difference between these values and the method of simultaneous fitting using the transmission data of Δ n = 0.0002, the lowest of all liquids. Again showing that the simultaneous fit had minimal effect on the refractive index values.

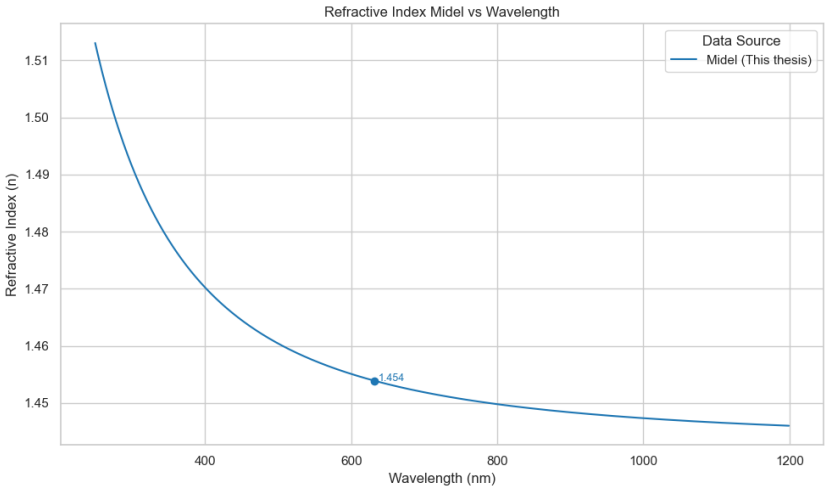

Figure 4.20: Refractive index of Midel 7131, there are no literature values available

Comparing refractive index

Overall, the determined refractive index values showed excellent agreement with literature values for water, glycerol, and PDMS, with deviations ranging from 0.005 to 0.009 as seen in Table 4.1. The largest deviation from literature was observed for glycol (Δ n = 0.042), most likely due to the use of InnoGreen SolarPro (based on glycol, but mixed with other unknown compounds and inhibitors), instead of pure glycol. For liquids lacking published values (e.g., Shell Diala, Mivolt, Midel 7131), these ellipsometry measurements and refractive indices serve as new reference values, supported by an excellent quality of fit (all $R^2 > 0.994$). As expected, glycerol showed the thickest roughness of 4.1 nm. The difference of the n values compared to the simultaneous transmission fit is minimal, as discussed earlier, PDMS has the highest with Δ n = 0.0025, which does not show up on the optical simulations as seen in the following chapter.

Table 4.1: Refractive index from Semilab ellipsometry measurement at 632 nm, compared to literature values and simultaneous transmission fit, showing minimal deviation. Cauchy model parameters A, B and the thickness of the surface/roughness interface layer, as well as the quality of fit R^2, which showed good fitting (green colour) of the simulated and measured values. The yellow colour highlights a higher difference compared to others, the green colour a lower difference.

Sample	n (632.8 nm)	Literature n (632.8 nm)	Delta n literature	Delta n simultaneous	R2	A	B	thicknes layer (nm)
Water	1.3377	1.3317	0.006	0.0002	0.9867	1.32888	0.003487	2.3
Glycerol	1.4718	1.4707	0.005	0.0006	0.9954	1.46175	0.004015	4.1
PDMS	1.4080	1.4055	0.009	0.0025	0.9762	1.39713	0.004374	0.4
Shell diala	1.4573	no data	-	0.0012	0.9948	1.44639	0.004376	1.8
Glycol	1.4116	1.4315	0.042	0.0015	0.9784	1.40077	0.004327	2.6
Mivolt	1.4569	no data	-	0.0009	0.9950	1.44592	0.004392	1.4
Midel 7131	1.4539	no data	-	0.0002	0.9940	1.44298	0.004356	1.6

For the liquids already present in literature showed expected results, the new liquids are especially interesting as they have never been characterised before. All three, Shell, Midel and Mivolt, show relatively high refractive index values, which is good for minimising the reflection, only being surpassed by glycerol as seen in Figure 4.21. The values of Shell and Mivolt almost seem to overlap, making it difficult to spot the curve of Shell. The values of Midel are quite close to them, which makes sense because it is also a synthetic ester like Mivolt. In the following section, the results of the extinction coefficient k will be presented.

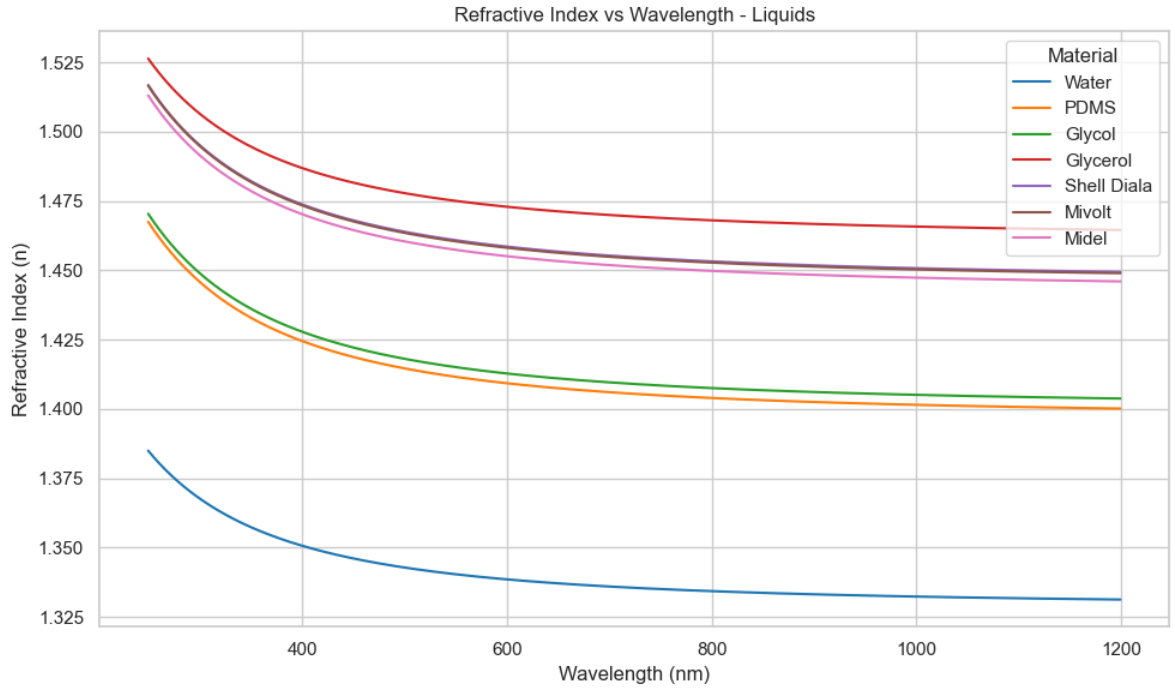

Figure 4.21: Refractive index (n) values obtained by ellipsometry at Semilab of all 7 liquids

4.3.2. Extinction coefficient (k) and transmission of liquids

Here, the results of the transmission measurements are displayed, and the process of obtaining the extinction values k is visualised. First, the process is displayed for water, followed by the end result of the other liquids. Finally, the cleanliness of the cuvettes is discussed, followed by the dual cuvette method k1 and the reference beam method k2.

Computing k values from transmittance

The transmission data can then be used to calculate the extinction coefficient (k), as described by the steps in the methodology. The procedure from processing from transmission to extinction coefficient will be performed on each liquid, but will be shown in more detail for water only to explain the process.

1. Normalise and correct transmission datasets

The method and process are explained in detail for water as an example. For water (and each other liquid), there are 9 transmission datasets (3 for each cuvette, 5 mm, 10 mm and reference beam method) which are first normalised and then corrected if needed. The normalisation is performed at each wavelength with the following equation:

$$T_{normalised}(\lambda) = \frac{T(\lambda)}{T_{100\%reference}(\lambda)} * 100\% \tag{4.5}$$

where $T(\lambda)$ is the measured transmittance at wavelength (λ) and $T_{100\%reference}(\lambda)$ is the 100% transmission measurements performed before each measurement without any sample to get a baseline of 100 % transmission (referred to as the 100% reference scan). Each liquid has its own 100 % reference measurements; for water, this is displayed in Figure 4.22, and has a standard and max deviation of 0.18 % and 0.75 %, respectively. As can be seen on the graph, the values show little deviation and therefore the normalisation has a minimal effect.

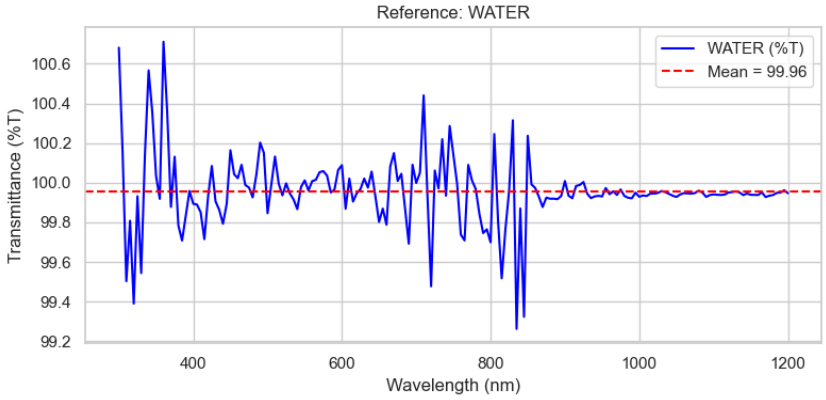

Figure 4.22: 100 % reference graph water used for normalising

For all liquids, besides water, a correction was applied for potential dirt on the walls of the cuvettes on the k1 method (not possible for k2). First, the two cuvettes were measured (air inside) when they came out of the packaging to establish a baseline ($T_{basline}(\lambda)$), which is visualised in Figure 4.23. After each cleaning protocol, the cuvettes are measured again ($T_{cleaning}(\lambda)$), visualised in Figure 4.24 for PDMS, which had the largest difference (2%) and was therefore cleaned multiple times (2 times for 10 mm and 3 times for 5 mm, as can be seen in the graph for the different curves). PDMS was by far the worst case and is therefore shown, all other liquids cleaning files showed significantly less (less than 1%) difference between the 5 and 10 mm cuvette. The absolute difference ($T_{Absolute\ difference}(\lambda)$) between the transmission values is computed according to the following formula.

$$T_{Absolute\ difference}(\lambda) = T_{basline}(\lambda) - T_{cleaning}(\lambda) \tag{4.6}$$

This $T_{Absolute\ difference}(\lambda)$ is then added to the transmission values of the liquid to compensate for the potential dirt on the cuvette.

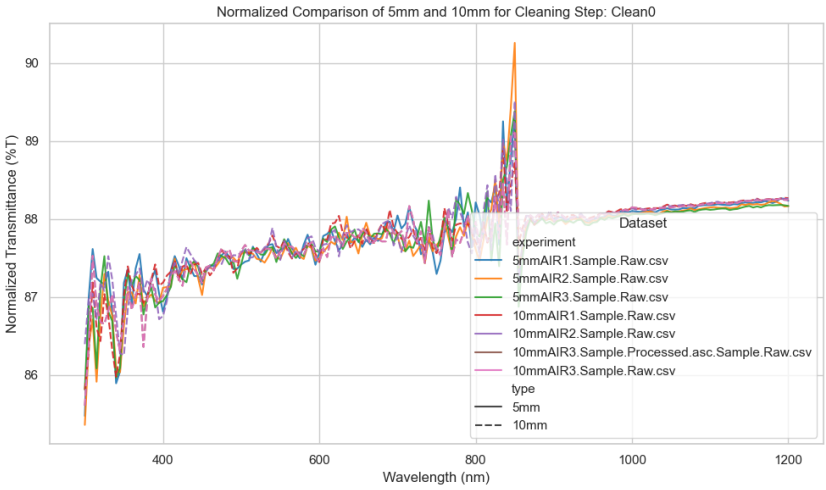

Figure 4.23: Baseline transmittance ($T_{basline}(\lambda)$) for the 5 and 10 mm cuvettes

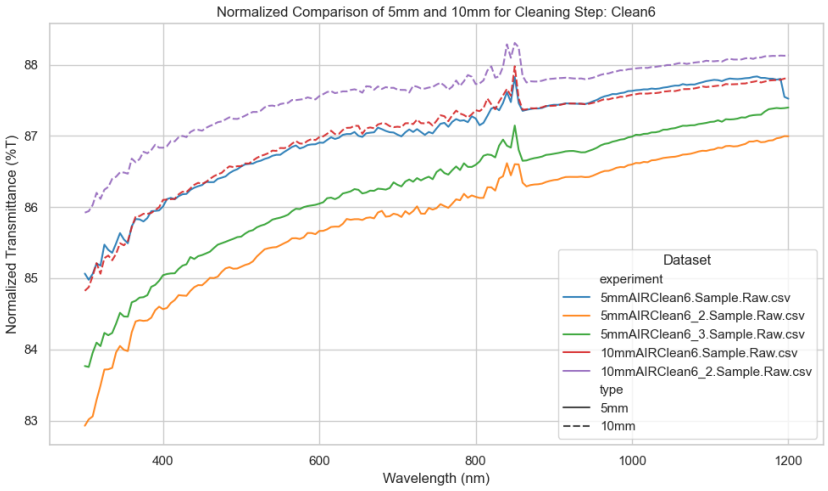

Figure 4.24: Transmission ($T_{cleaning}(\lambda)$) after cleaning protocol before the first PDMS measurements

Relative correction was also used and gave similar results; therefore, the absolute correction was eventually applied. As mentioned before, the dirt was minimal and only showed a maximum of 1% deviation from the baseline, except for PDMS, which was therefore measured again. When looking at the corrected PDMS measurement (Figure 4.25) and the second PDMS measurement (Figure 4.34), they align well, as can be seen when comparing the graphs, giving confidence in the correction method.

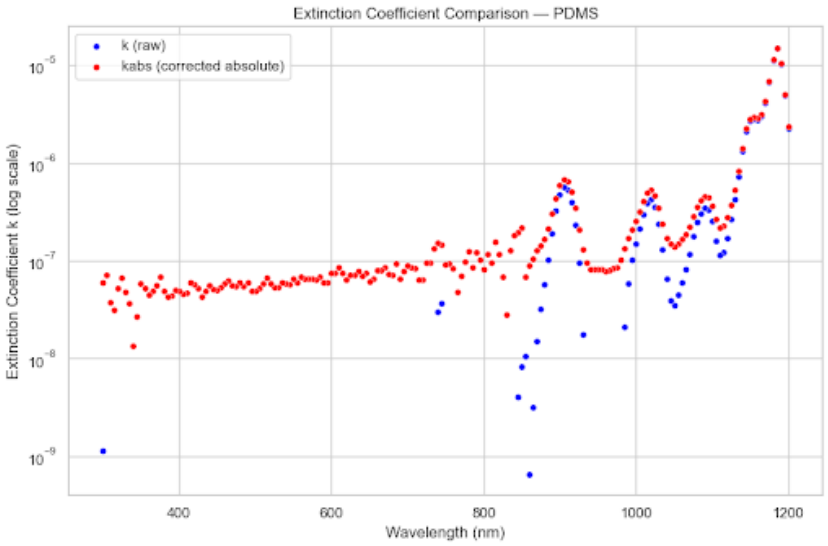

Figure 4.25: Extinction coefficient k of PDMS first measurement, plotted together with k abs corrected for the cleanliness of the cuvette

2. Mean and standard deviation measurements

After normalising and correcting, the standard deviation and maximum deviation from the mean are checked for the three measurements of each cuvette (5 and 10 mm). Water 5 mm cuvette has a standard and max deviation of 0.16% (highest STD of all liquids and cuvettes) and 1.33%, 10 mm cuvette 0.10% and 1.15%, respectively. They seem to match well with other uncertainty values reported around the 0.1% to 0.5% [168], [180].

The mean is taken from the three transmission measurements for each liquid and cuvette/method (5 mm, 10 mm, and reference beam). This reduces the influence of random noise and measurement variation, ensuring a more robust dataset for calculating the extinction coefficient. The mean of each experiment is shown in Figure 4.26. The 5 and 10 mm values overlap for a large part (300 - 700

nm) because there is almost no absorption in this region. This can also be seen in the reference beam method, which touches the 100% line and sometimes goes over. This can be explained by the earlier-mentioned effect of the ultra-low absorption of water in this region, which causes the difference in transmittance between the 5 and 10 mm water column to be nil, leading to experimental noise and potential dirt on the cuvette wall being dominant. This is also observed in other liquids around the same region, giving unphysical k data, which is why a confidence threshold is applied in the next section.

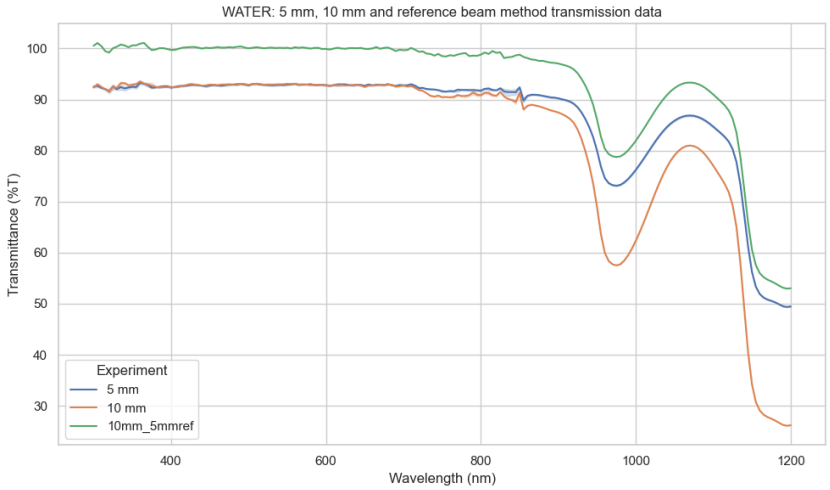

Figure 4.26: Transmission graph of water for the 5 mm, 10 mm cuvette and reference beam method

3. Compute extinction coefficient k1 and k2

As explained in the methodology, the k1 values are computed using the following equation:

$$k1(\lambda) = \frac{\lambda}{4\pi} \frac{ln(T_1/T_2)}{z_2 - z_1} \tag{4.7}$$

The k2 values are computed by using the following equation:

$$k2(\lambda) = \frac{\lambda \ln(T)}{4\pi x} \tag{4.8}$$

They are both visualised (with other literature values) in Figure 4.28, which will be commented on in the following step.

4. Calculate signal-to-noise ratio (SNR) threshold

In spectral regions (300 - 800 nm) with ultra-low absorption, minor noise dominates, and results can not be trusted. To find out where this cut-off happens for most liquids, SNR is computed in order to find an appropriate threshold to filter out unreliable data. Values below the threshold are replaced by the threshold value to avoid underestimating absorption (values are increased, creating a more conservative approach). Multiple threshold values for water are tested and compared in the optical simulations to see the different effects they have on the modelling in the next step.

SNR is defined by the Equation 4.9 and quantified by using the T table to get a desired confidence interval [181]–[183]. This was set at SNR = 10, giving a confidence of 99% which aligns well with the areas where more distortion is seen [181]–[183].

$$SNR(\lambda) = \frac{T_{sample\ mean}(\lambda) - T_{baseline/hypothesis}(\lambda)}{\sigma_{basline}} \tag{4.9}$$

where $T_{sample\ mean}(\lambda)$ is the mean of the 3 measurements of the sample, $T_{baseline/hypothesis}$ is the 100% reference measurement and $\sigma_{basline}$ is the standard deviation of the reference measurement.

This allows us to make a mask over the measurements to see which areas can be trusted and which can not. This is visualised in Figure 4.27, where it can be seen that values in the ultra-low absorption region (300 - 800 nm) are showing less trusted results as predicted. This trend is also seen for other liquids. Using the same equation, it is possible to calculate a maximum $T_{sample\ mean}(\lambda)$ which can be trusted. This was calculated to be 99.31% transmission, which corresponds to $k \approx 5 * 10^{-8}$. The threshold was set to this value and compared to other threshold values to see the effects on the optical simulations.

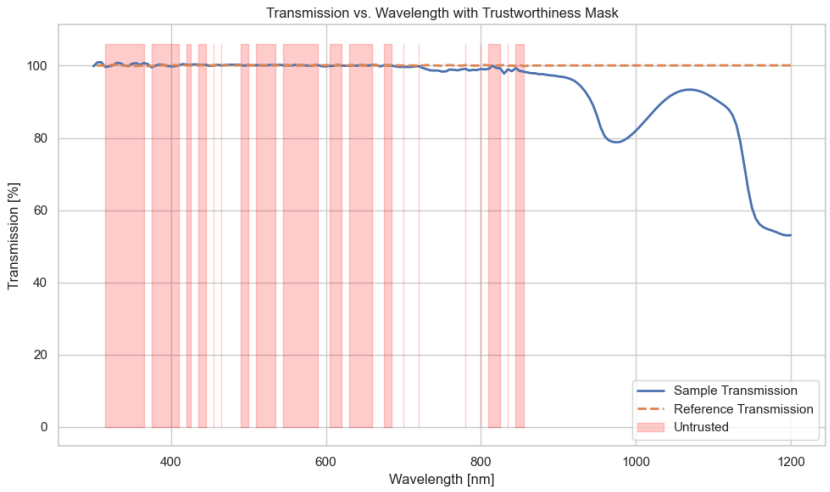

Figure 4.27: SNR mask for transmission values of water showing which values can be trusted, roughly translating to a threshold at 99.31%

5. Effect of threshold on optical simulations

To see the effect the threshold has on the optical simulations in GenPro4, the effect was tested on a PERC cell inside a solar module with water as encapsulation (thickness = 0.45 mm) using 5 different values for the threshold ($k = 3 * 10^{-7},\ 1 * 10^{-7},\ 5 * 10^{-8},\ 1 * 10^{-8},\ 0$). The effects on the photocurrent absorbed by the water encapsulation and generated by the absorber layer are noted for each threshold value in Table 4.2. Looking at the differences in photocurrent generated in the Si wafer compared to the k = 0 (no) threshold, the effect of the threshold is minimal. The calculated threshold of $5 * 10^{-8}$ is appropriate since it has a negligible difference (0.009 mA/cm^2) with the 0 threshold, and also an insignificant difference with a more conservative threshold such as $1 * 10^{-7}$ (0.021 mA/cm^2). The effect of this threshold will be taken into account when analysing the results of the optical simulations; values could be 0.01 mA/cm^2 higher or lower due to the threshold being chosen. Water is most affected by the threshold (most values below $5 * 10^{-8}$) compared to other liquids, thus concluding that the simulation effect of other liquids is lower.

Threshold (k)	$3 * 10^{-7}$	$1 * 10^{-7}$	$5 * 10^{-8}$	$1 * 10^{-8}$	**0**
Absorption Water (mA/cm^2)	0.525	0.470	0.458	0.449	0.448
absorption Si wafer (mA/cm^2)	40.765	40.818	40.829	40.836	40.838
Difference to 0 threshold (mA/cm^2)	0.074	0.021	0.009	0.002	0

Table 4.2: Effect of different threshold values on photocurrent generated in optical simulations with water encapsulation (thickness = 0.45 mm)

6. Compare k1, k2 and literature values

The two k datasets (k_1 and k_2) are plotted together and compared. This allows visual validation of consistency between methods. Where available, literature data for k is added to assess accuracy. For water, two literature values are used: Han et al [97], which measured water using a Lambda and dual cuvette method, and Segelstein [179], which is the benchmark for the complex refractive index of

water. As seen in the graph, there is good agreement between both methods and the literature values till $k \approx 5 * 10^{-8}$, where values deviate more from the Segelstein line, which is also observed in the Han et al. water values. Similar trends can be found in the other liquids, also seeing a growing difference in k1 and k2 values below this value, justifying the threshold set here.

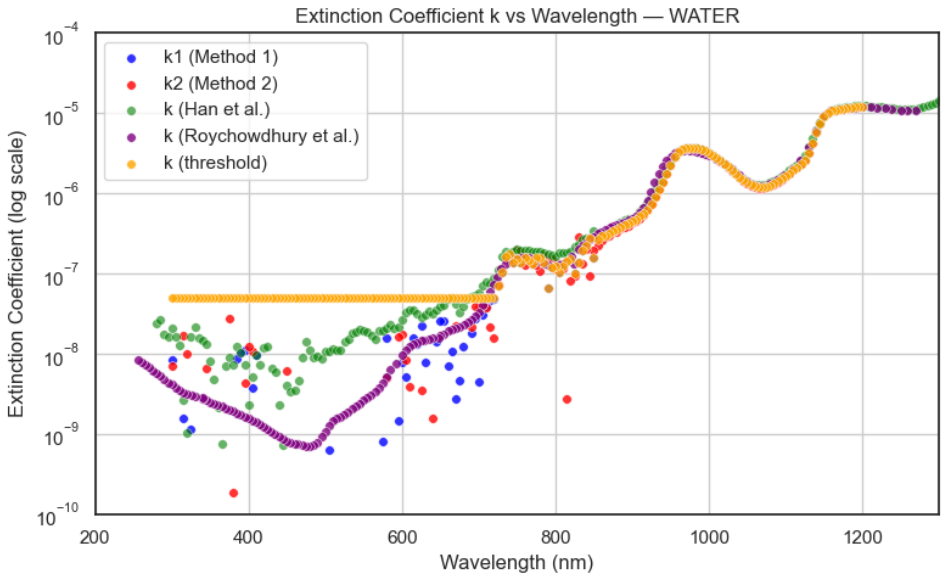

Figure 4.28: Extinction coefficient k for water from method k1 and k2, and k (threshold) from the applied threshold, literature values from Han et al. [97] and Segelstein [179]

7. Produce nk file

The eventual values used in GenPro for water are shown in Figure 4.28 called k (threshold). These values are combined with the n values measured by Semilab on the wavelength steps of the k/transmission values (300 - 1200 nm, 5 nm step size) to produce the needed nk files for optical modelling in GenPro.

Glycerol

Applying the same workflow as described for water to glycerol, and all other liquids that follow, yields the following results and observations.

Glycerol's 100 % reference scan was stable (Min = 99.26 %T, Max = 100.71 %T, Mean = 99.96 %T, Std Dev = 0.18 %T, Max Dev = 0.75 %T), and cuvette□cleaning corrections were below 0.1 % for both 5 mm and 10 mm cuvette so the correction shows little difference to the original. Repeatability across the three measurements remains excellent with a STD of 1.39% T and maximum deviation of 2.77%T (highest of all liquids) around the wavelength 860 nm, which can be explained by the added noise due to the switching of the Lambda detector.

After averaging and applying the correction for cuvette cleanliness, the k1 and k2 values are computed, as well as the kabs corrected values (for k1 corrected), which take the cuvette cleanliness into account as seen in Figure 4.29. k1 is slightly higher than k2 due to a marginally cleaner 5 mm cuvette, though the difference is negligible. Notably, glycerol exhibited higher absorption than expected (compared to literature values from Han et al.), possibly due to two reasons: (i) water content and (ii) trapped air bubbles. Han et al. do not mention the purity of the glycerol, but it is expected that it is mixed with water 5-10%, which is often done and allows for easier handling (less viscous). Because it is so viscous, it could be that minuscule air bubbles are trapped, which cannot be spotted with the eye but slightly decrease the transmission. During experiments, it was attempted to remove these air bubbles (if present at all) by placing the cuvette filled with glycerol in a vacuum chamber for a while, which could potentially suck out the air bubbles. Transmission was measured before and after this process, which showed no difference could mean either that there were no air bubbles to begin with or the vacuum chamber was unsuccessful in removing the air bubbles. Glycerol is not affected by the SNR threshold.

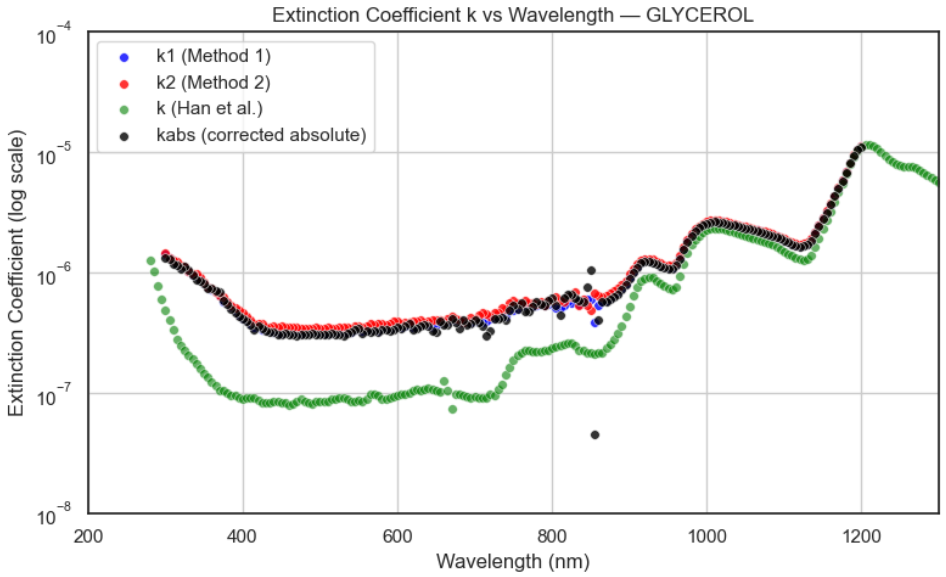

Figure 4.29: Extinction coefficient k for glycerol from method k1, k2, kabs corrected for cuvette cleanliness and k (threshold) from the applied threshold, literature values from Han et al. [97]

Glycol

Glycol's 100 % reference scan was stable (Min = 99.86 %T, Max = 100.28 %T, Mean = 100.07 %T, Std Dev = 0.05 %T, Max Dev = 0.21 %T), and no cuvette□cleaning corrections were applied. Repeatability across the three measurements remains excellent with a STD of 0.28 %T and maximum deviation of 0.55 %T around 855 nm, which can be explained by the added noise due to the Lambda detector switching.

After averaging, the k1 and k2 values are computed, visualised with the literature values from Han et al. [97] and Shah et al. [130], which can be seen in Figure 4.30. k2 follows k1 closely until entering the ultra-transparent region, where more distortion appears; k1 is slightly lower than k2, though the difference is small. There are no cleaning files for glycol (which is also why there is no kabs curve), which could have explained the small downward shift, as it does in other liquids for this region. Glycol's absorption curve matches Han et al.'s literature shape but is shifted downward, possibly due to additives in the glycol (not pure glycol was used). Glycol is slightly affected by the SNR threshold, aligning better with literature values as seen in Figure 4.30.

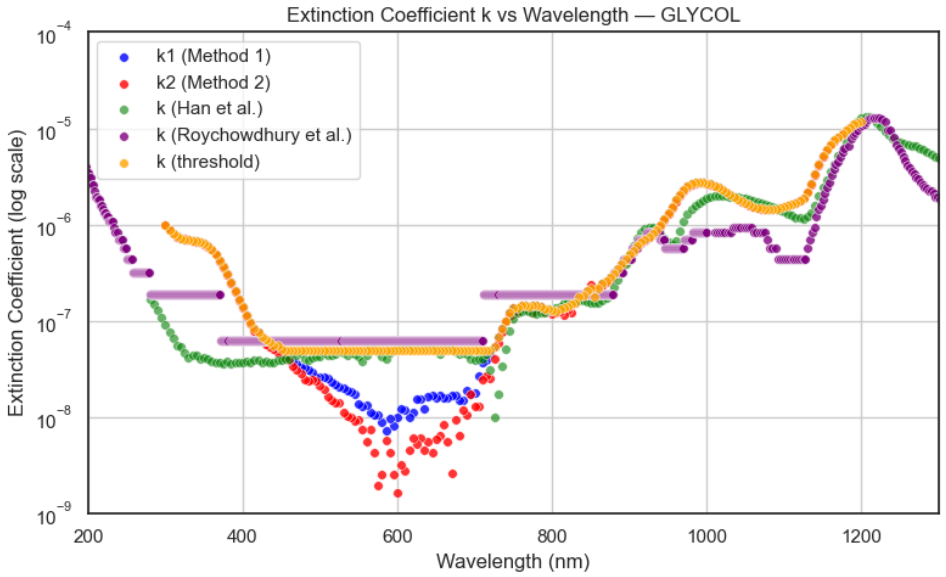

Figure 4.30: Extinction coefficient k for glycol from methods k1, k2, compared to Han et al. [97] and Shah et al. [130]

Mivolt

Mivolt's 100 % reference scan was stable (Min = 99.86 %T, Max = 100.28 %T, Mean = 100.07 %T, Std Dev = 0.05 %T, Max Dev = 0.21 %T). Repeatability across the three measurements per cuvette was again good, with a STD of 0.22 %T and a maximum deviation of 0.43 %T occurring around 850 nm (switching of Lambda detector).

There are no literature values for Mivolt, with almost all data points positive or non-zero and showing a smooth trend. Overall, the values are low and comparable to the other liquids documented in literature, which is a good sign for low absorption in the optical simulations. The cuvettes had a minor cleanliness difference (around 0.3%), which was not large enough to compromise the k1 method. As a result, all three methods, k1, k2, and Kabs, yield sensible values. After applying the correction, the extinction coefficients shifted slightly upward, which aligns with the expected impact of removing the small cleanliness difference.

Interestingly, in the ultra-transparent region, the k2 method produces slightly higher values than k1, which is contrary to most other liquids, where k2 tends to follow a lower path. This highlights the difficulty in drawing meaningful trends in the ultra-transparent regime where extinction coefficients drop below $5 * 10^{-8}$ and measurement uncertainty becomes more dominant. The SNR threshold has a minor effect on Mivolt as seen in the small difference between the kabs and k (threshold) curves.

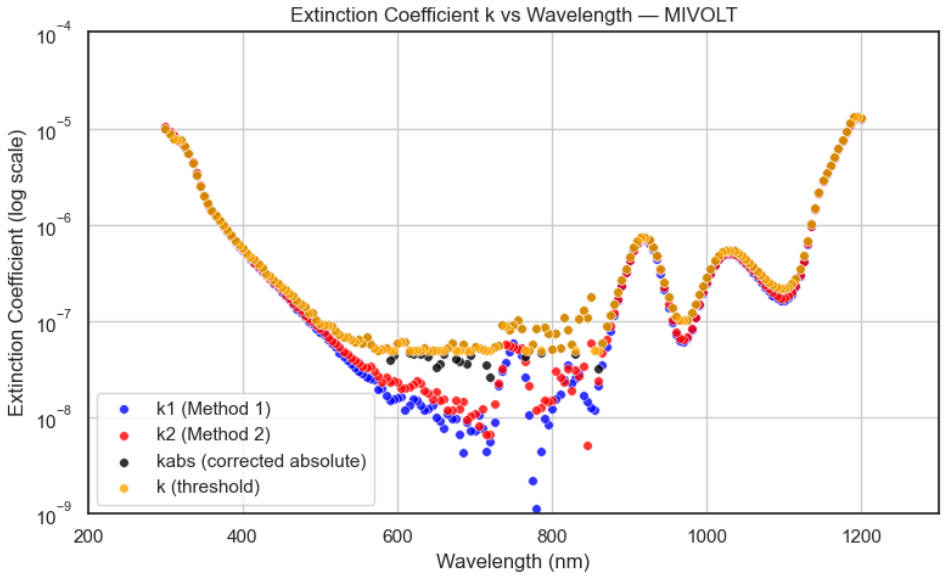

Figure 4.31: Extinction coefficient k for Mivolt from method k1, k2, kabs corrected for cuvette cleanliness and k (threshold) from the applied threshold

Midel

Midel's 100 % reference scan was stable (Min = 99.57 %T, Max = 100.79 %T, Mean = 100.00 %T, Std Dev = 0.08 %T, Max Dev = 0.79 %T), and cuvette□cleaning corrections were larger up to 1%, with the 10 mm cell notably dirtier than the 5 mm. Repeatability remains high with a STD of 0.24 %T and max deviation of 0.48 %T at 300 nm (instead of 860 nm, which also explains the significantly lower values).

After averaging and applying cleanliness corrections, k1 and k2 were computed (and kabs corrected) as shown in Figure 4.32 (no literature values are present for Midel). Midel is slightly yellowish when seen in bulk, this can be explained by the bump in absorption around 450 nm, which corresponds to blue light, creating a yellow colour because red, green and yellow are absorbed less. Interestingly, the extinction coefficient is low and comparable to the other liquids, meaning that a slightly yellow colour (125 hazen) could still be usable, as will be determined in the following chapter. This is an important finding as it could open the door to more liquids that may not appear perfectly clear, such as plant-based oils, for example.

The larger dirt-induced difference between the 5 and 10 mm cuvette makes uncorrected k1 unreliable below 10^{-7}, whereas k2 seems to partly cancel this by taking into account the dirt on the 5 mm reference cuvette. Once corrected, k1 follows a straight-line trend similar to other liquids, and the difference between k2 and corrected k2 is $\approx 1 \times 10^{-7}$, matching the 1 % cleanliness difference (86.5% vs. 87.5%) of the 5 and 10 mm cuvette. Midel is unaffected by the SNR threshold.

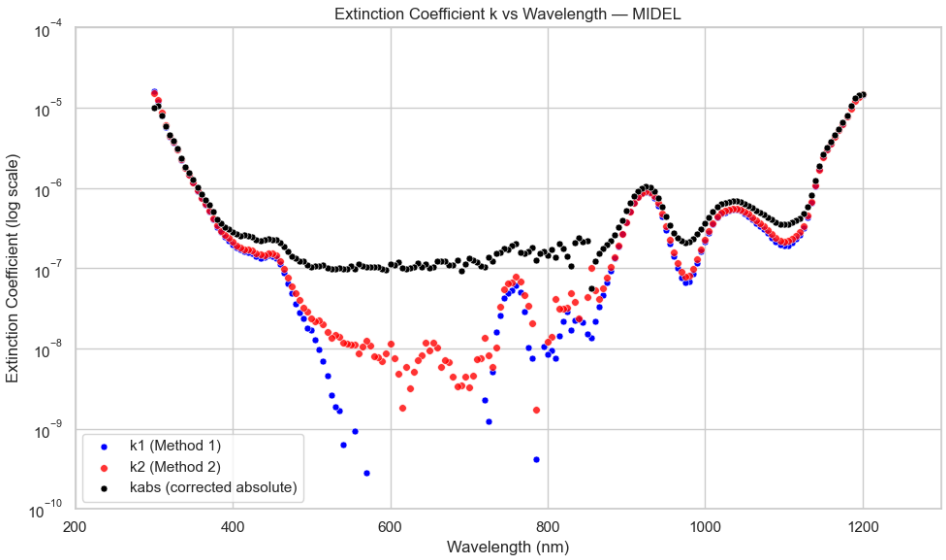

Figure 4.32: Extinction coefficient k for Midel from methods k1, k2, and kabs

Shell Diala

Shell Diala's 100 % reference scan showed good stability (Min = 99.65 %T, Max = 100.15 %T, Mean = 99.98 %T, Std Dev = 0.06 %T, Max Dev = 0.33 %T). Repeatability across the three measurements per cuvette was strong, with a STD of 0.26 %T and a maximum deviation of 0.51 %T around 850 nm (Lambda detector switching).

Also, Shell does not have any literature values, but is also slightly yellowish in bulk, again possible to explain by its step rise in absorption around 450 nm (absorbing blue, giving its yellow colour). As also mentioned for Midel, Shell Diala displays low extinction coefficient values, supporting the idea that slightly yellowish (ASTM D1500 0.5) liquids could be usable.

Because the cleanliness of the 5 and 10 mm cuvettes is already close to each other (max 0.2%), the k2 method, which subtracts the 5 mm dirt, yields lower extinction values than the k1 method, as the influence of residual dirt is partly removed as seen in Figure 4.33. This difference persists until the ultra-transparent region (600–800 nm) is reached, where measurement uncertainties increase and the values become less reliable.

Despite the generally clean cuvettes, a small residual cleanliness difference still exists, and this has a magnified effect in the ultra-transparent region. Correcting for cuvette cleanliness in the Kabs method leads to a shift upward in the extinction coefficient values. This is because the 5 mm cuvette was slightly dirtier than the 10 mm one, artificially reducing the observed transmission difference and thus yielding lower extinction coefficients. Removing this discrepancy results in a more accurate, slightly higher extinction curve that is consistent with expectations and follows a smoother trajectory. Shell is slightly affected by the SNR threshold and shifted further up as seen in Figure 4.33.

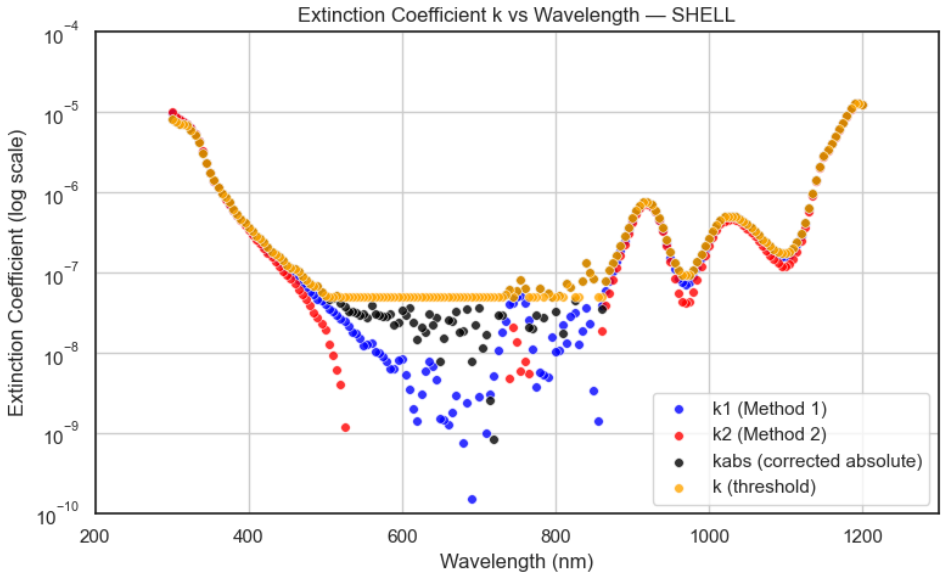

Figure 4.33: Extinction coefficient k for Shell Diala from method k1, k2, Kabs corrected for cuvette cleanliness and k (threshold) from the applied threshold

PDMS

PDMS is the only liquid measured twice because the cleanliness of the cuvette distorts the measurements too much, although the correction aligns well with the second measurement, giving more confidence in the cuvette dirt correction, as seen in Figure 4.34 The 100 % reference scan for PDMS showed good stability (Min = 99.53%T, Max = 100.27%T, Mean = 100.03%T, Std Dev = 0.06%T, Max Dev = 0.49%T). Repeatability across the three measurements per cuvette was good, with a maximum standard deviation of 0.16 %T and a maximum deviation of 0.29 %T at 1195 nm.

PDMS is one of the most transparent liquids tested, and the initial measurement was hindered by a large mismatch (max 2%) in cleanliness between the 5 and 10 mm cuvettes, as displayed in Figure 4.25. This resulted in many unusable values, prompting a second measurement. In the second set, the cleanliness of the cuvettes was more closely aligned (max 0.1%), which improved the data quality and cuvette correction gave similar results as expected, visualised in Figure 4.34. The extinction coefficients k1 and k2 follow a consistent and expected trend, similar to literature values. Roychowdhury et al. [137] have many missing values due to the ultra-low absorption of PDMS and potentially because of the reach of the ellipsometry transmission method. Han et al. [97] curves show a similar curve but slightly shifted down, which could be explained by the fact that a different PDMS is used. since the difference is rather small. It is interesting to note that PDMS has the lowest k values in the UV region, which has both positive and negative effects. It could boost its photocurrent as it allows more light through, but the solar cells can also be damaged by UV radiation, which means blocking the UV rays can be beneficial. Literature values have even lower k values deeper into the UV region.

The k2 values show a slight downward shift relative to the k1 values, which is consistent with the 5 mm cuvette being slightly dirtier than the 10 mm cuvette. However, because the cleanliness difference was small in the second measurement, this shift remains minor, and the overall trends remain reliable.

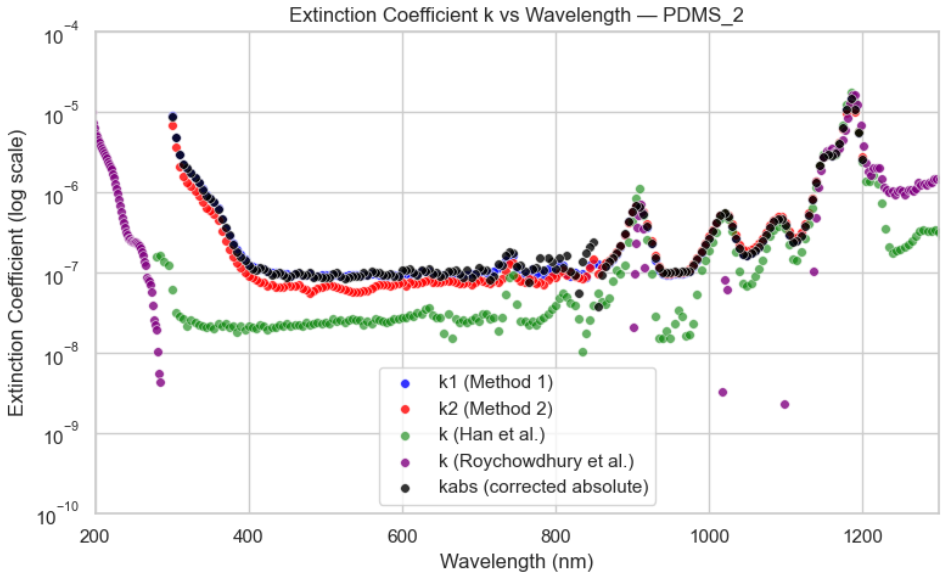

Figure 4.34: Extinction coefficient k for PDMS from method k1, k2, and Kabs corrected for cuvette cleanliness, compared to Han et al. [97] and Roychowdhury et al. [137]

Discussion extinction coefficient

The results, in general, show good agreement with the literature and make physical sense, giving confidence that they display reality fairly well. However, as seen in multiple liquids, more distortion is visible in the highly transparent region of 300 - 800 nm, where values drop below the $k = 10^{-7}$ and the absorption of light by the liquid is extremely small. Consequently, the measurement becomes highly sensitive to minor experimental flaws, causing divergent effects to be observed in different measurements and liquids. Some hypotheses will be discussed which try to explain the differences observed. It is important to note that it is difficult to draw hard conclusions because separate mechanisms play alternating dominant and subordinate roles between measurements.

Three main mechanisms are described to explain the differences between the k1 and k2 values per liquid and in-between liquids, as well as the general difference in k values in between liquids. (i) General experimental uncertainty; instrumental noise, calibration and measuring limits, systemic bias, observer inconsistencies, environmental deviations, among others, (ii) cleanliness of cuvettes, and (iii) fundamental differences between k1 and k2 methods. The last two mechanisms are further discussed as general experimental uncertainty will be present in all experiments; it is only noted to acknowledge its influence. As for the k1 and k2 method, it is important to note that the difference might look large on the log scale graphs, but they are in the order of k = 10^{-8} and have an insignificant effect on the optical simulations as seen with the various threshold values.

Cleanliness of the cuvettes

The cleanliness of the cuvettes plays a general role for all liquids and a specific role between k1 and k2 commented on in the following section. For all cuvettes, the 5 mm cuvette is dirtier, resulting in a lower overall transmittance in the 5 mm cuvette measurements. The lower transmittance is either caused by more absorption in the sample or absorption by the dirt on the cuvette; impossible to distinguish between them, and it is attributed towards more absorption by the 5 mm liquid sample. Higher ”absorption” or lower transmittance by the 5 mm liquid sample compared to the 10 mm sample results in a smaller difference between the transmittance values, leading to lower k values, which follows from Equation 4.4. As the extinction coefficient is coming closer to 0, the material is almost non-absorbing, and the cleanliness of the cuvette role becomes more dominant. This eventually causes the transmittance of the 5 mm to go below the 10 mm cuvette ($T_1 < T_2$), which gives unphysical results as the 5 mm sample cannot absorb more light than the 10 mm sample. This is seen in the graphs of Figure 4.25, Figure 4.28, Figure 4.32 and Figure 4.33, where gaps appear in the curves because of these unphysical results. No longer the difference in absorption of the liquid sample in the 5 and 10 mm cuvette is

measured, but the difference in cleanliness of the 5 and 10 mm cuvette.

This is evident when looking at the differences in the cleanliness of the 5 and 10 cuvettes per liquid. When the cleanliness is further apart (Midel, Mivolt, shell and PMDS1 (first measurement PDMS)), the graphs show more gaps. This hypothesis is strengthened by the fact that the correction of the dirt on the cuvette (kabs curve), shifts the values back up, nicely visualised in Figure 4.25 and the other graphs. This gave confidence in the approach of using the corrected kabs values. In future experiments, this problem could also be reduced by using larger optical path lengths for the cuvettes, such as 25 - 50 mm, which helps the absorption effect to stay the dominant reason for lower transmittance values measured.

Comparison k1 and k2 Methods

The k1 (dual cuvette) and k2 (reference beam) methods are designed to isolate the absorption of the liquid from the reflective and absorption losses arising from using cuvettes. However, they have some fundamental differences related to the exponential nature of light absorption and the handling of the cleanliness of the cuvettes.

The k1 method respects the exponential nature of light absorption and allows for correcting the data for cleanliness between the 5 and 10 mm cuvette, because each cuvette is measured independently. The k2 method subtracts the transmittance, which leads to a false linear assumption of light absorption. It automatically corrects for some of the dirt on the cuvettes (dirt of a 5 mm cuvette in the reference beam is taken into account). However. This assumes the 5 and 10 mm cuvettes to be identical, with identical cleanliness, which is not always the case, leading to a systematic error because the 5 mm cuvette is dirtier than the 10 mm cuvette. This can lead to the k2 values being lower because the difference between T_1 and T_2 is smaller. This is seen in the Glycol Figure 4.30 and Shell Diala Figure 4.33 graphs, but the Mivolt and Midel have lower k1 in the ultra-transparent region, which highlights again that drawing hard conclusions in this region remains difficult.

Although differences in the k1 and k2 methods exist, they are barely significant. The linear assumption of k2 does not seem that far from reality for extremely low k values and such short distances (exponential behaviour looks linear). The differences in cuvette cleanliness are small, and the effect of the automatic correction performed by the k2 method is therefore also small, as seen by the fact that k2 is not always lower than k1.

The k2 reference beam method offers a fast and easy measurement approach which delivers trustworthy results down to k = 10^{-7}. When used, it is important to keep its bias in mind, especially if there are questions about the cleanliness difference between cuvettes; if this is large, the k2 method becomes less reliable. Ultimately, the values of the k1 method with cleanliness correction (and threshold) were chosen as they allowed for correction and gave a more conservative approach in the optical modelling.

4.4. Conclusion

The primary goal of this chapter was to address the critical lack of optical data for potential liquid encapsulants by measuring the complex refractive index (n and k) of seven selected liquids over the solar spectrum (300 - 1200 nm). Through a hybrid approach combining spectroscopic ellipsometry and spectrophotometry, this work has successfully generated a complete and reliable dataset essential for accurate optical modelling.

For the refractive index (n), a specialised spectroscopic ellipsometer set-up from Semilab proved effective. The use of a 2-term Cauchy model yielded excellent fits ($R^2 > 0.97$) for all liquids. The results showed strong agreement with published literature for water, glycerol, and PDMS, validating the measurement methodology. For Shell Diala, Mivolt, and Midel 7131, for which no data were available, this work provides the first reliable reference values. The minimal impact of a simultaneous nk-fit on the n-values further justified the decoupled measurement approach, taking the dependent nature of nk into account.

Determining the extinction coefficient (k) was done by transmission measurements using a Lambda spectrophotometer; two methods were tried. The dual-cuvette (k1) transmission method, combined with careful cuvette cleaning protocols and corrections, proved to be the most robust technique. It successfully accounted for the complex reflection and absorption effects introduced by the cuvette, producing k values that aligned well with the literature. A SNR analysis established a confidence threshold at $k \approx 5 * 10^{-8}$, acknowledging that below this level, measurement noise and minor differences in cuvette cleanliness become the dominant factors over the liquid's absorption. The effect this threshold can have on the optical simulations was checked and is calculated to stay below 0.01 mA/cm^2 (compared to not setting the threshold), which is acceptable.

This chapter demonstrated that all tested liquids possess excellent optical transparency, even slightly yellowish liquids like Shell Diala and Midel, with subtle but important differences in their absorption profiles. The final output, a complete set of nk-files for all seven liquids, provides the crucial and previously unavailable data necessary for the detailed optical simulations presented in the following chapter. The data, n and k values, for all liquids are presented in Table B.2 in the appendix (additional data can be made available on request).

5

Optical model GenPro

To determine the difference in performance of liquid encapsulation compared to standard EVA and air, it is possible to perform optical modelling using the optical properties of the materials. In the previous chapter, the complex refractive index of 7 potential liquids was determined; in this chapter, this data will be used in the topical simulations of solar modules with liquid encapsulation. Therefore, the theory of optical modelling will shortly be explained, followed by the software used, GenPro 4. Then, the methodology will be explained with the set-up of the model, solar cell technologies used, different configurations modelled and the ARC effect on simulations. After which, the results of the simulations will be shown and discussed, identifying interesting trends and selecting the most promising liquids. These liquids will then be further optimised to see what kind of maximal performance can be achieved. Finally, these will be used in real-life modelling scenarios using the PVMD Toolbox to evaluate their expected performance in the field, followed by the conclusion.

5.1. Optical modelling theory and methods

Optical modelling is crucial in understanding the energy production and losses in solar cells, providing important preliminary information about the device performance before performing experiments on it. The optical simulations produce several useful outputs: the absorption profile per wavelength and layer, the photocurrent generated or lost in each layer, and the fractions of light that are transmitted, reflected, or absorbed. These optical phenomena are fundamental to the solar cell performance.

When light is incident on a photovoltaic device, part of it is reflected at the surface, part is transmitted through the device, and the remainder is absorbed within the various layers. Only the absorbed photons in the Si absorber have the potential to generate charge carriers (electron-hole pairs), which may contribute to electrical current if they are successfully collected.

The amount of light absorbed in each layer is visualised in the absorption profile plot, such as shown in Figure 5.5. However, not every absorbed photon leads to a collected electron. This is where the concept of External Quantum Efficiency (EQE) becomes important. EQE is defined as the ratio of the number of electrons collected to the number of photons incident at a specific wavelength:

$$\mathrm{EQE}(\lambda) = \frac{\text{electrons collected}}{\text{photons incident at } \lambda} \tag{5.1}$$

In contrast, the absorption profile merely shows the fraction of light absorbed per wavelength, without accounting for electrical losses such as recombination. Thus, EQE includes both optical and electrical effects, while absorption alone does not.

In simulations using GenPro, the EQE is typically approximated as equal to the absorption in the active (photo-generating) layer [184]. This means it assumes that every absorbed photon generates and contributes an electron to the current—an ideal case with no recombination or transport losses.

Based on the EQE and the incident photon flux under the AM1.5 solar spectrum, the short-circuit current density J_{sc}, a key performance metric for solar cells, can be calculated as follows:

$$J_{\mathrm{sc}} = -q \int_{\lambda_1}^{\lambda_2} \mathrm{EQE}(\lambda)\, \Phi_{\mathrm{ph},\lambda}^{\mathrm{AM1.5}}\, \mathrm{d}\lambda \tag{5.2}$$

where q is the elementary charge, $\mathrm{EQE}(\lambda)$ is the external quantum efficiency at wavelength λ, $\Phi_{\mathrm{ph},\lambda}^{\mathrm{AM1.5}}$ is the spectral photon flux density under the AM1.5 standard spectrum, λ_1 and λ_2 define the integration bounds, typically from 300 - 1200 nm for silicon-based devices.

This equation quantifies the total current density generated per unit area under standard illumination, assuming that each collected carrier contributes one unit of charge. This parameter is used in GenPro and will mainly be used in the following sections and simulations to show the performance of the cell with different encapsulation materials.

5.1.1. GenPro4

Accurate optical modelling is essential to evaluate and optimise solar module performance. Several optical software options were considered, such as CROWN and PV Lighthouse, among others. GenPro4 was selected for its fast and accurate simulations and its in-house availability [184], [185].

Most optical models use either wave optics or ray optics. Wave optics rigorously describes light as an electromagnetic wave, solving Maxwell's equations to account for interference, diffraction, and other wave effects. However, this approach is computationally intensive and is typically limited to periodic or small domains. In contrast, ray optics simplifies light into rays that travel and reflect or refract at interfaces based on Snell's law and Fresnel equations. While computationally efficient, ray optics neglects wave phenomena, making it unsuitable for subwavelength-scale textures.

GenPro4 combines the strengths of both approaches in a computationally efficient manner [184]. It treats solar cells as 1D multilayer stacks and employs the extended net-radiation method to calculate reflectance, transmittance, and absorptance as a function of wavelength. In this framework, thick layers are considered incoherent, where interference is negligible, while thin layers, or "coatings," are treated coherently to account for interference effects. This hybrid strategy allows GenPro4 to accurately simulate real-world solar cells with varying layer thicknesses and optical behaviour, all while maintaining low computational cost.

GenPro operates primarily in the frequency domain, modelling optical properties across the solar spectrum. Light propagation and interaction at flat interfaces are modelled using matrices derived from Fresnel equations and the Lambert–Beer law, while light scattering at textured interfaces is handled with specialised interface models. For subwavelength textures (>100 nm), a scalar scattering model is employed to simulate wave-based interference patterns using a Fourier approach [186], instead of solving the computationally heavy Maxwell equations. For larger textures, ray-tracing is applied to determine angular intensity distributions. In both cases, scattering matrices are constructed to describe reflection and transmission probabilities across all angular intervals, ensuring conservation of energy and adherence to the reciprocity theorem.

To simulate real devices, the hemisphere of possible light propagation directions is discretised into angular intervals—typically 30 per interface—forming scattering matrices of 30×30 elements. Each matrix quadrant represents reflection or transmission from above or below the interface. The use of vectorised flux equations allows GenPro to solve for reflectance R, transmittance T, and layer-wise absorptance A_i with high precision:

$$R = \sum \mathbf{q}_1^b, \quad T = \sum \mathbf{q}_I^d, \quad A_i = \sum (\mathbf{q}_{i-1}^d - \mathbf{q}_{i-1}^c + \mathbf{q}_i^b - \mathbf{q}_i^a) \tag{5.3}$$

GenPro's flexibility extends to current matching in multijunction solar cells, where optimal layer thicknesses are identified to equalise the generated photocurrent across different subcells, although not needed in this thesis. Because the scattering matrices are wavelength-dependent but layer-independent,

multiple thickness configurations can be simulated rapidly by reusing previously computed matrices, which will be useful.

In summary, GenPro4 offers a powerful and efficient platform for optical simulation of solar cells. By combining ray and wave optics within the extended net-radiation framework and supporting advanced texture models, GenPro enables both rapid prototyping and detailed optical analysis for novel photovoltaic designs. This makes it very suitable for testing the different encapsulation materials. The optical models developed in GenPro4 are explained in the following section, followed by validation of the optical model using experiments.

5.1.2. Anti-Reflection Coatings

Anti-reflection coatings have become a crucial part of solar modules to increase efficiency by reducing reflection. This is evident from the fact that over 90% of commercial solar modules include some form of ARC treatment [34], [187]. Another method for reducing reflection is texturing, which will be discussed in the following section. Three main aspects are important when using ARC: (i) the number of ARC layers, (ii) the location of ARC layers and (iii) the material of the ARC layers. The ARC can be one or multiple layers, which is discussed first, along with the working principle and optimal performance. Location will be explained in the methodology section. ARCs are typically applied at two primary interfaces: the outer surface of the front glass, where light enters the module from air, and the surface of the solar cell, where light transitions from the encapsulation into the silicon absorber layer. Another potentially interesting interface is the rear side of the front glass, where light moves from the glass into the encapsulation. Finally, the potential materials that can be used are addressed.

Single-Layer ARC Design

ARCs are designed to minimise reflection losses at optical interfaces. Their effectiveness is based on two key optical principles: refractive index grading and destructive interference.

When light travels from one material to another with a different refractive index, a portion of it is reflected due to a mismatch in the n values. The lower this mismatch, the lower the reflection losses, as the Fresnel equation shows. This is where refractive index grading comes in, where a material is introduced with a refractive index value between the values of the two other materials, reducing the reflection. For example, at the air-glass interface (with refractive indices $n = 1$ for air and $n = 1.5$ for glass), approximately 4% of the incident light is reflected at normal incidence. This value is even higher at the air–silicon interface, where silicon's refractive index is around 3.5. Reducing these reflection losses is therefore essential for maximising the light absorption in the solar cell.

The simplest type of ARC is a single-layer anti-reflection coating (SLARC) placed between two media. The optimal refractive index of the material used can be calculated at normal incidence with the following formula:

$$n_{\mathrm{ARC}}(\lambda) = \sqrt{n_1(\lambda) n_2(\lambda)} \tag{5.4}$$

where $n_{\mathrm{ARC}}(\lambda)$ is the optimal n values for the ARC material, $n_1(\lambda)$ and $n_2(\lambda)$ are the refractive indices of the adjacent materials. For instance, for air ($n = 1$) and silicon ($n = 3.5$), the optimal ARC material would have a refractive index around $n_{\mathrm{ARC}} = 1.87$.

Destructive interference happens when the electromagnetic waves cancel each other out because they are out of phase by half a wavelength, which reduces reflection. To ensure destructive interference of the reflected light waves at the coating's surfaces, the thickness d of the ARC layer is determined with the following formula for a specific design wavelength λ:

$$d_{ARC}(\lambda) = \frac{\lambda}{4 n_{\mathrm{ARC}}(\lambda)} \tag{5.5}$$

This configuration causes the two reflected waves to be out of phase by 180°, effectively cancelling each other out and minimising reflection at the design wavelength, commonly chosen around 550 nm, which corresponds to the peak of the solar spectrum.

As the refractive index is wavelength dependent, the optimal refractive index of the ARC $n_{\mathrm{ARC}}(\lambda)$ and the thickness $d_{ARC}(\lambda)$ are also wavelength dependent, which is visualised in Figure 5.1 for air and silicon. While for the refractive index it could be possible to have a curve (green) as seen in Figure 5.1, although finding a material exactly matching it will be challenging, the thickness of the layer can have one value (one thickness) and thus only be optimised for one wavelength. So the thickness (blue) curve in Figure 5.1 only visualises at which thickness, which wavelength is targeted, same for Figure 5.2, explained in the following paragraph.

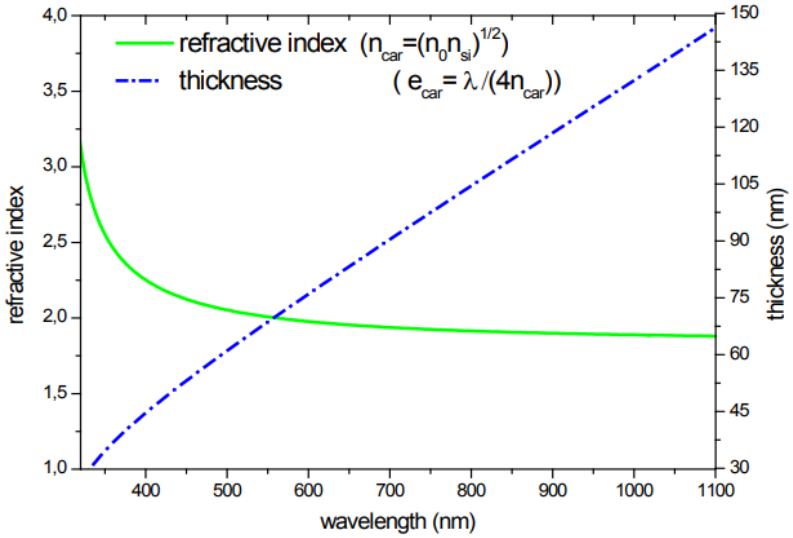

Figure 5.1: Optimal refractive index (n) and thickness (d) of a single idealised ARC layer between air and silicon [188]

Multi-Layer ARC

The effect of single-layer ARCs can be enlarged by adding more ARC layers, creating a smoother refractive index grading and destructive interference at another wavelength by choosing a different thickness. These extra layers do add extra complexity and are, therefore, more challenging and expensive to produce. They are produced in academic laboratories to boost efficiency, but common solar panel manufacturers limit themselves to one or 2 layers max, prioritising an easier/cheaper manufacturing process. Therefore, the ARCs are limited to double ARC layers in this thesis, which can be calculated in the following way.

Double-layer anti-reflection coatings (DLARC) offer a practical balance between complexity and performance. Average reflectivity can be reduced from approximately 9% for a single-layer ARC to below 2.4% with an optimised double-layer design [188]. For optimal performance, the refractive indices $n_{top}(\lambda)$ and $n_{bot}(\lambda)$ of the top and bottom layers should ideally satisfy [188]:

$$n_{ARCtop}(\lambda) = \left(n_0(\lambda)^2 n_2(\lambda)\right)^{1/3}, n_{ARCbot}(\lambda) = \left(n_0(\lambda) n_2(\lambda)^2\right)^{1/3} \tag{5.6}$$

ensuring a gradual refractive index transition from one medium to the other. Additionally, each layer should have a quarter-wavelength optical thickness to support destructive interference at the design wavelength:

$$d_{top}(\lambda) = \frac{\lambda}{4 \cdot n_{top}(\lambda)}, \quad d_{bot}(\lambda) = \frac{\lambda}{4 \cdot n_{bot}(\lambda)} \tag{5.7}$$

These formulas are again dependent on wavelength, plotting them gives the following graphs,Figure 5.2. Which now shows the optimal for a double-layer structure, these same methods can be applied to multilayer structures to achieve even broader spectral coverage and angular stability. These are typically

optimised using numerical simulation tools like the transfer matrix method (TMM)[188]. Again, noting that it is only possible to select one thickness per ARC layer.

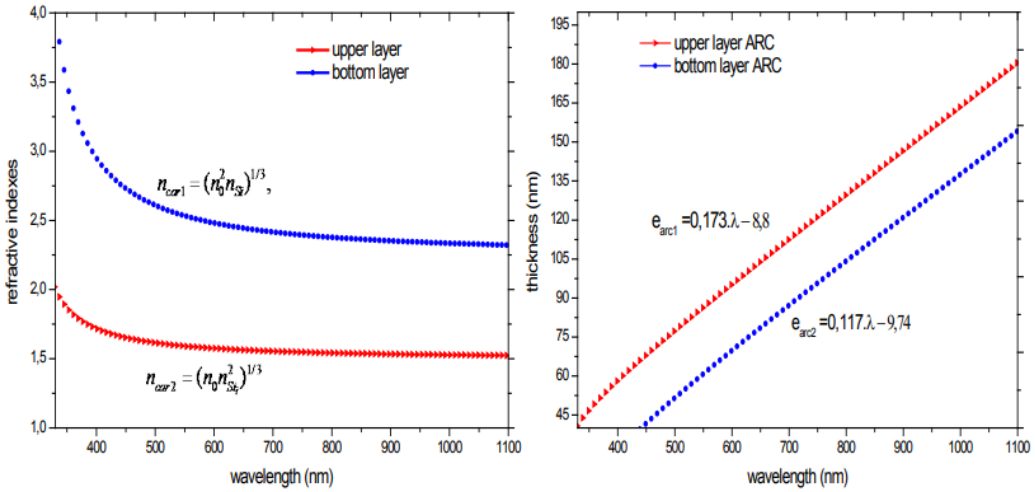

Figure 5.2: Optimal refractive index (n) and thickness (d) of a double idealised ARC layer between air and silicon [188]

ARC Materials

In practice, ideal refractive indices are often not available, so materials are selected based on a compromise between optical performance, transparency, chemical stability, and ease of manufacturing. In the following sections, the specific applications, materials, and performance characteristics of ARCs on the front glass and the solar cell surface will be discussed in more detail.

Glass ARC

The front glass of a solar module plays a crucial role in determining the overall light transmittance to the solar cell. Without anti-reflection measures, a significant portion of sunlight, typically 4–8% (increases with larger angles of incidence), can be lost due to surface reflection. To minimise these losses and enhance energy yield, ARCs are applied to the surface of the glass. It can be tricky to gain information from solar glass manufacturers about the specific ARC they use, as they rarely share information about the materials used or thicknesses. This can also form a problem for the recycling of the glass, if the materials present in the glass are not known, as addressed in chapter 1.

One of the most widely used materials in single-layer ARCs is porous silicon dioxide (SiO_2, or SiO_x) (n = 1.46) [187], [189], [190]. Nano-porous SiO_2 coatings, often deposited using sol-gel techniques, are designed to have a refractive index in the range of 1.11 to 1.46, closely matched to the ideal value for minimising reflectance at the air-glass interface [191], [192]. These coatings can reduce reflection losses by approximately 2–3% across a broad spectral range. However, while effective optically, porous coatings are inherently fragile and can suffer from weather conditions, cleaning and moisture ingress, which limit their long-term durability, especially in harsh outdoor environments. Therefore, it is a balance between ideal refractive index and long-term durability. Currently, ARCs on glass have an average lifetime of around 15 years, expected to increase to 25+ years in the future [34].

Another material commonly used in glass ARCs includes magnesium fluoride (MgF_2) (n = 1.39), a low-index material valued for its transparency and chemical stability. These coatings are applied using a range of deposition techniques, including sol-gel, spin-coating, and sputtering, depending on the required optical performance, production cost, and environmental stability.

A higher refractive index material, titanium dioxide (TiO_2) (n = 2.29), is used for the self-cleaning effects it has on the glass (often in combination with SiO_2) [189]. This self-cleaning might be important for some locations in which the ARC can hold dirt and become less effective [187]. To improve mechanical robustness, multilayer ARCs have been developed using alternating stacks of dense dielectric materials such as TiO_2 and zirconium dioxide (ZrO□) (n = 1.99) [188]. These coatings avoid the use

of porous structures and are therefore more resistant to environmental degradation. By carefully controlling the refractive index contrast and thickness of each layer, these multilayer coatings can achieve even lower average reflectance over a wider wavelength range than single-layer solutions. Although more expensive and complex to manufacture, they are increasingly used in premium solar modules and research applications.

Other coating materials are more niche; they could include PFAS-based materials, which have a low refractive index (n = 1.28) and are durable in weather conditions [193], [194]. There are concerns about using PFAS in solar modules because of their potential environmental and health risks, as also discussed for the liquids in chapter 3.

Solar cell surface ARC

Due to the relatively high refractive index of silicon (n = 3.5), it is important to apply ARC to lower the reflection at this interface. Multiple studies look into the effect of single and multilayer ARCs, of which the main options will be shortly discussed.

Silicon nitride (SiN_x) (n = 1.86) is the most commonly used ARC for crystalline silicon (c-Si) solar cells [188], [195]–[197]. It not only reduces reflectivity but also provides excellent surface passivation by introducing hydrogen to passivate surface defects. SiN□ is typically deposited using plasma-enhanced chemical vapour deposition (PECVD).

Similar materials to glass ARC can be used, often with a higher refractive index, such as titanium dioxide (TiO_2, n = 2.29), zirconium dioxide (ZrO_2, n = 1.99). Also frequently used in tandem with low-refractive-index materials like SiO_x (n = 1.47) and magnesium fluoride (MgF_2 n = 1.39) to form multilayer coatings.

In addition to conventional single- and multi-layer coatings, several advanced ARC approaches are being explored. Gradient refractive index (GRIN) and nanoporous layers allow for a smooth transition in refractive index from air to silicon, reducing reflection and enhancing adhesion [197]. Techniques such as refractive index tuning—by adjusting porosity or stoichiometry of materials like SiO_2 or SiN_x, enable multilayer behaviour using a single material. Furthermore, embedding nanoparticles (e.g., indium) into ARCs can enhance light scattering and trapping. These techniques are rather advanced and not used in the industry due to higher cost; they are therefore not considered for the modelling.

For glass surfaces, common ARC materials include tuned porous SiO_x and MgF_2. For silicon solar cell surfaces, SiN_x is mainly used, sometimes TiO_2 or MgF_2, and combinations of these in multilayer coatings are used. These materials can be deposited using various methods such as sol-gel processing, spin-coating, sputtering, or plasma-enhanced chemical vapour deposition (PECVD). How these ARCs will be applied in the optical simulations will be addressed, along with the other configurations, in the following section.

5.2. Simulated structures

In GenPro, it is possible to simulate multiple solar energy structures by adjusting different parameters such as layer build-up, materials, texturing, sunray and model settings. In this section, the solar module stack will be discussed along with the materials used and their optical properties (complex refractive index), texturing, ARC and different configurations. First, the texturing and ARCs will be addressed, followed by the various optical configurations that will be simulated, and at the end, the optimisation will be introduced.

5.2.1. Texturing

Reflection can be minimised by using an ARC, as discussed in the previous section, or texturing, which enables better sunlight collection through light trapping. The two main locations for texturing are the same as for ARCs: the solar cell surface is textured, often with pyramid shapes, and the front glass can be textured as well with different geometric shapes. For the solar cell surface, only the pyramid texturing is applied in combination with the ”ray” model in GenPro, for all solar cell technologies and configurations. For the glass texturing, 3 geometric shapes will be tested through simulations, and the best one will be chosen. The 3 shapes are visualised in Figure 5.3, note that the different orientation

for Alberino G does not affect GenPro, but would have an effect in real-life conditions, although in fabrication they are alternating like a chess board [198].

A decrease in reflection is expected for EVA, air and all liquids. Therefore, an increase in photocurrent, it is interesting to see how this will compare to the ARC used. In the optimisation stage, glass texturing could be combined with ARC to see if reflection can be minimised further, although it is important to note that the actual production of these combinations should be checked.

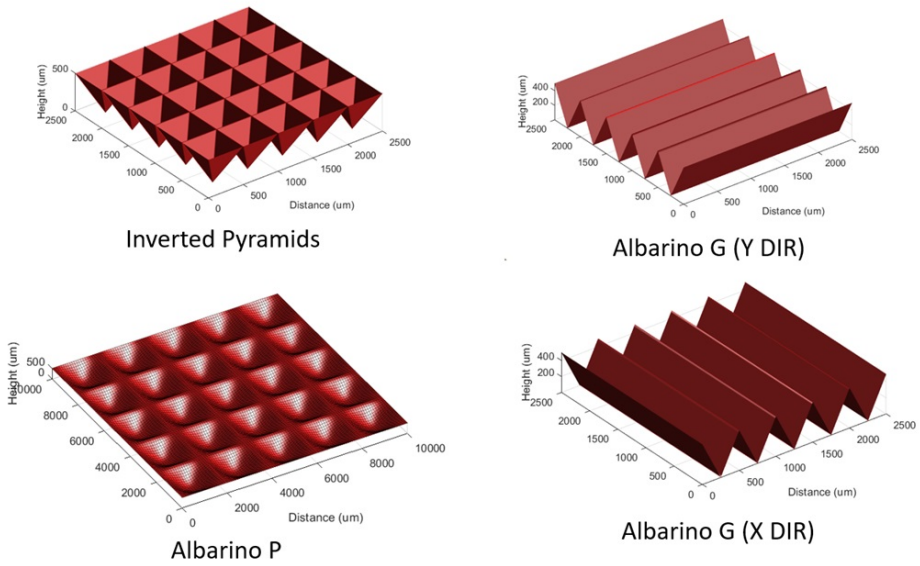

Figure 5.3: Different glass texture geometric shapes tested in optical simulations

absorption

5.2.2. Different configurations

To evaluate the optical performance of the 7 selected liquids, they are simulated and compared to air and EVA encapsulation in multiple configurations. The difference between the simulation scenarios and potential hypotheses will be discussed in this section. They differ mainly in layer and interface stack; some use different GenPro settings, which will be addressed in the following section. As mentioned before, the goal is to minimise reflection and absorption losses, both are governed by the material properties (complex refractive index) of the liquids. However, as shown, reflection can be reduced by introducing new layers and materials, especially beneficial for the liquids since they have lower n values than ideal/EVA. The absorption can be minimised by reducing the thickness of the material; some configurations look into this.

Solar cell technologies

As mentioned earlier, GenPro uses two different categories for building up its solar stack: thick layers and interfaces between layers. Thick layers (>1 µm, coherence length of incoming light) do not take into account interference effects (glass, EVA/encapsulation, Si absorber). For thinner layers, the interfaces (ARC, ITO, ect.), this assumption is no longer accurate and interference is modelled by the fluxes Equation 5.3 represented as complex amplitudes of electromagnetic waves [184].

To evaluate the difference between the standard EVA encapsulation, air and the 7 selected liquids, they are all modelled for different solar cell technologies (PERC, TOPCon and IBC), only changing the encapsulation layer (air, EVA-Conv, EVA-UVT and 7 liquids) as seen in Figure 5.4. A silicon heterojunction (SHJ) was also tested, but not shown in the results due to lower performance and usage in industry. All the solar stacks have the following layers and interfaces, along with their thicknesses [196], [199], [200]. Layers include: Air (t = infinite), glass front (same as backsheet) (t = 2 mm), encapsulation front (same as back) (t = 0.45 mm), silicon absorber (0.15 mm). For some configurations, these thicknesses are changed. The interfaces are different for the solar cell technologies, and some configurations, which

will be explained for each technology/configuration. The PERC (middle) is shown in Figure 5.4 (thicknesses not to scale), with its interfaces specific layers such as the SiN(2.09) and SiO2-Lem13. Note that the cell area between fingers is simulated (this is where light is collected), which is why interfaces such as P/N+ emitter or n/p polysilicon (TOPCon) are not included on the front. TOPCon (right) Figure 5.4 has an added npolySi layer on the back, compared to PERC. IBC has an additional a-Si(n) on the front and Emitter-G and ITO on the back of the cell as seen in (left) Figure 5.4.

It is not confirmed that these layers are the exact layer build-up of specific cells, so the exact thicknesses and materials might differ. For example, there is no ITO layer present in the Maxeon III IBC cell (which is taken as an example), but this layer is used to get a suitable refractive index (n 1.6) at NIR wavelengths (900 nm to 1200 nm) to increase a bit the reflectance in this range without inducing significant absorption losses. The reason is that in GenPro4, you cannot optically simulate the pitch of the IBC; therefore, including the metal will create significant reflection and absorption losses that do not match the measurements. Using SiO2 (n 1.45) also yielded a reflectance/transmittance mismatch. ITO was a better optical fit. However, optically, that ITO layer matches the behaviour of the IBC cell, as also confirmed through experiments and datasheets. Therfore, the IBC structure simulated in GenPro4 is not a real device, but one that matches the optical behaviour of one and since we are only interested in the optical aspect, that is sufficient. These models are validated with current measurements and datasheet values at the beginning of the results section. (IBC optical model and explanation are accredited to Juan CamilO Ortiz Lizcano).

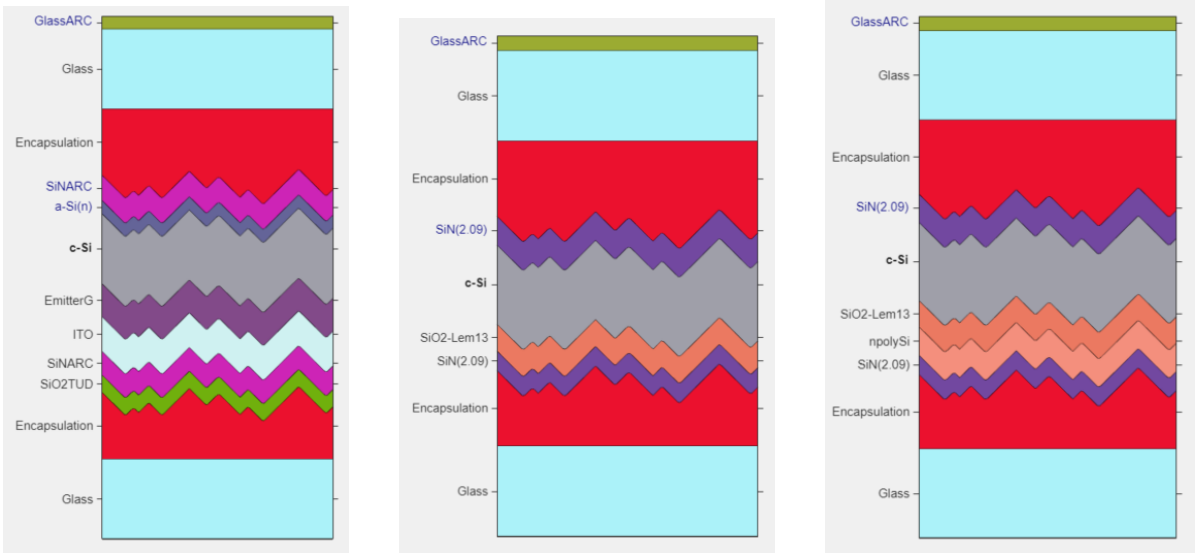

Figure 5.4: Layer build-up for IBC (left), PERC (middle) and TOPCon solar cell technology inside solar module, thickness of layers is not to scale

These 3 cell technologies are modelled to see if their layer build-up affects the change in encapsulation. It is expected that there are some differences, but they will be minimal and probably not have an effect on the ranking of best/worst performing liquids. For the following configurations, only TOPCon will be used since the focus is on the difference in encapsulation (not solar cell technology), and to limit the number of simulations. TOPCon is selected since the industry is moving more toward this technology, as seen in Figure 1.4, and Biosphere and TU Delft plan on using TOPCon cells in liquid-filled test modules [34].

Advanced ARC

As mentioned before, the ARC will be limited to a maximum of two ARC layers, positioned on the outside and inside of the front glass panel, and on the solar cell surface. The 3 standard solar cell technologies discussed before all have a glass ARC (SiO_2, n = 1.413 at 630 nm) and solar cell ARC (and passivation) layer of SiN_x (n = 2.09 at 633 nm), since this is industry standard and belongs to the solar cell architecture. This is compared to two cases, having no glass ARC (still SiN_x on cell surface) and an advanced DARC on both sides of the glass and solar cell ARC. The advanced version

is optimised for the largest reflector, air, with materials used in ARC. The TPedge concept also has ARC on the outside and inside of the glass, supporting the feasibility of this idea [51].

Several configurations were simulated using air as encapsulation and different materials for the glass and solar cell ARC. The optimal values of n can be seen in Figure 5.2, for outside of the glass the ideal values for n are: 1.143 top ARC, 1.31 bottom ARC, reversed for the inside of the glass. The silicon cell surface ideal n values are: 1.58 top, 2.49 bottom.

The materials available in the GenPro database that match the ideal n values the best are the following (some materials have more nk files in the database; their names appear as they do in GenPro, for an overview, please see Table 5.1). For the glass, SiO_2, AF2400 (n = 1.28) and MgF_2 (n = 1.39) were used. For the solar cell surface SiN_x (different n (1.91, 2.09, 2.13)), MgF_2, TiO_2 (n = 2.30), and multiple SiO_2 (n = 1.47).

These were simulated in different stacking orders, always forming a refractive index grading between the two media. The best results for air encapsulation are air/glass: AF2400 - Glass ARC (SiO_2), glass/encapsulation: Glass ARC (SiO_2) - AF2400, solar cell surface: + SiO_2 -TiO_2.

Table 5.1: Materials / nk files from the GenPro database used in this thesis, some materials have multiple nk files, the names are used as seen in GenPro.

Material / nk file (GenPro database)	Refractive index (n) 630 nm	TOPCon	IBC	PERC	Advanced ARC
c-Si-2015 (Si absorber)	3.869	x	x	x	x
Glass-Fe10ppmM1	1.512	x	x	x	x
GlassARC (SiO_x)	1.413	x	x	x	x
AF2400	1.28				x
npolySi	3.833	x			
SiN(2.09)	2.09	x		x	x
SiNARC	1.98		x		x
Emitter G	3.833		x		
a-Si(n)	4.136		x		
ITO	1.991		x		
TiO2	2.295				x
SiO2-Lem13	1.472	x		x	
SiOTUD / SiO2TUD	1.475		x		
EVA-UVT	1.492	x	x	x	x
PDMS	1.410	x	x	x	x
EVA-Conv	1.490	x	x	x	
MIDEL	1.458	x	x	x	
WATER	1.337	x	x	x	x
SHELL DIALA	1.459	x	x	x	
AIR	1.0	x	x	x	x
MIVOLT	1.459	x	x	x	
Tried but unused materials					
ZnO_x	1.99				x
MgF_2	1.39				x
SiO_2	1.47				x
SiN (1.91)	1.91				x
SiN (2.13)	2.13				x

It is expected that liquids with a lower refractive index benefit the most from this advanced ARC, because they reflect the most and because their n values are closer to air, for which the ARC is optimised. It could be that EVA is even going down in performance because of the refractive index grading on the inside of the glass and less optimal grading on the solar cell surface. Later on, at the optimisation stage, the ARC will be optimised for the most promising liquids and EVA to evaluate how much their performance can be boosted.

Multilayer encapsulation, Liquid and EVA

A small layer of EVA could be applied to the inside of the glass, which can eliminate leakage if the module breaks, while still having liquid in touch with the solar cells for easier dismantling. This idea is being explored by Biosphere and is already used by the CEA-INES concept, which holds the interconnections in place with a layer of ionomer on the inside of the glass. In this simulation, half of the encapsulation (0.225 mm) is EVA, and the other half is a liquid (or air).

It is expected that the EVA layer can help reduce reflection by enabling some refractive index grading to the lower n values of the liquids. It could potentially cancel this positive effect by also absorbing more, which needs to be checked.

Biosphere-TU Delft case

The biosphere-TU Delft case means having more encapsulation on the front (0.6 mm) than on the back (0.3 mm) of the solar cells, instead of having the cells in the middle (and no glass ARC). Whether this will be the case is not yet sure, but it could be possible. It is also anticipated that the liquid could sag when installed at an angle. The liquid is putting pressure on the lower half of the solar module, causing the glass panels to slightly bend. This leads to a thicker encapsulation layer on the bottom of the module (and thinner at the top), which could cause a current mismatch. If this happens, and if so, to what extent, has yet to be researched.

With this simulation, it can already be partially quantified. With a thicker encapsulation layer, more light is absorbed, so a lower photocurrent is expected.

5.2.3. Optimisation

For the optimisation, some options are already considered, while others will arise after the first simulations. They will be performed on the best-performing liquids to limit the number of simulations. They can be divided into two groups: optimisation with available resources and theoretical optimisation, to quantify the upper limit of performance and see how close we can get to this. The maximum possible (theoretical) photocurrent a crystalline solar cell can achieve under standard test conditions is 46 mA/cm^2, currently the measured record is around 42.60 mA/cm^2 [32], [201]. The liquid encapsulation could theoretically surpass the Shockley-Queisser Limit by improved (active) cooling of the solar cells. Although this cooling mainly reduces the thermalisation and V_{oc}.

Thickness layers

It is useful to see the effect of changing the thickness of the layers (Si absorber and especially glass and encapsulation) on the photocurrent generated. This can help Biosphere and TU Delft when considering a thicker glass panel in order to make up for lost mechanical strength by not using a solid encapsulation and potentially altering the thickness of the encapsulation, as also discussed before.

As mentioned before, a thicker layer absorbs more, and how much more depends on the extinction coefficient k of the material. If this is quantified, we can see if a thicker glass or encapsulation layer can be used or if this is causing too much reduction in photocurrent. The glass thickness ranges from 2000 to 5000 μm with a step size of 500 μm, the encapsulation thickness goes from 200 to 1000 μm step size of 50 μm and the Si absorber layer goes from 150 to 200 μm with a step size of 5 μm. Changing the Si absorber thickness might be difficult as the cells used are off-the-shelf products, but perhaps this can help decide which thickness when ordering the solar cells, although the industry is moving towards thinner absorbers in general [34].

Liquid specific ARC

As mentioned before, the advanced ARC was optimised for air encapsulation. In further optimisation, this will be optimised for the best-performing liquids using the same method, to see how much their reflection can be reduced. Combinations with ARC and glass texturing might also be interesting to simulate.

Theoretical optimisation

Theoretical optimisation involves artificially changing material properties such as the refractive index of some materials. Focused on two approaches, producing ARC layers with the optimal calculated n

values, which can quantify how close we are to the theoretical limit and help in searching for liquid-specific ARC. Changing the n values of the liquids to the calculated optimum, again quantifying the theoretical limit, and seeing the effect of raising the n values with additives. Numerous studies show that the refractive index of materials/liquids can be raised by adding additives [202], [203]. In this thesis, this is not investigated in detail, since additives will affect other properties (such as extinction coefficient, electrical conductivity, etc.) as well and are therefore only considered theoretically.

It is expected that photocurrent increases; it will be interesting to see what the theoretical limit is. For the refractive index of the liquids, the n value will have an optimum, which can be calculated, after which it will go down again.

5.2.4. GenPro settings

GenPro has several settings that can be adjusted to modify the speed and accuracy of the optical simulations. Most settings were not changed, as the main focus is on the difference in encapsulation. Other settings like wavelength range, step size, number of angular intervals, angle of incidence and number of rays, were adjusted and simulated for different values to see their effect, after which the fastest with proper accuracy were selected. Also, various assumptions are made, which are important to keep in mind when interpreting the results.

- The main assumption is that the liquids are a uniform static layer, no flow is considered, and the liquids behave optically similar to solids or gases
- The encapsulation is completely filled (no air bubbles). In reality, there will probably be one or multiple air bubbles left. This also implies that potentially different light scattering due to liquid droplets/bubbles, as explained by Clark et al., is not considered [65]. Also, different behaviour due to the vapour formation is not taken into account (as the liquid should not vaporise under standard conditions)
- The Temperature dependence of the complex refractive index is not considered as the effect is minimal (which will be shown) and applies to all materials [164], [165]

The wavelength range was set at 300 - 1200 nm with a 5 nm step size. The number of angular intervals and rays was set to the most accurate (longest computational time) to see the best result, after which it was tuned down for a shorter simulation time while still getting the same results (same to one decimal). The number of angular intervals was set to 18, and the number of rays to 500. Angle of incidence to 1, corresponding to the first angular interval (90/18 = first 5 degrees).

5.3. Results

In total, more than 34 different configurations were tested, resulting in over 240 liquid simulations run, with a total of 120+ hours of computational time. The results will be displayed and discussed in this section in the same order as the methodology.

As described at the beginning of this chapter, the GenPro simulations produce various parameters for analysing the performance of a solar cell stack. The focus of this research is evaluating the liquid encapsulation compared to air and standard EVA, therefore the most interesting parameters are the photocurrent generated in the Si absorber (layer: ”c-Si-2015”), parasitic absorption losses in the encapsulation layer (layer: ”SAMPLE”) and reflection losses (”Reflection”). These are influenced by the reflection, absorption and transmittance in other layers; therefore, these layers could explain more about what is happening in our focus layers. This is where the absorption profile can come in handy for explaining these differences, visualised in Figure 5.5.

First, the optical model is validated with literature, datasheet and experiments in the following section. Followed by the different simulation configurations described in the methodology and a real-life scenario is simulated using the PVMD toolbox. After analysing these, the optimisation starts and explores the performance of the best-performing liquids further.

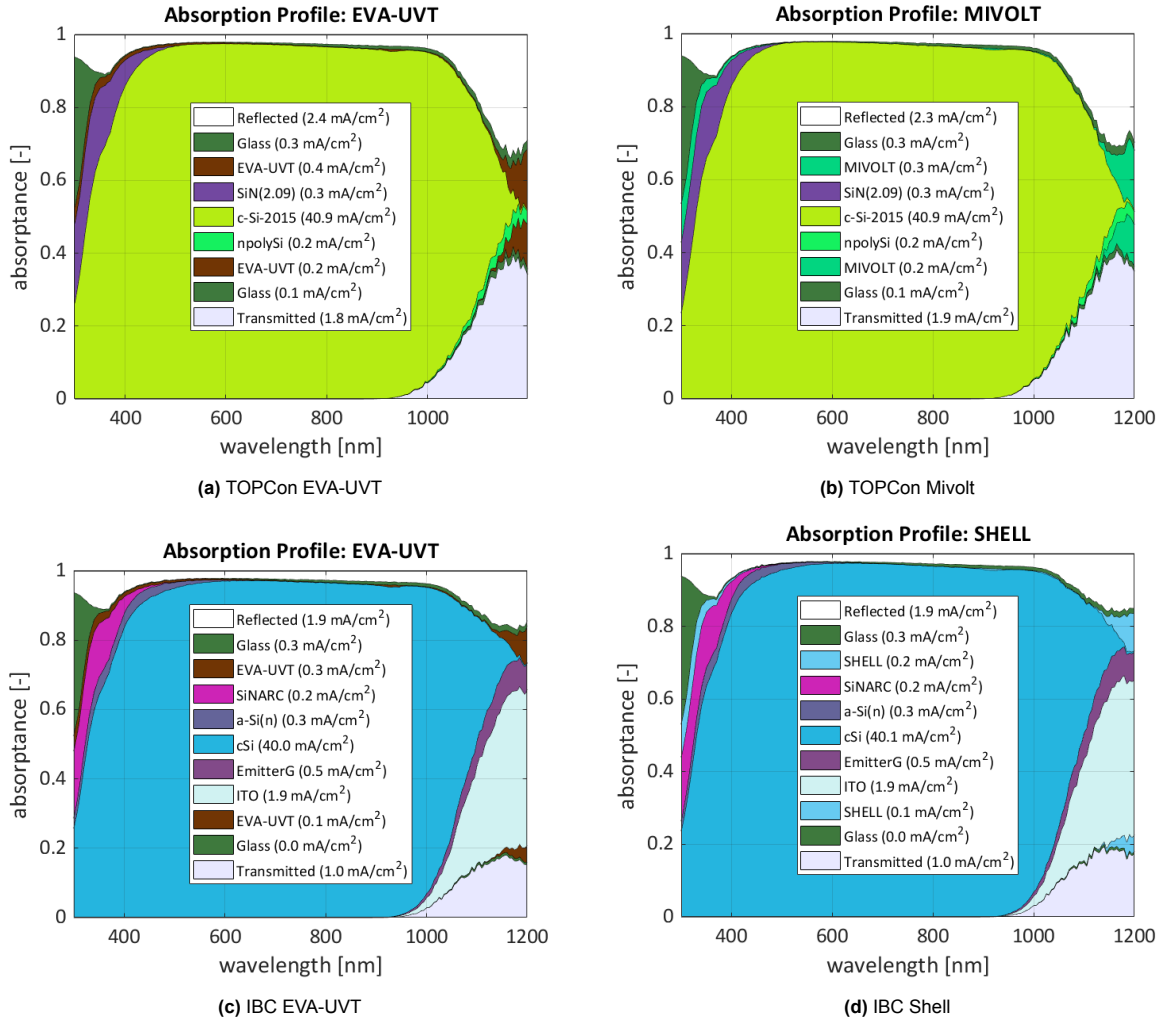

(a) TOPCon EVA-UVT

(b) TOPCon Mivolt

(c) IBC EVA-UVT

(d) IBC Shell

Figure 5.5: Absorption profile for TOPCon and IBC with EVA-UVT, Mivolt and Shell encapsulation

5.3.1. Validation optical model

In order to have more confidence in the results of the optical simulations, the model is validated with measurements and datasheets. It is expected that the simulations will be slightly higher because of two reasons: the assumption in GenPro that internal quantum efficiency (IQE) = 1, all photons absorbed produce an electron-hole pair, which is successfully collected [185]. This is an accurate assumption for state-of-the-art devices, leading to an identical shape for EQE and absorption in the Si absorber layer. If the recombination losses do play a role, this needs to be simulated in an electrical model (such as Sentaurus) to obtain the EQE. Secondly, finger/shading losses are not taken into account during simulations because the area between the fingers is simulated. The optical model and the simulated output are validated through three methods: (i) Literature validation, (ii) IBC and TOPCon datasheet values, and (iii) IBC liquid-filled 1-cell solar modules measurements.

Juan Camilo Ortiz Lizcano, researcher at the TU Delft, has performed measurements and validation on the Maxeon III IBC solar cell from SunPower using GenPro4 as well. This supplied us with a more detailed solar stack build-up and validation measurements performed by measuring the transmittance and reflection of a bare IBC cell using the Lambda spectrophotometer. The results are visualised in Figure 5.6, in which good agreement can be seen between the measured and simulated values, especially in the important absorption range of 400 - 1000 nm. The experimental setup is detailed in [204].

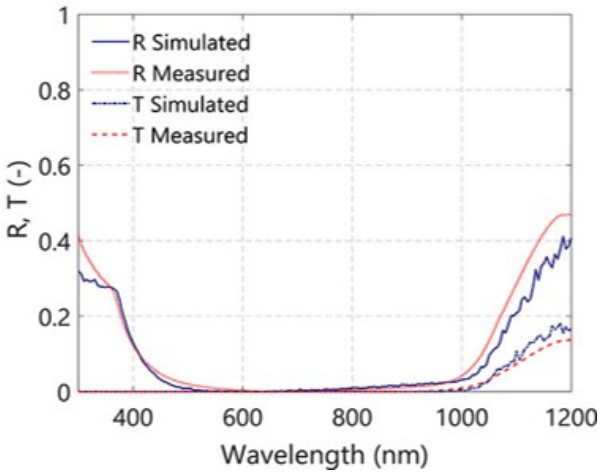

Figure 5.6: Validation of optical GenPro model of Sunpower Maxeon III IBC cell by measured transmittance and reflected using a Lambda spectrophotometer performed by Juan Camilo Ortiz Lizcano [204]

For further validation, the IBC and TOPCon simulated photocurrent was compared to their datasheet. For IBC Sunpower Maxeon generation III solar cell Ne3, the I_{sc} is 6.41 A, divided by the area of 155 cm^2 gives a J_{sc} of 41.35 mA/cm^2 [205]. The simulated value is 41.4 mA/cm^2, so this is in excellent agreement.

For TOPCon, the cell was not simulated to a specific cell (like Sunpower IBC cell), but to a general TOPCon layout. To still validate its layer configurations, a TOPCon cell with a similar thickness is selected, and values are taken from its datasheet. The SE-210M-18D1 from SunEvo Solar has a current I_{sc} of 18.37 A, divided by the 441 cm^2 area gives a J_{sc} of 41.66 mA/cm^2 [206]. This is in good agreement with the simulated value of 41.8 mA/cm^2, which is again slightly higher, as expected.

Lastly, the photocurrent was measured of the liquid-filled 1-cell modules fabricated by Sebastian Weemaes and Urvashi Bothra [58], [59]. They align very well with the simulated values, as all simulated values stay within the measurement uncertainty. The bare IBC cell has a measured photocurrent of 41.4±0.1 mA/cm^2 (±0.1 gives the measurement uncertainty as the measurements were performed three times, of which the average is given), which is the same as the simulated 41.4 mA/cm^2 value. The measured value for air 38±0.5 mA/cm^2 is again close to the simulated value of 38.24 mA/cm^2. Same for the EVA with a measured value of 39.8±0.9 mA/cm^2, which is very close to the EVA-UVT simulated photocurrent of 40.01 mA/cm^2 and in the measurement uncertainty for EVA-Conv with 39.46 mA/cm^2. For PDMS

the measured value is 39.8±0.1 mA/cm^2 and the simulated value is 40.0 mA/cm^2, all showing excellent agreement to measured values.

These experiments and datasheet values give confidence in the optical simulations, as these values match very well. The shape of the reflection and transmission of the IBC cell is similar to that seen in Figure 5.6. The datasheet values show a difference between the simulated photocurrent of 0.05 mA/cm^2 for IBC and 0.14 mA/cm^2 for TOPCon. The measured value of the bare IBC cell even matched completely, with 0.0 mA/cm^2 difference (measurement uncertainty of 0.1 mA/cm^2). The difference between the measured photocurrent of a complete solar module with an IBC cell and the simulated values ranges between 0.20 to 0.34 mA/cm^2, showing excellent agreement. IBC cells do not have fingers on the front side of the solar cells, same as for the optical model, which is simulating the solar cell without fingers, nicely see in their good alignment (TOPCon cell has good agreement as well).

5.3.2. Solar cell technologies

First, the 3 standard cell technologies(IBC, TOPCon, PERC) are simulated, which give interesting results regarding the performance of the liquids. First, the TOPCon simulation will be discussed, followed by the PERC and IBC, after which they will be compared to each other. The data gathered of all the liquids and all layers for the standard TOPCon simulation is noted in the top part of Table 5.2 to show which data is collected and analysed. In this table, multiple layers are not significantly absorbing (Glass ARC, SiO_2, among others), while others do not change much between simulations; they are therefore left out in other tables for easier reading (although still taken into account when analysing). It is important to keep in mind that the reflection discussed is the total reflection of all layers in the solar stack, not only the reflection of the encapsulation sample. This means that an encapsulation material, such as glycerol, might have a lower reflection itself but a higher reflection in total because of reflection in different layers that are absorbed at different wavelengths in the sample. Most of the reflection comes from the glass front panel.

For the standard TOPCon simulation see in the top part of Table 5.2, the EVA-UVT achieves the highest photocurrent of 40.92 mA/cm^2, due to its low reflection (2.37 mA/cm^2) and parasitic absorption (0.37 mA/cm^2), followed by all liquids, except water, within 0.17 mA/cm^2. Water and air score lower due to their higher reflection, EVA-Conv has the lowest reflection but the highest absorption, making it the second lowest performing sample.

Table 5.2: GenPro results TOPCon simulations, all values are expressed in photocurrent generated or lost (mA/cm^2), the yellow colour identifies the most relevant layers, green means best performing sample (or liquid) in that layer and red is worst performing. EVA-UVT achieves the highest photocurrent of 40.92 mA/cm^2, with low reflection (2.37 mA/cm^2) and parasitic absorption (0.37 mA/cm^2), followed by all liquids, except water, within 0.17 mA/cm^2.

Layer (mA/cm^2)	AIR	EVA-UVT	EVA-Conv	GLYCEROL	GLYCOL	MIDEL	MIVOLT	PDMS	SHELL	WATER
Reflected	4.82	2.37	2.31	2.36	2.38	2.36	2.34	2.43	2.35	2.54
GlassARC	0.00	0.00	0.00	0.00	0.00	0.00	0.00	0.00	0.00	0.00
Glass	0.30	0.34	0.34	0.34	0.32	0.33	0.33	0.32	0.33	0.31
SAMPLE	0.00	0.37	1.12	0.48	0.40	0.33	0.33	0.25	0.32	0.45
SiN(2.09)	0.23	0.30	0.16	0.30	0.29	0.29	0.29	0.29	0.29	0.28
c-Si-2015	39.15	40.92	40.35	40.75	40.75	40.87	40.90	40.85	40.89	40.68
SiO_2	0.00	0.00	0.00	0.00	0.00	0.00	0.00	0.00	0.00	0.00
npolySi	0.17	0.16	0.16	0.15	0.15	0.15	0.15	0.15	0.15	0.15
SiN(2.09)	0.00	0.00	0.00	0.00	0.00	0.00	0.00	0.00	0.00	0.00
SAMPLE	0.00	0.16	0.15	0.19	0.21	0.17	0.17	0.14	0.17	0.22
Glass	0.02	0.08	0.08	0.07	0.06	0.07	0.07	0.06	0.06	0.05
Transmitted	1.76	1.77	1.80	1.82	1.90	1.88	1.87	1.97	1.89	1.78
Glass texturing Inverted Pyramids										
Reflected	7.02	1.35	1.25	1.31	1.43	1.33	1.31	1.53	1.32	1.82
Glass	0.76	0.44	0.42	0.43	0.45	0.43	0.43	0.46	0.43	0.50
SAMPLE	0.00	0.44	1.72	1.01	0.83	0.66	0.66	0.51	0.62	0.90
c-Si-2015	36.46	41.49	40.57	41.14	41.24	41.48	41.49	41.41	41.54	40.83
Tranmitted	1.84	2.06	2.09	2.01	1.97	2.03	2.03	2.02	2.02	1.88
No ARC Glass										
Reflected	5.52	3.14	3.09	3.14	3.15	3.14	3.12	3.21	3.13	3.31
SAMPLE	0.00	0.37	1.11	0.47	0.40	0.33	0.33	0.25	0.31	0.44
c-Si-2015	38.47	40.16	39.61	39.98	40.01	40.13	40.16	40.09	40.15	39.94
Transmitted	1.74	1.77	1.78	1.82	1.88	1.86	1.86	1.96	1.87	1.76
Advanced ARC Glass and Cell										
Reflected	3.49	2.24	2.22	2.17	2.01	2.13	2.12	2.07	2.12	1.99
SAMPLE	0.00	0.37	1.12	0.48	0.41	0.33	0.33	0.25	0.31	0.45
c-Si-2015	40.44	41.06	40.46	40.97	41.10	41.13	41.15	41.22	41.17	41.25
Transmitted	1.88	1.88	1.89	1.91	2.04	1.99	1.97	2.08	1.98	1.86
Multilayer encapsulation EVA - Sample										
Reflected	4.48	2.31	2.30	2.30	2.32	2.29	2.30	2.36	2.30	2.45
EVA-Conv	0.78	0.81	0.80	0.81	0.80	0.80	0.80	0.80	0.80	0.79
SAMPLE	0.00	0.18	0.31	0.24	0.20	0.16	0.16	0.12	0.15	0.23
c-Si-2015	38.79	40.44	40.34	40.36	40.32	40.41	40.43	40.38	40.41	40.27
Transmitted	1.74	1.81	1.81	1.84	1.93	1.90	1.87	1.96	1.90	1.85
biosphere-TU Delft case, no glass ARC, thicker encapsulation										
Reflected	5.52	3.12	3.06	3.10	3.11	3.11	3.08	3.18	3.10	3.27
SAMPLE	0.00	0.47	1.50	0.81	0.68	0.55	0.55	0.42	0.53	0.74
c-Si-2015	38.47	40.09	39.37	39.85	39.92	40.06	40.10	40.06	40.10	39.84
Transmitted	1.74	1.81	1.79	1.81	1.90	1.87	1.87	1.96	1.88	1.77

The PERC simulations, seen in Table 5.3, show a similar pattern; the main difference between the PERC and TOPcon technology is the npolySi layer, which absorbs a fraction of the light, causing the PERC to generate a slightly higher photocurrent in all samples. EVA-UVT has the highest photocurrent of 40.95 mA/cm^2, again followed within 0.17 mA/cm^2 by all liquids but water.

Table 5.3: GenPro results PERC simulations, all values are expressed in photocurrent generated/lost (mA/cm^2), green colour identifies best performing sample (or liquid) in that layer. EVA-UVT has the highest photocurrent of 40.95 mA/cm^2, again followed within 0.17 mA/cm^2 by all liquids but water.

Layer (mA/cm^2)	AIR	EVA-UVT	EVA-Conv	GLYCEROL	GLYCOL	MIDEL	MIVOLT	PDMS	SHELL	WATER
Reflected	4.84	2.39	2.35	2.39	2.41	2.38	2.38	2.46	2.38	2.57
SAMPLE	0.00	0.37	1.13	0.48	0.41	0.34	0.34	0.26	0.32	0.45
c-Si-2015	39.18	40.95	40.37	40.79	40.78	40.92	40.94	40.88	40.94	40.73
Transmitted	1.87	1.86	1.86	1.88	1.98	1.95	1.92	2.04	1.94	1.83

The IBC, seen in Table 5.4, is performing significantly lower than the PERC and TOPCon, which can be explained by the absorption of the additional a-Si(n), EmitterG and, especially, the ITO layer. For IBC, the best performing sample is Shell Diala with 40.07 mA/cm^2 driven by a low reflection of 1.91 mA/cm^2 and even lower parasitic absorption of 0.23 mA/cm^2. Most other samples follow within 0.16 mA/cm^2, again water and air are further down because of their higher reflection and EVA-Conv because of high absorption losses.

Table 5.4: GenPro results IBC simulations, all values are expressed in photocurrent generated/lost (mA/cm^2), the yellow colour identifies the main difference with TOPCon/PERC, green means best performing sample (or liquid) in that layer. Shell Diala has the highest photocurrent with 40.07 mA/cm^2 driven by a low reflection of 1.91 mA/cm^2 and even lower parasitic absorption of 0.23 mA/cm^2. Most other samples follow within 0.16 mA/cm^2.

Layer mA/cm^2	AIR	EVA-UVT	EVA-Conv	GLYCEROL	GLYCOL	MIDEL	MIVOLT	PDMS	SHELL	WATER
Reflection	4.21	1.90	1.84	1.91	1.97	1.92	1.91	1.99	1.91	2.12
SAMPLE	0.00	0.28	1.04	0.38	0.30	0.24	0.24	0.18	0.23	0.33
a-Si(n)	0.25	0.27	0.23	0.27	0.27	0.27	0.27	0.27	0.27	0.26
cSi	38.24	40.01	39.46	39.91	39.93	40.04	40.05	40.00	40.07	39.83
ITO	1.93	1.94	1.94	1.89	1.83	1.88	1.88	1.87	1.88	1.86
Transmitted	0.96	0.96	0.99	1.01	1.09	1.05	1.05	1.11	1.05	1.00

The reason Shell, Mivolt and Midel are now outperforming EVA-UVT can be explained in the following way, the same logic can explain other differences between simulations as well. The IBC (compared to TOPCon and PERC) has additional absorption of the a-Si(n) layer in the region of 400 - 600 nm. In this region, Shell is the lowest absorber, followed by Mivolt, Midel and then EVA-UVT (between these four) as seen in Figure 5.5 (and also visible in the extinction coefficient Figure 4.33). Because of the new a-Si(n) layer compared to TOPCon/PERC, there is more parasitic absorption in this region (by the a-Si (n) layer), an effect that can be reduced by having a lower absorber, such as Shell, which makes it slightly outcompete the other two. This is how the different layers can affect the differences in photocurrent between simulations. Although the relative order of best/worst performing liquid only slightly changed between different cell technologies, with some liquid combinations that were already very close to each other swapping spots, such as glycerol and glycol, and Shell, Mivolt and EVA-UVT. This can be explained by slight changes in wavelength area, where one sample may reflect or absorb more than another. Due to a different layer build-up, this effect can be amplified or suppressed, making one liquid perform better than its partner.

The most interesting finding is the excellent transmission of all liquids, seen by the very low values for parasitic absorption losses in the ”SAMPLE” layer in all three tables (Table 5.2, Table 5.4, Table 5.3). Even the slightly yellowish liquids Midel 7131 and the Shell Diala show excellent transmission, opening up the door for other liquids with a light (yellow) colour, such as plant-based oils. This extremely low absorption makes up for the higher reflection losses most liquids have due to their lower refractive index. This makes all liquids slightly outperform the conventional EVA and have around the same performance as UV-transparent EVA. The conventional EVA absorbs significantly more in the UV region, something that the EVA-UVT solves. Especially the Midel, Mivolt and Shell show excellent performance, on the same level as EVA-UVT, due to their higher n values and thus lower reflection. Closely followed by PDMS, which has the lowest parasitic absorption of all samples (except for air). The air encapsulation scores lowest due to its high reflection, which was expected

When looking at which effect, reflection or absorption, is dominant in securing a better photocurrent, it seems that the order of the lowest reflector best resembles the highest photocurrent order. This can be explained by the fact that all the liquids have relatively low absorption, meaning the effect of reflection plays a more important role (there is less to gain with having an even lower absorption compared to lower reflection). Suggesting that the n values are more important than the k values when selecting a liquid. However, as discussed before, the k values are difficult/impossible to change, but reflection can be engineered and reduced by adding ARC layers or texturing, which will be addressed in the following section.

5.3.3. Glass texturing

For the following configurations, only the TOPCon technology is simulated to reduce the number of simulations and focus on the effect of different encapsulations when changing 1 parameter, such as glass texturing. To determine the best-performing glass texturing geometrical shape, several simulations with EVA-Conv and no ARC on the glass are performed. They showed that inverted pyramids (J = 41.0 mA/cm^2) performed best, compared to Albarino P (J = 39.5 mA/cm^2) and Albarino G (J = 40.9 mA/cm^2), which is why they selected for further simulations with the liquids. It could be that (perfectly geometrical-shaped) inverted pyramids are not possible to fabricate. In that case, this would be a theoretical simulation to see the effect of the best-performing texturing.

As seen by the low reflection values for all samples in Table 5.2, the glass texturing is very effective in reducing the reflection, except for air, which is addressed later on, achieving the lowest reflection, leading to the highest photocurrent, of all simulations performed so far. Shell has the highest photocurrent of 41.54 mA/cm^2, driven by its reduced reflection of 1.32 mA/cm^2 (decrease of 1.33 mA/cm^2), while slightly increasing its parasitic absorption to 0.62 mA/cm^2 (increase of 0.29 mA/cm^2, because of more internal reflection and longer optical path-lengths). Most simulations follow within 0.4 mA/cm^2, an increase in the difference between samples, caused by some interesting mechanisms that come into play, because of the glass texturing.

Due to the glass texturing, light is refracted and transported to the encapsulation layer at many different angles, which gives three main effects. First of all, the total reflection of light is lower due to more scattering, which is mainly directed to go inside the module, the effect that textured glass is known for [207]. Secondly, this scattering at different angles creates longer optical pathways, leading to higher parasitic absorption, which is seen by the higher losses in the encapsulation layer for all samples in Table 5.2. This effect is stronger at higher angles of incidence, which is visualised in Table 5.5, causing PDMS to slightly outperform EVA-UVT in photocurrent. This is very interesting as it could play a role in total energy generated by the solar module, since the angles of incidence are not always 0 - 5 $^\circ$ as used in most simulations. The effect is also tested with more simulations at various angles of incidence without glass texturing, visualised in the Table C.1 in the appendix. PDMS is again performing better than at 0 - 5°, although it is not a linear effect and PDMS and EVA-UVT alternate each other. The effects on the energy generated will be simulated with the PVMD Toolbox in a later section.

Table 5.5: Photocurrent of AIR, PDMS, EVA-UVT and MIVOLT with glass texturing at various angles of incidence, interestingly PDMS performs better at higher angles due to its lower absorption (compared to EVA-UVT)

Angle of incidence	**2.5**	**22.5**	**42.5**	**62.5**	**82.5**
AIR	36.46	38.29	36.80	25.09	12.81
EVA-UVT	41.50	39.96	39.49	37.10	30.93
MIVOLT	41.49	40.05	39.56	37.19	30.97
PDMS	41.41	40.06	39.55	37.17	30.93
Delta PDMS and EVA-UVT	-0.08	0.10	0.06	0.07	0.00

Lastly, another interesting effect comes into play; there is more internal reflection due to light reflected at higher angles than the critical angle, leading to more parasitic absorption losses. This effect is most evident in air, as it has the lowest refractive index and thus the lowest critical angle (41.8 °), which can be calculated with the following formula (the refractive index is wavelength-dependent, and thus the critical angle as well, but for these calculations it is only reported for 632 nm):

$$\sin\theta_{\text{crit}}(\lambda) = \frac{n_1(\lambda)}{n_2(\lambda)} \tag{5.8}$$

where θ_{crit} is the critical angle where all light is internally reflected, n1 and n2 are the refractive indices of medium 1 and 2, respectively.

The inverted pyramids have an angle of 45°. When light is coming in from 0 - 5°it will be refracted to 28.2 - 25.4°, leading to an angle of incidence on the encapsulation layer of 61.8 - 64.6°, according to Snell's law.

$$n_1 \sin\theta_i = n_2 \sin\theta_t \tag{5.9}$$

Since the critical angle for air is lower, this leads to more internal reflection, and this is the reason for the air encapsulation having an even higher reflection (7.02 compared to 4.82 mA/cm^2) than in the original simulation or without glass ARC, as seen in Table 5.2. As this seemed counterintuitive, glass texturing is supposed to reduce reflection, instead of increasing it; more simulations were performed to check if this was indeed the case. Therefore, the n values were artificially changed to 1.3, 1.2, 1.1 and 1.05, and other texturings were used for glass. Higher n values gave lower reflection, as expected,

but it was interesting to see that around 1.3 there is a turning point where the glass texturing works positively again, reducing reflection instead of increasing it. This is explained by the critical angle, which is 60.1 °for n = 1.3, just under the incidence angle of light for the encapsulation, creating more internal reflection and losses in the glass and encapsulation layer. This effect for was also checked by Juan Camilo Ortiz Lizcano, by adjusting the slopes of the inverted pyramids. Lower slope angles (20°- 35°), meaning light can come in below the critical angle, gave a slightly lower reflection, but higher glass absorption compared to flat glass. Increasing the slope increased both reflection and parasitic glass absorption, as expected.

When looking at the glass texturing values in Table 5.2, this effect of increased internal reflection in the glass layer is nicely seen in the higher parasitic absorption losses in the glass layers (they all increased by $\approx$ 0.1 mA/cm^2). In the original simulation, the glass absorption was almost identical, but now there is more deviation because of this internal reflection, especially for air, which has almost twice the losses compared to other samples and its original value (0.76 compared to 0.3 mA/cm^2). Also, for the total reflection, this effect plays a role, EVA-Conv reflection is not only reduced compared to the original simulations but also relatively to the other samples, difference with Mivolt was 0.03 mA/cm^2, which increased to 0.06 mA/cm^2, because of its lower internal reflection as a compounding effect.

Eventually, these effects give a balance in performance; as mentioned, EVA-Conv enjoys an absolute and relative decrease in total reflection, but at the same time sees an increase in parasitic absorption in the encapsulation and glass layer due to longer optical path lengths. EVA-UVT gives an interesting twist by absorbing less in its front encapsulation layer, but more in its back encapsulation layer, causing it to slightly underscore the Shell. The air encapsulation gives an interesting example of internal reflection and warns for the use of glass texturing when air is used. In the following paragraph, the other method, ARCs, for reducing reflection is discussed.

5.3.4. Advanced ARC glass and cell

As discussed in the methodology, an advanced ARC was developed, optimised for air, consisting of a maximum of 2 ARCs per interface. It successfully reduced the reflection in all samples, as can be seen in the advanced ARC section in Table 5.2. The positive effect is stronger for samples with a lower refractive index value, as expected, because their n values are closer to air. This means that now water is the best performing sample, with 41.25 mA/cm^2 having the closest n value to air, reducing its reflection to 1.99 mA/cm^2, while parasitic absorption stays the same. Most liquids follow within 0.15 mA/cm^2, with glycerol (Δ 0.28 mA/cm^2) and EVA-UVT (Δ 0.19 mA/cm^2) falling further behind because of their higher refractive index, giving higher index mismatching since the optimisation is performed for the low refractive index of air.

The advanced ARC and original TOPCon simulation was run for various angles of incidence, 2.5°, 22.5°, 42.5°, 62.5°, 82.5°. Because there are 18 angular intervals, the angles correspond to an interval, so 90/18 = 0 - 5 °interval, so noted as 2.5°. This is visualised for air encapsulation in Figure 5.7, which has the largest effect on reflection and photocurrent because of its lower refractive index (highest at 82.5°is 22.63 mA/cm^2 and 22.15 mA/cm^2 for reflection and photocurrent, respectively). The other samples follow a similar trend, all significantly decreasing after 60 °. This is good to keep in mind with the other simulations, as all of them show the ideal situation of 2.5 °angle of incidence.

Air encapsulation sees a significant increase in photocurrent (40.44 mA/cm^2, increase of 1.29 mA/cm^2), coming close to the original values of the other samples, giving confidence in this technique for increasing the performance of the samples. It will be interesting to see the performance of ARC optimised for the best-performing samples in the optimisation section, potentially in combination with glass texturing.

5.3.5. Multilayer encapsulation EVA - Sample

Multilayer encapsulation, first a layer of EVA-Conv followed by the samples, gives lower reflection but higher parasitic absorption, eventually producing lower photocurrents overall. The best performing sample is EVA-UVT with 40.44 mA/cm^2, followed closely by all liquids (within 0.12 mA/cm^2), except water, showing an increase in liquid performance. This is due to the higher n values of EVA, the layer acts as an ARC by refractive index grading, lowering the reflection. Unfortunately, the layer is also absorbing significantly more, cancelling any positive effects.

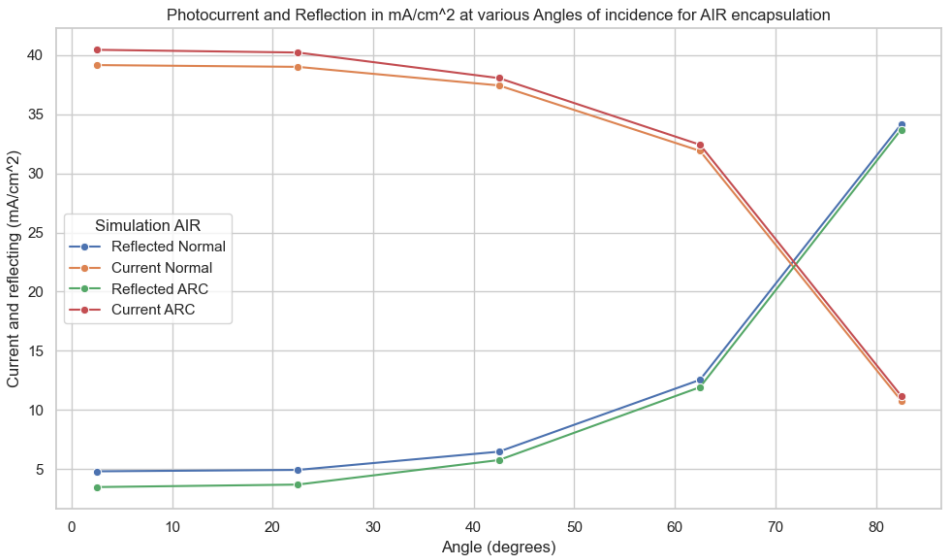

Figure 5.7: Photocurrent and reflection of AIR encapsulation with original and Advanced ARC simulation for various angles of incidence

The thickness of the EVA-Conv layer was now half of the total front encapsulation (225 μm). If this thickness is decreased, the parasitic absorption is decreased, which might make this configuration interesting again. This is checked with optimisation.

5.3.6. Biosphere-TU Delft case

In this configuration, there was a thicker encapsulation on the front (0.6 mm assumed) of the solar cells (and less on the back (0.3 mm)), in combination with no ARC on the glass, which is the case for some 1-cell modules currently produced. As expected, the overall parasitic absorption in the encapsulation layer is higher, and the reflection is higher, leading to a lower photocurrent in all samples. The highest performing sample is now Mivolt with 40.10 mA/cm^2, followed by the best-performing liquids (and EVA-UVT) within 0.04 mA/cm^2 and slightly further glycol, glycerol and water (0.26 mA/cm^2) because of their higher extinction coefficients compared to the other liquids. This is logical because the lower extinction coefficients of the liquids give them an advantage when the encapsulation layer is increased, since the absorption plays a more critical role.

This is important to note when changing the layer thickness of the encapsulation and deciding where the solar cells will be placed in the encapsulation. Also, as mentioned before, the glass could slightly deform because of the liquid pressing on it when installed at an angle. This could lead to different thicknesses in encapsulation (less liquid at the top, more at the bottom), leading to significantly different photocurrents, $\approx$0.8 mA/cm^2 when front encapsulation is changed from 450 to 600 μm, causing the whole string/module to operate at this lower current. Changing the encapsulation thickness is explored further in the optimisations.

5.3.7. Real application PVMD toolbox

As seen in the simulations, there are small differences between standard EVA encapsulation, liquids and different configurations. To see how these differences would affect the energy yield of a solar module, they are simulated in real-world conditions using the PVMD Toolbox from TU Delft [208]. For these simulations, the best performing liquids are selected; the highest photocurrent and lowest reflector: Mivolt, and the lowest absorber: PDMS, are compared to air and EVA-UVT encapsulation. These liquids are also used in the following optimisation chapter.

The EVA-UVT, AIR, PDMS and MIVOLT are simulated in the standard TOPCon cell configurations Figure 1.3 and their simulated values are the top row in Table 5.2. This configuration is of a typical solar module not designed for liquid encapsulation and therefore EVA-UVT produced slightly higher photocurrent (0.02 mA/cm^2 difference Mivolt). This is chosen to see the ”worst case” scenario where no

adjustments are made, but as seen in the other simulations (and following optimisation section), liquid encapsulation can produce the same or higher photocurrent than standard (or future) encapsulation material with adjustments.

The PVMD Toolbox is used to simulate real-life conditions from a solar cell to multiple solar module arrays under various configurations [208]. This is useful for quantifying the difference in power output between the liquid encapsulated solar modules and air or EVA, under real-world conditions. Therefore, a standard solar module configuration in Delft is simulated with weather data from 2005 for 1 year, keeping all parameters the same except for the encapsulation material. The following assumptions were made for the PVMD toolbox:

- Periodic simulations (1 solar module, no environment obstacles (shading), meaning lower computational time)
- Albedo = 0.2
- Weather data from 2005 (January 1 to December 31) in Delft (52.012, 4.359) with clouds at each hour from Meteonorm
- Efficiency TOPCon cell = 24% for thermal calculations (thermalisation of remaining solar energy)
- Modules composed of 72 M10 cells (12 x 6) with 3 bypass diodes
- Installed at 31 °tilt, facing south, 50 cm above ground
- Electrical parameters taken from SiliconV2023 (this is a SHJ cell, currently only one available in the PVMD toolbox)
- The thermal behaviour of Liquids and air is assumed to be similar to standard solid encapsulation. This is not the case, but more detailed thermal modelling would be needed to properly integrate this.
- electrical behaviour is assumed same as standard solid encapsulation, also not the case, but more detailed electrical modelling is needed to see the effect and integrate it into these simulations.

The output of the simulations includes the DC power generated and loss analysis, with per component the amount of energy lost, among others. The main focus is on the difference in DC output over the year between the different encapsulation materials. All outputs are in Table C.2 in the appendix, from which the relevant parameters are selected. The main parameter, DC energy output, compared between the different simulations is visualised in Table 5.6, together with the losses that fluctuated the most between the different encapsulation materials. It is important to note that there was still an unresolved bug in the PVMD toolbox simulation, causing the parasitic absorption to be positive (seen in Table 5.6 as a negative value), which is not correct. Although the reason for this still needs to be further investigated, the main hypothesis (accredited to Youri Blom) is that the assumption of using the electrical characteristics of an SHJ cell while optically using the TOPCon cell has the following effect. Part of the parasitic absorption losses in a SHJ cell can still be used to produce a photocurrent, but with TOPCon, this is smaller (or not possible). However, the simulation still assumes part of the parasitic absorption losses are generating a photocurrent; it might be that this assumed ”boost” (that is added to the overall photocurrent) is more than the parasitic absorption simulated by the TOPCon, resulting in a net positive parasitic absorption ”loss”. As this ”boost” is applied to all 4 encapsulation samples, it is assumed that the differences between simulations are still correct (but the absolute DC power output of all samples is incorrect, as it should be slightly lower). More research is needed to confirm this by either adjusting the electrical characteristics to match the TOPCon cell or using a SHJ cell in combination with the liquid encapsulation for the optical simulations. That being said, the real-life simulations gave some interesting insights.

Table 5.6: Real-world simulations using the PVMD toolbox and different encapsulation materials EVA-UVT, AIR, MIVOLT and PDMS, expressed in DC energy (Wh) produced in a year (2021) in Delft. Surprisingly, PDMS has the highest DC output, while in the optical simulations it has slightly lower photocurrent at 0 - 5 \deg angle of incidence. At lower angles of incidence, the effect of lower reflection becomes less dominant and the lower absorption of PDMS gives the highest photocurrent.

Loss/generation	EVA-UVT Energy (Wh)	EVA-UVT (%)	AIR Energy (Wh)	AIR (%)	MIVOLT Energy (Wh)	MIVOLT (%)	PDMS Energy (Wh)	PDMS (%)
Angle mismatch	397020	13.45	395250	13.38	396970	13.45	396670	13.44
Reflection	78139	2.65	149940	5.08	78176	2.65	79306	2.69
Parasitic absorption	-19520	-0.66	-20896	-0.71	-19520	-0.66	-20391	-0.69
DC Energy	**618190**	**20.948**	**570010**	**19.299**	**618090**	**20.946**	**618620**	**20.952**
DC difference EVA	**-**	**-**	**- 48180**	**-1.649**	**- 100**	**- 0.002**	**430**	**0.004**
Relative difference EVA	-	-	**- 7.79%**		**- 0.016%**		**0.070%**	

Surprisingly, PDMS has the highest DC output with 430 Wh (0.07%) more generation than EVA-UVT. The difference is rather small but shows an interesting principle and becomes more significant when imagining more solar modules. The main differences in losses (leading to the different DC outputs) are shown in Table 5.6; (i) angle mismatch, (ii) reflection, and (iii) parasitic absorption. As seen in the earlier simulations, PDMS has a higher reflection (-1167 Wh, 0.19% to EVA), but lower parasitic absorption (+871 Wh, 0.14% to EVA). The angle mismatch is affected by the lower parasitic absorption in the following way. The angle mismatch is affected by the difference between the voltage of the cell and the bandgap energy; the voltage of the cell is affected by the temperature, which in turn is affected by the amount of light absorbed within the solar module. Since the PDMS absorbs less light (and thus total energy), more light is reflected and transmitted through the solar module, as seen in Table 5.2, the temperature of the solar module is lower. If the temperature is lower, the voltage is lower and the mismatch losses are lower (+350 Wh, 0.057% to EVA-UVT), this can also be seen for air in Table 5.6, which also absorbs less light. This increased importance of low (parasitic) absorption is also seen by the following effect. While in the optical simulations, PDMS has a slightly lower photocurrent at 0 - 5 $^\circ$ angle of incidence. At lower angles of incidence, as shown before, the effect of lower reflection becomes less dominant, and the lower absorption of PDMS gives the highest photocurrent. Since the real-world simulations operated on multiple angles of incidence, the PDMS is performing better than originally in the optical simulations, with 0- 5 $^\circ$ usually used. The total difference is tipped in favour of PDMS by slightly lower losses in thermalisation and below bandgap losses, among others.

The Mivolt had a very similar photocurrent to the EVA-UVT in earlier simulations (0.02 mA/cm^2 difference, higher reflection but lower absorption), which produces almost identical DC output, 100 Wh (0.016 %) less over the year compared to EVA-UVT. This nicely highlights how the slightly higher reflection of the liquids can be compensated (and almost perfectly balanced out) by their lower absorption compared to EVA.

The air encapsulation is the worst performing, 48,180 Wh (7.79%) lower than EVA-UVT, which is significantly less. It is expected that this becomes even worse with the thermal behaviour of air, heating the panels more than solids or liquids.

The PVMD Toolbox simulations give interesting insights into the interrelated mechanisms and losses affected by using a liquid encapsulation. It reminds us that the optical behaviour is a part of a bigger picture for which future research is needed. This becomes evident when looking at the assumptions and their effect on the simulations, in which two key aspects stand out: electrical and thermal behaviour.

As mentioned before, the assumption of the electrical characteristics of an SHJ cell might be causing problems regarding the parasitic absorption ”losses”. Furthermore, the electrical behaviour of the liquids could have a positive effect (better solar cell surface passivation for example) on the performance, as addressed in chapter 2 and chapter 3. This calls for electrical modelling and experiments to be performed to map out the electrical effect of the liquids on the solar cell. The optical simulations are already influencing the thermal losses in the solar cell, even though the direct thermal effect of the liquid encapsulation is not taken into account yet. It is assumed (and calculated in [55]) that the liquids have improved heat dissipation, boosting their performance. However, more detailed thermal modelling is required to confirm this. This electrical and thermal research could strengthen the PVMD Toolbox results and give more confidence in the proper performance of liquids compared to EVA.

5.4. Optimisation

In this section, the best performing liquids (same as the PVMD Toolbox simulations, highest photocurrent and lowest reflector: MIVOLT, lowest absorber: PDMS) are selected and compared to Air and EVA-UVT encapsulation in various optimisation configurations.

5.4.1. Thickness layers

To see the effect that different layer thicknesses have on the simulations, the Glass, Encapsulation and Si absorber layers were adjusted. As mentioned before, the effect of increasing thickness is already known, and the simulations nicely followed this expectation. Thicker glass and encapsulation give more parasitic absorptions, leading to lower photocurrents; a thicker Si absorber gives higher photocurrent, as can be seen in Figure 5.8.

Changing the glass or Si Absorber thickness has a similar effect for all encapsulation materials, which is why the slope in each of the top two graphs, a and b, in Figure 5.8 is similar for all materials. As already mentioned and explained in chapter 4, light absorption follows an exponential trend according to Beer-Lambert's Law. This can be seen as the slight bend in the curves of glass and Si absorber, although it almost behaves linearly. For glass, this is due to its very low extinction coefficient k; higher k gives better visible exponential behaviour, and the distance; the exponential behaviour is better seen at lower thickness values (first 1000 μm). So a thicker material and step size would be needed to nicely visualise its exponential behaviour. Same for the Si Absorber, behaviour is better visualised at the start of the material, and increased step size and range.

In the data, this exponential behaviour is seen in the difference Δ in photocurrent between steps, which increases and decreases. To still quantify this Δ, we take the average Delta over the range, so we get an idea of the effect on the photocurrent in this range. For glass, this is a reduction in photocurrent of $\approx$ 0.060 mA/cm^2 for every 500 μm added to the glass over the range 2000 - 5000 μm (mA/cm^2). For the Si absorber layer, there is an increase of 0.032 mA/cm^2 for every 5 μm added to the Si absorber over the range 150 - 200 μm (mA/cm^2). For the encapsulation thickness, the effect also varies for each material (different extinction coefficient), which is addressed in the following paragraph.

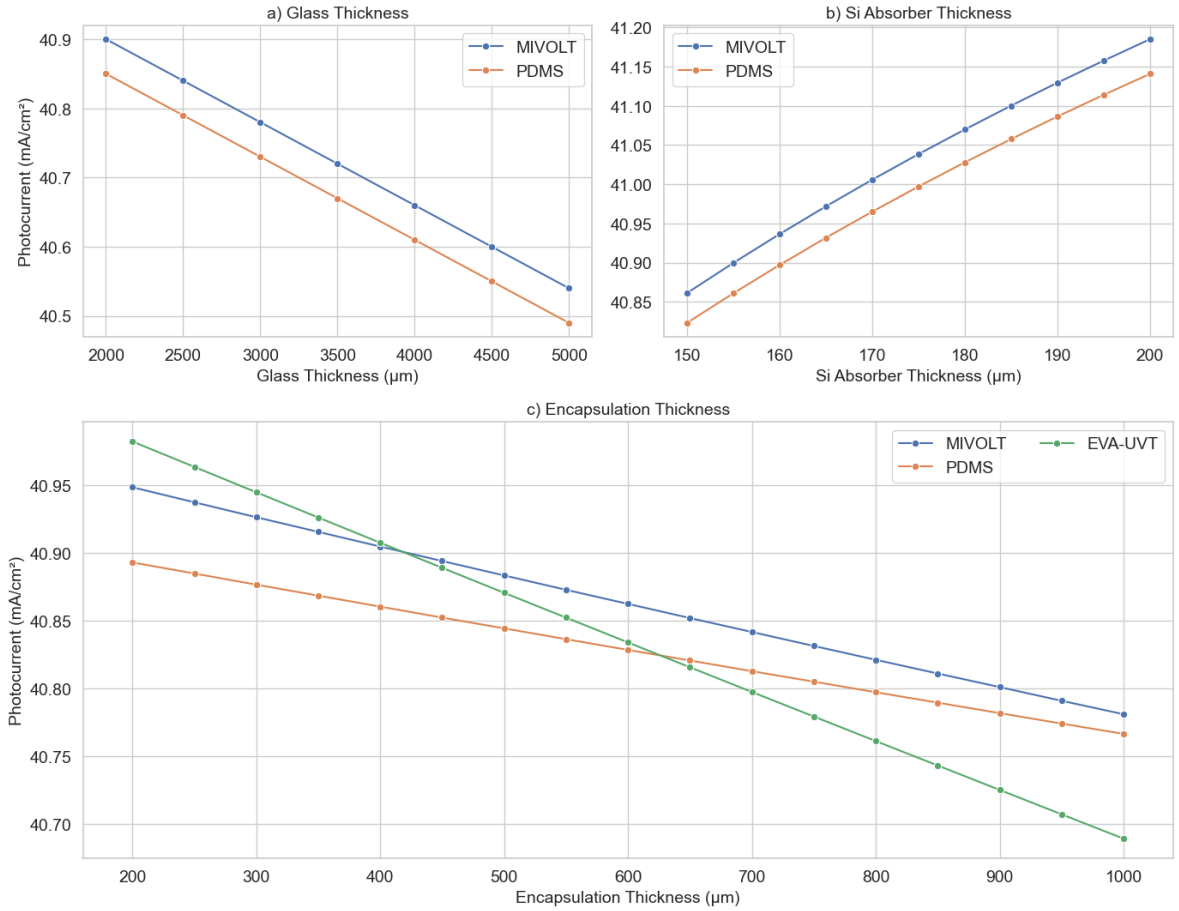

Figure 5.8: Layer thickness variation plots for Glass, Encapsulation and Si Absorber using PDMS, MIVOLT and EVA-UVT encapsulation. As expected, glass and Si absorber thickness changes have a similar effect on photocurrent, while encapsulation thickness has a different effect for various materials

When varying the encapsulation thickness, it produces a different effect on the photocurrent, in contrast to glass and Si absorber, due to the material-specific extinction coefficient k. That is why the slopes of the curves in Figure 5.8 (c) are not the same and even cross each other at certain points. This nicely highlights when the absorption mechanism becomes the dominant effect for determining the photocurrent, as opposed to the reflection. The EVA-UVT with higher n and k values is best performing with thinner encapsulation, but is surpassed by Mivolt around 450 μm encapsulation thickness (in agreement with the previous simulations with 450 μm where the difference between Mivolt and EVA-UVT was around the 0.02 mA/cm^2) and PDMS around 630 μm. Also, PDMS seems to head towards crossing Mivolt after 1000 μm, although this would be rather thick for (front) encapsulation, which usually ranges from 300 - 500 μm. It is interesting to see that the Mivolt would outcompete the EVA-UVT when a slightly thicker encapsulation is chosen. The values seen in Figure 5.8 are tabled in Table C.3 in the appendix, where the exponential behaviour is visualised by showing the decreasing Δ.

5.4.2. Theoretical optimisation

The theoretical optimal encapsulation does not absorb light (k = 0) and has minimal reflection. Setting k to zero might cause problems with the reflection, so through iteration, various k values (10^{-6} - 10^{-12} are simulated to find the lowest value. In general, the optimal n value for the encapsulation is the same n value as the glass, causing minimal reflection losses at this interface. However, to see if the encapsulation could perform refractive index grading, similar to an ARC, the same approach for calculating the ideal n value as for an ARC is taken. The encapsulation is assumed to be between the Glass (n = 1.512) and the SiN_x(n = 2.09), which leads to an idealised encapsulation material with n = 1.78 at 630 nm, whole range: 1.90 - 1.76. These ideal n values over the range 300 - 1200 nm are

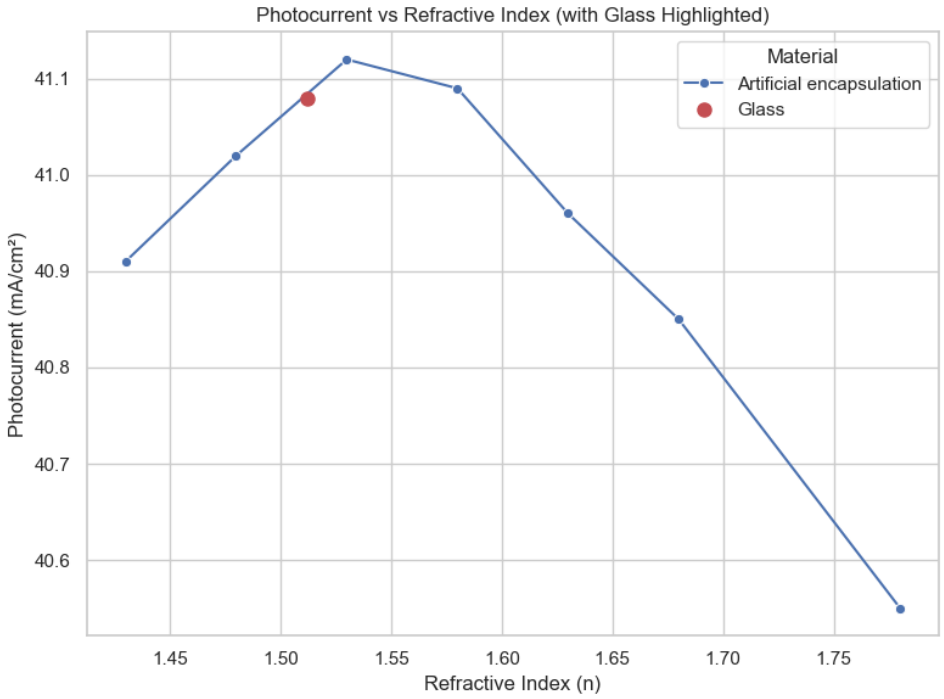

Figure 5.9: Photocurrent of the ideal artificial encapsulation material for various n values, peaking around n = 1.53 with 41.12 mA/cm^2

combined with k = 0 over the whole range to get an idea of the perfect encapsulation material and the theoretical maximum photocurrent to be obtained. However, as expected, setting k to zero does not work, nicely showing the dependent nature of n and k discussed earlier. It was found that k = 10^{-8} works by providing low reflection while not significantly absorbing.

Secondly, the optimal n value of the encapsulation is tied to its extinction coefficient k and cannot be as easily calculated as done for the ARC, also because the material is way thicker and handled as a layer instead of an interface in GenPro. This was also discovered when adjusting the n values for PDMS, as discussed in the following paragraph. Therefore, for the optimal encapsulation material, the n values were changed from 1.43 to 1.78, and k was set to 10^{-8} for all wavelengths. Also, the n values of glass were used in combination with k = 10^{-8}, to see if this produces the best match. Through this method, the theoretical optimal photocurrent (optimal encapsulation material) was calculated to be 41.12 mA/cm^2 around n = 1.53, as seen in Figure 5.9. Interestingly, the n value is close to the glass value but not the same; slightly higher is beneficial, so some index grading seems beneficial. Also, the earlier simulated values are quite close to the theoretical optimum values found in this configuration.

To see how close we can get to this optimal encapsulation material, the n values of the lowest absorber, PDMS, are artificially changed from their original value of n = 1.41 to 1.91 with a step size of 0.1, to see the effects additives could potentially have. This is plotted in Figure 5.10, where we can see that the value n = 1.51 (delta n = 0.1) gives the maximum photocurrent of 41.02 mA/cm^2. The CEA-INES concept performed a similar optimisation, which can be seen in their supportive material, where glycerol peaked around n = 1.517, with a maximum photocurrent of 37.0 mA/cm^2 [55]. From this, we conclude that the optimal n value (n $\approx$ 1.52) for the encapsulation material is slightly above glass, and depends on the k values of the material.

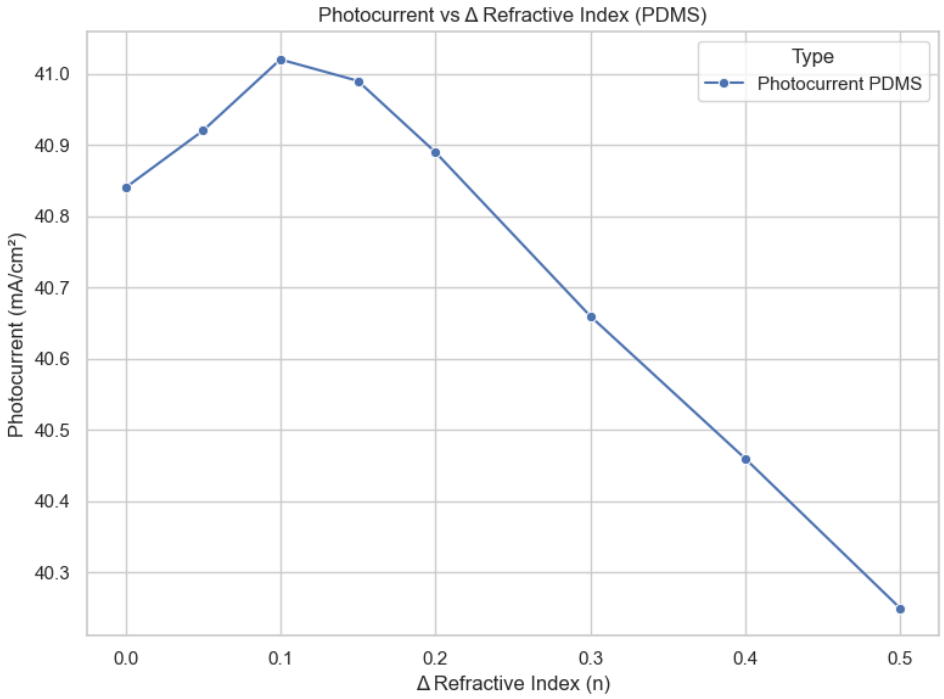

Figure 5.10: Effect on photocurrent by increasing the Refractive index of PDMS artificially, optimum value around n ≈ 1.51

From these simulations and graphs, it is possible to get an idea of the influence of the refractive index on the photocurrent. On average, for PDMS, the photocurrent increases by 0.077 mA/cm^2 for every Δ n = 0.1 towards the optimum value. This value highly depends on how far away from the optimum point you are, as it is not linear. It also depends on the material and the extinction coefficient, so it should be carefully applied to other materials. That being said, it quantifies the influence a higher or lower refractive index value can have. For example, the 0.02 difference in n different temperatures can have would have an insignificant effect of 0.00154 mA/cm^2 [164].

5.4.3. ARC optimised per sample

The previously produced advanced DARC was optimised for air; the same approach will be taken for the other samples (EVA-UVT, PDMS and MIVOLT). The outside glass DARC will be kept the same (AF2400 n = 1.28, GlassARC/SiO_2 n = 1.413), the inside will be adjusted accordingly, as well as the ARC on the solar cell. To see where the most reflection takes place, the layers and interfaces are simulated one for one. The largest reflection takes place at the first interface, going from air to glass, so placing the correct ARC here has the most effect. Multiple ARC materials are tried that come close to the ideal calculated refractive index value per encapsulation material. Some materials (such as SiN_x and SiO_x) have multiple nk files in GenPro with slightly different n and k, which are all tried, and their names are shown as they appear in GenPro4. See also Table 5.1 for the overview of materials and their nk files.

AIR

The effect of an advanced ARC for air has already been simulated and produced a maximum photocurrent of 40.44 mA/cm^2 as seen in Table 5.2.

EVA-UVT

The optimal value for the DARC for the inside of the glass can be calculated in the following way, where bottom refers to the position of the lowest ARC material and top to the highest positioned ARC material when looking at the DARC stack. The inside of the glass DARC is between the glass (n = 1.51) and the EVA-UVT encapsulation (n = 1.492), which produces an optimal refractive index value for the bottom ARC material (so touching the encapsulation) of n = 1.499 and n = 1.51 for the top ARC (touching the

glass). Currently, no ARC material in the GenPro database possesses such refractive index values. The refractive index of EVA is already very close to glass, so the reflection at this interface is limited.

For the DARC on the solar cell surface, the DARC is between the EVA-UVT encapsulation (n = 1.492) and the Si Absorber (n = 3.869), producing a bottom n = 2.050 and top n = 2.816. The closest materials for this would be the SiN(n = 2.089) and TiO_2 (n = 2.295). This combination produces a photocurrent of 41.38 mA/cm ^{2}.

The combination was also tried without the TiO_2 layer, since most reflection is at the air/glass interface, which produced very similar, but slightly higher, results (41.52 mA/cm^2) as can be seen in Table 5.7. The SiN(2.09) was switched for SiNARC (different nk file in GenPro, similar material) because this has lower absorption, again showing that the refractive index values at this interface play a submissive role compared to the absorption. Removing the SiN_xwould not make sense as it would remove the passivation layer.

Table 5.7: Optimisation of ARC for multiple samples with available ARC materials in the GenPro4 database, Mivolt achieved the highest photocurrent of 41.54 mA/cm^2. Green colour is the best performing value, and yellow are the layers that are changed in-between samples.

Layer (mA/cm^2)	EVA-UVT		PDMS		MIVOLT (no EVA)	MIVOLT (EVA)
Reflected	1.79	Reflected	1.96	Reflected	1.64	1.65
AF2400	0.00	AF2400	0.00	AF2400	0.00	0.00
GlassARC	0.00	GlassARC	0.00	GlassARC	0.00	0.00
Glass	0.35	Glass	0.33	Glass	0.33	0.33
		GlassARC	0.00	SiO2TUD	0.00	0.00
		SiO2TUD	0.00	(No) EVA-UVT		0.00
EVA-UVT	0.37	PDMS	0.25	MIVOLT	0.34	0.34
SiNARC	0.21	SiNARC	0.21	SiNARC	0.17	0.18
				TiO_2	0.06	0.06
c-Si-2015	41.52	c-Si-2015	41.35	c-Si-2015	41.54	41.51
SiO2-Lem13	0.00	SiO2-Lem13	0.00	SiO2-Lem13	0.00	0.00
npolySi	0.16	npolySi	0.15	npolySi	0.16	0.16
SiN(2.09)	0.00	SiN(2.09)	0.00	SiN(2.09)	0.00	0.00
EVA-UVT	0.16	PDMS	0.14	MIVOLT	0.17	0.18
Glass	0.08	Glass	0.06	Glass	0.06	0.06
Transmitted	1.82	Transmitted	2.01	Transmitted	1.98	2.00

PDMS

The optimal value for the DARC for the inside of the glass can be calculated in the same way; the DARC is between the glass (n = 1.512) and the PDMS encapsulation (n = 1.410), which produces an n = 1.443 for the bottom and n = 1.477 for the top. For which the closest materials are GlassARC (1.413) and SiOTUD(1.4755), it was also tried with SiO2-lem13 (1.472) and EVA-UVT (1.492), but these gave slightly lower results. (n = ..., will be left out in the upcoming paragraphs for easier reading).

For the solar cell surface, the ARC is between the PDM encapsulation (n = 1.410) and the Si Absorber (n = 3.869), producing a bottom n = 1.974 and top n = 2.764. The optimal candidates for this would be SiNARC (1.98) and TiO_2 (2.295). This combination gave a photocurrent of 41.32 mA/cm^2.

Again, the combination was tried without the TiO_2 layer, as this worked beneficial for EVA-UVT, and this also had a small positive effect on PDMS, with a slightly higher photocurrent of 41.35 mA/cm^2 as seen in Table 5.7.

MIVOLT

The optimal value for the DARC for the inside of the glass can be calculated in the same way; the DARC is between the glass (1.512) and the MIVOLT encapsulation (n = 1.459), which produces an n = 1.477 for the bottom and n = 1.494 for the top. The ARC material that comes close are SiOTUD(1.4755) and EVA-UVT (1.492). The EVA-UVT is also tried, which resembles the multilayer configurations already tried, now with a thinner layer of 0.1 mm, which will be further examined in the following section.

For the solar cell surface, the ARC is between the MIVOLT encapsulation (n = 1.459) and the Si Absorber (n = 3.869), producing a bottom n = 2.020 and top n = 2.795. For which the following ARC

materials come close: SiNARC (1.98) and TiO_2 (2.295), ZnO_x (1.994) was also tried, but absorbed more. This combination produced a photocurrent of 41.54 mA/cm^2, which is the highest simulated value so far (along with the SHELL glass texturing), as can be seen in Table 5.7.

Also for Mivolt, the combination was tried without the TiO_2 layer; interestingly, this produces slightly lower values (41.52 mA/cm^2), in contrast to the effect on EVA-UVT and PDMS. This can be explained in the following way: when looking at the calculated optimal n values for the ARCs and the n values of the ARC materials actually available, we see the smallest mismatch for Mivolt. This results in Mivolt having the lowest reflection, leading to the highest photocurrent. The reason that the Mivolt is benefiting from the additional TiO_2 layer is that the largest reflection (the glass interfaces) is already reduced, while for EVA-UVT and PDMS, they are still high, and the light that the TiO_2 layer could help "catch" is already reflected. That is why the additional TiO_2 layer will not have a positive effect until the reflection at the glass is reduced, so it can do its part later on in the solar stack. The area where this takes place is around the 300 - 450 nm, where the reflection is lower for Mivolt as can be seen in Figure 5.11a.

The differences are again very small, and the added complexity of having a DARC (or TiO_2 layer) on the solar cell surface will probably not be worth it. Combine this with the results of EVA-UVT and PDMS, and it is safe to conclude that the SiN_xalone should be appropriate for the solar cell surface when using a liquid. The focus on reducing the reflection should be on the front and back sides of the glass; therefore, glass texturing with ARC is tried in the following section.

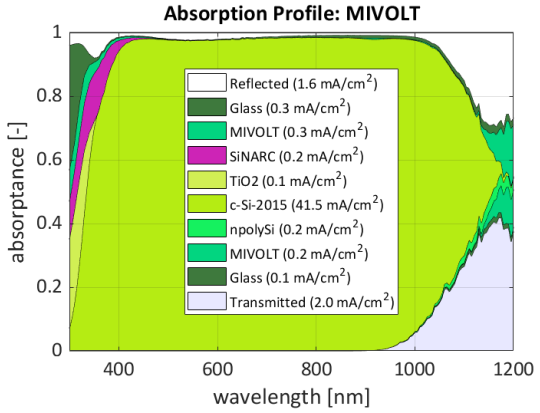

(a) Mivolt advanced ARC obtaining the highest photocurrent (41.54 mA/cm^2) so far, using ARC materials from the GenPro database

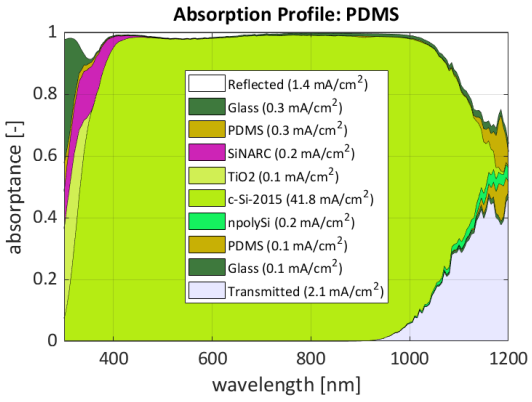

(b) PDMS theoretical ARC with a photocurrent of 41.75 mA/cm^2 using artificially generated ARC nk data

Figure 5.11: Comparison of absorption results for Mivolt using materials available in the GenPro4 database and theoretical optimal calculated ARC for PDMS

Theoretical ARC

To see the effect the calculated optimum ARC material would have, the values are again artificially changed to get an idea of the theoretical maximum. For the glass ARCs, this is not such a bad assumption, as the refractive index of SiO_x and SiN_x can be tuned [191], [192]. EVA-UVT, Mivolt and PDMS are optimised for this configuration.

The glass front side will be the same for all samples, for which the optimal values were already calculated: n = 1.146 top and n = 1.317 bottom. Which are in the range for porous SiO_2 tuning [191].

For EVA-UVT, the optimal ARC material on the inside of the glass is the following: bottom is n = 1.499 and the optimum top is n = 1.510, which produces a photocurrent of 41.81 mA/cm^2, the highest photocurrent for all simulations. What we can achieve with available materials in the GenPro database is quite close (41.52 mA/cm^2).

For Mivolt, the optimal ARC material on the inside of the glass is the following: bottom is n = 1.477 and the optimum top is n = 1.494, which produces a photocurrent of 41.81 mA/cm^2. This is the same as achieved for EVA-UVT, nicely showing the theoretical maximum achievable for this TOPCon solar module configuration.

For PDMS, the optimal ARC material on the inside of the glass is the following: bottom is n = 1.443 and the optimum top is n = 1.477, which produces a photocurrent of 41.75 mA/cm^2. Again, very close to the maximum of Mivolt (and EVA-UVT) and what is achievable with available materials, as seen in the comparison in Figure 5.11.

These theoretical optimisations nicely show how potential reflection losses from using a liquid, which generally have lower refractive index values, can be mitigated by ARCs. Compared to the record measured photocurrent of 42.60 mA/cm^2, the simulated values (max of 41.81 mA/cm^2 Mivolt) are not that far off. Important to note that this comparison is not fair as this is a measured value regarding a bare solar cell without any glass/encapsulation/etc, but it helps put the simulations into perceptive. Most can be gained by tuning the ARCs on both sides of the glass, instead of the solar cell surface ARC, which was already difficult to influence since the solar cells are off-the-shelf products. Developing special solar cells for liquids has a lower priority. In the following section, the ARCs will be combined with glass texturing to see if this could boost the performance even further.

5.4.4. Glass texturing with ARC

So far, the glass texturing has been most effective in reducing reflection by using inverted pyramids on the glass surface. To further reduce the reflection, ARC layers are applied to the texturing; whether this is currently done or can be produced by industry is not known, which is good to keep in mind. Only ARCs on both sides of the glass are applied, similar to the previous section. Using AF2400 and GlassARC (SiO) on the front of the glass and GlassARC, and SiOTUD at the inside for PDMS and MIVOLT. Texturing on the inside of the glass was also tried, but did not produce sensible results.

The glass texturing and the DARC on the front side of the glass gave the following results. A photocurrent of 41.59 mA/cm^2 for EVA-UVT, 41.70 mA/cm^2 for Mivolt, 41.65 mA/cm^2 for PDMS and 39.76 mA/cm^2 for AIR. Which is slightly higher than the advanced ARC values in Table 5.7. Especially the liquids are performing well, with values coming close to the theoretically maximum ARC achieved in the previous section.

Now, adding DARC on the inside of the glass as well for PDMS and MIVOLT gave similar, slightly lower results. A photocurrent of 41.61 mA/cm^2 for PDMS and 41.70 mA/cm^2 for Mivolt. Again, close to the theoretical maximum of the ARC optimisation. Therefore, Mivolt was also tested with its artificial optimum ARCs, which produced 41.71 mA/cm^2, slightly below the ARC theoretical optimum.

The glass texturing performs well in reducing reflection, which is further enhanced by adding ARCs; again, this helped the liquids perform on the same level (or slightly above) the EVA. This shows the good optical performance that liquids can achieve, potentially by adding ARC layers or glass texturing. As mentioned before, it is important to note that it is not confirmed that the glass texturing with ARC is (or can be) produced by the industry for an affordable price. Also, the inverted pyramids used in simulations are perfect geometrical shapes created through modelling and not microscopic scanning of the surface, meaning that the eventual fabrication will probably produce imperfect pyramids. If these look more like the previously tested Albarino P (known to be fabricated), which produced a photocurrent of 40.04 mA/cm^2 for EVA-UVT, this results in a lower value than without texturing [198]. Meaning the results for textured glass might be less beneficial than simulated here, although the added value is mainly focused on lower angles of incidence [209]. Therefore, the glass texturing with inverted pyramids and P Albarino texturing are both simulated for larger angles of incidence, which are shown in Figure 5.12. This shows that Albarino P has lower photocurrent at 0 - 30 $^\circ$ angles of incidence, but surpasses inverted pyramids at higher angles. For these simulations, PDMS seems to be slightly lower at higher angles of incidence, making it difficult to draw hard conclusions.

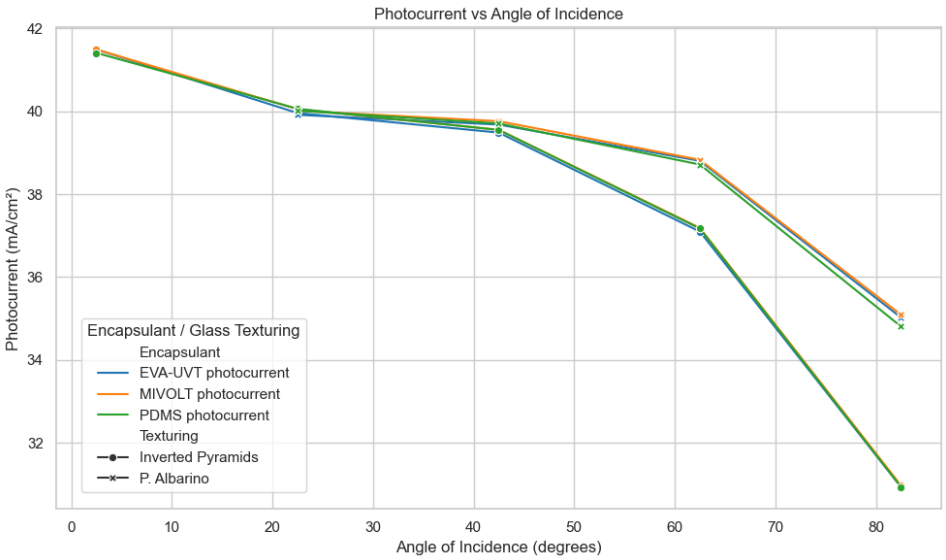

Figure 5.12: Comparison of glass texturing on photocurrent of EVA-UVT, MIVOLT and PDMS, inverted pyramids vs Albarino P. Albarino P seems to perform better on higher angles of incidence

Therefore, the DARC approach might be more viable, tuning these ARCs for a specific liquid. This depends on the glass manufacturers, who are not always keen on sharing their ARC properties or production techniques.

5.4.5. Multilayer encapsulation

The multilayer encapsulation, layer of solid EVA followed by a liquid, was simulated and depicted in Table 5.2, which showed lower reflection, but this was cancelled by more parasitic absorption from the EVA-Conv layer. Therefore, a thinner layer of EVA-UVT (which is more transparent) is proposed to reduce the parasitic absorption.

Mivolt, PDMS and air (0.35 mm) were simulated with this thin (0.1 mm) layer of EVA-UVT, which gave the following results: 40.88 mA/cm^2 for MIVOLT, 40.81 mA/cm^2 for PDMS and 39.20 mA/cm^2 for air. Again, slightly lower (Δ 0.04 mA/cm^2) than the original simulation (slightly improved for air), but acceptable in case such a layer is used for post-breakage or securing the solar cells/interconnections.

5.4.6. Different solid encapsulation materials

As already discussed in chapter 1, more solid encapsulation materials besides EVA exist, and the industry is currently moving away from EVA [34]. That is why some of the other encapsulation materials are also simulated, to compare the performance of the liquids to these new materials. The two new materials used are Polyolefin (POE) and a mixture of POE and EVA (no nk data available for this mixture, so produced by a multilayer with glass-side 0.225 mm POE and cell-side 0.225 mm EVA stacked). Solid silicone is no longer used as encapsulation, but simulated for comparison.

The results are visualised in Table 5.8, as expected, silicone is performing the worst (40.54 mA/cm^2), but comparable to conventional EVA (Δ 0.19 mA/cm^2) as seen in Table 5.2. Both polyolefin (40.82 mA/cm^2) and EVA/POE mixture (40.89 mA/cm^2) perform well and achieve similar results to EVA-UVT (40.92 mA/cm^2) and the best-performing liquids such as Mivolt (40.90 mA/cm^2). This means that the liquids are also on par or slightly outperforming the newer encapsulation to which the industry is moving.

Table 5.8: Different solid encapsulation materials with similar generated photocurrent, slightly below EVA-UVT (40.92 mA/cm^2) and MIVOLT (40.90 mA/cm^2)

Layer (mA/cm^2)	Silicone-UVT	Polyolefin-UVT	EVA/POE
Reflected	2.42	2.34	2.36
SAMPLE	0.55	0.46	0.39
c-Si-2015	40.54	40.82	40.89
Transmitted	1.98	1.78	1.78

5.4.7. Glycerol literature values

Glycerol makes a good candidate with its proper material compatibility, biodegradability, it is widely available and has a high refractive index; unfortunately, it was underperforming in this optical analysis due to higher extinction coefficient values k. As already mentioned in chapter 4, the values looked shifted compared to values found in literature, meaning the measurements performed could be slightly lower due to air bubbles present. Therefore, the glycerol is also simulated with the values found in literature to see if that makes a difference, and higher performance can be expected.

The simulations show similar results with the literature values, as seen in Figure 5.13, achieving a higher photocurrent of 40.84 mA/cm^2, coming very close to the other liquids as seen in Table 5.2, (Δ 0.06 mA/cm^2 to Mivolt). The glycerol is absorbing a bit less, but the most absorption of glycerol occurs in the region of 900 - 1200 nm, where the measured glycerol and the literature values align better. The difference in k values is within the 300 - 800 nm, but since the values are already extremely low here, there is little to no gain.

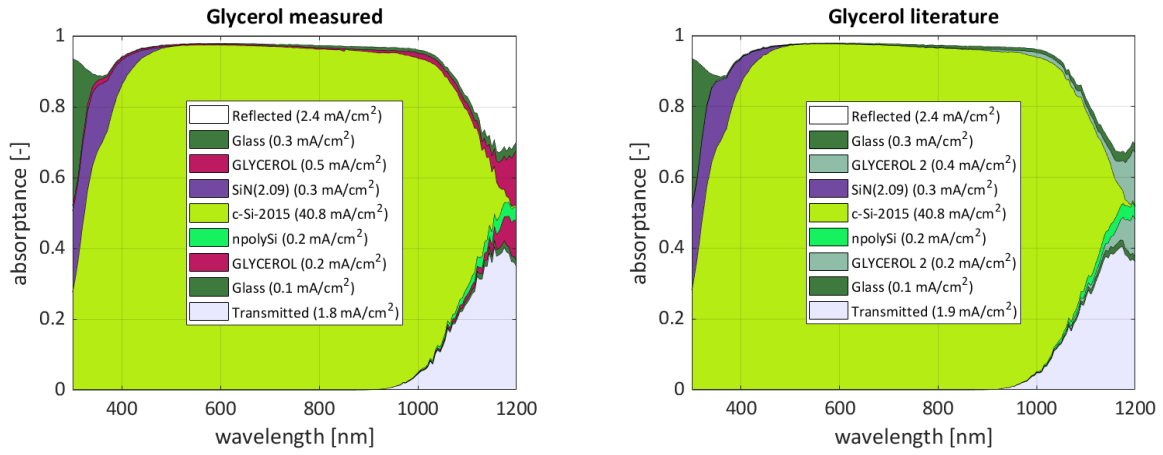

(a) Glyerol with measured extinction coefficient k values, producing a photocurrent of 40.75 mA/cm^2

(b) Glyerol with literature extinction coefficient k values [96], producing a photocurrent of 40.84 mA/cm^2

Figure 5.13: Comparison of absorption results for measured and literature values of glycerol, difference is lower than expected

5.5. Conclusion

This chapter performed extensive optical simulations to determine if liquid encapsulation could optically compete with standard EVA, air, and newer materials, including POE. The simulations in GenPro have shown that liquids are indeed a very viable option, offering a competitive, and in some optimised scenarios, a superior optical performance. The optical model was validated through comparison of simulated photocurrents to datasheet and measured values. Both showed excellent agreement with a difference compared to simulated values of Δ = 0.05 - 0.14 mA/cm^2 for datasheet photocurrents, Δ = 0.1 mA/cm^2 for bare IBC cell measurement, and between the Δ = 0.20 - 0.34 mA/cm^2 for EVA, air and PDMS filled 1-cell solar modules measured.

Initial simulations on standard TOPCon, PERC, and IBC cell stacks showed an interesting balance. A key finding is that all tested liquids demonstrated excellent transparency, even liquids with a slight yellow tint, a positive sign that other potential liquids may also outperform solid encapsulants in this aspect.

While their generally lower refractive indices led to higher reflection losses compared to EVA, this was largely compensated by their extremely low parasitic absorption. This allowed the best-performing liquids, notably Mivolt (highest photocurrent and lowest reflection, 40.90 - 41.81 mA/cm^2) and PDMS (lowest absorption, 40.85 - 41.75 mA/cm^2), to generate a photocurrent comparable (Δ 0.02 mA/cm^2 to EVA-UVT without optimisation) to, or even slightly higher than, UV-transparent EVA (40.92 - 41.81 mA/cm^2). However, the optical performance of the other liquids was very close (especially Midel and Shell, but also glycerol and glycol, within 0.17 mA/cm^2), meaning that based on optics alone, they should not be excluded, as other design benefits might justify their selection.

The real-world simulations using the PVMD Toolbox revealed an interesting insight. While Mivolt and EVA-UVT performed best at a normal angle of incidence, it was PDMS that delivered the highest annual energy yield (0.07% higher than EVA-UVT, 0.086% to Mivolt). This happens because of two reasons: (i) across the wide range of real-world incidence angles encountered throughout a day and year, the benefit of lower absorption can outweigh the penalty of slightly higher reflection, a trend confirmed in the simulations at various angles. (ii) The lower light and thus energy absorption of PDMS resulted in lower module temperature, increasing its efficiency. These real-life conditions were simulated under various assumptions, which call for more detailed electrical and thermal modelling and measurements to ensure more confidence in the results.

Finally, the optimisation configurations showed how and where liquid encapsulation could be improved. By applying advanced ARCs specifically tailored to each sample, reflection losses were significantly reduced, allowing the liquids to slightly outperform EVA-UVT. The highest photocurrent (41.81 mA/cm²) was achieved when perfect ARCs were assumed, providing a theoretical maximum for this TOPCon solar module configuration, that might be reachable with future tuning of ARC material properties. Glass texturing had an interesting effect on the air encapsulation, and warns for using glass texturing in combination with air, due to increased reflection. Glass texturing combined with ARC achieved similar, but slightly lower, photocurrents (41.70 mA/cm^2 Mivolt), but give an additional benefit at lower angles of incidence, especially for lower absorbing samples such as PDMS and air. The optimal refractive index value for the encapsulation material was found to be around the n $\approx$ 1.52, but it depends on the extinction coefficient of the material. Layer thickness of glass, encapsulation and Si absorber were adjusted to see the effect on the photocurrent, which can help with making design considerations about glass and encapsulation thickness.

In summary, this chapter confirms that the main optical drawback of liquids, their higher reflection, is compensated by lower parasitic absorption and can also be effectively engineered and mitigated. With proper design, liquid encapsulation can match and even exceed the optical performance of current solid encapsulants like EVA and newer materials involving POE. The most reachable and impactful configuration is applying a suitable ARC to the front side of the glass, as this reduces the most significant reflection losses. While this would also benefit an EVA-encapsulated module, it is a crucial first step for optimising liquid designs. More advanced solutions like glass texturing or liquid-specific ARCs on the inside of the glass showed further gains, but their added cost and manufacturing complexity must be further examined. Purely from an optical perspective, these results provide a strong justification for further investigating the other potential advantages of liquids, such as their expected benefits in thermal management, electrical behaviour, and module circularity.

6

Conclusion

This thesis set out to answer a central question: Can liquid encapsulation be a viable optical alternative to standard solid EVA in silicon solar modules? To address this, the work was structured around three key sub-goals: developing a liquid selection strategy, optical characterisation through experiments, and performing detailed optical modelling to evaluate the best-performing liquids and optimisation options. By systematically achieving each of these goals, this thesis provides a conclusive answer, demonstrating that liquids are not only optically competitive but, in optimised designs, can even be superior.

The first step was to develop a strategy for liquid selection. By reviewing existing literature on liquids in PV applications, related patents, dielectric liquids, datasheets and contact with industry and experts, a framework of critical criteria and suitable liquid groups was established, focusing on optical properties, electrical insulation, chemical stability with module components (especially the PIB edge-seal) and fluid characteristics. A quick comparison of raw material costs was made, which showed, under various assumptions, that liquids can have comparable or even cheaper prices compared to EVA and POE. This process filtered a wide range of candidates down to seven promising liquids for further testing: deionised water, glycerol, InnoGreen SolarPro glycol, PDMS, Shell Diala S4 XZ-I, Midel 7131, and Mivolt. After the optical analysis, the running material compatibility test confirmed Shell Diala to be incompatible with the PIB sealant, excluding mineral oils when using PIB.

With the candidates selected, the next goal was to obtain their complex refractive index from 300 - 1200 nm wavelength through experiments, as this data was largely unavailable. A hybrid method combining spectroscopic ellipsometry (for refractive index, n) and a dual cuvette spectrophotometry technique (for extinction coefficient, k) was successfully employed. This produced the first complete and reliable nk-dataset for many of these liquids over the 300–1200 nm range, which is crucial for accurate optical modelling. The experiments confirmed that all liquids possess excellent transparency and established a confidence threshold of $k = 5 * 10^{-8}$ through SNR analysis.

Using these new nk values, it was possible to perform optical modelling and simulation with GenPro. The optical model was validated through datasheets and experiments, showing a difference with simulated photocurrents between the Δ = 0.05 - 0.14 mA/cm^2 (datasheets) and Δ = 0.1 - 0.34 mA/cm^2 (bare cell and liquid-filled solar module measurement). An important finding is the extremely high transparency of all liquids, creating very low absorption, even for slightly yellowish liquids such as Midel and Shell, broadening the scope for potentially suitable liquids which are not perfectly clear/transparent, such as plant-based oils. The simulations of standard solar modules revealed a fundamental trade-off: the liquids' lower refractive indices caused higher reflection losses than conventional EVA with UV blocking additives, but their excellent transparency resulted in lower parasitic absorption. This balance allowed the top-performing liquids, notably Mivolt (40.90 - 41.81 mA/cm^2) and PDMS (40.85 - 41.75 mA/cm^2), to generate a photocurrent comparable to, or even higher than, UV-transparent EVA (40.92 - 41.81 mA/cm^2). It is important to note that the optical performance of the other liquids, Midel 7131, Shell Diala, glycerol and glycol, is very close to the best performing samples (within Δ 0.17 mA/cm^2), suggesting that based on optics alone, they should not be excluded, as other design benefits might

justify their selection.

A critical insight came from real-world energy yield simulations with the PVMD Toolbox, which showed that PDMS, due to its extremely low absorption (better optical performance at lower angles of incidence and thermal management), delivered the highest annual energy output (0.07% more energy than EVA-UVT, 0.086% more than Mivolt), even though it was not the top performer under standard, normal-incidence simulation conditions.

Finally, the last goal was to identify the best-performing liquids and evaluate optimisation options. The models clearly showed that mitigating reflection is the key to unlocking the full potential of liquid encapsulation. By applying tailored anti-reflection coatings or glass texturing, the liquids slightly outperformed standard solid encapsulants, with idealised ARC designs indicating a high theoretical ceiling for performance (41.81 mA/cm^2). The combination of using glass texturing and air showed an interesting effect and might be disadvantageous, as it could reflect more light instead of less. The focus for optically improving the liquid encapsulation should be on applying suitable ARCs of the front side of the glass panel, followed by liquid-specific ARCs on the inside of the glass or a combination with glass texturing, depending on the cost-effectiveness of these adjustments.

In conclusion, this thesis successfully demonstrates that from an optical standpoint, liquid encapsulation is a highly promising technology. Its main drawback, higher reflection, is not only compensated for by its superior transparency, but can also be effectively overcome with existing technologies like ARCs and glass texturing. By establishing a robust methodology for liquid selection, characterisation, and modelling, this work provides a strong foundation for future research. While the optical viability has been confirmed, the next steps should focus on some key aspects described in the following section in more detail. Priority when selecting a liquid should be on confirming the fluid properties on the identified crucial criteria, checking material compatibility with glass, PIB and solar cells at various temperatures (-40° to 85 ° C), optical characterisation over 300 - 1200 nm, potentially optical/electrical/thermal modelling or measurements followed by long term degradation and field testing in liquid-filled solar modules.

6.1. Future research

The findings of this thesis confirm the optical viability of liquid encapsulation and provide a strong foundation for further research. While the optical performance has been thoroughly analysed, several critical aspects regarding electrical interactions, thermal management, long-term reliability, and economic feasibility remain.

The following areas are proposed for future work to advance this technology towards practical implementation. The priority of the research should be on these areas, as these are less researched areas, and there are still major challenges to overcome for liquid encapsulation to be a success. That being said, further optical research is also interesting and will be briefly discussed first, to see how to improve and extend on the work presented in this thesis.

6.1.1. Potential extended optical research

The current thesis could be deepened and extended as liquid encapsulation develops further. On the liquid selection, more in the following paragraph. Regarding the measurements of the complex refractive index, More liquids can be measured, and the measurement range can be extended to 2500 nm, for example, to also support detailed thermal modelling.

For the measurements themselves, easier methods for optical characterisation can be tested to facilitate faster experiments. The k2 method can be a good example for this. Perhaps measurement of only a few wavelengths for the refractive index can be enough for less detailed optical modelling. In case more detail is needed (although it was shown that the achieved level of detail was sufficient for the analysis performed), simultaneous ellipsometry fitting could again be tried with updated ellipsometry software, allowing easier transmission measurement integration. More complex models, besides Cauchy, could be tried to perform the fitting. Regarding the extinction coefficient, three main improvements could be made: (i) a clean, unused cuvette for each liquid could be used to ensure complete cleanliness. (ii) Extended calibration of the Lambda spectrophotometer could help reduce noise and give more accurate measurements. (iii) Cuvettes with a longer optical pathway (25 - 50 mm) could be used in combination with the dual cuvette method, ensuring that the absorption of the liquid sample is

the dominant effect. Measuring with FTIR or Ramen for absorption peaks might be interesting to learn more about the absorption of the liquids.

For the simulations, more configurations can be tested, trying more materials, ARCs, glass texturing and their combinations, also with new liquids. Especially simulations at more angles of incidence are interesting, as they might show an added benefit for lower absorbing liquids, but also solids, at lower angles, as was seen in some simulations. The effect was also different and altered for different glass texturing, which can be further investigated. The two reasons for this effect should be further explored (i) at lower angles of incidence, the absorption becomes more important as optical partway lengths of the light through the encapsulation increase. (ii) Lower absorbing materials absorb less light/energy, resulting in a lower module temperature and thus increased efficiency. This research is not only interesting for liquids but is also applicable to solids, as a lower absorbing material might get underscored without proper testing and simulation of multiple angles of incidence. The PVMD Toolbox simulations need to be extended, and the mentioned bug regarding parasitic absorption losses needs to be fixed. Extended electrical and thermal modelling will help with this. This will give more confidence in the energy yield calculations, which then can be used for economic comparisons, discussed in the following section

6.1.2. Liquid candidates

This thesis considered a vast amount of potentially suitable liquids, but this search can always be extended. Especially with the fact that the slightly yellowish liquids Midel 7131 and Shell Diala had excellent transparency and extremely low parasitic absorption, opening up the door to other slightly yellowish liquids. This enables more liquids to qualify, especially plant-based oils, which were first excluded based on their yellow appearance (and potential material compatibility/oxidation problems, which should also be checked). One study (which was discovered after the liquid selection) already looks into the optical properties of sunflower, soybean and peanut oil, noting good optical performance [122].

It is difficult to determine a strict step-by-step process for selecting liquid candidates, as their properties are more or less reported and differ in the influence they have on the performance. It is advised to first check the fluid properties on the identified crucial criteria. Especially long-term material compatibility with glass, PIB and solar cells at various temperatures (-40° to 85 ° C), which should be confirmed with experiments. If not known, optical characterisation over 300 - 1200 nm, especially transmission measurements using the dual cuvette method, refractive index measurements preferably with ellipsometry, but if not possible, measuring n at one or multiple wavelengths and comparing to similar values in this thesis. Potentially followed by optical/electrical/thermal modelling or measurements to identify best-performing liquids. Finally, long-term degradation and field testing of liquid-filled solar modules, compared to EVA, air and POE encapsulations.

6.1.3. Chemical behaviour

Material compatibility is a key factor in the suitability of the liquid. The material compatibility issues between liquids and the PIB sealant must be resolved. Research into this has been conducted by Biosphere Solar and TU Delft by Sebastian Weemaes and Urvashi Bothra, and should be expanded [58], [59]. As seen in chapter 3, material compatibility tests were performed for Shell Diala and Midel 7131, which showed good results for Midel 7131 but excluded Shell. More tests like PIB dissolved in liquids at lower (-40 ° C) and higher temperatures (85 ° C), and damp-heat cycles with mini modules need to be performed to properly check the material compatibility.

The performance of the liquids themselves can be further enhanced through material science. Pptimisation with additives: The effect of additives should be systematically studied when one or two liquids are selected for further research. Additives could perform improved refractive index matching: adding high refractive index nanoparticles (e.g., TiO_2, ZrO_2) to base fluids to increase their refractive index (possible to the ideal n $\approx$ 1.52 calculated) and reduce reflection losses. Using nanofluids could also improve other properties of the encapsulation. It is crucial that any study on additives evaluates the full range of properties, as an improvement in one area, such as refractive index, could negatively impact another, such as extinction coefficient or dielectric strength. UV and thermal stability: incorporating UV absorbers and antioxidants to enhance the long-term stability of liquids that show degradation potential.

Multilayer encapsulation concepts: The idea of using a thin solid layer of a material like polyolefin (POE), EVA or ionomer, in combination with the liquid could be explored further. This hybrid approach could offer the best of both worlds: the solid layer would provide mechanical support and secure the cell interconnections, while the liquid would provide the optical and thermal benefits, and facilitate end-of-life disassembly. The simulations showed a small decline in photocurrent with these configurations, but this could be justified if it improves on other design criteria.

It will be interesting to see the behaviour of liquid encapsulation with other solar cells and configurations, especially perovskite solar cells. It might be that a hydrophobic fluid (such as most oils) could better seal perovskite cells and protect them from degradation.

6.1.4. Electrical and thermal modelling and measurements

As mentioned before, a key unknown is the direct electrical impact of the liquid on the solar cell surface. The liquid could have a positive effect on the solar cell, as observed in some studies, potentially due to increased passivation, reducing recombination losses, as also discussed in chapter 2 [61], [63]. This effect was partly described in some papers, but there was no clear conclusion on what is happening at the surface of the solar cell. The hypothesis is that polar liquids may provide ”field-effect passivation”, which needs to be tested. This can be done by measuring the effective charge carrier lifetime of silicon wafers immersed in various liquids in which Semilab is also interested; previous research into such a set-up has been conducted [210]. Comparing the results for a bare, unpassivated wafer versus a state-of-the-art, well-passivated solar cell would help understand the additional passivation liquids might have.

These insights could also be integrated into an electrical model (such as Sentaurus), to see the effects of the liquid encapsulation on the electrical parameters of the solar cell. As seen in the real-world conditions simulations using the PVMD Toolbox, the electrical (and thermal) assumptions made should be further explored to strengthen the results from these simulations.

Thermal modelling and measurements can confirm the potential improved thermal management of liquid encapsulation (as also seen in [55]), boosting the efficiency further. The PVMD Toolbox simulations already showed an improved thermal effect due to the lower absorption of light/energy by PDMS. It will be interesting to see the effect of the heat dissipation from the liquid encapsulation.

6.1.5. Mechanical and long-term reliability

The long-term performance and structural integrity of a liquid-filled module are crucial for commercial viability. The long-term degradation was studied in the thesis of Sebastian Weemaes and is currently investigated by Urvashi Bothra at the TU Delft [58], [59].

When installed at a tilt angle, the liquid will exert hydrostatic pressure on the glass and edge seal. Finite element analysis (FEA) could be used to model the stress distribution, glass deflection (sag), and pressure on the PIB sealant under various tilt angles and operating temperatures (accounting for thermal expansion). This would help predict mechanical failure points and inform the design of the module frame and sealant geometry. As well as potential thicker (bottom of module) and thinner (top of module) encapsulation spots due to the sagging, leading to higher parasitic absorption (at the bottom) and thus lower photocurrents, overall lowering the operating current of the panel, as discussed in chapter 5.

6.1.6. Techno-Economic Analysis

Finally, for the technology to be adopted, it must be economically viable. A comprehensive techno-economic analysis is needed to compare the levelised cost of energy (LCOE) of a liquid-encapsulated module to that of a conventional module. For this analysis, the expected energy yield from liquid-filled solar modules is needed, already briefly addressed in this thesis; more research is needed to confirm and expand the current findings.

The analysis should not only include the raw material costs as focused on in chapter 3, but also potential savings from simplified, lower-temperature manufacturing processes and the significant value proposition of easier, more complete material recovery at the module’s end-of-life. As mentioned before, it should be checked if additional ARCs or glass texturing are cost-effective.

Life cycle assessment of the liquid-filled module could be performed to see the expected benefits of easier repairs and recycling. In a broader context, it would be interesting to see if these benefits outweigh potential disadvantages such as adjusting manufacturing lines, current recycling practices, the life time of the model, among others.

Future work

Parts of this thesis will be published as a scientific paper, as part of the research of Urvashi Bothra in ”Liquid PV module encapsulation to enable circular design ” [59], and another paper focused on the complex refractive index measurements of liquids will be published in collaboration with the ellipsometry R&D application group at Semilab Hungary.

Furthermore, this thesis was nominated for the ”Young Energy Leader Award” at the Recharge Earth conference in Rotterdam (September 17 and 18).

References

[1] *Outlook for electricity – World Energy Outlook 2020 – Analysis*, en-GB. [Online]. Available: https://www.iea.org/reports/world-energy-outlook-2020/outlook-for-electricity (visited on 01/23/2025).

[2] M. Roser, "Why did renewables become so cheap so fast?" en, *Our World in Data*, Dec. 2020. [Online]. Available: https://ourworldindata.org/cheap-renewables-growth (visited on 01/23/2025).

[3] *Renewable Power Generation Costs in 2023*, en, Sep. 2024. [Online]. Available: https://www.irena.org/Publications/2024/Sep/Renewable-Power-Generation-Costs-in-2023 (visited on 04/16/2025).

[4] *World Energy Outlook 2024 – Analysis*, en-GB, Oct. 2024. [Online]. Available: https://www.iea.org/reports/world-energy-outlook-2024 (visited on 01/31/2025).

[5] *Eu-market-outlook-for-solar-power-2024-2028 - SolarPower Europe*. [Online]. Available: https://www.solarpowereurope.org/insights/outlooks/eu-market-outlook-for-solar-power-2024-2028#download (visited on 01/31/2025).

[6] *Empirical approach shows PV is getting cheaper than all the forecasters expect*, en-US, Dec. 2023. [Online]. Available: https://www.pv-magazine.com/2023/12/05/empirical-approach-shows-pv-is-getting-cheaper-than-all-the-forecasters-expect/ (visited on 01/31/2025).

[7] *Renewable capacity statistics 2025*, en, Mar. 2025. [Online]. Available: https://www.irena.org/Publications/2025/Mar/Renewable-capacity-statistics-2025 (visited on 04/17/2025).

[8] "End-of-Life Solar PV Panels," en-US, Aug. 2016. [Online]. Available: https://iea-pvps.org/key-topics/irena-iea-pvps-end-of-life-solar-pv-panels-2016/ (visited on 04/16/2025).

[9] X. Wang, X. Tian, X. Chen, L. Ren, and C. Geng, "A review of end-of-life crystalline silicon solar photovoltaic panel recycling technology," *Solar Energy Materials and Solar Cells*, vol. 248, p. 111 976, Dec. 2022, ISSN: 0927-0248. DOI: 10.1016/j.solmat.2022.111976. [Online]. Available: https://www.sciencedirect.com/science/article/pii/S0927024822003932 (visited on 04/16/2025).

[10] *Circular and blue economy: What's the difference? – BlueCity*, en. [Online]. Available: https://www.bluecity.nl/en/nieuws/de-circulaire-en-de-blauwe-economie-wat-is-eigenlijk-het-verschil (visited on 04/01/2025).

[11] A. Knight, *How is a circular economy different from a linear economy?* en-GB, Nov. 2021. [Online]. Available: https://www.aandapackaging.co.uk/how-is-a-circular-economy-different-from-a-linear-economy/ (visited on 03/31/2025).

[12] *Fairphone Shop*, nl-NL. [Online]. Available: https://shop.fairphone.com/nl/shop-home (visited on 08/04/2025).

[13] *Patagonia Outdoor Clothing & Gear*, en-US. [Online]. Available: https://www.patagonia.com/home/ (visited on 08/04/2025).

[14] *Critical raw materials - European Commission*, en. [Online]. Available: https://single-market-economy.ec.europa.eu/sectors/raw-materials/areas-specific-interest/critical-raw-materials_en (visited on 04/01/2025).

[15] *Climate risk and decarbonization: What every mining CEO needs to know | McKinsey*. [Online]. Available: https://www.mckinsey.com/capabilities/sustainability/our-insights/climate-risk-and-decarbonization-what-every-mining-ceo-needs-to-know (visited on 03/31/2025).

[16] *Total GHG Emissions of Major Metals and Mining Companies Worldwide by Revenue in 2021*, en-us. [Online]. Available: https://www.linkedin.com/company/globaldataplc/ (visited on 03/31/2025).

[17] P. Söderholm and T. Ekvall, "Metal markets and recycling policies: Impacts and challenges," en, *Mineral Economics*, vol. 33, no. 1, pp. 257–272, Jul. 2020, ISSN: 2191-2211. DOI: 10.1007/s13563-019-00184-5. [Online]. Available: https://doi.org/10.1007/s13563-019-00184-5 (visited on 03/31/2025).

[18] *Executive summary – Recycling of Critical Minerals – Analysis*, en-GB. [Online]. Available: https://www.iea.org/reports/recycling-of-critical-minerals/executive-summary (visited on 03/31/2025).

[19] EARTHDAY.ORG, *How Our Trash Impacts the Environment*, en, Jul. 2024. [Online]. Available: https://www.earthday.org/how-our-trash-impacts-the-environment/ (visited on 03/31/2025).

[20] S. M. Parvez, F. Jahan, M.-N. Brune, *et al.*, "Health consequences of exposure to e-waste: An updated systematic review," English, *The Lancet Planetary Health*, vol. 5, no. 12, e905–e920, Dec. 2021, Publisher: Elsevier, ISSN: 2542-5196. DOI: 10.1016/S2542-5196(21)00263-1. [Online]. Available: https://www.thelancet.com/journals/lanplh/article/PIIS2542-5196(21)00263-1/fulltext (visited on 03/31/2025).

[21] Y.-S. Zimmermann, A. Schäffer, P. F.-X. Corvini, and M. Lenz, "Thin-Film Photovoltaic Cells: Long-Term Metal(loid) Leaching at Their End-of-Life," *Environmental Science & Technology*, vol. 47, no. 22, pp. 13 151–13 159, Nov. 2013, Publisher: American Chemical Society, ISSN: 0013-936X. DOI: 10.1021/es402969c. [Online]. Available: https://doi.org/10.1021/es402969c (visited on 03/19/2025).

[22] M. Tammaro, A. Salluzzo, J. Rimauro, S. Schiavo, and S. Manzo, "Experimental investigation to evaluate the potential environmental hazards of photovoltaic panels," *Journal of Hazardous Materials*, vol. 306, pp. 395–405, Apr. 2016, ISSN: 0304-3894. DOI: 10.1016/j.jhazmat.2015.12.018. [Online]. Available: https://www.sciencedirect.com/science/article/pii/S0304389415302788 (visited on 03/19/2025).

[23] C. Xu, O. Isabella, and M. R. Vogt, "Future material demand for global silicon-based PV modules under net-zero emissions target until 2050," *Resources, Conservation and Recycling*, vol. 210, p. 107 824, Nov. 2024, ISSN: 0921-3449. DOI: 10.1016/j.resconrec.2024.107824. [Online]. Available: https://www.sciencedirect.com/science/article/pii/S0921344924004178 (visited on 03/17/2025).

[24] X. Xu, D. Lai, G. Wang, and Y. Wang, "Nondestructive silicon wafer recovery by a novel method of solvothermal swelling coupled with thermal decomposition," *Chemical Engineering Journal*, vol. 418, p. 129 457, Aug. 2021, ISSN: 1385-8947. DOI: 10.1016/j.cej.2021.129457. [Online]. Available: https://www.sciencedirect.com/science/article/pii/S1385894721010445 (visited on 03/19/2025).

[25] A. K. Schnatmann, F. Schoden, and E. Schwenzfeier-Hellkamp, "Sustainable PV Module Design: Review of State-of-the-Art Encapsulation Methods," *Sustainability*, vol. 14, p. 9971, Aug. 2022. DOI: 10.3390/su14169971.

[26] A. Perelman, V. Barth, F. Mandorlo, and E. Voroshazi, "Critical materials and PV cells interconnection," en, *EPJ Photovoltaics*, vol. 15, p. 4, 2024, Publisher: EDP Sciences, ISSN: 2105-0716. DOI: 10.1051/epjpv/2023034. [Online]. Available: https://www.epj-pv.org/articles/epjpv/abs/2024/01/pv230011/pv230011.html (visited on 01/14/2025).

[27] Y. Zhang, M. Kim, L. Wang, P. Verlinden, and B. Hallam, "Design considerations for multi-terawatt scale manufacturing of existing and future photovoltaic technologies: Challenges and opportunities related to silver, indium and bismuth consumption," en, *Energy & Environmental Science*, vol. 14, no. 11, pp. 5587–5610, Nov. 2021, Publisher: The Royal Society of Chemistry, ISSN: 1754-5706. DOI: 10.1039/D1EE01814K. [Online]. Available: https://pubs.rsc.org/en/content/articlelanding/2021/ee/d1ee01814k (visited on 01/14/2025).

[28] E. Gerold and H. Antrekowitsch, “Advancements and Challenges in Photovoltaic Cell Recycling: A Comprehensive Review,” en, *Sustainability*, vol. 16, no. 6, p. 2542, Jan. 2024, Number: 6 Publisher: Multidisciplinary Digital Publishing Institute, ISSN: 2071-1050. DOI: 10.3390/su16062542. [Online]. Available: https://www.mdpi.com/2071-1050/16/6/2542 (visited on 03/17/2025).

[29] *How Are Solar Panels Made?* en-US, Section: Energy, Oct. 2022. [Online]. Available: https://blog.ucsusa.org/charlie-hoffs/how-are-solar-panels-made/ (visited on 01/31/2025).

[30] *Responsible minerals sourcing for renewable energy*, en, Jan. 2021. [Online]. Available: https://www.uts.edu.au/isf/explore-research/projects/responsible-minerals-sourcing-renewable-energy (visited on 01/31/2025).

[31] A. Ilias, M. Rentoumis, Y. Katsigiannis, and N. Bilalis, “Integration & assessment of recycling into c-Si photovoltaic module’s life cycle,” *International Journal of Sustainable Engineering*, vol. 11, pp. 1–10, Jan. 2018. DOI: 10.1080/19397038.2018.1428833.

[32] A. Smets, K. Jäger, O. Isabella, R. van Swaaij, and M. Zeman, *Solar Energy: The physics and engineering of photovoltaic conversion, technologies and systems*. Cambridge: UIT Cambridge Limited, 2016, ISBN: 978-1-906860-32-5. [Online]. Available: https://www.amazon.com/Solar-Energy-Engineering-Photovoltaic-Technologies/dp/1906860327 (visited on 08/16/2025).

[33] G. A. Heath, T. J. Silverman, M. Kempe, *et al.*, “Research and development priorities for silicon photovoltaic module recycling to support a circular economy,” en, *Nature Energy*, vol. 5, no. 7, pp. 502–510, Jul. 2020, Publisher: Nature Publishing Group, ISSN: 2058-7546. DOI: 10.1038/s41560-020-0645-2. [Online]. Available: https://www.nature.com/articles/s41560-020-0645-2 (visited on 04/03/2025).

[34] *International Technology Roadmap for Photovoltaic (ITRPV) - vdma.org - VDMA*, nl-NL. [Online]. Available: https://www.vdma.eu/international-technology-roadmap-photovoltaic (visited on 07/22/2025).

[35] *Photovoltaics Report - Fraunhofer ISE*, en. [Online]. Available: https://www.ise.fraunhofer.de/en/publications/studies/photovoltaics-report.html (visited on 04/02/2025).

[36] Späth, M., Wieclawska, S.M., Sommeling, P.M., and Lenzmann, F.O., *Balancing costs and revenues for recycling end-of-life PV panels in the Netherlands*. [Online]. Available: https://publications.tno.nl/publication/34640523/crl8a6/TNO-2022-R10860.pdf.

[37] P. J. M. Isherwood, “Reshaping the Module: The Path to Comprehensive Photovoltaic Panel Recycling,” en, *Sustainability*, vol. 14, no. 3, p. 1676, Jan. 2022, ISSN: 2071-1050. DOI: 10.3390/su14031676. [Online]. Available: https://www.mdpi.com/2071-1050/14/3/1676 (visited on 03/17/2025).

[38] K. Wambach, C. Libby, and S. Shaw, “Advances in Module Recycling – Literature Review and Update to Empirical LCI Data and Patent Review,” en-US, Jun. 2024. [Online]. Available: https://iea-pvps.org/key-topics/advances-in-module-recycling-literature-review-and-update-to-empirical-lci-data-and-patent-review/ (visited on 01/23/2025).

[39] *The eight essential materials for solar panels*, en. [Online]. Available: https://www.maysunsolar.eu/blog/the-eight-essential-materials-for-solar-panels (visited on 02/21/2025).

[40] *Addressing uncertain antimony content in solar glass for recycling*, en-GB, Apr. 2023. [Online]. Available: https://solaralliance.eu/wp-content/uploads/2023/10/Recommendation-on-Addressing-uncertain-antimony-content-in-solar-glass-for-recycling.pdf (visited on 06/09/2025).

[41] S. K. Chunduri and M. Schmela, *Market Survey on Backsheets and Encapsulation 2022-2023*. Feb. 2023. DOI: 10.13140/RG.2.2.11206.45124.

[42] *Visualizing the abundance of elements in the Earth’s crust*, en, Dec. 2021. [Online]. Available: https://www.weforum.org/stories/2021/12/abundance-elements-earth-crust/ (visited on 01/31/2025).

[43] R. F. M. Lange, Y. Luo, R. Polo, and J. Zahnd, “The lamination of (multi)crystalline and thin film based photovoltaic modules,” en, *Progress in Photovoltaics: Research and Applications*, vol. 19, no. 2, pp. 127–133, 2011, ISSN: 1099-159X. DOI: 10.1002/pip.993. [Online]. Available: https://onlinelibrary.wiley.com/doi/abs/10.1002/pip.993 (visited on 04/03/2025).

[44] J. Tracy, N. Bosco, C. Delgado, and R. Dauskardt, “Durability of ionomer encapsulants in photovoltaic modules,” *Solar Energy Materials and Solar Cells*, vol. 208, p. 110 397, May 2020, ISSN: 0927-0248. DOI: 10.1016/j.solmat.2020.110397. [Online]. Available: https://www.sciencedirect.com/science/article/pii/S0927024820300052 (visited on 04/08/2025).

[45] G. Beaucarne, A. Dupont, D. Puthenmadom, N. Shephard, and T. Sample, “Material study of photovoltaic modules with silicone encapsulation after long-term outdoor exposure,” *Solar Energy Materials and Solar Cells*, vol. 230, p. 111 298, Sep. 2021, ISSN: 0927-0248. DOI: 10.1016/j.solmat.2021.111298. [Online]. Available: https://www.sciencedirect.com/science/article/pii/S0927024821003408 (visited on 12/10/2024).

[46] V. Poulek, D. S. Strebkov, I. S. Persic, and M. Libra, “Towards 50 years lifetime of PV panels laminated with silicone gel technology,” *Solar Energy*, vol. 86, no. 10, pp. 3103–3108, Oct. 2012, ISSN: 0038-092X. DOI: 10.1016/j.solener.2012.07.013. [Online]. Available: https://www.sciencedirect.com/science/article/pii/S0038092X12002642 (visited on 04/03/2025).

[47] M. Calì, B. Hajji, G. Nitto, and A. Acri, “The Design Value for Recycling End-of-Life Photovoltaic Panels,” en, *Applied Sciences*, vol. 12, no. 18, p. 9092, Jan. 2022, Number: 18 Publisher: Multidisciplinary Digital Publishing Institute, ISSN: 2076-3417. DOI: 10.3390/app12189092. [Online]. Available: https://www.mdpi.com/2076-3417/12/18/9092 (visited on 05/11/2025).

[48] R. Deng, N. L. Chang, Z. Ouyang, and C. M. Chong, “A techno-economic review of silicon photovoltaic module recycling,” *Renewable and Sustainable Energy Reviews*, vol. 109, pp. 532–550, Jul. 2019, ISSN: 1364-0321. DOI: 10.1016/j.rser.2019.04.020. [Online]. Available: https://www.sciencedirect.com/science/article/pii/S1364032119302321 (visited on 04/07/2025).

[49] M. S. Chowdhury, K. S. Rahman, T. Chowdhury, *et al.*, “An overview of solar photovoltaic panels’ end-of-life material recycling,” *Energy Strategy Reviews*, vol. 27, p. 100 431, Jan. 2020, ISSN: 2211-467X. DOI: 10.1016/j.esr.2019.100431. [Online]. Available: https://www.sciencedirect.com/science/article/pii/S2211467X19301245 (visited on 01/31/2025).

[50] V. Fiandra, L. Sannino, and C. Andreozzi, “Photovoltaic waste as source of valuable materials: A new recovery mechanical approach,” *Journal of Cleaner Production*, vol. 385, p. 135 702, Jan. 2023, ISSN: 0959-6526. DOI: 10.1016/j.jclepro.2022.135702. [Online]. Available: https://www.sciencedirect.com/science/article/pii/S0959652622052763 (visited on 03/17/2025).

[51] M. Mittag, T. Neff, S. Hoffmann, M. Ebert, U. Eitner, and H. Wirth, *TPedge: glass-glass photovoltaic module for BiPV-applications*. May 2016. [Online]. Available: https://www.researchgate.net/publication/318226349_TPedge_glass-glass_photovoltaic_module_for_BiPV-applications.

[52] J. Dupuis, E. Saint-Sernin, O. Nichiporuk, P. Lefillastre, D. Bussery, and R. Einhaus, “NICE module technology - From the concept to mass production: A 10 years review,” in *2012 38th IEEE Photovoltaic Specialists Conference*, ISSN: 0160-8371, Jun. 2012, pp. 003 183–003 186. DOI: 10.1109/PVSC.2012.6318254. [Online]. Available: https://ieeexplore.ieee.org/document/6318254 (visited on 04/07/2025).

[53] D. Kray, S. Bandyopadhyay, L. Heuberger, *et al.*, “N.I.C.E.-Wire: Next Generation Robust Eco-Friendly Bifacial PV Modules With High Efficiency,” *IEEE Journal of Photovoltaics*, vol. 12, no. 1, pp. 38–44, Jan. 2022, Conference Name: IEEE Journal of Photovoltaics, ISSN: 2156-3403. DOI: 10.1109/JPHOTOV.2021.3124168. [Online]. Available: https://ieeexplore.ieee.org/document/9624987 (visited on 04/07/2025).

[54] R. Einhaus, F. Madon, J. Degoulange, *et al.*, "Recycling and Reuse potential of NICE PV-Modules," in *2018 IEEE 7th World Conference on Photovoltaic Energy Conversion (WCPEC) (A Joint Conference of 45th IEEE PVSC, 28th PVSEC & 34th EU PVSEC)*, ISSN: 0160-8371, Jun. 2018, pp. 561–564. DOI: 10.1109/PVSC.2018.8548307. [Online]. Available: https://ieeexplore.ieee.org/document/8548307 (visited on 04/07/2025).

[55] A. Perelman, V. Barth, F. Mandorlo, and E. Voroshazi, "Innovative Design-for-Recycling for Critical Material-Free Interconnection of PV Modules," en, *Progress in Photovoltaics: Research and Applications*, vol. n/a, no. n/a, ISSN: 1099-159X. DOI: 10.1002/pip.3869. [Online]. Available: https://onlinelibrary.wiley.com/doi/abs/10.1002/pip.3869 (visited on 01/13/2025).

[56] Youp Kroon, *PV Solar Exploration: The Circular Photovoltaic-Thermal panel of the future*. [Online]. Available: https://www.biosphere.solar/repositories/research (visited on 04/07/2025).

[57] Hongyi Chen, *The optical property and degradation of liquid encapsulated solar cells*. [Online]. Available: https://www.biosphere.solar/repositories/research (visited on 04/07/2025).

[58] S. Weemaes, "Performance and Reliability of Liquid Encapsulated PV Modules," en, 2025. [Online]. Available: https://repository.tudelft.nl/record/uuid:255062db-fc7d-4874-b8fa-45bfca7fea7e (visited on 08/07/2025).

[59] U. Bothra, S. Weemaes, T. Rijsman, *et al.*, "Liquid PV module encapsulation to enable circular design [IN PREPERATION]."

[60] *BIOSPHERE SOLAR V1.4-TOPCon datasheet*, 2025. [Online]. Available: https://www.biosphere.solar/product (visited on 08/05/2025).

[61] Y. Wang, Z. Fang, L. Zhu, Q. Huang, Y. Zhang, and Z. Zhang, "The performance of silicon solar cells operated in liquids," *Applied Energy*, vol. 86, no. 7, pp. 1037–1042, Jul. 2009, ISSN: 0306-2619. DOI: 10.1016/j.apenergy.2008.08.020. [Online]. Available: https://www.sciencedirect.com/science/article/pii/S0306261908002134 (visited on 12/12/2024).

[62] Y. Wang, Z. Zhang, L. Zhu, L. Han, Q. Huang, and Z. Fang, "Accelerated Ultraviolet Test and High Temperature Test on Dielectric Liquid for Immersing Solar Cells," en, in *Proceedings of ISES World Congress 2007 (Vol. I – Vol. V)*, D. Y. Goswami and Y. Zhao, Eds., Berlin, Heidelberg: Springer, 2009, pp. 1381–1385, ISBN: 978-3-540-75997-3. DOI: 10.1007/978-3-540-75997-3_281.

[63] X. Han and Y. Wang, "Electrical and thermal performance of silicon concentrator solar cells immersed in dielectric liquids," *Applied Energy*, vol. 88, no. 12, pp. 4481–4489, Dec. 2011, ISSN: 0306-2619. DOI: 10.1016/j.apenergy.2011.05.037. [Online]. Available: https://www.sciencedirect.com/science/article/pii/S0306261911003321 (visited on 12/11/2024).

[64] M. Vivar and V. Everett, "A review of optical and thermal transfer fluids used for optical adaptation or beam-splitting in concentrating solar systems," en, *Progress in Photovoltaics: Research and Applications*, vol. 22, no. 6, pp. 612–633, 2014, ISSN: 1099-159X. DOI: 10.1002/pip.2307. [Online]. Available: https://onlinelibrary.wiley.com/doi/abs/10.1002/pip.2307 (visited on 03/11/2025).

[65] M. Clarke, "Investigations on photovoltaic receivers in linear concentrating systems," en, Accepted: 2020-06-30T02:14:55Z, Thesis, Technische Universität Wien, 2012. [Online]. Available: https://repositum.tuwien.at/handle/20.500.12708/9850 (visited on 05/07/2025).

[66] X. Han, Q. Wang, and J. Zheng, "Determination and evaluation of the optical properties of dielectric liquids for concentrating photovoltaic immersion cooling applications," *Solar Energy*, vol. 133, pp. 476–484, Aug. 2016, ISSN: 0038-092X. DOI: 10.1016/j.solener.2016.04.036. [Online]. Available: https://www.sciencedirect.com/science/article/pii/S0038092X1630069X (visited on 01/13/2025).

[67] *Fully recyclable new generation of solar panels | TNO*, en. [Online]. Available: https://www.tno.nl/en/sustainable/energy-supply/sustainable-solar-panels/silicon-solar-panels-circular-design/made-in-europe/ (visited on 05/11/2025).

[68] "PV Module Design for Recycling Guidelines," en-US, Dec. 2021. [Online]. Available: https://iea-pvps.org/key-topics/pv-module-design-for-recycling-guidelines/ (visited on 05/11/2025).

[69] T. Doi, I. TSUDA, K. SAKUTA, and G. MATSUI, “Development of a recyclable PV-module: Trial manufacturing and evaluation,” *Proceedings of the 3rd World Conference on Photovoltaic Energy Conversion*, Jan. 2003.

[70] *Future LCA on the Solar panels of Solarge for comparison with conventional solar panels and finding possible improvements*, en. [Online]. Available: https://research.tue.nl/en/studentTheses/future-lca-on-the-solar-panels-of-solarge-for-comparison-with-con (visited on 05/11/2025).

[71] T. Ugumori and M. Ikeya, “Efficiency Increase of Solar Cells Operated in Dielectric Liquid,” en, *Japanese Journal of Applied Physics*, vol. 20, no. S2, p. 77, Jan. 1981, Publisher: IOP Publishing, ISSN: 1347-4065. DOI: 10.7567/JJAPS.20S2.77. [Online]. Available: https://iopscience.iop.org/article/10.7567/JJAPS.20S2.77/meta (visited on 12/11/2024).

[72] K. Tanaka, “Solar energy converter using optical concentration through a liquid,” Jan. 2003. [Online]. Available: https://patents.google.com/patent/US20030005957A1/en (visited on 12/10/2024).

[73] K. Tanaka, “Solar energy converter using a solar cell in a shallow liquid-gel layer,” US7244888B1, Jul. 2007. [Online]. Available: https://patents.google.com/patent/US7244888B1/en (visited on 12/10/2024).

[74] J. A. Muaddi and M. A. Jamal, “Spectral response and efficiency of a silicon solar cell below water surface,” *Solar Energy*, vol. 49, no. 1, pp. 29–33, Jul. 1992, ISSN: 0038-092X. DOI: 10.1016/0038-092X(92)90123-R. [Online]. Available: https://www.sciencedirect.com/science/article/pii/0038092X9290123R (visited on 04/30/2025).

[75] Y. A. Abramyan, G. G. Karamyan, A. A. Murodyan, V. I. Stafeev, and V. I. Serago, “Effect of liquid dielectrics on the efficiency of silicon solar cells,” en, *Semiconductors*, vol. 33, no. 12, pp. 1320–1321, Dec. 1999, ISSN: 1090-6479. DOI: 10.1134/1.1187917. [Online]. Available: https://doi.org/10.1134/1.1187917 (visited on 12/11/2024).

[76] Y. A. Abrahamyan, V. I. Serago, V. M. Aroutiounian, *et al.*, “The efficiency of solar cells immersed in liquid dielectrics,” *Solar Energy Materials and Solar Cells*, vol. 73, no. 4, pp. 367–375, Aug. 2002, ISSN: 0927-0248. DOI: 10.1016/S0927-0248(01)00220-3. [Online]. Available: https://www.sciencedirect.com/science/article/pii/S0927024801002203 (visited on 12/11/2024).

[77] M. Victoria, S. Askins, C. Domínguez, I. Antón, and G. Sala, “Durability of dielectric fluids for concentrating photovoltaic systems,” *Solar Energy Materials and Solar Cells*, vol. 113, pp. 31–36, Jun. 2013, ISSN: 0927-0248. DOI: 10.1016/j.solmat.2013.01.039. [Online]. Available: https://www.sciencedirect.com/science/article/pii/S0927024813000548 (visited on 12/11/2024).

[78] L. Zhu, R. F. Boehm, Y. Wang, C. Halford, and Y. Sun, “Water immersion cooling of PV cells in a high concentration system,” *Solar Energy Materials and Solar Cells*, vol. 95, no. 2, pp. 538–545, Feb. 2011, ISSN: 0927-0248. DOI: 10.1016/j.solmat.2010.08.037. [Online]. Available: https://www.sciencedirect.com/science/article/pii/S0927024810005374 (visited on 12/16/2024).

[79] L. Liu, L. Zhu, Y. Wang, Q. Huang, Y. Sun, and Z. Yin, “Heat dissipation performance of silicon solar cells by direct dielectric liquid immersion under intensified illuminations,” *Solar Energy*, vol. 85, no. 5, pp. 922–930, May 2011, ISSN: 0038-092X. DOI: 10.1016/j.solener.2011.02.007. [Online]. Available: https://www.sciencedirect.com/science/article/pii/S0038092X11000387 (visited on 01/29/2025).

[80] Y. Sun, Y. Wang, L. Zhu, B. Yin, H. Xiang, and Q. Huang, “Direct liquid-immersion cooling of concentrator silicon solar cells in a linear concentrating photovoltaic receiver,” *Energy*, vol. 65, pp. 264–271, Feb. 2014, ISSN: 0360-5442. DOI: 10.1016/j.energy.2013.11.063. [Online]. Available: https://www.sciencedirect.com/science/article/pii/S0360544213010335 (visited on 12/13/2024).

[81] X. Han, Y. Wang, L. Zhu, H. Xiang, and H. Zhang, “Mechanism study of the electrical performance change of silicon concentrator solar cells immersed in de-ionized water,” *Energy Conversion and Management*, vol. 53, no. 1, pp. 1–10, Jan. 2012, ISSN: 0196-8904. DOI: 10.1016/j.enconman.2011.08.011. [Online]. Available: https://www.sciencedirect.com/science/article/pii/S0196890411002238 (visited on 12/13/2024).

[82] R. Winston and H. Hinterberger, “Principles of cylindrical concentrators for solar energy,” *Solar Energy*, vol. 17, no. 4, pp. 255–258, Sep. 1975, ISSN: 0038-092X. DOI: 10.1016/0038-092X(75)90007-9. [Online]. Available: https://www.sciencedirect.com/science/article/pii/0038092X75900079 (visited on 05/06/2025).

[83] D. R. Mills, “Two-stage tilting solar concentrators,” *Solar Energy*, vol. 25, no. 6, pp. 505–509, Jan. 1980, ISSN: 0038-092X. DOI: 10.1016/0038-092X(80)90082-1. [Online]. Available: https://www.sciencedirect.com/science/article/pii/0038092X80900821 (visited on 05/06/2025).

[84] D. R. Mills and J. E. Giutronich, “Ideal prism solar concentrators,” *Solar Energy*, vol. 21, no. 5, pp. 423–430, Jan. 1978, ISSN: 0038-092X. DOI: 10.1016/0038-092X(78)90175-5. [Online]. Available: https://www.sciencedirect.com/science/article/pii/0038092X78901755 (visited on 05/06/2025).

[85] I. R. Edmonds, I. R. Cowling, and H. M. Chan, “The design and performance of liquid filled stationary concentrators for use with photovoltaic cells,” *Solar Energy*, vol. 39, no. 2, pp. 113–122, Jan. 1987, ISSN: 0038-092X. DOI: 10.1016/S0038-092X(87)80039-7. [Online]. Available: https://www.sciencedirect.com/science/article/pii/S0038092X87800397 (visited on 05/06/2025).

[86] I. R. Edmonds, “The performance of bifacial solar cells in static solar concentrators,” *Solar Energy Materials*, vol. 21, no. 2, pp. 173–190, Dec. 1990, ISSN: 0165-1633. DOI: 10.1016/0165-1633(90)90052-3. [Online]. Available: https://www.sciencedirect.com/science/article/pii/0165163390900523 (visited on 05/06/2025).

[87] M. Victoria, S. Askins, C. Domínguez, I. Antón, and G. Sala, *FluidReflex Concentrator: From Elementary Unit to Module*. Dec. 2011, vol. 1407, Pages: 256. DOI: 10.1063/1.3658338.

[88] X. Han, Y. Wang, and L. Zhu, “The performance and long-term stability of silicon concentrator solar cells immersed in dielectric liquids,” *Energy Conversion and Management*, vol. 66, pp. 189–198, Feb. 2013, ISSN: 0196-8904. DOI: 10.1016/j.enconman.2012.10.009. [Online]. Available: https://www.sciencedirect.com/science/article/pii/S0196890412004050 (visited on 01/08/2025).

[89] B. Zhang, Y. Wang, Q. Huang, J. Feng, Y. Cui, and Y. Zhang, “Study on the performance of cooling composite materials for liquid-immersed concentrating photovoltaic systems,” *Solar Energy*, vol. 119, pp. 543–552, Sep. 2015, ISSN: 0038-092X. DOI: 10.1016/j.solener.2015.05.012. [Online]. Available: https://www.sciencedirect.com/science/article/pii/S0038092X15002352 (visited on 12/17/2024).

[90] A. G. Imenes and D. R. Mills, “Spectral beam splitting technology for increased conversion efficiency in solar concentrating systems: A review,” *Solar Energy Materials and Solar Cells*, International Solar Energy Society World Congress 2003, vol. 84, no. 1, pp. 19–69, Oct. 2004, ISSN: 0927-0248. DOI: 10.1016/j.solmat.2004.01.038. [Online]. Available: https://www.sciencedirect.com/science/article/pii/S0927024804001394 (visited on 05/08/2025).

[91] M. A. C. Chendo, M. R. Jacobson, and D. E. Osborn, “Liquid and thin-film filters for hybrid solar energy conversion systems,” *Solar & Wind Technology*, vol. 4, no. 2, pp. 131–138, Jan. 1987, ISSN: 0741-983X. DOI: 10.1016/0741-983X(87)90039-7. [Online]. Available: https://www.sciencedirect.com/science/article/pii/0741983X87900397 (visited on 05/08/2025).

[92] D. E. Osborn, M. A. C. Chendo, M. A. Hamdy, *et al.*, “Spectral selectivity applied to hybrid concentration systems,” *Solar Energy Materials*, vol. 14, no. 3, pp. 299–325, Nov. 1986, ISSN: 0165-1633. DOI: 10.1016/0165-1633(86)90055-9. [Online]. Available: https://www.sciencedirect.com/science/article/pii/0165163386900559 (visited on 05/08/2025).

[93] M. Sabry, R. Gottschalg, T. Betts, *et al.*, “Optical filtering of solar radiation to increase performance of concentrator systems,” in *Conference Record of the Twenty-Ninth IEEE Photovoltaic Specialists Conference, 2002.*, ISSN: 1060-8371, May 2002, pp. 1588–1591. DOI: 10.1109/PVSC.2002.1190918. [Online]. Available: https://ieeexplore.ieee.org/abstract/document/1190918 (visited on 05/08/2025).

[94] R. A. Powell, “Variable aperture, variable flux density, aerospace solar collector,” US4719903A, Jan. 1988. [Online]. Available: https://patents.google.com/patent/US4719903A/en (visited on 05/08/2025).

[95] R. Looser, M. Vivar, and V. Everett, “Spectral characterisation and long-term performance analysis of various commercial Heat Transfer Fluids (HTF) as Direct-Absorption Filters for CPV-T beam-splitting applications,” *Applied Energy*, vol. 113, pp. 1496–1511, Jan. 2014, ISSN: 0306-2619. DOI: 10.1016/j.apenergy.2013.09.001. [Online]. Available: https://www.sciencedirect.com/science/article/pii/S030626191300737X (visited on 03/10/2025).

[96] X. Han, Y. Guo, Q. Wang, and P. Phelan, “Optical characterization and durability of immersion cooling liquids for high concentration III-V photovoltaic systems,” *Solar Energy Materials and Solar Cells*, vol. 174, pp. 124–131, Jan. 2018, ISSN: 0927-0248. DOI: 10.1016/j.solmat.2017.08.034. [Online]. Available: https://www.sciencedirect.com/science/article/pii/S0927024817304828 (visited on 03/10/2025).

[97] X. Han, D. Xue, J. Zheng, S. M. Alelyani, and X. Chen, “Spectral characterization of spectrally selective liquid absorption filters and exploring their effects on concentrator solar cells,” *Renewable Energy*, vol. 131, pp. 938–945, Feb. 2019, ISSN: 0960-1481. DOI: 10.1016/j.renene.2018.07.125. [Online]. Available: https://www.sciencedirect.com/science/article/pii/S0960148118309224 (visited on 03/10/2025).

[98] *Freezing Points of Glycerol and Its Aqueous Solutions.* | *Industrial & Engineering Chemistry*. [Online]. Available: https://pubs.acs.org/doi/10.1021/ie50189a017 (visited on 07/03/2025).

[99] D. Chemisana, E. F. Fernandez, A. Riverola, and A. Moreno, “Fluid-based spectrally selective filters for direct immersed PVT solar systems in building applications,” *Renewable Energy*, vol. 123, pp. 263–272, Aug. 2018, ISSN: 0960-1481. DOI: 10.1016/j.renene.2018.02.018. [Online]. Available: https://www.sciencedirect.com/science/article/pii/S0960148118301617 (visited on 05/07/2025).

[100] S. S. Joshi and A. S. Dhoble, “Experimental investigation of solar photovoltaic thermal system using water, coconut oil and silicone oil as spectrum filters,” en, *Journal of the Brazilian Society of Mechanical Sciences and Engineering*, vol. 39, no. 8, pp. 3227–3236, Aug. 2017, ISSN: 1806-3691. DOI: 10.1007/s40430-017-0802-0. [Online]. Available: https://doi.org/10.1007/s40430-017-0802-0 (visited on 01/13/2025).

[101] Y. Ma, X. Han, Z. Chen, and D. Zheng, “Performance evaluation of a semi-transparent cells filtered concentrated photovoltaic/thermal system,” *Applied Thermal Engineering*, vol. 266, May 2025, ISSN: 1359-4311. DOI: 10.1016/j.applthermaleng.2025.125760. [Online]. Available: https://www.sciencedirect.com/science/article/pii/S1359431125003515 (visited on 05/07/2025).

[102] M. Kumar, S. Kumar, and S. Singh, “A critical review of concentrating and nanofluid-based hybrid PV/T systems utilizing beam splitting technique: Progress, challenges, and way forward,” en, *Environmental Science and Pollution Research*, vol. 30, no. 36, pp. 84 850–84 873, Aug. 2023, ISSN: 1614-7499. DOI: 10.1007/s11356-023-27972-5. [Online]. Available: https://doi.org/10.1007/s11356-023-27972-5 (visited on 05/08/2025).

[103] P. Belkhode, M. Giripunje, M. Dhande, *et al.*, “Nanomaterials applications in solar energy: Exploring future prospects and challenges,” *Materials Today: Proceedings*, Apr. 2024, ISSN: 2214-7853. DOI: 10.1016/j.matpr.2024.04.035. [Online]. Available: https://www.sciencedirect.com/science/article/pii/S2214785324002232 (visited on 05/08/2025).

[104] Z. Chen, X. Han, L. Wang, and D. Zheng, “Experimental and numerical study of stable TiN plasmonic nanofluids for direct absorption parabolic trough collector,” en, *Journal of the Brazilian Society of Mechanical Sciences and Engineering*, vol. 47, no. 4, p. 167, Mar. 2025, ISSN: 1806-3691. DOI: 10.1007/s40430-025-05483-3. [Online]. Available: https://doi.org/10.1007/s40430-025-05483-3 (visited on 05/08/2025).

[105] S. Yar Khan, S. Rauf, S. Liu, W. Chen, Y. Shen, and M. Kumar, “Revolutionizing the solar photovoltaic efficiency: A comprehensive review on the cutting-edge thermal management methods for advanced and conventional solar photovoltaics,” en, *Energy & Environmental Science*, 2025, Publisher: Royal Society of Chemistry. DOI: 10.1039/D4EE03525A. [Online]. Available: https://pubs.rsc.org/en/content/articlelanding/2025/ee/d4ee03525a (visited on 01/08/2025).

[106] C. R. Russell, “Optical concentrator and cooling system for photovoltaic cells,” US4052228A, Oct. 1977. [Online]. Available: https://patents.google.com/patent/US4052228A/en (visited on 04/30/2025).

[107] G. Carcangiu, M. Sardo, I. Carcangiu, and R. Sardo, “Photovoltaic panel and solar-panel unit made using photovoltaic panels of the same sort,” US20090145425A1, Jun. 2009. [Online]. Available: https://patents.google.com/patent/US20090145425A1/en (visited on 01/08/2025).

[108] O. V. Vasilinina, J. K. Kidyashev, V. N. Potapov, S. V. Ryabikov, A. M. Stepanov, and D. S. Strebkov, “Solar Photoelectric conversion apparatus with cooling means,” US4211581A, Jul. 1980. [Online]. Available: https://patents.google.com/patent/US4211581A/en (visited on 01/08/2025).

[109] N. S. Kapany, E. E. Hardy, and T. A. Orofino, “Solar energy collector,” US4143233A, Mar. 1979. [Online]. Available: https://patents.google.com/patent/US4143233A/en?q=(pv+liquid+encapsulation)&oq=pv+liquid+encapsulation (visited on 05/11/2025).

[110] M. VITE, R. F. D. ALMEIDA, M. Hidalgo, and F. ZANARDO, “Procédé permettant l’encapsulation de cellules photovoltaïques d’un module photovoltaïque par voie liquide,” fr, WO2018042136A1, Mar. 2018. [Online]. Available: https://patents.google.com/patent/WO2018042136A1/en?q=(silicon+pv+liquid+encapsulation)&oq=silicon+pv+liquid+encapsulation (visited on 05/11/2025).

[111] K. JOSHI, P. KUMAR, V. Kumar, R. MARKAN, and R. RAJAK, “Method of manufacturing a photovoltaic cell module,” en, WO2014192010A1, Dec. 2014. [Online]. Available: https://patents.google.com/patent/WO2014192010A1/en?q=(silicon+pv+liquid+encapsulation)&oq=silicon+pv+liquid+encapsulation (visited on 05/11/2025).

[112] K. Tange, “Coolant sealing structure for a solar cell,” US6005185A, Dec. 1999. [Online]. Available: https://patents.google.com/patent/US6005185A/en (visited on 01/08/2025).

[113] W. Mook, “Solar panels with liquid superconcentrators exhibiting wide fields of view,” Aug. 2006. [Online]. Available: https://patents.google.com/patent/US20060185713A1/en (visited on 12/16/2024).

[114] H.-C. Francke, “Solar panel, and systems for interconnecting multiple solar panels,” en, Jul. 2011. [Online]. Available: https://patents.google.com/patent/NO20100113A1/en (visited on 08/17/2025).

[115] G. Baret and H. Lauvray, “Procede de realisation d’un module photovoltaique et module photovoltaique realise par ce procede,” fr, FR2853993A1, Oct. 2004. [Online]. Available: https://patents.google.com/patent/FR2853993A1/en?q=(photovoltaic)&assignee=apollon+solar&oq=apollon+solar+photovoltaic (visited on 05/11/2025).

[116] G. Baret and H. Lauvray, “Procede de realisation d’un module photovoltaique et module photovoltaique realise par ce procede,” fr, FR2850489A1, Jul. 2004. [Online]. Available: https://patents.google.com/patent/FR2850489A1/en?q=(photovoltaic)&assignee=apollon+solar&oq=apollon+solar+photovoltaic&page=1 (visited on 05/11/2025).

[117] B. Cheviet, G. Perrod, K. W. Bamberg, and S. E. Saint, “Ensemble de support et de raccordement electrique pour une cellule photovoltaique a contacts arriere, module photovoltaique comprenant un tel ensemble et procede de fabrication d’un tel module,” fr, FR2956248A1, Aug. 2011. [Online]. Available: https://patents.google.com/patent/FR2956248A1/fr?q=(photovoltaic)&assignee=apollon+solar&oq=apollon+solar+photovoltaic&page=2 (visited on 05/11/2025).

[118] H. Lauvray and R. Einhaus, “Procede de fabrication d’un module photovoltaique et module obtenu,” fr, FR2862427A1, May 2005. [Online]. Available: https://patents.google.com/patent/FR2862427A1/en?q=(photovoltaic)&assignee=apollon+solar&oq=apollon+solar+photovoltaic&page=1 (visited on 05/11/2025).

[119] E. Saint-Sernin and H. Lauvray, “Module photovoltaïque à dépression contrôlée, utilisation d’un getter d’oxygène dans un module photovoltaïque et procédé de fabrication d’un tel module,” fr, EP2647058A1, Oct. 2013. [Online]. Available: https://patents.google.com/patent/EP2647058A1/en?q=(photovoltaic)&assignee=apollon+solar&oq=apollon+solar+photovoltaic&page=1 (visited on 05/11/2025).

[120] G. Baret, H. Lauvray, R. Einhaus, and K. Bamberg, “MODULE PHOTOVOLTAIQUE ET PROCEDE DE FABRICATION D’UN TEL MODULE,” fr, EP1614165A2, Jan. 2006. [Online]. Available: https://patents.google.com/patent/EP1614165A2/en?assignee=apollon+solar&oq=apollon+solar (visited on 05/11/2025).

[121] J.-P. Reyal, J. Giusti, and K. Bamberg, “Photovoltaic module and energy or light production modules,” US20100089438A1, Apr. 2010. [Online]. Available: https://patents.google.com/patent/US20100089438A1/en?assignee=apollon+solar&oq=apollon+solar (visited on 05/11/2025).

[122] X. C. Li, J. M. Zhao, L. H. Liu, and J. Y. Tan, “Optical properties of edible oils within spectral range from 300 to 2500 nm determined by double optical pathlength transmission method,” EN, *Applied Optics*, vol. 54, no. 13, pp. 3886–3893, May 2015, Publisher: Optica Publishing Group, ISSN: 2155-3165. DOI: 10.1364/AO.54.003886. [Online]. Available: https://opg.optica.org/ao/abstract.cfm?uri=ao-54-13-3886 (visited on 02/21/2025).

[123] *Refractive Index List of Common Household Liquids - Gem Society*, en-US, Jul. 2021. [Online]. Available: https://www.gemsociety.org/article/refractive-index-list-of-common-household-liquids/ (visited on 08/04/2025).

[124] *Refractive Index common Liquids, Solids and Gases*, en. [Online]. Available: https://www.engineeringtoolbox.com/refractive-index-d_1264.html (visited on 08/04/2025).

[125] M. N. Lyutikova, A. V. Ridel, and A. A. Konovalov, “Dielectric Liquids: Past, Present, Future (Review),” en, *Power Technology and Engineering*, vol. 57, no. 4, pp. 615–622, Nov. 2023, ISSN: 1570-1468. DOI: 10.1007/s10749-024-01709-x. [Online]. Available: https://doi.org/10.1007/s10749-024-01709-x (visited on 02/25/2025).

[126] *2.6.1: Like Dissolves Like*, en, Aug. 2024. [Online]. Available: https://chem.libretexts.org/Workbench/Survey_of_Chemistry_and_Physics/02%3A_Structure_of_Matter/2.06%3A_Solutions/2.6.01%3A_Like_Dissolves_Like (visited on 03/13/2025).

[127] *Polyisobutylene – scipoly.com*, en-US. [Online]. Available: https://scipoly.com/shop/polyisobutylene-9/ (visited on 03/13/2025).

[128] *Safety Data Sheet PIB*. [Online]. Available: https://www.trc-corp.com/wp-content/uploads/2016/05/PIB-240.pdf#:~:text=Water%20Solubility%20nil%20%E2%80%93%20below,Molecular%20Weight%20average%204400%20grams%2Fmole.

[129] *Polyisobutene (PIB) safety sheet*. [Online]. Available: https://www.braskem.com.br/cms/usa/ModuloProduto/Download?id=i24SrHnOR4I=&pasta=u+NLUW2hd4tbZe90oWKjdQ==&idioma=&guid=9899d1e7-4235-48da-84a2-8558caa83480.

[130] D. Shah, T. Roychowdhury, J. N. Hilfiker, and M. R. Linford, “Polyethylene glycol: Optical constants from 191 to 1688 nm (0.735–6.491 eV) by spectroscopic ellipsometry,” *Surface Science Spectra*, vol. 27, no. 1, p. 016 001, Jan. 2020, ISSN: 1055-5269. DOI: 10.1116/1.5095949. [Online]. Available: https://doi.org/10.1116/1.5095949 (visited on 02/03/2025).

[131] I.-C. B.V, *SolarPro*, en-US. [Online]. Available: https://innogreenchem.com/product/solarpro/ (visited on 08/05/2025).

[132] Shanshan Wang and David A. DeVore, *A study of polymer additives in mineral oil and vegetable oil-based greases*. [Online]. Available: http://functionalproducts.com/documents/articles/Biobased/PolymerAdditivesInMineralVegetableOil-ELGI2011.pdf.

[133] *Comparison of Dielectric Fluids for Immersive Liquid Cooling of IT Equipment | Schneider Electric*, en. [Online]. Available: https://www.se.com/ww/en/download/document/SPD_WP291_EN/ (visited on 08/17/2025).

[134] D. Sundin, *ElectroCool® Dielectric Coolants - Electronics Cooling*, en-US, Aug. 2022. [Online]. Available: https://www.engineeredfluids.com/products/electrocool/ (visited on 07/03/2025).

[135] *OptiCool Fluid, Dielectric Heat Transfer Fluid, Electronics Cooling, DSI Ventures, Soltex Inc.* en. [Online]. Available: https://soltexinc.com/product/products/thermal-fluids/opticool-fluids/opticool-fluid/ (visited on 07/03/2025).

[136] *SLIC Product Material Compatibility Guide | Engineered Fluids*, en-US, Aug. 2022. [Online]. Available: https://www.engineeredfluids.com/our-resources/compatibility-guides/ (visited on 07/03/2025).

[137] T. Roychowdhury, C. V. Cushman, R. A. Synowicki, and M. R. Linford, "Polydimethylsiloxane: Optical properties from 191 to 1688 nm (0.735–6.491 eV) of the liquid material by spectroscopic ellipsometry," *Surface Science Spectra*, vol. 25, no. 2, p. 026 001, Nov. 2018, ISSN: 1055-5269. DOI: 10.1116/1.5046735. [Online]. Available: https://doi.org/10.1116/1.5046735 (visited on 01/21/2025).

[138] L. Makai, B. Kalas, and G. Tiborcz, "Spectroscopic ellipsometry investigation of free liquid-liquid and liquid-air interfaces," *Thin Solid Films*, vol. 764, p. 139 634, Jan. 2023, ISSN: 0040-6090. DOI: 10.1016/j.tsf.2022.139634. [Online]. Available: https://www.sciencedirect.com/science/article/pii/S0040609022005363 (visited on 01/21/2025).

[139] L. Zhu, Y. Wang, Z. Fang, Y. Sun, and Q. Huang, "An effective heat dissipation method for densely packed solar cells under high concentrations," *Solar Energy Materials and Solar Cells*, vol. 94, no. 2, pp. 133–140, Feb. 2010, ISSN: 0927-0248. DOI: 10.1016/j.solmat.2009.08.014. [Online]. Available: https://www.sciencedirect.com/science/article/pii/S0927024809002943 (visited on 01/08/2025).

[140] M. A. G. Martins, "Vegetable oils, an alternative to mineral oil for power transformers- experimental study of paper aging in vegetable oil versus mineral oil," *IEEE Electrical Insulation Magazine*, vol. 26, no. 6, pp. 7–13, Nov. 2010, ISSN: 1558-4402. DOI: 10.1109/MEI.2010.5599974. [Online]. Available: https://ieeexplore.ieee.org/document/5599974 (visited on 07/03/2025).

[141] S. Ab Ghani, N. A. Muhamad, Z. A. Noorden, H. Zainuddin, N. Abu Bakar, and M. A. Talib, "Methods for improving the workability of natural ester insulating oils in power transformer applications: A review," *Electric Power Systems Research*, Advances in HV Transmission Systems, vol. 163, pp. 655–667, Oct. 2018, ISSN: 0378-7796. DOI: 10.1016/j.epsr.2017.10.008. [Online]. Available: https://www.sciencedirect.com/science/article/pii/S0378779617304121 (visited on 07/03/2025).

[142] F. S. Javadi, R. Saidur, and M. Kamalisarvestani, "Investigating performance improvement of solar collectors by using nanofluids," *Renewable and Sustainable Energy Reviews*, vol. 28, pp. 232–245, Dec. 2013, ISSN: 1364-0321. DOI: 10.1016/j.rser.2013.06.053. [Online]. Available: https://www.sciencedirect.com/science/article/pii/S1364032113004449 (visited on 02/14/2025).

[143] *Deionized_water*. [Online]. Available: https://www.chemeurope.com/en/encyclopedia/Deionized_water.html (visited on 03/05/2025).

[144] *BestSolv™ 7300 Engineered Fluid | Novec™ 7300 Replacement*, en-US. [Online]. Available: https://bestsolv.com/3m-novec-replacements/bestsolv-7300/ (visited on 07/03/2025).

[145] *3M™ Solar Encapsulant Films polyolefin POE*, en-US, Archive Location: US Layout: Luxury. [Online]. Available: https://www.3m.com/3M/en_US/p/d/b00022822/ (visited on 08/05/2025).

[146] *3M™ Novec™ 7300 Engineered Fluid*, en-US, Archive Location: US Layout: Luxury. [Online]. Available: https://www.3m.com/3M/en_US/p/d/b40044871/ (visited on 07/03/2025).

[147] V. Everett, Y. Wu, A. Resch, *et al.*, "Towards an innovative spectral-splitting hybrid PV-T micro-concentrator," *AIP Conference Proceedings*, vol. 1477, no. 1, pp. 230–234, Oct. 2012, ISSN: 0094-243X. DOI: 10.1063/1.4753875. [Online]. Available: https://doi.org/10.1063/1.4753875 (visited on 07/03/2025).

[148] *Xiameter PMX561 Silicone Transformer Fluid*, en. [Online]. Available: https://croylek.com/products/pmx-561-silicone-transformer-fluid (visited on 08/05/2025).

[149] Mike, *Ethylene vinyl acetate (EVA) price index*, en-US, Oct. 2020. [Online]. Available: https://businessanalytiq.com/procurementanalytics/index/ethylene-vinyl-acetate-eva-price-index/ (visited on 08/05/2025).

[150] *HIGH QUALITY EVA FILM FOR ENCAPSULATING SOLAR PANELS / GLASSES*, 2025. [Online]. Available: https://cdn.enfsolar.com/Product/pdf/EVA/597be38b8898a.pdf.

[151] *Polyolefin Elastomer (POE) Prices, News, Forecast*, en. [Online]. Available: https://www.imarcgroup.com/polyolefin-elastomer-pricing-report (visited on 08/05/2025).

[152] *Datasheet Glycerol*, 2023. [Online]. Available: https://www.sigmaaldrich.com/NL/en/sds/sigma/g5516?userType=anonymous.

[153] Mike, *Glycerol price index*, en-US, Jul. 2020. [Online]. Available: https://businessanalytiq.com/procurementanalytics/index/glycerol-price-index/ (visited on 08/06/2025).

[154] *Datasheet Glycol*, 2025. [Online]. Available: https://www.sigmaaldrich.com/NL/en/sds/sial/398039?userType=anonymous.

[155] Mike, *Propylene glycol price index*, en-US, Jul. 2020. [Online]. Available: https://businessanalytiq.com/procurementanalytics/index/propylene-glycol-price-index/ (visited on 08/05/2025).

[156] *Gedemineraliseerd water 10L Online kopen | Huchem*. [Online]. Available: https://www.huchem.nl/demi-water.html (visited on 08/05/2025).

[157] *XIAMETER™ PMX-561 Transformer Liquid*, en-US. [Online]. Available: https://www.dow.com/en-us/pdp.xiameter-pmx-561-transformer-liquid.01496204z.html (visited on 08/05/2025).

[158] *Pmx 561 Imports Under HS Code 39100020 | pmx 561 import price | Zauba*. [Online]. Available: https://www.zauba.com/import-pmx-561/hs-code-39100020-hs-code.html (visited on 08/05/2025).

[159] *Shell Diala S4 Imports | shell diala s4 import price | Zauba*. [Online]. Available: https://www.zauba.com/import-shell-diala-s4-hs-code.html (visited on 08/05/2025).

[160] *Shell Diala S4 ZX-I Datasheet*, nl-BE, 2025. [Online]. Available: https://www.shell.com/business-customers/lubricants-for-business/sector-expertise/power-industry/wind-power/windeurope-electric-city/_jcr_content/root/main/section/simple_2118681472/text.multi.stream/1726581236629/30ce6e8d9d69ebdcb19c946c00e1644ec7507965/shell-diala-s4-zx-i-tds.pdf (visited on 08/06/2025).

[161] *MIDEL 7131*, en-GB. [Online]. Available: https://static.mimaterials.com/midel/documents/technical/MIDEL_7131_UK.pdf (visited on 08/05/2025).

[162] *Midel 7131 Imports | midel 7131 import price | Zauba*. [Online]. Available: https://www.zauba.com/import-midel-7131-hs-code.html (visited on 08/05/2025).

[163] *MIVOLT DF7 - Single Phase Immersion Cooling Liquid*, en-GB. [Online]. Available: https://www.mivolt.com/wp-content/uploads/2021/10/MIVOLT-DF7-Brochure_Mar23.pdf (visited on 08/05/2025).

[164] X. C. Li, C. C. Wang, J. M. Zhao, and L. H. Liu, "Temperature-dependent optical constants of highly transparent solids determined by the combined double optical pathlength transmission-ellipsometry method," EN, *Applied Optics*, vol. 57, no. 5, pp. 1260–1266, Feb. 2018, Publisher: Optica Publishing Group, ISSN: 2155-3165. DOI: 10.1364/AO.57.001260. [Online]. Available: https://opg.optica.org/ao/abstract.cfm?uri=ao-57-5-1260 (visited on 06/25/2025).

[165] C. C. Wang, J. Y. Tan, C. Y. Jing, and L. H. Liu, “Temperature-dependent optical constants of liquid isopropanol, n-butanol, and n-decane,” EN, *Applied Optics*, vol. 57, no. 12, pp. 3003–3011, Apr. 2018, Publisher: Optica Publishing Group, ISSN: 2155-3165. DOI: 10.1364/AO.57.003003. [Online]. Available: https://opg.optica.org/ao/abstract.cfm?uri=ao-57-12-3003 (visited on 02/03/2025).

[166] S. A. Khodier, “Refractive index of standard oils as a function of wavelength and temperature,” *Optics & Laser Technology*, vol. 34, no. 2, pp. 125–128, Mar. 2002, ISSN: 0030-3992. DOI: 10.1016/S0030-3992(01)00101-3. [Online]. Available: https://www.sciencedirect.com/science/article/pii/S0030399201001013 (visited on 02/17/2025).

[167] M. Izdebski, R. Ledzion, and S. Węgrzynowski, “Extremely Weak Electro-Optic Kerr Effect in Methyl Silicone Oils,” *Materials*, vol. 17, p. 1850, Apr. 2024. DOI: 10.3390/ma17081850.

[168] *LAMBDA 1050+ UV/Vis/NIR Spectrophotometer*. [Online]. Available: https://shop.perkinelmer.com/product/L6020055 (visited on 08/11/2025).

[169] T. P. Otanicar, P. E. Phelan, and J. S. Golden, “Optical properties of liquids for direct absorption solar thermal energy systems,” *Solar Energy*, vol. 83, no. 7, pp. 969–977, Jul. 2009, ISSN: 0038-092X. DOI: 10.1016/j.solener.2008.12.009. [Online]. Available: https://www.sciencedirect.com/science/article/pii/S0038092X08003496 (visited on 01/14/2025).

[170] M. Stchakovsky, Y. Battie, and A. E. Naciri, “An original method to determine complex refractive index of liquids by spectroscopic ellipsometry and illustrated applications,” *Applied Surface Science*, 7th_International Conference on Spectroscopic Ellipsometry, vol. 421, pp. 802–806, Nov. 2017, ISSN: 0169-4332. DOI: 10.1016/j.apsusc.2016.12.001. [Online]. Available: https://www.sciencedirect.com/science/article/pii/S0169433216327015 (visited on 01/21/2025).

[171] X. Li, C. Wang, L. Ma, and L. Liu, “Ellipsometry-transmission measurement of the complex refractive indices for a series of organic solvents in the 200–1700 nm spectral range,” *Infrared Physics & Technology*, vol. 125, p. 104 313, Sep. 2022, ISSN: 1350-4495. DOI: 10.1016/j.infrared.2022.104313. [Online]. Available: https://www.sciencedirect.com/science/article/pii/S1350449522002948 (visited on 02/03/2025).

[172] *Spectroscopic Ellipsometry: Principles and Applications | Wiley*, en. [Online]. Available: https://www.wiley.com/en-us/Spectroscopic+Ellipsometry%3A+Principles+and+Applications-p-9780470016084 (visited on 06/26/2025).

[173] X. Li, C. Wang, J. Zhao, and L. Liu, “A New Method for Determining the Optical Constants of Highly Transparent Solids,” EN, *Applied Spectroscopy*, vol. 71, no. 1, pp. 70–77, Jan. 2017, Publisher: Society for Applied Spectroscopy. [Online]. Available: https://opg.optica.org/as/abstract.cfm?uri=as-71-1-70 (visited on 06/26/2025).

[174] X. Li, L. Liu, J. Zhao, and J. Tan, “Optical-Properties of Sodium Chloride Solution within the Spectral Range from 300 to 2500 nm at Room Temperature,” EN, *Applied Spectroscopy*, vol. 69, no. 5, pp. 635–640, May 2015, Publisher: SAGE Publications Ltd STM, ISSN: 0003-7028. DOI: 10.1366/14-07769R. [Online]. Available: https://doi.org/10.1366/14-07769R (visited on 06/26/2025).

[175] *Systematic errors in rotating-compensator ellipsometry*. [Online]. Available: https://opg.optica.org/josaa/fulltext.cfm?uri=josaa-11-9-2550&id=822 (visited on 08/12/2025).

[176] “Introduction to Spectroscopic Ellipsometry,” en, in *Spectroscopic Ellipsometry*, John Wiley & Sons, Ltd, 2007, pp. 1–11, ISBN: 978-0-470-06019-3. DOI: 10.1002/9780470060193.ch1. [Online]. Available: https://onlinelibrary.wiley.com/doi/abs/10.1002/9780470060193.ch1 (visited on 08/12/2025).

[177] M. Khardani, M. Bouaicha, and B. Bessaïs, “Bruggeman effective medium approach for modelling optical properties of porous silicon: Comparison with experiment,” *physica status solidi (c)*, vol. 4, pp. 1986–1990, May 2007. DOI: 10.1002/pssc.200674420.

[178] *Hellma cuvettes 5 and 10 mm optical pathway*, 2025. [Online]. Available: https://www.hellma.com/fileadmin/fos/Website/Broschueren_Flyer_Handhabung/Hellma_Analytics/English/Hellma_Kuevettenkatalog_EN_2025_gross.pdf (visited on 08/11/2025).

[179] D. J. Segelstein, “The complex refractive index of water,” en_US, Thesis, University of Missouri–Kansas City, 1981. [Online]. Available: https://mospace.umsystem.edu/xmlui/handle/10355/11599 (visited on 05/30/2025).

[180] “Transfer spectrophotometer,” en, *NIST*, Nov. 2009, Last Modified: 2023-02-07T10:09-05:00. [Online]. Available: https://www.nist.gov/laboratories/tools-instruments/transfer-spectrophotometer (visited on 08/12/2025).

[181] *T Table*, en-US. [Online]. Available: https://www.tdistributiontable.com/ (visited on 06/30/2025).

[182] Y. Mattley, *The Importance of Dynamic Range and Signal to Noise Ratio in Spectrometers*, en-US, Nov. 2021. [Online]. Available: https://www.oceanoptics.com/high-sensitivity-spectrometers/dynamic-range-and-signal-to-noise-ratio-spectrometers/ (visited on 06/30/2025).

[183] G. Wells, *Signal, Noise, and Detection Limits in Mass Spectrometry*, Jun. 2023. [Online]. Available: https://www.agilent.com/cs/library/technicaloverviews/public/5990-7651EN.pdf.

[184] R. Santbergen, A. H. M. Smets, and M. Zeman, “Optical model for multilayer structures with coherent, partly coherent and incoherent layers,” EN, *Optics Express*, vol. 21, no. 102, A262–A267, Mar. 2013, Publisher: Optica Publishing Group, ISSN: 1094-4087. DOI: 10.1364/OE.21.00A262. [Online]. Available: https://opg.optica.org/oe/abstract.cfm?uri=oe-21-S2-A262 (visited on 04/30/2025).

[185] R. Santbergen, T. Meguro, T. Suezaki, G. Koizumi, K. Yamamoto, and M. Zeman, “GenPro4 Optical Model for Solar Cell Simulation and Its Application to Multijunction Solar Cells,” *IEEE Journal of Photovoltaics*, vol. PP, pp. 1–8, Mar. 2017. DOI: 10.1109/JPHOTOV.2017.2669640.

[186] K. Jäger, M. Fischer, R. A. C. M. M. van Swaaij, and M. Zeman, “A scattering model for nano-textured interfaces and its application in opto-electrical simulations of thin-film silicon solar cells,” *Journal of Applied Physics*, vol. 111, no. 8, p. 083 108, Apr. 2012, ISSN: 0021-8979. DOI: 10.1063/1.4704372. [Online]. Available: https://doi.org/10.1063/1.4704372 (visited on 04/24/2025).

[187] A. M. Law, L. O. Jones, and J. M. Walls, “The performance and durability of Anti-reflection coatings for solar module cover glass – a review,” *Solar Energy*, vol. 261, pp. 85–95, Sep. 2023, ISSN: 0038-092X. DOI: 10.1016/j.solener.2023.06.009. [Online]. Available: https://www.sciencedirect.com/science/article/pii/S0038092X23004061 (visited on 04/15/2025).

[188] M. Diop, A. Diaw, N. Mbengue, *et al.*, “Optimization and Modeling of Antireflective Layers for Silicon Solar Cells: In Search of Optimal Materials,” *Materials Sciences and Applications*, vol. 09, pp. 705–722, Jan. 2018. DOI: 10.4236/msa.2018.98051.

[189] A. S. Sarkın, N. Ekren, and Ş. Sağlam, “A review of anti-reflection and self-cleaning coatings on photovoltaic panels,” *Solar Energy*, vol. 199, pp. 63–73, Mar. 2020, ISSN: 0038-092X. DOI: 10.1016/j.solener.2020.01.084. [Online]. Available: https://www.sciencedirect.com/science/article/pii/S0038092X20300918 (visited on 04/15/2025).

[190] N. Ekren, “Researches on Anti-reflection Coating (ARC) Methods Used in PV Systems,” *Balkan Journal of Electrical and Computer Engineering*, vol. 6, pp. 42–46, Feb. 2018. DOI: 10.17694/bajece.402004.

[191] S. Yang and Y. Zhang, “Spectroscopic ellipsometry investigations of porous SiO2 films prepared by glancing angle deposition,” en, *Surface and Interface Analysis*, vol. 45, no. 11-12, pp. 1690–1694, 2013, ISSN: 1096-9918. DOI: 10.1002/sia.5308. [Online]. Available: https://onlinelibrary.wiley.com/doi/abs/10.1002/sia.5308 (visited on 07/24/2025).

[192] M. Vogt, R. Witteck, T. Gewohn, *et al.*, “Boosting PV Module Efficiency Beyond the Efficiency of Its Solar Cells – A Raytracing Study with Daidalos Now Available to the Scientific Community,” en, *36th European Photovoltaic Solar Energy Conference and Exhibition; 795-800*, 6 pages, 9903 kb, 2019. DOI: 10.4229/EUPVSEC20192019-4BO.11.3. (visited on 08/17/2025).

[193] M. K. Yang, “Optical properties of Teflon® AF amorphous fluoropolymers,” en, *Journal of Micro/-Nanolithography, MEMS, and MOEMS*, vol. 7, no. 3, p. 033 010, Jul. 2008, ISSN: 1932-5150. DOI: 10.1117/1.2965541. [Online]. Available: http://nanolithography.spiedigitallibrary.org/article.aspx?doi=10.1117/1.2965541 (visited on 04/15/2025).

[194] P. Nain and A. Anctil, “Per- and polyfluoroalkyl substances (PFAS) in solar photovoltaic modules,” *Renewable and Sustainable Energy Reviews*, vol. 215, p. 115 562, Jun. 2025, ISSN: 1364-0321. DOI: 10.1016/j.rser.2025.115562. [Online]. Available: https://www.sciencedirect.com/science/article/pii/S1364032125002357 (visited on 05/09/2025).

[195] A. Diaw, A. Dieye, O. Ngom, *et al.*, “Optimization of Antireflective Layers of Silicon Solar Cells: Comparative Studies of the Efficiency Between Single and Double Layer at the Reference Wavelength,” *American Journal of Physics and Applications*, vol. 9, p. 133, Nov. 2021. DOI: 10.11648/j.ajpa.20210906.11.

[196] P. Procel-Moya, Y. Zhao, and O. Isabella, “Unlocking the potential of carrier-selective contacts: Key insights for designing c-Si solar cells with efficiency beyond 28 %,” *Solar Energy Materials and Solar Cells*, vol. 285, p. 113 504, Jun. 2025, ISSN: 0927-0248. DOI: 10.1016/j.solmat.2025.113504. [Online]. Available: https://www.sciencedirect.com/science/article/pii/S0927024825001059 (visited on 02/18/2025).

[197] C. Ji, W. Liu, Y. Bao, *et al.*, “Recent Applications of Antireflection Coatings in Solar Cells,” en, *Photonics*, vol. 9, no. 12, p. 906, Dec. 2022, Number: 12 Publisher: Multidisciplinary Digital Publishing Institute, ISSN: 2304-6732. DOI: 10.3390/photonics9120906. [Online]. Available: https://www.mdpi.com/2304-6732/9/12/906 (visited on 04/15/2025).

[198] A. Nositschka, *Sun-light harvesting with surface patterned glass for photovoltaics*, Saint-Gobain Sekurit Deutschland, Pittsburgh, PA, Nov. 2008. [Online]. Available: https://www.lehigh.edu/imi/teched/SolarWS/T3f_Nositschka.pdf.

[199] S. Sadhukhan, S. Acharyya, T. Panda, *et al.*, “Evaluation of dominant loss mechanisms of PERC cells for optimization of rear passivating stacks,” *Surfaces and Interfaces*, vol. 27, p. 101 496, Dec. 2021, ISSN: 2468-0230. DOI: 10.1016/j.surfin.2021.101496. [Online]. Available: https://www.sciencedirect.com/science/article/pii/S2468023021005733 (visited on 07/08/2025).

[200] J. Xu, C. Chen, C. Liu, *et al.*, “High efficiency TOPCon solar cells with micron/nano-structured emitter for a balance of light-trapping and surface passivation,” *Solar Energy Materials and Solar Cells*, vol. 238, p. 111 606, May 2022, ISSN: 0927-0248. DOI: 10.1016/j.solmat.2022.111606. [Online]. Available: https://www.sciencedirect.com/science/article/pii/S092702482200307 (visited on 07/08/2025).

[201] M. A. Green, E. D. Dunlop, M. Yoshita, *et al.*, “Solar cell efficiency tables (Version 64),” en, *Progress in Photovoltaics: Research and Applications*, vol. 32, no. 7, pp. 425–441, 2024, ISSN: 1099-159X. DOI: 10.1002/pip.3831. [Online]. Available: https://onlinelibrary.wiley.com/doi/abs/10.1002/pip.3831 (visited on 08/16/2025).

[202] K. Lee, J. T. Kunjappu, S. Jockusch, *et al.*, “Amplification of the Index of Refraction of Aqueous Immersion Fluids by Ionic Surfactants,” en, vol. 5753, pp. 537–553, 2005. DOI: 10.7916/D8SX6KG2. [Online]. Available: https://doi.org/10.7916/D8SX6KG2 (visited on 07/09/2025).

[203] J. Reis, I. Lampreia, A. Santos, M. Moita, and G. Douhéret, “Refractive Index of Liquid Mixtures: Theory and Experiment,” *Chemphyschem : a European journal of chemical physics and physical chemistry*, vol. 11, pp. 3722–33, Dec. 2010. DOI: 10.1002/cphc.201000566.

[204] N. None, “Optimal Design of Multilayer Optical Color Filters for Building-Integrated Photovoltaic (BIPV) Applications,” en, 2023. [Online]. Available: https://repository.tudelft.nl/record/uuid:354e9b05-5175-4d54-a93e-10c3a18d69ec (visited on 07/17/2025).

[205] Sunpower, *IBC Sunpower Maxeon Gen III*. [Online]. Available: https://oceanplanetenergy.com/wp-content/uploads/2023/11/Maxeon_3_Solar_Cell_ds_en_a4_166_519452E-final.pdf.

[206] E. N. F. SunEvo Solar Co, *210 mono-crystalline Bifacial solar cell (SE-210M-18D1)*, en. [Online]. Available: https://cdn.enfsolar.com/z/pp/2023/12/5c8kb9b82ow9qwi3a/TOPCon-210-18BB.pdf?_gl=1*mgcoto*_gcl_au*MTEyNTY4NzQ2MS4xNzUyNzU5OTcz (visited on 07/18/2025).

[207] M. S. Kim, J. H. Lee, and M. K. Kwak, “Review: Surface Texturing Methods for Solar Cell Efficiency Enhancement,” en, *International Journal of Precision Engineering and Manufacturing*, vol. 21, no. 7, pp. 1389–1398, Jul. 2020, ISSN: 2005-4602. DOI: 10.1007/s12541-020-00337-5. [Online]. Available: https://doi.org/10.1007/s12541-020-00337-5 (visited on 07/21/2025).

[208] M. R. Vogt, C. R. Tobon, A. Alcañiz, *et al.*, “Introducing a comprehensive physics-based modelling framework for tandem and other PV systems,” *Solar Energy Materials and Solar Cells*, vol. 247, p. 111 944, Oct. 2022, ISSN: 0927-0248. DOI: 10.1016/j.solmat.2022.111944. [Online]. Available: https://www.sciencedirect.com/science/article/pii/S0927024822003622 (visited on 08/15/2025).

[209] M. Hofmann, L. Stevens, P. Hör, *et al.*, “Improvement Options for PV Modules by Glass Structuring,” en, 2023. DOI: 10.4229/EUPVSEC2023/3DO.18.3. [Online]. Available: https://publica.fraunhofer.de/handle/publica/464568 (visited on 07/25/2025).

[210] *Might Silicon Surface Be Used for Electronic Tongue Application? | ACS Applied Materials & Interfaces*. [Online]. Available: https://pubs.acs.org/doi/10.1021/am5058162 (visited on 07/27/2025).

A

Chapter 3, Liquid selection

Encapsulation Material	Refractive Index (n)	Pour Point (°C)	Flash Point (°C)	thermal conductivity ($W/m^2 \cdot K$)	heat capacity (kJ/kg·K)	thermal expansion (1/K)	Density (g/cm^3)	Kinematic Viscosity ($cSt)/(mm^2/s$)	Electrical resistivity (Ω*cm)	Dielectric Constant (kV/cm)
EVA [70]	1.48	X	270	0.23	1.40	-	0.95	-	$1.0 * 10^{15}$	200
Air	1.00	-213	X	0.03	1.01	0.0034	0.001	-	$1.3 * 10^{16}$	30
Demi water	1.33	0	X	0.62	4.18	0.0002	0.997	0.89	$1.8 * 10^{7}$	29
Glycerol [76]	1.47	19	199	0.29	2.38	0.0005	1.25	1130	$1.0 * 10^{9}$	43
MPG [77]	1.41	-57	104	0.18	2.48	0.0006	1.04	42.1	$2.3 * 10^{7}$	32
PDMS [78]	1.40	-70	318	0.15	1.51	0.0010	0.96	50	$1.0 * 10^{15}$	40
Mivolt [79]	1.46	-50	250	0.14	1.90	0.0008	0.97	75	$9.0 * 10^{8}$	75
Midel 7131 [80]	1.46	-56	260	0.14	-	-	0.97	29	$2.0 * 10^{12}$	75
shell Diala [81]	1.45	-45	191	0.14	2.14	0.0008	0.81	9.8	$9.0 * 10^{10}$	78

Figure A.1: Material properties of the selected liquids [58]

B

Chapter 4, complex refractive index

Liquid	Cuvette	Mean Std (%T)	Max Std (%T)	Max Dev (%T)	Wavelength (nm)
Water	5 mm	0.1604	0.6895	1.3292	835.0
	10 mm_5mmref	0.1240	0.3604	1.1209	300.0
	10 mm	0.1003	0.8144	1.1517	375.0
Glycerol	5 mm	0.1434	0.5994	1.1988	845.0
	10 mm_5mmref	0.1175	1.3943	2.7661	855.0
	10 mm	0.1129	0.6348	1.2688	850.0
Glycol	5 mm	0.0321	0.1330	0.2557	855.0
	10 mm_5mmref	0.0364	0.2836	0.5498	855.0
	10 mm	0.0222	0.2501	0.4622	850.0
Mivolt	5 mm	0.0303	0.2192	0.4347	850.0
	10 mm_5mmref	0.0231	0.1259	0.2495	855.0
	10 mm	0.0350	0.1906	0.3322	855.0
Midel	5 mm	0.0390	0.1239	0.2307	345.0
	10 mm_5mmref	0.0369	0.2413	0.4755	300.0
	10 mm	0.0225	0.1219	0.2423	855.0
Shell Diala	5 mm	0.0217	0.1448	0.2727	855.0
	10 mm_5mmref	0.0470	0.2643	0.5142	850.0
	10 mm	0.0218	0.1133	0.2232	805.0
PDMS	5 mm	0.1409	1.0687	0.1916	300.0
	10 mm_5mmref	0.0305	0.1626	0.2947	1195.0
	10 mm	0.2150	0.3320	0.4173	300.0

Table B.1: Measurement statistics for each liquid and cuvette combination

Table B.2: Complex refractive index (n and k) values for all 7 liquids measured in this thesis, as described in Chapter 4 (first part)

Liquid	Water		Glycerol		SP Glycol		PDMS		Mivolt		Midel		Shell Diala	
Wavelength (nm)	**n**	**k**	**n**	**k**	**n**	**k**	**n**	**k**	**n**	**k**	**n**	**k**	**n**	**k**
300	1.376	5.00E-08	1.513	1.34E-06	1.454	9.80E-07	1.450	8.95E-06	1.500	9.95E-06	1.496	5.00E-08	1.503	8.27E-06
305	1.374	5.00E-08	1.512	1.31E-06	1.453	8.75E-07	1.448	4.89E-06	1.498	8.87E-06	1.495	4.73E-06	1.501	7.77E-06
310	1.372	5.00E-08	1.510	1.19E-06	1.451	8.04E-07	1.446	2.94E-06	1.497	7.71E-06	1.493	5.49E-06	1.499	7.16E-06
315	1.371	5.00E-08	1.509	1.15E-06	1.450	7.58E-07	1.445	2.23E-06	1.495	7.59E-06	1.492	4.77E-06	1.498	7.12E-06
320	1.370	5.00E-08	1.507	1.09E-06	1.448	7.22E-07	1.443	2.02E-06	1.494	7.57E-06	1.490	3.95E-06	1.496	6.99E-06
325	1.368	5.00E-08	1.506	1.13E-06	1.447	7.05E-07	1.442	1.78E-06	1.492	6.52E-06	1.489	3.38E-06	1.495	6.10E-06
330	1.367	5.00E-08	1.504	1.05E-06	1.445	6.95E-07	1.441	1.54E-06	1.491	5.57E-06	1.488	2.73E-06	1.493	5.29E-06
335	1.366	5.00E-08	1.503	9.55E-07	1.444	6.86E-07	1.440	1.34E-06	1.490	4.37E-06	1.487	2.02E-06	1.492	4.17E-06
340	1.365	5.00E-08	1.502	8.69E-07	1.443	6.70E-07	1.438	1.10E-06	1.488	3.31E-06	1.485	1.57E-06	1.490	3.11E-06
345	1.364	5.00E-08	1.501	8.46E-07	1.442	6.54E-07	1.437	9.17E-07	1.487	2.52E-06	1.484	1.28E-06	1.489	2.31E-06
350	1.363	5.00E-08	1.499	8.25E-07	1.441	6.36E-07	1.436	8.46E-07	1.486	2.01E-06	1.483	1.04E-06	1.488	1.78E-06
355	1.362	5.00E-08	1.498	7.48E-07	1.439	5.99E-07	1.435	7.75E-07	1.485	1.66E-06	1.482	8.03E-07	1.487	1.42E-06
360	1.361	5.00E-08	1.497	7.42E-07	1.438	5.51E-07	1.434	6.31E-07	1.484	1.41E-06	1.481	6.31E-07	1.486	1.16E-06
365	1.360	5.00E-08	1.496	7.06E-07	1.437	4.96E-07	1.433	4.71E-07	1.483	1.25E-06	1.480	5.12E-07	1.485	9.91E-07
370	1.359	5.00E-08	1.495	6.86E-07	1.436	4.31E-07	1.432	3.61E-07	1.482	1.11E-06	1.480	4.17E-07	1.484	8.67E-07
375	1.358	5.00E-08	1.494	5.85E-07	1.436	3.72E-07	1.431	3.01E-07	1.481	9.95E-07	1.479	3.33E-07	1.483	7.58E-07
380	1.357	5.00E-08	1.493	5.43E-07	1.435	3.08E-07	1.430	2.27E-07	1.480	8.77E-07	1.478	2.37E-07	1.482	6.17E-07
385	1.356	5.00E-08	1.493	5.06E-07	1.434	2.52E-07	1.430	1.86E-07	1.479	7.75E-07	1.477	1.83E-07	1.481	5.43E-07
390	1.356	5.00E-08	1.492	4.65E-07	1.433	2.08E-07	1.429	1.60E-07	1.478	6.72E-07	1.476	1.50E-07	1.480	4.75E-07
395	1.355	5.00E-08	1.491	4.41E-07	1.432	1.70E-07	1.428	1.45E-07	1.478	6.22E-07	1.476	1.31E-07	1.479	4.22E-07
400	1.354	5.00E-08	1.490	4.15E-07	1.431	1.40E-07	1.427	1.23E-07	1.477	5.66E-07	1.475	1.05E-07	1.478	3.71E-07
405	1.353	5.00E-08	1.490	3.97E-07	1.431	1.17E-07	1.427	1.13E-07	1.476	5.15E-07	1.474	8.65E-08	1.478	3.28E-07
410	1.353	5.00E-08	1.489	3.73E-07	1.430	9.67E-08	1.426	1.10E-07	1.475	4.68E-07	1.474	6.82E-08	1.477	2.90E-07
415	1.352	5.00E-08	1.488	3.37E-07	1.429	8.34E-08	1.425	1.17E-07	1.475	4.39E-07	1.473	7.41E-08	1.476	2.70E-07
420	1.352	5.00E-08	1.487	3.65E-07	1.429	7.68E-08	1.425	1.13E-07	1.474	3.94E-07	1.472	6.98E-08	1.475	2.40E-07
425	1.351	5.00E-08	1.487	3.41E-07	1.428	6.84E-08	1.424	1.03E-07	1.474	3.54E-07	1.472	5.56E-08	1.475	2.09E-07
430	1.350	5.00E-08	1.486	3.26E-07	1.427	6.45E-08	1.423	9.33E-08	1.473	3.14E-07	1.471	5.00E-08	1.474	1.81E-07
435	1.350	5.00E-08	1.486	3.21E-07	1.427	6.07E-08	1.423	9.72E-08	1.472	2.93E-07	1.471	5.00E-08	1.473	1.72E-07
440	1.349	5.00E-08	1.485	3.19E-07	1.426	5.53E-08	1.422	9.94E-08	1.472	2.71E-07	1.470	5.00E-08	1.473	1.60E-07
445	1.349	5.00E-08	1.485	3.06E-07	1.426	5.49E-08	1.422	9.40E-08	1.471	2.48E-07	1.470	5.00E-08	1.472	1.41E-07
450	1.348	5.00E-08	1.484	3.07E-07	1.425	5.08E-08	1.421	8.75E-08	1.471	2.24E-07	1.469	5.00E-08	1.472	1.23E-07
455	1.348	5.00E-08	1.483	3.13E-07	1.425	5.00E-08	1.421	8.96E-08	1.470	2.13E-07	1.469	5.00E-08	1.471	1.17E-07
460	1.347	5.00E-08	1.483	3.09E-07	1.424	5.00E-08	1.420	9.89E-08	1.470	1.96E-07	1.468	5.00E-08	1.471	1.13E-07
465	1.347	5.00E-08	1.483	3.07E-07	1.424	5.00E-08	1.420	1.01E-07	1.469	1.82E-07	1.468	5.00E-08	1.470	1.03E-07
470	1.347	5.00E-08	1.482	3.00E-07	1.423	5.00E-08	1.419	9.53E-08	1.469	1.61E-07	1.467	5.00E-08	1.470	8.94E-08
475	1.346	5.00E-08	1.482	3.11E-07	1.423	5.00E-08	1.419	9.46E-08	1.468	1.48E-07	1.467	5.00E-08	1.469	8.09E-08
480	1.346	5.00E-08	1.481	3.10E-07	1.422	5.00E-08	1.418	9.98E-08	1.468	1.41E-07	1.466	5.00E-08	1.469	7.47E-08
485	1.345	5.00E-08	1.481	3.08E-07	1.422	5.00E-08	1.418	8.75E-08	1.467	1.24E-07	1.466	5.00E-08	1.468	6.80E-08
490	1.345	5.00E-08	1.480	3.18E-07	1.422	5.00E-08	1.418	9.18E-08	1.467	1.21E-07	1.466	5.00E-08	1.468	6.79E-08
495	1.345	5.00E-08	1.480	3.04E-07	1.421	5.00E-08	1.417	8.71E-08	1.467	1.04E-07	1.465	5.00E-08	1.467	5.72E-08
500	1.344	5.00E-08	1.480	3.05E-07	1.421	5.00E-08	1.417	8.82E-08	1.466	9.51E-08	1.465	5.00E-08	1.467	5.14E-08
505	1.344	5.00E-08	1.479	3.09E-07	1.420	5.00E-08	1.416	8.90E-08	1.466	9.18E-08	1.465	5.00E-08	1.467	5.00E-08
510	1.343	5.00E-08	1.479	3.05E-07	1.420	5.00E-08	1.416	9.60E-08	1.465	9.01E-08	1.464	5.00E-08	1.466	5.00E-08
515	1.343	5.00E-08	1.478	3.14E-07	1.420	5.00E-08	1.416	1.03E-07	1.465	8.96E-08	1.464	5.00E-08	1.466	5.26E-08
520	1.343	5.00E-08	1.478	3.09E-07	1.419	5.00E-08	1.415	9.09E-08	1.465	7.90E-08	1.464	5.00E-08	1.465	5.00E-08
525	1.343	5.00E-08	1.478	3.09E-07	1.419	5.00E-08	1.415	8.60E-08	1.464	7.22E-08	1.463	5.00E-08	1.465	5.00E-08
530	1.342	5.00E-08	1.477	3.01E-07	1.419	5.00E-08	1.415	8.83E-08	1.464	6.74E-08	1.463	5.00E-08	1.465	5.00E-08
535	1.342	5.00E-08	1.477	3.14E-07	1.418	5.00E-08	1.415	9.08E-08	1.464	6.81E-08	1.463	5.00E-08	1.464	5.00E-08
540	1.342	5.00E-08	1.477	3.20E-07	1.418	5.00E-08	1.414	9.05E-08	1.463	6.36E-08	1.462	5.00E-08	1.464	5.00E-08
545	1.341	5.00E-08	1.477	3.39E-07	1.418	5.00E-08	1.414	9.19E-08	1.463	6.00E-08	1.462	5.00E-08	1.464	5.00E-08
550	1.341	5.00E-08	1.476	3.47E-07	1.418	5.00E-08	1.414	9.94E-08	1.463	6.35E-08	1.462	5.00E-08	1.463	5.00E-08
555	1.341	5.00E-08	1.476	3.15E-07	1.417	5.00E-08	1.413	9.45E-08	1.463	5.87E-08	1.462	5.00E-08	1.463	5.00E-08
560	1.341	5.00E-08	1.476	3.30E-07	1.417	5.00E-08	1.413	1.06E-07	1.462	6.86E-08	1.461	5.00E-08	1.463	5.00E-08
565	1.340	5.00E-08	1.475	3.21E-07	1.417	5.00E-08	1.413	1.03E-07	1.462	5.75E-08	1.461	5.00E-08	1.463	5.00E-08
570	1.340	5.00E-08	1.475	3.33E-07	1.416	5.00E-08	1.413	1.01E-07	1.462	5.27E-08	1.461	5.00E-08	1.462	5.00E-08
575	1.340	5.00E-08	1.475	3.19E-07	1.416	5.00E-08	1.412	9.54E-08	1.462	5.00E-08	1.461	5.00E-08	1.462	5.00E-08
580	1.340	5.00E-08	1.475	3.35E-07	1.416	5.00E-08	1.412	9.45E-08	1.461	5.06E-08	1.460	5.00E-08	1.462	5.00E-08
585	1.339	5.00E-08	1.474	3.36E-07	1.416	5.00E-08	1.412	9.79E-08	1.461	5.28E-08	1.460	5.00E-08	1.462	5.00E-08
590	1.339	5.00E-08	1.474	3.26E-07	1.415	5.00E-08	1.412	9.11E-08	1.461	5.00E-08	1.460	5.00E-08	1.461	5.00E-08
595	1.339	5.00E-08	1.474	3.38E-07	1.415	5.00E-08	1.411	9.07E-08	1.461	5.00E-08	1.460	5.00E-08	1.461	5.00E-08
600	1.339	5.00E-08	1.474	3.50E-07	1.415	5.00E-08	1.411	1.10E-07	1.460	5.90E-08	1.459	5.00E-08	1.461	5.00E-08
605	1.339	5.00E-08	1.473	3.43E-07	1.415	5.00E-08	1.411	1.09E-07	1.460	6.15E-08	1.459	5.00E-08	1.461	5.00E-08
610	1.338	5.00E-08	1.473	3.62E-07	1.415	5.00E-08	1.411	1.13E-07	1.460	6.09E-08	1.459	5.00E-08	1.460	5.00E-08
615	1.338	5.00E-08	1.473	3.78E-07	1.414	5.00E-08	1.411	9.95E-08	1.460	5.00E-08	1.459	5.00E-08	1.460	5.00E-08
620	1.338	5.00E-08	1.473	3.34E-07	1.414	5.00E-08	1.410	9.41E-08	1.460	5.00E-08	1.459	5.00E-08	1.460	5.00E-08
625	1.338	5.00E-08	1.473	3.42E-07	1.414	5.00E-08	1.410	1.09E-07	1.459	5.00E-08	1.458	5.00E-08	1.460	5.00E-08
630	1.338	5.00E-08	1.472	3.57E-07	1.414	5.00E-08	1.410	1.05E-07	1.459	5.00E-08	1.458	5.00E-08	1.459	5.00E-08
635	1.337	5.00E-08	1.472	3.74E-07	1.414	5.00E-08	1.410	1.12E-07	1.459	5.21E-08	1.458	5.00E-08	1.459	5.00E-08
640	1.337	5.00E-08	1.472	3.63E-07	1.413	5.00E-08	1.410	9.66E-08	1.459	5.00E-08	1.458	5.00E-08	1.459	5.00E-08
645	1.337	5.00E-08	1.472	3.30E-07	1.413	5.00E-08	1.409	1.02E-07	1.459	5.00E-08	1.458	5.00E-08	1.459	5.00E-08
650	1.337	5.00E-08	1.472	3.23E-07	1.413	5.00E-08	1.409	8.95E-08	1.458	5.00E-08	1.458	5.00E-08	1.459	5.00E-08
655	1.337	5.00E-08	1.472	4.01E-07	1.413	5.00E-08	1.409	9.36E-08	1.458	5.00E-08	1.457	5.00E-08	1.459	5.00E-08
660	1.337	5.00E-08	1.471	3.67E-07	1.413	5.00E-08	1.409	1.06E-07	1.458	5.00E-08	1.457	5.00E-08	1.458	5.00E-08
665	1.337	5.00E-08	1.471	3.66E-07	1.413	5.00E-08	1.409	1.05E-07	1.458	5.28E-08	1.457	5.00E-08	1.458	5.00E-08
670	1.336	5.00E-08	1.471	4.12E-07	1.412	5.00E-08	1.409	1.08E-07	1.458	5.83E-08	1.457	5.00E-08	1.458	5.00E-08
675	1.336	5.00E-08	1.471	3.91E-07	1.412	5.00E-08	1.409	9.60E-08	1.458	5.00E-08	1.457	5.00E-08	1.458	5.00E-08
680	1.336	5.00E-08	1.471	3.47E-07	1.412	5.00E-08	1.408	8.71E-08	1.457	5.00E-08	1.457	5.00E-08	1.458	5.00E-08
685	1.336	5.00E-08	1.471	4.04E-07	1.412	5.00E-08	1.408	1.10E-07	1.457	5.73E-08	1.457	5.00E-08	1.458	5.00E-08
690	1.336	5.00E-08	1.470	3.68E-07	1.412	5.00E-08	1.408	8.92E-08	1.457	5.00E-08	1.456	5.00E-08	1.457	5.00E-08
695	1.336	5.00E-08	1.470	3.77E-07	1.412	5.00E-08	1.408	9.79E-08	1.457	5.00E-08	1.456	5.00E-08	1.457	5.00E-08
700	1.336	5.00E-08	1.470	4.05E-07	1.412	5.00E-08	1.408	1.15E-07	1.457	5.40E-08	1.456	5.00E-08	1.457	5.00E-08
705	1.335	5.00E-08	1.470	3.85E-07	1.411	5.00E-08	1.408	1.09E-07	1.457	5.29E-08	1.456	5.00E-08	1.457	5.00E-08
710	1.335	5.00E-08	1.470	3.65E-07	1.411	5.00E-08	1.408	1.09E-07	1.457	5.16E-08	1.456	5.00E-08	1.457	5.00E-08
715	1.335	5.00E-08	1.470	3.01E-07	1.411	5.00E-08	1.407	8.26E-08	1.456	5.00E-08	1.456	5.00E-08	1.457	5.00E-08
720	1.335	5.00E-08	1.470	3.27E-07	1.411	5.00E-08	1.407	8.98E-08	1.456	5.00E-08	1.456	5.00E-08	1.456	5.00E-08
725	1.335	7.05E-08	1.470	4.12E-07	1.411	5.49E-08	1.407	1.30E-07	1.456	5.39E-08	1.456	5.00E-08	1.456	5.00E-08
730	1.335	1.04E-07	1.469	4.14E-07	1.411	6.80E-08	1.407	1.23E-07	1.456	5.53E-08	1.455	5.00E-08	1.456	5.00E-08
735	1.335	1.64E-07	1.469	4.28E-07	1.411	8.33E-08	1.407	1.63E-07	1.456	9.02E-08	1.455	5.00E-08	1.456	5.47E-08
740	1.335	1.78E-07	1.469	4.02E-07	1.411	9.99E-08	1.407	1.84E-07	1.456	8.89E-08	1.455	5.00E-08	1.456	6.23E-08
745	1.334	1.40E-07	1.469	4.89E-07	1.410	1.22E-07	1.407	1.75E-07	1.456	8.18E-08	1.455	5.00E-08	1.456	5.07E-08
750	1.334	1.54E-07	1.469	5.40E-07	1.410	1.36E-07	1.407	1.21E-07	1.456	9.24E-08	1.455	5.00E-08	1.456	5.93E-08

Table B.3: Complex refractive index (n and k) values for all 7 liquids measured in this thesis, as described in Chapter 4 (second part)

Liquid	Water		Glycerol		SP Glycol		PDMS		Mivolt		Midel		Shell Diala	
Wavelength (nm)	**n**	**k**	**n**	**k**	**n**	**k**	**n**	**k**	**n**	**k**	**n**	**k**	**n**	**k**
755	1.334	1.37E-07	1.469	5.02E-07	1.410	1.36E-07	1.406	1.23E-07	1.455	1.03E-07	1.455	5.00E-08	1.456	8.21E-08
760	1.334	1.62E-07	1.469	5.65E-07	1.410	1.46E-07	1.406	1.03E-07	1.455	8.37E-08	1.455	5.00E-08	1.455	6.39E-08
765	1.334	1.48E-07	1.469	4.80E-07	1.410	1.44E-07	1.406	7.77E-08	1.455	5.00E-08	1.455	5.00E-08	1.455	5.00E-08
770	1.334	1.35E-07	1.468	4.82E-07	1.410	1.43E-07	1.406	1.12E-07	1.455	5.00E-08	1.455	5.00E-08	1.455	5.00E-08
775	1.334	1.60E-07	1.468	5.20E-07	1.410	1.44E-07	1.406	1.17E-07	1.455	5.70E-08	1.455	5.00E-08	1.455	5.00E-08
780	1.334	1.59E-07	1.468	5.79E-07	1.410	1.46E-07	1.406	1.52E-07	1.455	8.47E-08	1.454	5.00E-08	1.455	6.53E-08
785	1.334	1.37E-07	1.468	5.45E-07	1.410	1.40E-07	1.406	1.10E-07	1.455	5.00E-08	1.454	5.00E-08	1.455	5.00E-08
790	1.334	6.66E-08	1.468	5.32E-07	1.409	1.32E-07	1.406	1.56E-07	1.455	8.66E-08	1.454	5.00E-08	1.455	5.60E-08
795	1.334	1.21E-07	1.468	5.92E-07	1.409	1.32E-07	1.406	1.39E-07	1.455	7.50E-08	1.454	5.00E-08	1.455	5.03E-08
800	1.333	1.25E-07	1.468	6.13E-07	1.409	1.29E-07	1.406	1.13E-07	1.455	5.08E-08	1.454	5.00E-08	1.455	5.00E-08
805	1.333	1.03E-07	1.468	5.43E-07	1.409	1.25E-07	1.406	1.51E-07	1.454	7.55E-08	1.454	5.00E-08	1.455	5.13E-08
810	1.333	1.25E-07	1.468	4.51E-07	1.409	1.32E-07	1.405	1.15E-07	1.454	5.24E-08	1.454	5.00E-08	1.454	5.00E-08
815	1.333	1.45E-07	1.468	6.19E-07	1.409	1.38E-07	1.405	1.64E-07	1.454	1.10E-07	1.454	5.00E-08	1.454	7.36E-08
820	1.333	1.53E-07	1.468	6.56E-07	1.409	1.41E-07	1.405	1.06E-07	1.454	8.09E-08	1.454	5.00E-08	1.454	6.62E-08
825	1.333	1.03E-07	1.467	6.67E-07	1.409	1.51E-07	1.405	9.34E-08	1.454	5.75E-08	1.454	5.00E-08	1.454	5.00E-08
830	1.333	1.38E-07	1.467	6.22E-07	1.409	1.56E-07	1.405	5.52E-08	1.454	5.00E-08	1.454	5.00E-08	1.454	5.00E-08
835	1.333	1.94E-07	1.467	5.90E-07	1.409	1.78E-07	1.405	1.38E-07	1.454	1.06E-07	1.454	5.00E-08	1.454	7.88E-08
840	1.333	2.29E-07	1.467	5.69E-07	1.409	1.82E-07	1.405	1.79E-07	1.454	1.31E-07	1.453	5.00E-08	1.454	1.36E-07
845	1.333	2.82E-07	1.467	7.53E-07	1.409	2.09E-07	1.405	2.09E-07	1.454	1.09E-07	1.453	5.00E-08	1.454	1.03E-07
850	1.333	1.58E-07	1.467	1.06E-06	1.408	2.17E-07	1.405	2.39E-07	1.454	1.78E-07	1.453	5.00E-08	1.454	8.59E-08
855	1.333	2.68E-07	1.467	5.00E-08	1.408	1.77E-07	1.405	5.00E-08	1.454	5.00E-08	1.453	5.00E-08	1.454	5.00E-08
860	1.332	2.98E-07	1.467	4.06E-07	1.408	2.19E-07	1.405	9.47E-08	1.454	5.00E-08	1.453	5.00E-08	1.454	5.00E-08
865	1.332	2.99E-07	1.467	5.75E-07	1.408	2.45E-07	1.405	1.20E-07	1.453	5.94E-08	1.453	5.00E-08	1.454	7.91E-08
870	1.332	3.23E-07	1.467	5.74E-07	1.408	2.63E-07	1.404	1.38E-07	1.453	8.79E-08	1.453	5.00E-08	1.453	1.07E-07
875	1.332	3.40E-07	1.467	6.06E-07	1.408	2.84E-07	1.404	1.55E-07	1.453	1.17E-07	1.453	5.00E-08	1.453	1.34E-07
880	1.332	3.60E-07	1.467	6.33E-07	1.408	3.12E-07	1.404	1.75E-07	1.453	1.49E-07	1.453	5.00E-08	1.453	1.65E-07
885	1.332	3.82E-07	1.467	6.63E-07	1.408	3.46E-07	1.404	2.18E-07	1.453	1.98E-07	1.453	5.00E-08	1.453	2.15E-07
890	1.332	4.04E-07	1.466	7.35E-07	1.408	3.87E-07	1.404	3.04E-07	1.453	2.68E-07	1.453	5.00E-08	1.453	2.83E-07
895	1.332	4.27E-07	1.466	7.89E-07	1.408	4.34E-07	1.404	4.32E-07	1.453	3.51E-07	1.453	1.09E-07	1.453	3.67E-07
900	1.332	4.47E-07	1.466	8.98E-07	1.408	4.87E-07	1.404	5.89E-07	1.453	4.68E-07	1.453	2.25E-07	1.453	4.84E-07
905	1.332	4.73E-07	1.466	1.01E-06	1.408	5.44E-07	1.404	6.82E-07	1.453	5.82E-07	1.453	3.50E-07	1.453	5.96E-07
910	1.332	5.13E-07	1.466	1.12E-06	1.408	5.98E-07	1.404	6.66E-07	1.453	6.86E-07	1.452	4.88E-07	1.453	6.98E-07
915	1.332	5.61E-07	1.466	1.20E-06	1.408	6.51E-07	1.404	5.39E-07	1.453	7.41E-07	1.452	6.05E-07	1.453	7.53E-07
920	1.332	6.29E-07	1.466	1.24E-06	1.407	7.01E-07	1.404	3.76E-07	1.453	7.44E-07	1.452	6.91E-07	1.453	7.56E-07
925	1.332	7.46E-07	1.466	1.25E-06	1.407	7.52E-07	1.404	2.37E-07	1.453	6.90E-07	1.452	7.23E-07	1.453	7.02E-07
930	1.332	9.15E-07	1.466	1.22E-06	1.407	8.12E-07	1.404	1.54E-07	1.453	5.95E-07	1.452	6.90E-07	1.453	6.10E-07
935	1.332	1.13E-06	1.466	1.18E-06	1.407	8.90E-07	1.404	1.16E-07	1.453	4.74E-07	1.452	5.86E-07	1.453	4.89E-07
940	1.332	1.40E-06	1.466	1.14E-06	1.407	9.96E-07	1.404	1.02E-07	1.453	3.50E-07	1.452	4.37E-07	1.452	3.65E-07
945	1.331	1.75E-06	1.466	1.10E-06	1.407	1.14E-06	1.404	9.97E-08	1.452	2.51E-07	1.452	2.80E-07	1.452	2.59E-07
950	1.331	2.26E-06	1.466	1.07E-06	1.407	1.32E-06	1.404	1.02E-07	1.452	1.78E-07	1.452	1.45E-07	1.452	1.83E-07
955	1.331	2.87E-06	1.466	1.08E-06	1.407	1.55E-06	1.403	1.04E-07	1.452	1.36E-07	1.452	5.00E-08	1.452	1.36E-07
960	1.331	3.34E-06	1.466	1.15E-06	1.407	1.81E-06	1.403	1.02E-07	1.452	1.11E-07	1.452	5.00E-08	1.452	1.07E-07
965	1.331	3.56E-06	1.466	1.31E-06	1.407	2.07E-06	1.403	1.03E-07	1.452	1.02E-07	1.452	5.00E-08	1.452	9.57E-08
970	1.331	3.67E-06	1.466	1.55E-06	1.407	2.30E-06	1.403	1.05E-07	1.452	1.02E-07	1.452	5.00E-08	1.452	9.36E-08
975	1.331	3.72E-06	1.465	1.81E-06	1.407	2.49E-06	1.403	1.06E-07	1.452	1.04E-07	1.452	5.00E-08	1.452	9.50E-08
980	1.331	3.72E-06	1.465	2.04E-06	1.407	2.63E-06	1.403	1.25E-07	1.452	1.21E-07	1.452	5.00E-08	1.452	1.10E-07
985	1.331	3.65E-06	1.465	2.23E-06	1.407	2.72E-06	1.403	1.51E-07	1.452	1.50E-07	1.452	5.00E-08	1.452	1.37E-07
990	1.331	3.53E-06	1.465	2.36E-06	1.407	2.75E-06	1.403	1.85E-07	1.452	1.87E-07	1.452	5.00E-08	1.452	1.72E-07
995	1.331	3.38E-06	1.465	2.48E-06	1.407	2.75E-06	1.403	2.25E-07	1.452	2.35E-07	1.452	5.00E-08	1.452	2.15E-07
1000	1.331	3.20E-06	1.465	2.57E-06	1.407	2.70E-06	1.403	2.69E-07	1.452	2.87E-07	1.452	5.00E-08	1.452	2.66E-07
1005	1.331	3.01E-06	1.465	2.63E-06	1.407	2.64E-06	1.403	3.33E-07	1.452	3.51E-07	1.452	1.07E-07	1.452	3.26E-07
1010	1.331	2.80E-06	1.465	2.65E-06	1.407	2.54E-06	1.403	4.22E-07	1.452	4.21E-07	1.451	1.81E-07	1.452	3.93E-07
1015	1.331	2.58E-06	1.465	2.64E-06	1.406	2.43E-06	1.403	5.15E-07	1.452	4.85E-07	1.451	2.55E-07	1.452	4.55E-07
1020	1.331	2.36E-06	1.465	2.62E-06	1.406	2.31E-06	1.403	5.58E-07	1.452	5.25E-07	1.451	3.02E-07	1.452	4.95E-07
1025	1.331	2.15E-06	1.465	2.57E-06	1.406	2.18E-06	1.403	4.99E-07	1.452	5.42E-07	1.451	3.21E-07	1.452	5.09E-07
1030	1.331	1.95E-06	1.465	2.52E-06	1.406	2.06E-06	1.403	3.83E-07	1.452	5.42E-07	1.451	3.32E-07	1.452	5.09E-07
1035	1.331	1.77E-06	1.465	2.47E-06	1.406	1.95E-06	1.403	2.73E-07	1.452	5.33E-07	1.451	3.48E-07	1.451	4.99E-07
1040	1.331	1.62E-06	1.465	2.43E-06	1.406	1.84E-06	1.403	2.03E-07	1.452	5.09E-07	1.451	3.49E-07	1.451	4.77E-07
1045	1.331	1.48E-06	1.465	2.38E-06	1.406	1.75E-06	1.403	1.72E-07	1.451	4.77E-07	1.451	3.30E-07	1.451	4.45E-07
1050	1.331	1.37E-06	1.465	2.34E-06	1.406	1.67E-06	1.403	1.67E-07	1.451	4.41E-07	1.451	3.00E-07	1.451	4.07E-07
1055	1.330	1.29E-06	1.465	2.30E-06	1.406	1.61E-06	1.403	1.74E-07	1.451	4.05E-07	1.451	2.62E-07	1.451	3.70E-07
1060	1.330	1.23E-06	1.465	2.27E-06	1.406	1.55E-06	1.402	1.90E-07	1.451	3.69E-07	1.451	2.20E-07	1.451	3.31E-07
1065	1.330	1.20E-06	1.465	2.22E-06	1.406	1.51E-06	1.402	2.11E-07	1.451	3.31E-07	1.451	1.82E-07	1.451	2.93E-07
1070	1.330	1.19E-06	1.465	2.17E-06	1.406	1.48E-06	1.402	2.49E-07	1.451	3.01E-07	1.451	1.52E-07	1.451	2.63E-07
1075	1.330	1.21E-06	1.465	2.13E-06	1.406	1.45E-06	1.402	3.03E-07	1.451	2.77E-07	1.451	1.23E-07	1.451	2.41E-07
1080	1.330	1.25E-06	1.465	2.09E-06	1.406	1.45E-06	1.402	3.72E-07	1.451	2.55E-07	1.451	9.00E-08	1.451	2.16E-07
1085	1.330	1.32E-06	1.464	2.04E-06	1.406	1.45E-06	1.402	4.35E-07	1.451	2.38E-07	1.451	6.16E-08	1.451	1.99E-07
1090	1.330	1.41E-06	1.464	1.98E-06	1.406	1.47E-06	1.402	4.76E-07	1.451	2.24E-07	1.451	5.00E-08	1.451	1.84E-07
1095	1.330	1.53E-06	1.464	1.92E-06	1.406	1.50E-06	1.402	4.70E-07	1.451	2.20E-07	1.451	5.00E-08	1.451	1.74E-07
1100	1.330	1.66E-06	1.464	1.85E-06	1.406	1.54E-06	1.402	3.94E-07	1.451	2.19E-07	1.451	5.00E-08	1.451	1.75E-07
1105	1.330	1.80E-06	1.464	1.79E-06	1.406	1.58E-06	1.402	2.93E-07	1.451	2.26E-07	1.451	5.00E-08	1.451	1.82E-07
1110	1.330	1.94E-06	1.464	1.73E-06	1.406	1.63E-06	1.402	2.42E-07	1.451	2.44E-07	1.451	5.00E-08	1.451	2.04E-07
1115	1.330	2.11E-06	1.464	1.69E-06	1.406	1.69E-06	1.402	2.47E-07	1.451	2.80E-07	1.451	5.00E-08	1.451	2.39E-07
1120	1.330	2.31E-06	1.464	1.66E-06	1.406	1.77E-06	1.402	2.89E-07	1.451	3.47E-07	1.451	7.17E-08	1.451	3.04E-07
1125	1.330	2.63E-06	1.464	1.66E-06	1.406	1.91E-06	1.402	3.81E-07	1.451	4.73E-07	1.451	1.29E-07	1.451	4.26E-07
1130	1.330	3.21E-06	1.464	1.72E-06	1.406	2.17E-06	1.402	5.26E-07	1.451	6.86E-07	1.451	2.35E-07	1.451	6.38E-07
1135	1.330	4.24E-06	1.464	1.86E-06	1.406	2.63E-06	1.402	8.08E-07	1.451	1.01E-06	1.451	4.48E-07	1.451	9.65E-07
1140	1.330	5.76E-06	1.464	2.10E-06	1.406	3.33E-06	1.402	1.36E-06	1.451	1.49E-06	1.451	8.49E-07	1.451	1.44E-06
1145	1.330	7.52E-06	1.464	2.43E-06	1.406	4.21E-06	1.402	2.16E-06	1.451	2.17E-06	1.451	1.50E-06	1.451	2.12E-06
1150	1.330	9.10E-06	1.464	2.78E-06	1.405	5.16E-06	1.402	2.79E-06	1.451	2.91E-06	1.450	2.22E-06	1.451	2.84E-06
1155	1.330	1.01E-05	1.464	3.18E-06	1.405	6.04E-06	1.402	2.96E-06	1.451	3.49E-06	1.450	2.75E-06	1.451	3.42E-06
1160	1.330	1.07E-05	1.464	3.68E-06	1.405	6.82E-06	1.402	2.89E-06	1.451	4.16E-06	1.450	3.33E-06	1.451	4.09E-06
1165	1.330	1.10E-05	1.464	4.31E-06	1.405	7.50E-06	1.402	3.08E-06	1.451	5.06E-06	1.450	4.11E-06	1.450	4.99E-06
1170	1.330	1.12E-05	1.464	5.01E-06	1.405	8.13E-06	1.402	4.08E-06	1.451	6.20E-06	1.450	4.94E-06	1.450	6.11E-06
1175	1.330	1.14E-05	1.464	5.81E-06	1.405	8.76E-06	1.402	6.44E-06	1.451	7.59E-06	1.450	5.91E-06	1.450	7.48E-06
1180	1.330	1.16E-05	1.464	6.84E-06	1.405	9.47E-06	1.402	1.08E-05	1.451	9.35E-06	1.450	7.39E-06	1.450	9.20E-06
1185	1.330	1.18E-05	1.464	8.10E-06	1.405	1.03E-05	1.402	1.49E-05	1.451	1.15E-05	1.450	9.77E-06	1.450	1.13E-05
1190	1.330	1.20E-05	1.464	9.39E-06	1.405	1.10E-05	1.402	1.10E-05	1.450	1.31E-05	1.450	1.22E-05	1.450	1.28E-05
1195	1.330	1.21E-05	1.464	1.05E-05	1.405	1.16E-05	1.402	5.50E-06	1.450	1.32E-05	1.450	1.32E-05	1.450	1.29E-05
1200	1.330	1.21E-05	1.464	1.12E-05	1.405	1.19E-05	1.402	2.59E-06	1.450	1.27E-05	1.450	1.36E-05	1.450	1.25E-05

C

Chapter 5: Optical model GenPro

Table C.1: Simulation without glass texturing at various angles of incidence for EVA-UVT, AIR, MIVOLT and PDMS, expressed in mA/cm^2. Surprisingly, PDMS surpasses EVA-UVT mutliple times at lower angles of incidence, probably due to the effect of lower reflection becomes less dominant and the lower absorption of PDMS gives the highest photocurrent.

Angle of incidence	AIR	EVA-UVT	MIVOLT	PDMS	Delta PDMS and EVA-UVT
2.5	39.14487	40.89172	40.89096	40.84020	-0.05152
7.5	39.16202	40.90761	40.90742	40.88093	-0.02668
12.5	39.17733	40.92134	40.92173	40.91952	-0.00182
17.5	39.10909	40.88682	40.88857	40.90060	0.01378
22.5	39.00531	40.85310	40.85235	40.85762	0.00452
27.5	38.83915	40.79686	40.79234	40.78751	-0.00935
32.5	38.45489	40.69421	40.68868	40.68499	-0.00921
37.5	38.23469	40.59478	40.58902	40.58705	-0.00773
42.5	37.43932	40.42381	40.41690	40.42548	0.00167
47.5	37.05927	40.20759	40.20084	40.20437	-0.00322
52.5	35.76928	39.86958	39.86261	39.84882	-0.02075
57.5	35.21091	39.27294	39.26615	39.25300	-0.01994
62.5	31.90738	38.32901	38.32337	38.31008	-0.01893
67.5	30.50250	36.70843	36.70302	36.69307	-0.01536
72.5	28.38661	34.03271	34.02770	34.01971	-0.01300
77.5	17.35280	29.66445	29.66147	29.70628	0.04183
82.5	10.80522	22.14628	22.14423	22.18626	0.03997
87.5	4.49691	9.21964	9.21879	9.23693	0.01729

Table C.2: Real world simulations using the PVMD toolbox and different encapsulation materials EVA-UVT, AIR, MIVOLT and PDMS, expressed in DC energy (Wh) produced in a year (2021) in Delft. Surprisingly, PDMS has the highest DC output, while in the optical simulations it has slightly lower photocurrent at 0 - 5 $^{\circ}$ angle of incidence. At lower angles of incidenc, the effect of lower reflection becomes less dominant and the lower absorption of PDMS gives the highest photocurrent.

Loss/generation	EVA-UVT Energy (Wh)	EVA-UVT (%)	AIR Energy (Wh)	AIR (%)	MIVOLT Energy (Wh)	MIVOLT (%)	PDMS Energy (Wh)	PDMS (%)
Thermalization	942920	31.95	943750	31.95	942880	31.95	943430	31.95
Below bandgap	519220	17.60	519660	17.59	519200	17.60	519520	17.60
Emission	49302	1.67	49143	1.66	49311	1.67	49250	1.67
Carnot losses	78076	2.65	77729	2.63	78067	2.65	78008	2.64
Angle mismatch	397020	13.45	395250	13.38	396970	13.45	396670	13.44
Gain	-39273	-1.33	-39541	-1.34	-39222	-1.33	-39309	-1.33
Cell spacing	54791	1.86	55001	1.86	54788	1.86	54863	1.86
Metal shading	18979	0.64	19051	0.65	18978	0.64	19004	0.64
Reflection	78139	2.65	149940	5.08	78176	2.65	79306	2.69
Parasitic absorption	-19520	-0.66	-20896	-0.71	-19520	-0.66	-20391	-0.69
Recombination I	37039	1.26	34422	1.17	37038	1.26	37211	1.26
Shunt resistance	17	0.00	15	0.00	17	0.00	17	0.00
Series Resistance	71	0.00	66	0.00	71	0.00	71	0.00
Connection loss	41840	1.42	36235	1.23	41829	1.42	41840	1.42
Recombination V	168180	5.70	157830	5.34	168170	5.70	168460	5.71
Mismatch losses	6012	0.20	5896	0.20	6029	0.20	6042	0.20
DC Energy	**618190**	**20.948**	**570010**	**19.299**	**618090**	**20.946**	**618620**	**20.952**
DC difference EVA	**0**		**-48180**		**-100**		**430**	
Total	2951000	100.00	2953600	100.00	2950900	100.00	2952600	100.00

Table C.3: Varying encapsulation thickness for MIVOLT, PDMS, EVA-Conv and EVA-UVT encapsulation, which has various effects on their photocurrent (mA/cm^2) due to different extinction coefficient k values. Also, the difference Delta between steps is different because of the exponential nature of light absorption from Beer_Lambert's Law

Thickness Encapsulation	200	250	300	350	400	450	500	550	600	650	700	750	800	850	900	950	1000
MIVOLT (mA/cm^2)	40.95	40.94	40.93	40.92	40.90	40.89	40.88	40.87	40.86	40.85	40.84	40.83	40.82	40.81	40.80	40.79	40.78
Delta (mA/cm^2)	0.0111	0.0110	0.0109	0.0108	0.0107	0.0106	0.0105	0.0105	0.0104	0.0103	0.0103	0.0102	0.0101	0.0101	0.0100	0.0100	**0.0105**
PDMS (mA/cm^2)	40.89	40.88	40.88	40.87	40.86	40.85	40.84	40.84	40.83	40.82	40.81	40.80	40.80	40.79	40.78	40.77	40.77
Delta (mA/cm^2)	0.0083	0.0082	0.0081	0.0081	0.0080	0.0080	0.0079	0.0079	0.0079	0.0078	0.0077	0.0078	0.0077	0.0077	0.0077	0.0076	**0.0079**
EVA-Conv (mA/cm^2)	40.54	40.49	40.45	40.41	40.36	40.33	40.29	40.25	40.21	40.18	40.14	40.11	40.08	40.04	40.01	39.98	39.95
Delta (mA/cm^2)	0.0467	0.0445	0.0427	0.0410	0.0396	0.0384	0.0373	0.0363	0.0354	0.0347	0.0339	0.0333	0.0327	0.0322	0.0317	0.0313	**0.0370**
EVA-UVT (mA/cm^2)	40.98	40.96	40.94	40.93	40.91	40.89	40.87	40.85	40.83	40.82	40.80	40.78	40.76	40.74	40.73	40.71	40.69
Delta (mA/cm^2)	0.0188	0.0187	0.0186	0.0185	0.0185	0.0184	0.0184	0.0183	0.0182	0.0182	0.0181	0.0180	0.0180	0.0180	0.0180	0.0179	**0.0183**